

A Toolbox of Humanized Recombinant Antibody Fragments for Prion Diseases

by

Vineet Subhash Rathod

A thesis submitted in partial fulfillment of the requirements for the degree of

Doctor of Philosophy

Department of Biochemistry
University of Alberta

© Vineet Subhash Rathod, 2022

ABSTRACT

Prion diseases are rare, inexorably progressive, and fatal neurodegenerative disorders, with no therapy other than palliation. The key event in the pathogenesis of prion diseases is the conformational conversion of the cell-surface glycoprotein (PrP^C), from a predominantly α -helical structure into an infectious, aggregated isoform (PrP^{Sc}), with β -sheet oligomers and amyloid fibrils. Multiple abnormal PrP structures have been observed both in vivo and in vitro, and determining which are relevant to disease, that is, infectious and/or toxic, is a major challenge. Recently high-resolution structures of brain-derived prion strains revealed a parallel in-register intermolecular β -sheet (PIRIBS) structure, which is in conflict with brain-derived X-ray fiber diffraction patterns proposing a four-rung β -solenoid (4R β S) architecture.

Antibodies are powerful tools for protein purification and molecular detection. Although conventional antibodies are ideal for most applications, the performance of certain assays is enhanced by using antibody fragments. Fab fragments (Fabs) are small antibody derivatives that maintain antigen-binding capacity. One of the advantages of Fabs over intact antibodies is they are small in size, which allows them to penetrate deeper into protein aggregates, such as amyloid fibrils. However, having antibodies that are conformational dependent on proteins such as the pathologic conformation of PrP^{Sc} recognizing the toxic oligomers and fibrils has enormous value for biomedical research and therapeutics of prion diseases.

I established a pipeline to produce recombinant humanized antibody fragments for prions derived from phage display technology and hybridoma clones. The fully functional and soluble antibody fragments were characterized extensively using linear PrP peptides and via structural epitope

mapping of PrP^{Sc}-specific antibody fragments. This allowed me to build a toolbox of various recombinant antibody fragments, including engineered conformational PrP^{Sc}-specific antibody fragments and small conjugated antibody derivatives. I used these to perform ultrastructural analyses of animal and human prions using immunogold labelling, direct detection of prions, and in-vitro structural analysis of genetic prions using time-dependent folding immunoassay.

Taken together, these recombinant humanized antibody fragments provide an alternate approach to understand the structural relationships and pathophysiological roles of various prion ultrastructures and offer potential therapeutic candidates for prion diseases.

PREFACE

This thesis is an original work of Vineet Subhash Rathod, under the supervision of Dr. Holger Wille. This thesis begins with Chapter 1 which includes a general introduction and ends with Chapter 5 the overall conclusion and future directions.

The literature review described in chapter 1 is my original work. Parts of chapter 1 has been Published at as Flores-Fernandez*, J. M., V. Rathod* and H. Wille (2018). "Comparing the Folds of Prions and Other Pathogenic Amyloids." Pathogens 7(2). This review was equally written by the FFJM and VR. * Authors contributed equally to this work.

Chapter 2 of this thesis includes collaborative research with colleagues from the University of Zürich in Switzerland. The immunogold labelling experiment was performed by me and was published at as Kamali-Jamil, R., E. Vazquez-Fernandez, B. Tancowny, V. Rathod, S. Amidian, X. Wang, X. Tang, A. Fang, A. Senatore, S. Hornemann, S. Dudas, A. Aguzzi, H. S. Young and H. Wille (2021). "The ultrastructure of infectious L-type bovine spongiform encephalopathy prions constrains molecular models." PLoS Pathog 17(6): e1009628. The second immunogold labelling experiment for a different study was also performed by and was published at as Vanni, I., L. Pirisinu, C. Acevedo-Morantes, R. Kamali-Jamil, V. Rathod, M. A. Di Bari, C. D'Agostino, S. Marcon, E. Esposito, G. Riccardi, S. Hornemann, A. Senatore, A. Aguzzi, U. Agrimi, H. Wille and R. Nonno (2020). "Isolation of infectious, non-fibrillar and oligomeric prions from a genetic prion disease." Brain 143(5): 1512-1524.

Parts of other immunogold labelling data presented in chapter 2 were performed by me as well and the manuscript is in preparation (Amidian et al., CWD prions).

Engineering of the PrP^{Sc}-specific antibodies discussed in Chapter 3 of this thesis is an immune response from the PrP^{Sc}-vaccine project in the Wille lab. A patent published as A. Fang, Flores-

Fernández, J. M., V.Rathod, X.Tang, H.Wille (2018). "An innocuous, structured scaffold for structure-based amyloid disease vaccines and antigens". The formation of the hybridoma clone of Parent YEG Sc-G1, M63 and M18 and activity assays performed in various prion isolated were primarily performed and graphed (Figure 3-1.A-B) by Dr. Xinli Tang. The production of 14R1 vaccine/antigen for performing activity assays was kindly provided by Dr. Andrew Fang and Madeleine Fleming.

All the cell-culture work described in this thesis (Chapters 2 and 3) was performed with assistance from our collaborators from the Sim Lab; Hailey Pineau, and Grant Norman. They kindly provided me with all the cells to perform the experiment.

The experiments presented in Chapter 4 are all my original work except for Figure 4-1 was adapted from our collaborator's recent paper (Vanni et al., 2020) which was also an inspiration to perform the study described in this chapter.

All the molecular dynamic simulation and docking experiments were performed by Dr. Lyudmyla Dorosh.

The electron micrographs were collected with the help of Drs. Xiongyao Wang, Yongliang Wang, Sara Amidian and Razieh Kamali-Jamil.

The conclusive remarks discussed in Chapter 5 is my original work.

All the projects that required the use of animals received animal research ethics approval from the University of Alberta Animal Care and Use Committee and followed the guidelines provided by the Canadian Council on Animal Care (CCAC). The research protocols of these results were approved under AUP00000884, titled "Structural biology of infectious mammalian prions", and AUP00000424, titled "Production of antibodies for neurodegenerative disease Research".

Experiments utilizing human samples were given approval from the Health Research Ethics

Board Biomedical Panel of the University of Alberta under study “Pro0004244”, titled “Human prions and other misfolded proteins – analyzing the molecular structure of the misfolded conformers”.

What kept me going...

“It will be difficult, but difficult does not equal impossible”

-Subhash Rathod (Dad)

“When you believe in yourself, you have unlimited power”

-Priti Rathod (Mom)

“When life gives you lemons, you make a lemonade out of it”

-Dr. Holger Wille (Supervisor)

“Always keep your chin up”

-Dr. Adrienne Wright (Canadian mom/Mentor)

“I plan, you plan, he is the best of the planner”

-Sayyada Andani (Best friend)

ACKNOWLEDGEMENTS

I would like to begin by thanking my supervisor, Dr. Holger Wille, for believing in me and encouraging me to pursue a graduate degree in his lab and under his supervision. His constant assistance, counsel, and support throughout my time in his lab made my PhD path very pleasant and comfortable. I recall him introducing me to the project at the beginning of my master's degree, and a year later he inspired me to believe I could obtain a PhD. I admired his great leadership, critical thinking, and inspiration, which all led to my success and productivity.

Next, I would like to sincerely thank my supervisory committee Dr. Marek Michalak and Dr. Valerie Sim for their continuous support and guidance, which have always helped me to improve my work. They were always welcoming and available to have discussions. Their critical comments and encouragement have helped me improve my scientific reasoning and skills. I am very fortunate to have a team of mentors who gave me their time whenever I needed for helping me with my academic, extra-curricular activities and research.

Special thanks to Dr. Nicolas Touret of the University of Alberta and Dr. Mark Zabel of the Colorado State University for their time and kind willingness to be on my PhD examining committee.

I would like to thank all the members of the Wille lab, Sara Amidian, Dr. Lyudmyla Dorosh, Dr. Andrew Fang, Dr. Jose Flores Fernandez, Dr. Xinli (lili) Tang, Dr. Razieh Kamali-Jamil, Madeleine Fleming, Aishwairya Sriraman, Dr. Aliza Bornstein, Brian Tancowny, Shelaine Fleck, Victoria Foster, Dr. Xiongyao Wang (former member), Dr. Yongliang Wang (former member) for all their help, support and their precious friendship was a great source of joy and happiness.

I would also like to thank all my undergraduate students (BIOCH 499), Emily McNamara, Jimmy Lu, Gabrielle Gate, Jessica Cashion, Chey Zwicker, as well as international exchange student, Alina Hebestreit, and volunteering students, Tolu Abonduwa, Milan Shah, and Maddison Charlton for their time, dedication and experimental help in moving my projects forwards.

I am really grateful to my collaborators for their outstanding support, and contributions especially, Dr. Adrianno Aguzzi from the University of Zürich, Switzerland for kindly providing us with the anti-PrP antibody phage library. I am very thankful to Hailey Pineau from whom I initially learned the cell culture technique and for training me to use a confocal microscope as well as Grant Normal and Dr. Valerie Sim for providing us CAD 5/CAD5 RML cells. I am also thankful to Dr. Ilaria Vanni and Dr. Romolo Nonno at the Istituto Superiore di Sanita, Italy for performing our bioassays in bank voles. Also, I would like to acknowledge Isa Dzhabrailov and Dr. Debbie Mckenzie for performing PMCA and RT-QuIC analysis.

I am grateful to everyone at the Centre for Prions and Protein Folding Diseases. You all have contributed scientifically and socially with which I have a lot of enjoyable memories over the years of my PhD journey. I would like to thank Dr. Debbie Mckenzie, Dr. Judd Aiken, Dr. David Westaway, Dr. Kar Satyabatra, Dr. Ted Allison, Dr. Serene Wohlgemuth, Klinton Shmeit, Grant Norman. I would also like to extend my gratitude to my supportive friends, Danielle Gushue, Dr. Elizabeth Triscott, Dr. Satish Nemani, Dr. Bibin Anand, Abhishek Dahal and Andrew Schmaus.

I would like to thank all the past and present members of the Department of Biochemistry, especially Dr. David Stuart for his continuous support and advice as a graduate program coordinator, Dr. Charles Holmes (former chair) and Dr. Mark Glover (current chair) for

supporting me in various academic events, 3MT competition, academic talks, seminars, and providing a great environment for trainees. I cannot thank enough Ms. Lisa Dublin and Ms. Kelsey Robertson for being amazing graduate program advisors and for supporting me throughout my graduate degree program. Lastly, I would like to thank all the biochemistry graduate students for showing their support and believing in representing the biochemistry graduate student body as vice president and president of the Biochemistry Graduate Students' Association (BCGSA).

I would like to thank my mentors, especially Dr. Adrienne Wright and Dr. Jo Parrish for providing me with teaching opportunities in various introductory, structural and metabolic biochemistry courses as well as for running the biochemistry student lab course. I truly appreciate your continuous support and encouragement which allowed me to complete my Graduate Teaching and Learning Program at the UofA.

I would like to thank FGSR, FoMD and Instructors for providing me with various opportunities and experiences to develop my professional network, especially Dr. Hanne Ostergaard (former Dean of Research) and Dr. Alan Underhill (MD/PhD Director) for their valued mentorship and supporting me that led me to found a student initiative named, [the Bench to Bedside Students' Association](#) at the UofA which aims at fostering collaboration and networking between FoMD graduate and medical trainees. I would also like to thank FGSR, especially Charity Slobod for her time, support and guidance which allowed me to be in the top 15 finalists in presenting my [thesis in 3 minutes](#) (3MT).

I would like to express my gratitude to the University of Alberta International especially Mrs. Lubna Ahmed and Mrs. Kumarie Achaibar-Morrisson for providing me a home away from home

since [my undergraduate studies](#). Thank you for always being my go-to for all my concerns, be it school-related, immigration, or life in Canada.

I would like to thank my friends Isa Dzhabrailov, Jessi Bak, Dr. Mary Hernando, Anissa Viveiros, Dr. Darpan Malhotra, Dr. Rashmi Panigrahi, Dr. Asad Makhani, Graeden Winkelaar, and Steffane McLennan who provided me with an entire village and supported me tirelessly throughout my degree. You were the people I could always count on. Thank you for being there for laughter and venting my frustrations and keeping me sane throughout this whole process.

Lastly, I would like to thank my family for their unwavering support and for shaping me into the person I am today. I am grateful to mom and dad for their continuous support, unconditional love and providing me a better life and all the opportunities. To my twin sister Vineeta Patel and younger sister Aneeka Rathod, thank you for the unconditional love and care which were my greatest strengths and sources of motivation, and they are priceless in my life.

This chapter of my life could not have been completed without the support from all my family members, mentors, friends, and colleagues.

TABLE OF CONTENTS

ABSTRACT	ii
PREFACE	iv
What kept me going.....	vii
ACKNOWLEDGEMENTS	ix
LIST OF TABLES	xvii
LIST OF FIGURES	xviii
ABBREVIATIONS	xxi
AMINO ACIDS	xxv
Chapter 1: General Introduction	1
1.1 BIOCHEMISTRY OF PROTEINS: THE GOOD, THE BAD AND THE UGLY	2
1.2 THE CELLULAR PRION PROTEIN	3
1.3 THE DISEASE-CAUSING AGENT PRP ^{Sc}	5
1.3.1 In-vivo and in-vitro generation of infectious PrP ^{Sc}	7
1.4 PRION STRAINS.....	9
1.5 SPECIES BARRIER	9
1.6 PRION DISEASES	10
1.7 PRION DISEASES IN ANIMALS.....	11
1.7.1 Scrapie	12
1.7.2 Bovine spongiform encephalopathy (BSE)	13
1.7.3 Chronic wasting disease (CWD).....	15
1.8 PRION DISEASES IN HUMANS.....	16
1.8.1 Sporadic human prion diseases.....	17
1.8.2 Inherited human prion diseases.....	18
1.8.3 Acquired human prion diseases	19
1.9 STRUCTURES OF THE INFECTIOUS PRP ^{Sc}	20
1.9.1 Four-rung beta solenoid model (4RβS)	21
1.9.2 Parallel in-register intermolecular beta-sheet structure (PIRIBS)	24
1.10 STRUCTURES OF OTHER PATHOGENIC PROTEINS.....	27
1.11 HUMAN IMMUNOGLOBULINS	29
1.11.1 Antibody architecture	29
1.11.2 An abundant class of immunoglobulin: IgG	31
1.11.3 Engineering a toolbox of recombinant antibody fragments	31
1.11.4 How are antibodies generated?	32
1.12 ROLE OF ANTIBODIES IN PRION DISEASES	37
1.12.1 Antibodies and structure of prion protein	38
1.12.2 Antibodies in direct detection of prions.....	39
1.12.3 Antibodies as passive immunotherapeutic tools	40
1.13 AIM AND THESIS OUTLINE	42
Chapter 2: Characterizing Select Epitopes of PrP using Humanized Recombinant Anti-PrP antibody fragments	44

2.1 INTRODUCTION	45
2.2 EXPERIMENTAL PROCEDURES.....	48
2.2.1 Fab Library.....	48
2.2.2 Expression of selected anti-PrP Fabs.....	49
2.2.3 Nickel ion affinity chromatography purification of PrP Fabs.....	50
2.2.4 SDS-PAGE gels for Coomassie staining and Western blotting.....	51
2.2.5 PrP peptide library.....	52
2.2.6 Enzyme-Linked Immunosorbent Assay (ELISA) for epitope mapping	52
2.2.7 Activity assays	53
2.2.7.1 Dot blotting.....	53
2.2.7.2 ELISA using brain homogenates.....	53
2.2.7.3 Histoblots from RML infected and uninfected mouse brain slices.....	54
2.2.7.4 Immunohistochemistry using CAD 5 and CAD 5 - RML infected cells.....	56
2.2.8 Isolation of RML prions	57
2.2.9 Silver staining	58
2.2.10 Western blotting	59
2.2.11 Negative Staining electron microscopy.....	59
2.2.12 Immunogold labelling.....	60
2.3 RESULTS.....	62
2.3.1 Generation of the anti-PrP Fab library via phage display technology.....	62
2.3.2 Expression and purification of selected anti-PrP Fabs	63
2.3.3 Summary table of expressed and purified anti-PrP Fabs from the Fab library	66
2.3.4 Epitope mapping of anti-PrP Fabs	67
2.3.5 Epitope confirmation via activity assays	71
2.3.5.1 Histoblot analysis using anti-PrP Fabs	74
2.3.5.2 Validation by immunocytochemistry assay.....	75
2.3.6 Isolation of RML prions	79
2.3.7 The activity of anti-PrP Fabs towards prions.....	82
2.3.8 Ultrastructure of PTA-Purified RML using electron microscopy	85
2.3.9 Immunogold Labelling of RML, BSE and CWD fibrils using anti-PrP Fabs	91
2.4 DISCUSSION.....	112

Chapter 3: Engineering and Characterizing Humanized PrP^{Sc} – Specific Recombinant Antibody Fragments as Tools for Prion Disease 117

3.1 INTRODUCTION	118
3.2 EXPERIMENTAL PROCEDURES.....	127
3.2.1 Cell lines and generation of hybridomas.....	127
3.2.2 RNA isolation and cDNA synthesis	127
3.2.3 In silico primer design	128
3.2.4 PCR amplification of variable regions.....	129
3.2.5 PCR product clean-up and gel extraction	130
3.2.6 Sequencing of antibody variable regions	130
3.2.7 Designing of PrP ^{Sc} -specific Fabs, scFv and nanobodies	131
3.2.8 Cloning of variable region amplicons	132
3.2.8.1 Engineered antibody fragments	132

3.2.8.2 Digestion and ligation.....	133
3.2.9 Antibody expression and purification	134
3.2.10 SDS-PAGE Gel for Coomassie staining and Western blotting.....	134
3.2.11 Enzyme-Linked Immunosorbent Assay (ELISA) for epitope mapping	135
3.2.12 Activity assay	136
3.2.12.1 Indirect ELISA.....	136
3.2.12.2 Two-step indirect competition ELISA	136
3.2.13 Immunogold labelling.....	137
3.2.14 Immunocytochemistry assay.....	138
3.2.14.1 Thresholding	141
3.2.15 Immunoprecipitation assay.....	141
3.2.16 Homology modelling of antibody fragments	143
3.2.16.1 Homology modeling of Fab G1, scFv G1 and Nano G1 and preparing of huPrP ^{Sc} conformer for simulations.....	143
3.2.16.2 Homology modeling of scFv G1 conjugated to eGFP.....	144
3.2.16.3 Homology modeling of human four–ring beta solenoid (4R β S) model (huPrP ^{Sc})	144
3.2.17 Molecular dynamics simulations of modelled systems for stabilization.....	145
3.2.18 Docking and Analysis tools and following simulations of docked systems	146
3.2.19 Following MD simulation of docked complexes.....	146
3.3 RESULTS.....	147
3.3.1 Antibody variable region sequence identification workflow	147
3.3.2 PCR amplification of the immunoglobulin variable regions	147
3.3.3 DNA sequence analysis.....	151
3.3.4 Engineering a toolbox of PrP ^{Sc} -specific antibody fragments	159
3.3.5 Design of PrP ^{Sc} -specific Fabs.....	161
3.3.6 Expression and purification of selected PrP ^{Sc} -specific antibody fragments	164
3.3.7 Epitope mapping of YEG Sc – G1, M18 and M63.....	167
3.3.8 Epitope confirmation via activity assays	172
3.3.9 Comparative <i>in silico</i> modelling and docking of Fab G1.....	175
3.3.10 Immunogold labelling of RML prions using YEG Sc – G1 and YEG Sc – M63	177
3.3.11 Immunoprecipitation of fibrillized 14R1 vaccine/antigen.....	189
3.3.12 Validation by immunocytochemistry assay.....	194
3.3.13 Design of single-chain antibody fragments and their conjugates	199
3.3.13.1 Design of PrP ^{Sc} -specific single-chain variable fragment	199
3.3.13.2 Design of PrP ^{Sc} -specific single-chain variable fragment with a cell penetratin linker	200
3.3.13.3 Design of PrP ^{Sc} -specific fluobody (scFv G1 – eGFP)	200
3.3.14 Cloning, Expression and activity of engineered scFv's	203
3.3.15 Comparative <i>in silico</i> modelling and docking of scFv G1 and with its eGFP conjugate.....	208
3.3.16 Labelling of native PrP ^{Sc} in RML-infected CAD 5 cells using PrP ^{Sc} -specific fluobody	211
3.3.17 Design of PrP ^{Sc} -specific nanobody.....	217
3.3.18 The activity of variable heavy chain only	221
3.3.19 Comparative <i>in-silico</i> modelling and docking of VHH-G1 and huPrP ^{Sc}	222
3.4 DISCUSSION.....	225

Chapter 4: Analyzing the Fold of Synthetic A117V – Gerstmann Sträubler-Scheinker Peptide using a PrP^{Sc}-specific Antibody..... 231

4.1 INTRODUCTION232

4.2 EXPERIMENTAL PROCEDURES.....238

4.2.1 Synthetic GSS-A117V peptide design238

4.2.2 Preparation of GSS-A117V peptide238

4.2.3 PrP^{Sc} – specific antibody239

4.2.4 Designing GSS fold assay using different biochemical conditions.....239

4.2.5 Synthetic GSS-A117V time-dependent folding immunoassay240

4.2.6 Modelling and molecular docking of antigen-antibody complex.....241

4.2.7 Indirect and competitive Enzyme-Linked Immunosorbent Assays (ELISAs).....242

4.2.8 Negative stain electron microscopy243

4.2.9 Immunogold labelling.....244

4.2.10 PK-Digestion245

4.2.11 Methanol precipitation245

4.2.12 Western blotting246

4.2.13 ThT fluorescence assay.....246

4.2.14 Circular Dichroism spectroscopy (CD)247

4.2.15 Bioassays248

4.3 RESULTS.....249

4.3.1 Synthetic GSS-A117V peptide design249

4.3.2 Specificity of PrP^{Sc}-specific antibody to brain-derived infected prion isolates249

4.3.3 Computational studies confirm the binding of human GSS-A117V to YEG Sc-G1 monoclonal antibody250

4.3.4 Time-dependent folding immunoassay of GSS-A117V peptide254

4.3.5 Aggregated synthetic GSS-A117V are morphologically heterogenous at different biochemical conditions.....260

4.3.6 Immunogold labelling using recombinant anti-PrP Fab 69 and PrP^{Sc} – Fab G1.....266

4.3.7 GSS-A117V peptide promotes the formation of protease-resistant PrP at week 4271

4.3.8 Aggregated GSS-A117V binds ThT amyloid dye273

4.3.9 Circular Dichroism spectroscopy275

4.3.10 Bioassays280

4.4 DISCUSSION.....283

Chapter 5: Conclusion and Future Directions..... 289

5.1 The role of antibodies in understanding the prion protein290

5.2 Recombinant anti-PrP antibody fragments.....291

5.3 Engineered PrP^{Sc}-specific antibody fragments.....293

5.4 Orientation of H110 and D146 in a 4R β S and PIRIBS conformation295

5.5 Is 2R β S or 4R β S a precursor to PIRIBS fibril formation?.....297

5.6 Future directions.....299

REFERENCES:301

LIST OF TABLES

TABLE 2-1: SUMMARY TABLE OF CHARACTERIZED HUMANIZED RECOMBINANT PRP FABS.....	66
TABLE 2-2: MOUSE PRP PEPTIDE LIBRARY	68
TABLE 3-1: LIST OF REPORTED PRP ^{Sc} -SPECIFIC ANTIBODIES	121
TABLE 3-2: PRIMER SEQUENCES FOR MOUSE IMMUNOGLOBULIN PCR AMPLIFICATION AND SEQUENCING	128
TABLE 3-3: LIST OF ANTIBODIES USED FOR ICC ASSAY	140
TABLE 3-4: RECOMBINANT ANTIBODY FRAGMENT DERIVATIVES OF YEG Sc, PRP ^{Sc} – SPECIFIC MONOCLONAL ANTIBODY	160
TABLE 4-1: SYNTHETIC GSS-A117V PEPTIDE RECONSTITUTED IN SODIUM – ACETATE BUFFER, PH 5.0	240
TABLE 4-2: SYNTHETIC GSS-A117V PEPTIDE RECONSTITUTED IN SODIUM–PHOSPHATE BUFFER, PH8.0	240

LIST OF FIGURES

FIGURE 1-1: SCHEMATIC STRUCTURE OF CELLULAR PRION PROTEIN (PrP ^C).	4
FIGURE 1-2: PROTEINASE-RESISTANT PrP ^{Sc} FRAGMENT (PrP ^{RES}) OF SPORADIC AND GENETIC PRIONS.	7
FIGURE 1-3: 4RBS AND 2RBS MODEL OF PK-RESISTANT PrP ^{Sc}	24
FIGURE 1-4: RECENT CRYO-EM PIRIBS STRUCTURE OF PK-RESISTANT PrP ^{Sc}	27
FIGURE 1-5: PIRIBS STRUCTURE OF OTHER AMYLOIDOGENIC PROTEINS.	28
FIGURE 1-6: OVERVIEW OF THE RIBBON STRUCTURE OF FULL-LENGTH AND FRAGMENT ANTIBODIES.	34
FIGURE 1-7: SCHEMATIC REPRESENTATION OF IGG, IGM AND ITS SMALLER ANTIBODY DERIVATIVES.	36
FIGURE 1-8: SCHEMATIC REPRESENTATION OF ANTI-PRP ANTIBODY CLEARANCE USING PrP ^C AND PrP ^{Sc} -SPECIFIC ANTIBODY.	41
FIGURE 2-1: PRP FAB LIBRARY.	64
FIGURE 2-2: PURIFICATION OF HUMANIZED RECOMBINANT ANTI-PRP FAB FRAGMENTS.	66
FIGURE 2-3: EPITOPE CHARACTERIZATION.	70
FIGURE 2-4: ACTIVITY ASSAY.	73
FIGURE 2-5: ACTIVITY ASSAY VIA HISTOBLOTS.	75
FIGURE 2-6: IMMUNOCYTOCHEMISTRY OF UNINFECTED CAD 5 CELLS USING HUMANIZED RECOMBINANT ANTI-PRP FABS.	77
FIGURE 2-7: IMMUNOCYTOCHEMISTRY OF RML INFECTED CAD 5 CELLS USING HUMANIZED RECOMBINANT ANTI-PRP FABS.	79
FIGURE 2-8: PURIFICATION OF RML PRIONS.	81
FIGURE 2-9: IMMUNOREACTIVITY OF RECOMBINANT ANTI-PRP FABS USING PURIFIED PRIONS.	83
FIGURE 2-10: SUCROSE STEP GRADIENT PURIFICATION OF RML PRIONS.	87
FIGURE 2-11: NEGATIVELY STAINED ELECTRON MICROGRAPHS OF RML PELLET 1.	88
FIGURE 2-12: NEGATIVELY STAINED ELECTRON MICROGRAPHS OF RML PELLET 2.	89
FIGURE 2-13: NEGATIVELY STAINED ELECTRON MICROGRAPHS OF RML PELLET WASH.	90
FIGURE 2-14: NEGATIVELY STAINED ELECTRON MICROGRAPHS OF ANIMAL PRIONS.	95
FIGURE 2-15: IMMUNOGOLD ELECTRON MICROSCOPY OF SEMI-PURIFIED RML FIBRILS WITH RECOMBINANT ANTI-PRP FAB 3 ANTIBODY.	97
FIGURE 2-16: IMMUNOGOLD ELECTRON MICROSCOPY OF SEMI-PURIFIED RML FIBRILS WITH RECOMBINANT ANTI-PRP FAB 69 ANTIBODY.	99
FIGURE 2-17: IMMUNOGOLD ELECTRON MICROSCOPY OF SEMI-PURIFIED RML FIBRILS WITH ANTI-PRP FAB 29 ANTIBODY.	101
FIGURE 2-18: IMMUNOGOLD ELECTRON MICROSCOPY OF PURIFIED L-TYPE BSE FIBRILS WITH ANTI-PRP FAB 69 ANTIBODY.	103
FIGURE 2-19: IMMUNOGOLD ELECTRON MICROSCOPY OF PURIFIED L-TYPE BSE FIBRILS WITH ANTI-PRION FAB 29 ANTIBODY.	105
FIGURE 2-20: IMMUNOGOLD ELECTRON MICROSCOPY OF PURIFIED CWD FIBRILS WITH ANTI-PRION FAB 3 ANTIBODY.	107
FIGURE 2-21: IMMUNOGOLD ELECTRON MICROSCOPY OF PURIFIED CWD FIBRILS WITH ANTI-PRION FAB 29 ANTIBODY.	109
FIGURE 2-22: EPITOPE ORIENTATION OF HUMANIZED ANTI-PRION FABS IN PrP ^C STRUCTURE, DIMERIC 4RBS PrP ^{Sc} MODEL AND 263K PrP ^{Sc} PIRIBS STRUCTURE.	111
FIGURE 3-1: YEG Sc – G1, A PrP ^{Sc} -SPECIFIC MONOCLONAL ANTIBODY REACTS WITH NATIVE PrP ^{Sc} ONLY.	123
FIGURE 3-2: CONVENTIONAL AND RECOMBINANT ANTIBODY COMPOUNDS THAT HAVE BEEN DEVELOPED AGAINST THE PRION PROTEIN.	126
FIGURE 3-3: SCHEMATIC REPRESENTATION OF ENGINEERING DIFFERENT PrP ^{Sc} – SPECIFIC ANTIBODY FRAGMENTS CURRENTLY IN OUR RESEARCH TOOLBOX.	150
FIGURE 3-4: PCR AMPLIFICATION OF FULL-LENGTH HEAVY CHAIN AND LIGHT CHAIN OF MONOCLONAL ANTIBODIES IGG-61D8 AND IGG-63G4 cDNA (1 μG/μL).	154
FIGURE 3-5: PCR AMPLIFICATION OF HEAVY CHAIN AND LIGHT CHAIN OF MONOCLONAL ANTIBODY IGM63 cDNA (YEG Sc-M63) (1 μG/μL).	156

FIGURE 3-6: PCR AMPLIFICATION OF HEAVY CHAIN AND LIGHT CHAIN OF MONOCLONAL ANTIBODY IgM18 cDNA (YEG Sc-M18) (1 μ G/ μ L).....	158
FIGURE 3-7: DESIGN OF RECOMBINANT PrP ^{Sc} – SPECIFIC FABS.	162
FIGURE 3-8: DOUBLE RESTRICTION DIGEST OF RECOMBINANT FAB G1, FAB M63 AND FAB M18 CONSTRUCTS AND HUMAN FAB VECTOR.	163
FIGURE 3-9: EXPRESSION AND PURIFICATION OF RECOMBINANT PrP ^{Sc} – SPECIFIC FABS.	165
FIGURE 3-10: 14R1 REVERT MUTANTS TO IDENTIFY THE CORE EPITOPE OF FAB G1.	169
FIGURE 3-11: EPITOPE MAPPING OF RECOMBINANT FAB YEG SC G1 AND FULL-LENGTH MOUSE-DERIVED YEG SC G1 USING 14R1 REVERT MUTANTS TO IDENTIFY THE CORE EPITOPE OF FAB G1.....	170
FIGURE 3-12: EPITOPE MAPPING OF RECOMBINANT FAB M18 AND FAB M63 USING 14R1 REVERT MUTANTS TO IDENTIFY THE CORE EPITOPE OF FAB M18 AND FAB M63.	171
FIGURE 3-13: ACTIVITY ASSAY OF FAB G1 TOWARDS PrP ^{Sc} – VACCINE/ANTIGEN (14R1) AND PRIONS.	174
FIGURE 3-14. MOLECULAR DYNAMICS SIMULATION OF FAB G1 AND HUMAN PRP 27-30 STABILIZED FOR 140 NS.	177
FIGURE 3-15: IMMUNOGOLD ELECTRON MICROSCOPY OF PURIFIED RML PRIONS WITH PrP ^{Sc} -SPECIFIC YEG SC – G1 ANTIBODY.	180
FIGURE 3-16: IMMUNOGOLD LABELLING OF RECOMBINANT FAB YEG SC - G1 WITH PURIFIED (P2) AND PELLET WASH RML PRIONS.	182
FIGURE 3-17: IMMUNOGOLD LABELLING OF RECOMBINANT FAB YEG SC – M63 WITH PTA PURIFIED RML PRIONS.....	186
FIGURE 3-18: EPITOPE ORIENTATION OF THE MAb YEG SC-G1 IN MOUSE 4-RUNG-BETA SOLENOID (4RbS) MODEL AND BRAIN-DERIVED RML, PARALLEL IN-REGISTER INTERMOLECULAR BETA SHEET (PIRIBS) STRUCTURE.	188
FIGURE 3-19: ANALYSIS OF PROTEIN IMMUNOPRECIPITATED WITH FAB G1 IN A COMPLEX WITH PrP ^{Sc} VACCINE/ANTIGEN 14R1 IN ITS FIBRILLAR CONFORMATION.	190
FIGURE 3-20: ANALYSIS OF PROTEIN IMMUNOPRECIPITATED WITH scFv – G1 IN A COMPLEX WITH PrP ^{Sc} VACCINE/ANTIGEN 14R1 IN ITS FIBRILLAR CONFORMATION.	191
FIGURE 3-21: ANALYSIS OF PROTEIN IMMUNOPRECIPITATED WITH FAB – G1 IN A COMPLEX WITH PrP ^{Sc} VACCINE/ANTIGEN 14R1 IN ITS FIBRILLAR CONFORMATION AND CELLULAR MOUSE PRION PROTEIN.	193
FIGURE 3-22: IMMUNOCYTOCHEMISTRY OF CAD 5 PRP / RML INFECTED CELLS USING MOUSE-DERIVED FULL-LENGTH YEG SC – G1.	196
FIGURE 3-23: IMMUNOCYTOCHEMISTRY OF CAD 5 PRP / RML INFECTED CELLS USING RECOMBINANT FAB YEG SC – G1.	198
FIGURE 3-24: CONSTRUCT DESIGN OF SINGLE CHAIN ANTIBODY FRAGMENTS AND THEIR CONJUGATES.	202
FIGURE 3-25: DOUBLE RESTRICTION DIGEST OF RECOMBINANT SINGLE-CHAIN ANTIBODY FRAGMENTS AND THEIR CONJUGATES: scFv-G1, scFv-G1 CPP AND scFv-G1 GFP CONSTRUCTS AND HUMAN FAB VECTOR.	204
FIGURE 3-26: EXPRESSION AND PURIFICATION OF SINGLE-CHAIN ANTIBODY FRAGMENTS AND THEIR CONJUGATES.	205
FIGURE 3-27: ACTIVITY ASSAY OF SINGLE-CHAIN ANTIBODY FRAGMENTS AGAINST PrP ^{Sc} VACCINE/ANTIGEN (14R1).	207
FIGURE 3-28: MOLECULAR DYNAMICS SIMULATION OF scFv-G1 GFP AND HUMAN PRP 27-30 STABILIZED FOR 140 NS.	210
FIGURE 3-29: IMMUNOCYTOCHEMISTRY OF CAD 5 PRP / RML INFECTED CELLS USING RECOMBINANT scFv YEG SC – G1 CONJUGATED TO ENHANCED GREEN FLUORESCENT PROTEIN (scFv G1 – GFP).....	214
FIGURE 3-30: IMMUNOCYTOCHEMISTRY OF CAD 5 PRP / RML INFECTED CELLS USING RECOMBINANT ENHANCED GREEN FLUORESCENT PROTEIN AS A CONTROL.	216
FIGURE 3-31: CONSTRUCT DESIGN OF SINGLE DOMAIN ANTIBODY FRAGMENT AND THEIR BISPECIFIC CONJUGATES.	219
FIGURE 3-32: EXPRESSION AND PURIFICATION OF SINGLE DOMAIN ANTIBODY FRAGMENTS AND THEIR CONJUGATES.....	220
FIGURE 3-33: ACTIVITY ASSAY OF VARIABLE HEAVY SINGLE DOMAIN ANTIBODY FRAGMENT AGAINST PrP ^{Sc} –VACCINE/ANTIGEN (14R1).....	221
FIGURE 3-34: MOLECULAR DYNAMICS SIMULATION OF VHH G1 AND HUMAN PRP 27-30 STABILIZED FOR 140 NS.	224
FIGURE 4-1: BIOCHEMICAL AND STRUCTURAL CHARACTERIZATION OF HUMAN GSS-A117V BRAIN SAMPLE.	235
FIGURE 4-2: SYNTHETIC GSS-A117V PEPTIDE AND ITS INTERACTION WITH MAb YEG SC-G1 ANTIBODY.....	253
FIGURE 4-3: TIME-DEPENDENT FOLDING IMMUNOASSAY OF SYNTHETIC GSS ^{A117V} PEPTIDE IN DIFFERENT BIOCHEMICAL CONDITIONS USING MAb YEG SC-G1.....	257
FIGURE 4-5: EPITOPE ORIENTATION OF THE MAb YEG SC-G1 IN MOUSE 4-RUNG-BETA SOLENOID (4RbS) MODEL AND BRAIN-DERIVED GSS-F198S AND HAMSTER 263K, PARALLEL IN-REGISTER INTERMOLECULAR BETA SHEET STRUCTURE (PIRIBS).....	259

FIGURE 4-6: NEGATIVE STAIN ELECTRON MICROGRAPHS FROM WEEK 4 SYNTHETIC GSS ^{A117V} PEPTIDE AT PH 5.0.	263
FIGURE 4-7: NEGATIVE STAIN ELECTRON MICROGRAPHS FROM WEEK 4 SYNTHETIC GSSA117V PEPTIDE AT PH 8.0.	265
FIGURE 4-8: IMMUNOGOLD LABELLING OF WEEK 4 SYNTHETIC GSS-A117V SAMPLE USING FAB 69.....	268
FIGURE 4-9: IMMUNOGOLD LABELLING OF WEEK 4 SYNTHETIC GSS ^{A117V} SAMPLE USING FAB G1.	270
FIGURE 4-10: COMPARISON OF ~6.6 kDa PRP ^{RES} BAND FROM SYNTHETIC GSS-A117V PEPTIDE AT WEEK 4 AGGREGATED SAMPLE VERSUS LINEAR PEPTIDE AT WEEK 0.....	272
FIGURE 4-11: THT FLUORESCENCE OF THE LINEAR AND AGGREGATED SYNTHETIC GSS-A117V PEPTIDE IN VARIOUS BIOCHEMICAL CONDITIONS.	274
FIGURE 4-12: CIRCULAR DICHROISM SPECTRA OF WEEK 0 LINEAR AND WEEK 4 AGGREGATED SYNTHETIC GSS-A117V AT PH 5.0.....	277
FIGURE 4-13: CIRCULAR DICHROISM SPECTRA OF WEEK 0 LINEAR AND WEEK 4 AGGREGATED SYNTHETIC GSS-A117V AT PH 8.0.....	279
FIGURE 4-14: MOLECULAR DYNAMICS SIMULATIONS OF HUMAN PRP 90-150 STABILIZED FOR 40 NS AND 60 NS.	282

ABBREVIATIONS

2R β S	Two rung beta – solenoid
2D	Two - dimensional
4R β S	Four rung beta – solenoid
6 x His-tag	6 x histidine-tag
A β	Amyloid-Beta
AD	Alzheimer’s Disease
BBB	Blood brain barrier
BH	Brain homogenate
Bp	Base pairs
BSA	Bovine serum albumin
BSE	Bovine spongiform encephalopathy
CC1	Charged cluster 1 region
CC2	Charged cluster 2 region
CD	Circular dichroism
cDNA	Circular deoxyribonucleic acid
CDR	Complementarity determining region
CJD	Creutzfeldt-Jakob Disease
CNS	Central nervous system
DNA	Deoxyribonucleic acid
<i>E.coli</i>	<i>Escherischia coli</i>
ECL	Enhanced chemiluminescence

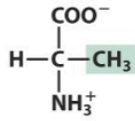
ELISA	Enzyme-linked immunosorbent assay
EM	Electron microscope
Fab	Fragment antigen-binding
FBS	Fetal bovine serum
FFI	Fatal familial insomnia
FTIR	Fourier transform infrared spectroscopy
GD	Globular domain
GPI	Glycosyl-phosphatidylinositol
GSS	Gerstmann-Sträussler-Scheinker
HR	Hydrophobic Region
HRP	Horseradish peroxidase
ICC	Immunocytochemistry
IF	Immunofluorescence
IgG	Immunoglobulin G
IgM	Immunoglobulin M
IMG	Immunogold labelling
IP	Immunoprecipitation
Kbp	kilobase pair
kDa	kilodalton
kV	Kilovolt
L-Type BSE	Low type bovine spongiform encephalopathy
mAbs	Monoclonal antibodies
MBM	Meat and bone meal

MD	Molecular dynamics
MW	Molecular weight
N/A	Not applicable
N/D	Not determined
NMR	Nuclear magnetic resonance
OD	Optical density
OD ₄₅₀	OD at 450 nm
OR	Octapeptide repeat region
PCR	Polymerase chain reaction
PD	Parkinson's disease
PDB	Protein Data Bank
PE	Pronase E
PIRIBS	Parallel In-Register Intermolecular Beta-Sheet
PK	Proteinase K
PMCA	Protein misfolding cyclic amplification
PMSF	Phenylmethylsulfonyl Fluoride
<i>PRNP</i>	Prion protein gene
<i>Prnp</i> ^{-/-}	PrP knockout
PrP ^C	Cellular prion protein
PrP ^{Sc}	Scrapie prion protein
PTA	Phosphotungstate anion
RecPrP	Recombinant prion protein
RML	Rocky mountain laboratory, mouse adapted scrapie prion

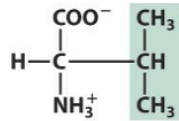
RT-QuIC	Real-time quaking-induced conversion
scFv	Single chain antibody fragment
SDS-PAGE	Sodium dodecyl sulfate-polyacrylamide gel electrophoresis
TBS	Tris-buffered saline
Tg	Transgenic
TSE	Transmissible spongiform encephalopathy
vCJD	Variant Creutzfeldt-Jakob Disease
VHH	Single domain antibody /Nanobody
WB	Western blot
WT	Wild type

AMINO ACIDS

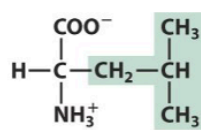
Hydrophobic amino acids



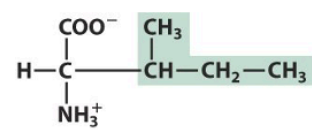
Alanine (Ala, A)



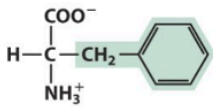
Valine (Val, V)



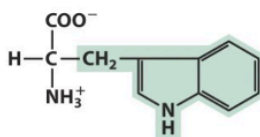
Leucine (Leu, L)



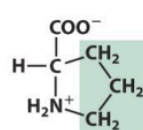
Isoleucine (Ile, I)



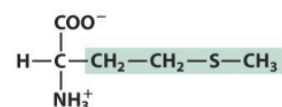
Phenylalanine (Phe, F)



Tryptophan (Trp, W)

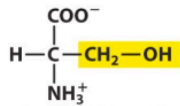


Proline (Pro, P)

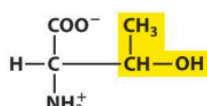


Methionine (Met, M)

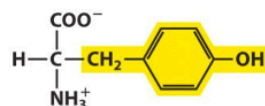
Polar amino acids



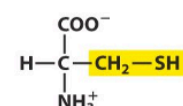
Serine (Ser, S)



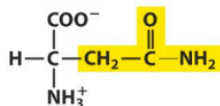
Threonine (Thr, T)



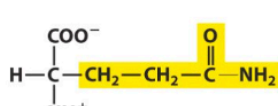
Tyrosine (Tyr, Y)



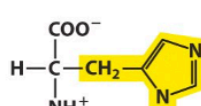
Cysteine (Cys, C)



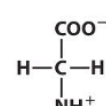
Asparagine (Asn, N)



Glutamine (Gln, Q)

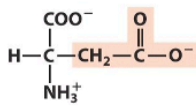


Histidine (His, H)

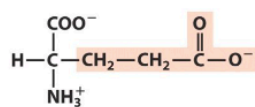


Glycine (Gly, G)

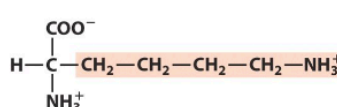
Charged amino acids



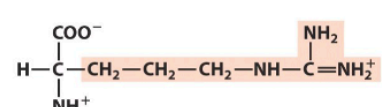
Aspartate (Asp, D)



Glutamate (Glu, E)



Lysine (Lys, K)



Arginine (Arg, R)

Chapter 1: General Introduction

1.1 BIOCHEMISTRY OF PROTEINS: THE GOOD, THE BAD AND THE UGLY

Proteins are commonly thought of as nutrients in food or as the main component of muscles, but they are also small molecules inside cells that perform a variety of vital functions. A human cell can have between 20,000 and 100,000 different types of proteins, composed of the 20 common amino acids that are hydrophobic, hydrophilic or charged (J. Wang, Li, Dangott, & Wu, 2006). These amino acids are covalently bonded together, and the order of the chain dictates how the protein folds upon itself and, eventually, its function. When protein folding goes awry, the resulting misfolded proteins cause problems ranging from bad to ugly, when proteins collapse their crucial role inside cells (Hafner Bratkovic, 2017). Among the misfolded proteins, one sticks out and deserves special attention. A misfolded protein gone rogue is the "prion" protein whose misfunction is associated with a variety of animal and human prion diseases (Mead et al., 2003). The misfolded prion protein is known to spread throughout the brain by converting the "normal" prion protein into the "misfolded" state. Despite significant advances, several key questions remain unanswered, including the function of the prion protein, molecular mechanisms of infection and cellular impairment, and the structure and replication mechanism of prions. Thus, no successful treatment exists yet and therefore prion diseases remain invariably fatal neurodegenerative diseases (Aguzzi & Zhu, 2012).

1.2 THE CELLULAR PRION PROTEIN

The cellular prion protein (PrP^C) is a cell surface glycoprotein expressed in various organs and tissues, with the central nervous systems having the highest levels of expression. The whole protein-coding open-reading frame in mice is encoded by the third exon of the *PRNP* gene, which is located on chromosome 20 in humans (chromosome 2 in mice). The human prion protein is translated as 253 amino acids long that undergoes several post-translational modifications (Oesch et al., 1985; Westaway et al., 1994). During protein processing in the ER, the 22-amino acid long N-terminal ER-targeting signal sequence (residues 1-22) and the 23-amino acid GPI-anchoring sequence at the C-terminal (residues 231-253) are removed, yielding a mature human prion protein of 208 amino acids (Stahl, Borchelt, Hsiao, & Prusiner, 1987) (Figure 1-1.A). The length of the PrP polypeptide chain varies depending on the species however, the primary structure of PrP^C remains highly conserved among mammalian species (Wulf, Senatore, & Aguzzi, 2017).

PrP^C adopts its physiological structure after translation and co-translational extrusion into the endoplasmic reticulum lumen, with an N-terminal flexible tail and a C-terminal globular domain (Riek, Hornemann, Wider, Glockshuber, & Wuthrich, 1997). The N-terminal flexible tail consists of two charged clusters (CC1 and CC2), an octarepeat region (OR), and a hydrophobic region (HR) make up the N-terminal tail. Furthermore, two N-glycosylation sites are found in the globular domain, N181 and N197 at the C-terminus, upstream of the sialylated GPI-anchor (Aguzzi, Baumann, & Bremer, 2008) (Figure 1-1.A). The globular domain of the prion protein contains three α -helices and two antiparallel β -strands (Figure 1-1.B) (Stevens et al., 2009). PrP^C is found extracellularly in lipid rafts after being transported to the cell membrane, where it is

at the C-terminus of PrP protein. **(B)** Schematic representation of membrane-bound PrP^C consisting of N-terminal unstructured region and the ordered C-terminal domain determined by solution NMR is shown (Stevens et al., 2009). The C-terminal domain consists of three α -helices, shown in red, and two β -strands shown in yellow whereas the N-terminal domain has been added on in a “random” configuration and Cu²⁺ (blue) binding sites are shown at the octapeptide repeat region.

1.3 THE DISEASE-CAUSING AGENT PRP^{Sc}

According to the protein-only hypothesis, the infectious agent that causes transmissible spongiform encephalopathies (TSE) is made up entirely of protein and lacks any informative nucleic acids (Prusiner et al., 1982). Dr. Stanley Prusiner coined the term "prion" – small proteinaceous infectious particles as the pathogenic agent, PrP^{Sc} (Prusiner, 1982).

Studies supporting the theory that PrP^{Sc} is devoid of nucleic acids emerged when prions showed to be resistant to a variety of nucleic acid-damaging treatments, but they were easily inactivated by protein-denaturing agents (Prusiner, 1982; Prusiner et al., 1980). The infectious, proteinaceous amyloid or prions from a scrapie-infected hamster brain were successfully purified using sucrose gradient-based ultracentrifugation in the early 1980s, validating the protein-only hypothesis (Bolton, McKinley, & Prusiner, 1982; Prusiner et al., 1983). Furthermore, the purified scrapie-infected hamster prions were resistant to the proteinase-K (PK) digestion resulting in a PK-resistant N-terminally truncated resistant core (~90-231) (Figure 1-2.B), yielding a 27-30 kDa (PrP²⁷⁻³⁰) resistant protein in SDS-PAGE, unlike a similar fraction from an uninfected brain (Bolton et al., 1982). The PK-treated PrP²⁷⁻³⁰ (PrP^{Sc}) usually forms three bands in Western blot analysis, corresponding to the un-, mono-, and di-glycosylated isoforms of

the prion protein (Figure 1-2.D) (Weissmann, 2004). Antibodies against PrP²⁷⁻³⁰ reacted with proteins with molecular weights of 33-35 kDa in crude extracts from scrapie-infected and control brains (Prusiner et al., 1993).

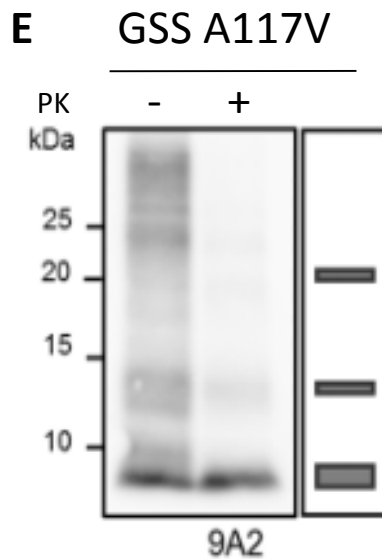
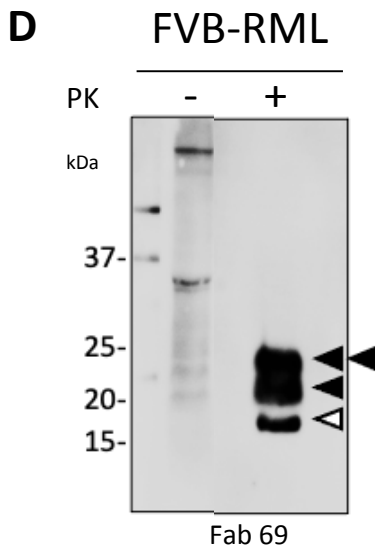
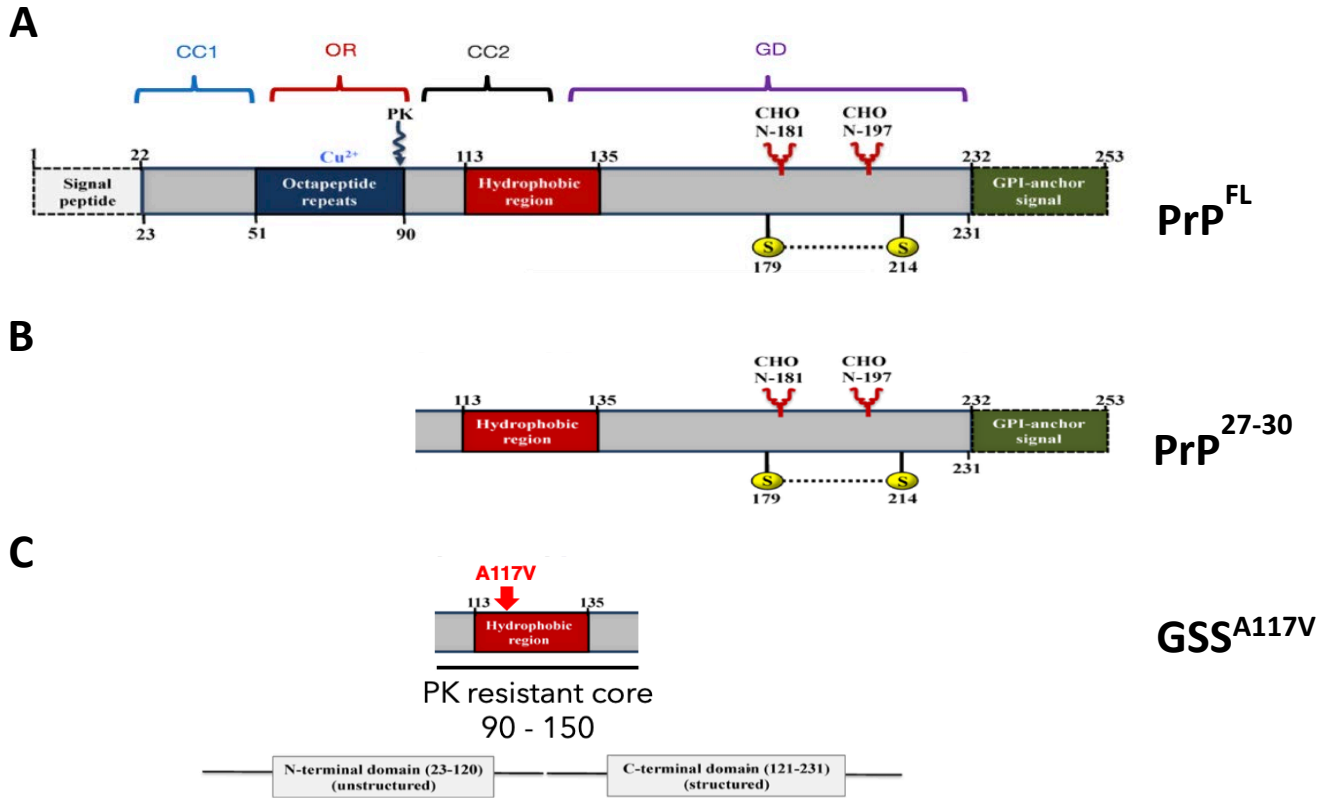


Figure 1-2: Proteinase-resistant PrP^{Sc} fragment (PrP^{res}) of sporadic and genetic prions.

Schematic representation of approximate cleavage sites for (A-C) classical/sporadic human prions and genetic prion diseases. Shown are approximate protease-resistant cores for classical and genetic human prions based on the PE and PK-cleavage sites and immunoreactivity with different anti-prion antibodies. (A) Treatment with Pronase-E (PE), digests the cellular prion protein and other endogenous proteins keeping the full-length PrP^{Sc} (PrP^{FL}) intact, spanning from residues ~23-231. (B) After PK treatment for sporadic prion diseases, the N-terminal domain is completely digested by the enzyme leaving the protease-resistant core intact spanning from residues ~90-231 (PrP²⁷⁻³⁰). (C) Genetic prions, such as GSS prions, have a unique PK-resistant PrP fragment spanning from residues 90-150 (GSS^{A117V}), devoid of the N- and C-terminus of the prion protein. (D-E) Western blot analysis of classical and atypical prions. PK-treated brain homogenates of (D) FVB-RML prions using anti-PrP Fab 69 antibody revealed 3 characteristic bands corresponding to un-, mono-, and di-glycosylated PrP²⁷⁻³⁰ as indicated by the unfilled and filled arrows, respectively. (E) The A117V-GSS human prions detected using a 9A2 monoclonal antibody, that recognizes the central region of PrP revealed a characteristic un-glycosylated band of the 7kDa PrP^{res} fragment (Vanni et al., 2020).

1.3.1 In-vivo and in-vitro generation of infectious PrP^{Sc}

The protein-only hypothesis is now largely accepted, and prions, which cause prion diseases, are viewed as infectious, misfolded proteins with no genetic material. Many studies have been formed after the generation of infectious *de novo* prions *in vivo* and *in vitro* to support the protein-only hypothesis (Castilla, Saa, Hetz, & Soto, 2005; Legname et al., 2004). The first approach used a method called PMCA (protein misfolding cyclic amplification), in which PrP^{res} can be amplified by incubating and sonicating PrP^{res}-containing brain homogenate diluted in uninfected brain homogenate as PrP^C substrate (Castilla et al., 2005; Saborio, Permanne, & Soto,

2001). Furthermore, Soto and colleagues used PMCA in serial dilutions to amplify PrP^{res} produced from scrapie-infected hamsters indefinitely. PrP^{res} amplification was accompanied by an increase in the infectivity (Barria, Mukherjee, Gonzalez-Romero, Morales, & Soto, 2009; Deleault, Harris, Rees, & Supattapone, 2007). For a long time, all attempts to employ recombinant PrP as a substrate for PMCA failed.

However, Caughey and colleagues successfully described the use of bacterially expressed hamster PrP as a substrate in generating amyloid fibrils *in vitro*, through another approach now known as RT-QuIC (Real-time quaking-induced conversion) (Orru, Favole, et al., 2015; Orru, Groveman, et al., 2015). This approach utilizes a dye, Thioflavin T that fluoresces when bound to amyloid and the fluorescence increases over the course of many intermittent shaking rounds in RT-QuIC to detect the amyloid formation. These assays exploit the fundamental self-propagating activity of prions to amplify the presence of prion seeds by as much as a trillion-fold (B. Caughey et al., 2017).

A second strategy involves creating infectivity by misfolding synthetic PrP peptides and subsequently inoculating wild-type animals. A 55-residue peptide encompassing the GSS mutation P101L was refolded *in vitro* to a beta-sheet-rich peptide and could induce disease similar to GSS in transgenic mice expressing PrP in one attempt (P101L) (Kaneko et al., 1995; H. Zhang et al., 1995). Later, an in-vitro generated misfolded portion of the prion protein (amino acid residues 89-231) was transmitted to wild-type mice. Legname and colleagues purified recombinant PrP (89-231) which subsequently formed amyloid fibrils in-vitro. These fibrils caused prion disease in transgenic mice overexpressing PrP (89-231) (Legname et al., 2004).

1.4 PRION STRAINS

Prion pathology is caused by misfolding of PrP^C into an aggregation-prone and β -sheet rich form, PrP^{Sc}. Although the host genome encodes PrP^C, prions themselves encode several phenotypic prion variants known as prion strains (Weissmann, 1991). Prion strains are infectious isolates that demonstrate diverse prion-disease phenotypes when transmitted to identical hosts. The phenotypic traits may include duration in incubation time, histological lesion profiles, and specific neuronal target locations are examples of phenotypic features (Nonno et al., 2006). Studies have shown that the molecular basis of prion strains lies in the distinct conformation of PrP^{Sc} molecules and moreover, each conformation exhibits different biochemical and structural properties; for example, the differences in the relative abundance of the main glycosylated moieties and the size of proteinase-K digested PrP^{Sc} can be used to identify prion strains (Vanni et al., 2020). The biochemical manifestation such as the glycopattern of each strain is sometimes determined by the incoming infectious agent's characteristics (Aguzzi, Heikenwalder, & Polymenidou, 2007).

1.5 SPECIES BARRIER

The presence of distinct prion strains and differences in PrP sequences among mammals creates a species barrier (also a transmission barrier). It was discovered that prions generally transmit far more efficiently within species when the donor and host's primary structures are identical, and prion transmission could be impeded due to the difference in primary structure (Aguzzi et al.,

2007). For example, the transmission of mouse-adapted scrapie in mice was relatively efficient, however, transmission to hamsters and rats required a prolonged incubation period, which was attributed to the "species barrier" (Kimberlin, Cole, & Walker, 1987).

However, the species barrier, cannot be explained solely by discrepancies in PrP amino acid sequences. Despite the fact that prions produced from patients with sporadic CJD and vCJD are typically made of PrP^{Sc} with the human amino acid sequence, sporadic CJD prion was barely transmissible to inbred FVB mice, whereas vCJD prion was (Hill, Desbruslais, et al., 1997).

Interestingly, host species capable of overcoming transmission barriers and proliferating diverse prion strains, such as bank voles, have been reported. Bank voles are regarded as a "universal host," and bank vole PrP is regarded as a universal acceptor of most prions, including human CJD, BSE, scrapie, and CWD (Watts et al., 2014).

According to these studies, the species barrier is directly related to the properties of prion strains, and strains should be defined by specific conformations of PrP^C or conformations of PrP^{Sc} aggregates. It is still unclear how conformational features contribute to the species barrier, but new structural investigations have revealed intriguing insights.

1.6 PRION DISEASES

Prion diseases are rare, progressive transmissible spongiform encephalopathies (TSEs) characterized by a unique spongiform appearance in the brain, caused by neuronal death and gliosis. Mammalian prion diseases, unlike other neurodegenerative diseases, affect both animals and humans and are invariably fatal (Prusiner, 1982, 1998b). Naturally occurring prion diseases

in animals include scrapie in sheep and goats, bovine spongiform encephalopathy (BSE) in cattle, chronic wasting disease (CWD) in cervids, and transmissible mink encephalopathy (TME) in mink (Houston & Andreoletti, 2019). Recently, camel prion disease (CPD) was discovered in the dromedary camels (Babelhadj et al., 2018).

Human prion disease can cause Creutzfeldt-Jakob disease (CJD), which can be 85-90% of the time sporadic (sCJD), 10-15% of the time genetic, or <1% of the cases are acquired (Collinge, 2001). The most common type of CJD is sCJD. Gerstmann-Strausler-Scheinker (GSS), familial CJD (fCJD), and fatal familial insomnia (FFI) are all inherited types of human prion diseases (K. Brown & Mastrianni, 2010; Collinge, 2001). Exogenous infection from TSE-contaminated tissues and substances causes acquired prion disorders. Kuru, iatrogenic CJD (iCJD), and variant CJD (vCJD) are a few instances (Chen & Dong, 2016).

1.7 PRION DISEASES IN ANIMALS

Animal prion diseases have been reported since 1732 when scrapie was diagnosed in a merino sheep in Spain, and subsequently, it was thoroughly analyzed in sheep from Great Britain.

Scrapie-like diseases in mink and deer were identified in North America during the 1960s and were later recognized as transmissible mink encephalopathy (TME) and chronic wasting disease (CWD), respectively. However, it wasn't until 1986 that animal prion diseases became increasingly prevalent. It was the first report of a scrapie-like illness afflicting cattle that year.

That new disease was known as BSE (Wells et al., 1987), and its impact was greater than that of other prion diseases due to the economic importance of cattle. When BSE was linked to a type of

CJD in humans known as variant-CJD (vCJD) and was thus classified as a zoonosis in 1996, interest in these diseases skyrocketed (Bruce et al., 1997; Will et al., 1996). Due to the risk to both animals and humans, strong measures to limit BSE transmission were successfully implemented, and the incidence of new cases has dropped drastically in recent years. CWD has now become the most concerning animal prion disease since it has been demonstrated to be sustained in wildlife animals and has spread across broad areas. Initially limited to a few states in the United States of America (USA) and Canada, CWD cases have lately been discovered in other parts of both nations as well as in Norway, Sweden, Finland and South Korea (Rivera, Brandt, Novakofski, & Mateus-Pinilla, 2019).

1.7.1 Scrapie

The transmissible nature of scrapie has been proposed since the 1800s affecting sheep and goats. Clinical signs vary between groups and include behavioural problems, visual impairment, ataxia, uncoordinated movement, hyperexcitability, itching, and tremors. The neuropathological profile in the brain is presented as spongiform lesions, gliosis, and PrP^{Sc} deposition.

The exact natural route of infection is unknown, however, it is agreed that horizontal transmission occurs. Following the oral route, it was discovered that PrP^{Sc} is deposited in lymphoid tissue such as Peyer's patches, mesenteric lymph nodes, and gut-associated lymphoid tissue (GALT) after entering (Andreoletti et al., 2000). The agent then spreads to the enteric nervous system, which is part of the peripheral nervous system (PNS) (McBride et al., 2001). Scrapie, like other transmissible diseases, could be spread through sources of environmental

contamination. Affected individuals' secretions and excretions may contribute to horizontal transmission. PrP^{Sc} was found in the feces of sheep infected with scrapie in both preclinical and clinical stages (L. A. Terry et al., 2011). Another mode of scrapie in goat and sheep herds appears through vertical transmission. Scrapie is more common in the offspring of naturally infected ewes (Hoinville, Tongue, & Wilesmith, 2010), albeit this could be due to a variety of transmission mechanisms.

Aside from classical scrapie, atypical scrapie has also been reported. Nor98, for example, was first detected in Norwegian sheep and had different biological features than conventional scrapie in terms of clinical symptoms, PK sensitivity of PrP^{Sc}, banding profile in SDS-PAGE, and neuropathology (Detwiler, 1992).

1.7.2 Bovine spongiform encephalopathy (BSE)

Bovine spongiform encephalopathy (BSE), colloquially known as “mad cow disease” was first discovered in the United Kingdom in the 1980s (Wells et al., 1987). The first case of classical BSE (C-BSE) was reported in 1986 (Wells et al., 1987), and its transmissibility was confirmed two years later through inoculation in mice (Fraser et al., 1988). The incidence of BSE was shown to be higher in dairy herds than in beef herds, which could be due to differences in feeding practices between the two production systems (Bradley, 1991; Wilesmith et al., 1992).

The clinical presentation of C-BSE includes tremors, gait abnormalities in the hind limb, ataxia, aggressiveness, apprehension, and hypersensitivity to stimuli. BSE has an incubation period of

two to eight years, with the majority of cases being detected in dairy animals aged four to five years (Mitra et al., 2009).

Based on these epidemiological findings and the lack of direct horizontal transmission, it was determined that the primary source of BSE infection was the meat and bone meal (MBM) provided to the cattle (Anderson et al., 1996). This observation led to the prohibition of feeding ruminant proteins to cattle in various nations. The pathogenesis of BSE via the oral route is comparable to scrapie in the early stages. PrP^{BSE} is first found in Peyer's patches, GALT, and tonsils before being transported to the CNS via the PNS (Terry et al., 2003; Wells et al., 2005; Hoffmann et al., 2007, 2011). Except for those already mentioned, the fundamental difference between BSE and scrapie is that individuals with BSE have little or no dispersion of prions in lymphoid tissue and as consequence, there is no shedding.

In 2004, cases of BSE detected in Italy and France showed differences from the typical cases. After digestion with proteases, the isolated prions revealed pieces of peptides with varying molecular weights. The one containing an unglycosylated fragment of higher molecular mass than previous cases of BSE was named H-BSE, while the other with a lower molecular mass was named L-BSE. The neurological hallmark of L-type BSE is the formation of amyloid plaques in the brain; this condition is also known as bovine amyloidotic spongiform encephalopathy (BASE). A substantial amount of PrP-positive amyloid plaques associated with L-type BSE have been found in the thalamus, subcortical white matter, and olfactory bulb, which are histopathological characteristics of the BASE (Kamali-Jamil et al., 2021).

Unlike the classical form of these diseases, atypical BSE typically affects aged animals and has a scattered distribution and low incidence (P. Brown, McShane, Zanusso, & Detwile, 2006; Sala et

al., 2012). To date, the specific characteristics and genesis of atypical BSE strains are unknown, and it is speculated that they may have first appeared in cattle intermittently, similar to sporadic CJD (sCJD) in people (Costassa et al., 2016).

1.7.3 Chronic wasting disease (CWD)

Since the late 1960s, CWD has been recognized as a syndrome affecting captive mule deer and white-tailed deer. CWD was classified as a spongiform encephalopathy clinically and pathologically in 1980 (Williams & Young, 1980). The first case of CWD was described in a captive mule deer in Colorado in 1967 when the animal developed a wasting disease with progressive neurological dysfunction. More than ten years later, in 1978, a neuropathological examination of the affected animal's brain by the late Elizabeth Williams established CWD to be a TSE in the cervids (Williams & Young, 1980). CWD has become endemic to both captive and free-ranging cervid species in North America, including mule deer, white-tailed deer, moose, and elk; it has impacted animals in 30 states in the United States and 4 provinces in Canada (Baeten, Powers, Jewell, Spraker, & Miller, 2007; Spraker et al., 1997). To date, no CWD cases have been reported in free-roaming caribou in Canada.

Based on other animal prion diseases, it is assumed that the major route of entry for PrP^{CWD} is oral, which has been experimentally accomplished in numerous cervid species (Kreeger, Montgomery, Jewell, Schultz, & Williams, 2006; Mitchell et al., 2012; Sigurdson et al., 1999). The etiology and tissue distribution of PrP^{CWD} appear to be comparable to that observed in scrapie-infected sheep. The pathogen first appears in lymphoid tissue, then spreads to the CNS,

PNS, and other organs (Sigurdson et al., 2002; Sigurdson, Spraker, Miller, Oesch, & Hoover, 2001; Sigurdson et al., 1999). However, unlike in scrapie-infected sheep, PrP^{CWD} accumulation was larger in retropharyngeal lymph nodes than in CWD-infected deer Peyer's patches (Fox, Jewell, Williams, & Miller, 2006; Sigurdson et al., 1999).

It was discovered in 2004 that susceptible animals (mule deer) could get CWD after being exposed to contaminated environments or infected animals (M. W. Miller & Wild, 2004). This investigation has looked into saliva, urine, and feces as potential sources of natural infection. Oral delivery of infected animal saliva to healthy deer that acquired CWD after exposure confirmed the infectivity of the infected animal saliva (Mathiason et al., 2009; Mathiason et al., 2006).

There is significant concern about the risk of CWD prion transmission to humans; nevertheless, there has been no report of CWD's association with prion diseases in humans. Under experimental conditions, CWD has been transmitted to humanized mice (Hannaoui et al., 2022). CWD has been demonstrated to be transmissible in laboratory mice, cattle, mink, squirrels, monkeys, cats, sheep, and goats (Bartz, Marsh, McKenzie, & Aiken, 1998).

1.8 PRION DISEASES IN HUMANS

CJD was first described in 1920 and 1921 by neurologist Hans Gerhard Creutzfeldt and neuropathologist Alfons Maria Jakob, who characterized a "nosologically extremely closely associated if not identical disease" in multiple individuals (Creutzfeldt, 1989). Kuru received attention in the first half of the twentieth century after being described among cannibalistic tribes

in Papua New Guinea; the disease is now considered extinct (Liberski, 2013). The most recent form of TSE, variant CJD (vCJD), was initially diagnosed in 1996 in the United Kingdom (Hill, Zeidler, Ironside, & Collinge, 1997; Will et al., 1996), which continues to have the most cases (178) out of a total of 232 worldwide (Ritchie, Peden, & Barria, 2021). Human prion diseases are rare in comparison to other infectious diseases, with a disease incidence of about 1.5 per million people per year (Jankovska et al., 2021). sCJD is the most frequent human prion disease (85-90% of cases). Around 10-15% of cases are genetic (including fCJD, FFI, and GSS), whereas the acquired type (iCJD and vCJD) accounts for <1% of all cases (Jankovska et al., 2021).

1.8.1 Sporadic human prion diseases

Sporadic prion diseases, which include Creutzfeldt-Jakob disease (CJD) and fatal sporadic insomnia, are more common in humans than hereditary and acquired variants (FFI) (Sikorska, Knight, Ironside, & Liberski, 2012). In approximately 85% of CJD cases, a sporadic conversion of physiological PrP^C to pathologic misfolded PrP^{Sc} occurs. The global incidence of sCJD is estimated to be one to two cases per million people (Uttley, Carroll, Wong, Hilton, & Stevenson, 2020). In contrast to vCJD, clinical symptoms and neuropathological findings vary from case to case, which is likely due to distinct molecular phenotypes (Manix et al., 2015). The disease normally lasts a few months, no more than a year. The disease must last less than two years; longer durations cases represent atypical prion diseases (Manix et al., 2015).

1.8.2 Inherited human prion diseases

Gerstmann, Strüssler, and Scheinker described GSS, a familial disease with autosomal dominant inheritance, in 1936 (Kalman et al., 1997). Since then, the term GSS has been used to represent a diverse set of neurodegenerative illnesses with a familial origin, infrequent myoclonus and diagnostic EEG, and a neuropathologic hallmark of many amyloid plaques. GSS is typically characterized by cerebellar ataxia and slowly progressive dementia (Galatioto, Ruggeri, & Gullotta, 1995), but extrapyramidal symptoms, visual and hearing impairment, myoclonus, spastic paraparesis, and hyporeflexia or areflexia in the lower extremities have also been reported as prevalent symptoms. GSS is a genetic prion disease associated with *PRNP* mutations such as proline (P) to leucine (L) substitution at codon 102 (P102L), alanine (A) to valine (V) substitution at 117 (A117V), and phenylalanine (F) to serine (S) substitution codon 198 (F198S), and mainly presents as a slow progressive disease with ataxia and motor dysfunction (K. Brown & Mastrianni, 2010; Ghetti et al., 1995).

GSS typically contains a 7-8 kDa protease-resistant fragment (PrP^{res}), which is N- and C-terminally truncated, spanning from residues 90-150 (Figure 1-2.C,E) (Vanni et al., 2020).

Among other inherited prion diseases, fatal familial insomnia (FFI) was coined in 1986 by Lugaresi and colleagues to describe a 52-year-old man who came with worsening sleeplessness and autonomic dysfunction, followed by dysarthria, tremor, and myoclonus; the patient's two sisters and many other relatives had died of a similar disease across three generations (Lugaresi et al., 1986). FFI is an autosomal dominant genetic condition caused by the D178N mutation in the *PRNP* gene, which is linked to the existence of the MM polymorphism at codon 129 (Medori

et al., 1992). The average survival time after the initiation of the clinical symptoms is 18 months (Gambetti, Parchi, Petersen, Chen, & Lugaresi, 1995).

1.8.3 Acquired human prion diseases

Following exposure to infectious resources, acquired forms of prion disease may occur. Human acquired prion diseases include kuru, iatrogenic CJD, and vCJD.

The UK government's expert advisory group announced on March 20, 1996, that the agent causing BSE may have transferred to humans, based on the identification of 10 people with a newly recognized variant form of CJD (Collinge, Sidle, Meads, Ironside, & Hill, 1996). Variant CJD (vCJD) is associated with the consumption of BSE-agent contaminated foods. The clinical presentation begins with psychiatric and behavioural symptoms, as well as severe paresthesia or dysesthesia, and progresses to ataxia and dementia (Bonda et al., 2016).

Following mouse transmission experiments, the lesion profiles in the mouse brain generated by vCJD prions were similar to those caused by BSE prions but distinct from those induced by sCJD prions, demonstrating that the vCJD and BSE prions were a single strain (Bruce et al., 1997). The polymorphism at codon 129 in the human PRNP gene is shown to have a significant role in vCJD susceptibility; until now, all vCJD patients had homozygous Met at codon 129, save for two heterozygous cases, implying a partial protective impact of valine on the BSE prions (Collinge, Palmer, & Dryden, 1991). Furthermore, acquired cases of vCJD reported as a result of blood transfusions from preclinical vCJD-infected donors, as well as surveillance data

identifying latent vCJD in some people in the UK, have posed a substantial public health risk (Peden, Head, Ritchie, Bell, & Ironside, 2004).

The iatrogenic variant occurs when pathologically misfolded prions are transferred during medical or surgical operations. Iatrogenic CJD is highly uncommon, accounting for fewer than 1% of all cases in CJD (Will, 2003). However, no reports of individual transmission of the CJD agent were published until 1974, when Duffy and colleagues described a 55-year-old patient who got CJD 18 months after getting a corneal transplant from a CJD donor (Duffy et al., 1974). More reports of iatrogenic CJD variant from human growth hormone, dura mater graft and the use of contaminated EEG depth electrodes have been reported (P. Brown et al., 2006).

Kuru is another acquired form of human prion disease that was discovered in the late 1950s in the Fore population of Papua New Guinea's Eastern Highlands and neighbouring linguistic groups for practising ritualistic cannibalism (eating the brains of dead relatives) (Collinge et al., 2006). Kuru was the first human prion disease shown to be transmitted to chimpanzees and later into rodent models and revealed that the strain characteristics of Kuru prions were similar to typical sCJD (Gajdusek, Gibbs, & Alpers, 1966; Wadsworth et al., 2008). The Kuru cases decreased after the cease of the act of endocannibalism in 1956 and no Kuru patient was born after that. The incubation period of Kuru was suggested to be more than 50 years (Collinge et al., 2006).

1.9 STRUCTURES OF THE INFECTIOUS PRP^{Sc}

The infectious prion protein, termed PrP^{Sc}, has the ability to convert native PrP^C into a copy of

itself, adopting a non-native conformation that has the propensity to self-assemble into amyloid fibrils (H. Wille & J. Requena, 2018). The main features that distinguish PrP^{Sc} from PrP^C are its high content in the β -structure (B. W. Caughey et al., 1991), its partial resistance to proteases (Prusiner et al., 1982), its insolubility, and its propensity to aggregate into amyloid fibrils and other quaternary structures, which accumulate over time, resulting in brain cell and tissue damage (Vazquez-Fernandez et al., 2016). Based on its structural properties, PrP^{Sc} differs in a number of epitopes from those that are recognized by antibodies targeting PrP^C (Horiuchi et al., 2009). Over the years, many structural models for PrP^{Sc} have been proposed; however, the most prominent ones are the β -solenoid (Govaerts, Wille, Prusiner, & Cohen, 2004), the β -spiral (DeMarco & Daggett, 2004), and the parallel in-register β -sheet models (Cobb, Sonnichsen, McHaourab, & Surewicz, 2007). The insoluble nature and the propensity of PrP^{Sc} to aggregate make it difficult to determine its structure. Hence, the high-resolution structure of PrP^{Sc} has long been elusive. Although efforts have been made to gain insights by combining techniques, such as X-ray fiber diffraction (Wille, Bian, et al., 2009), electron microscopy (EM) (Wille et al., 2002), and limited proteolysis using proteinase K (Vazquez-Fernandez et al., 2012). Together, these data indicate that due to the heterogeneity of various folds adopted by PrP^{Sc}, it has two defined structures which are a β -solenoid fold, consisting of 4-stacked β -rungs or possible two-stacked β -rungs (Vazquez-Fernandez et al., 2016; Wille, Bian, et al., 2009) and parallel in-register intermolecular β -sheet structure (PIRIBS) (B. Caughey, Standke, Artikis, Hoyt, & Kraus, 2022).

1.9.1 Four-rung beta solenoid model (4R β S)

β -solenoid proteins are characterized by a polypeptide chain that folds into more or less regular

“solenoidal windings”, while the canonical β -helical proteins follow a more stringent helical geometry (Kajava & Steven, 2006a). β -solenoid proteins contain between two to well above 100 β -rungs (Kajava & Steven, 2006b; Wasmer et al., 2008). Each β -rung contains two to four β -strands and they are connected by tight turns, β -arcs (two to six residues), or longer loops. Overall, the β -rungs have a length of between 12 and 30 amino acids. A β -rung corresponds to a complete turn of the amino acid backbone to where the next β -rung begins with an axial rise of $4.8 \pm 0.2 \text{ \AA}$ (Kajava, Baxa, & Steven, 2010; Kajava & Steven, 2006a).

The first suggestive β -solenoidal model was reported based on the results of the TEM examination of 2D crystals of brain-derived PrP27-30 (Wille et al., 2002). Fourier-transform infrared (FTIR) spectroscopy provided the first experimental evidence that the N-terminally truncated PrP27-30 contains predominantly β -structure (B. W. Caughey et al., 1991; Pan et al., 1993). Electron crystallography analyses on 2D crystals of PrP27-30 and an engineered variant of only 106 residues, PrP^{Sc}106, suggested the presence of a β -solenoid fold as a key feature of the infectious conformer (Govaerts et al., 2004; Wille et al., 2002). Subsequently, X-ray fiber diffraction determined the molecular height of PrP27-30 in amyloid fibrils to be 19.2 \AA , corresponding to the height of 4 β -strands ($19.2 \text{ \AA} = 4 \times 4.8 \text{ \AA}$) (Wille, Bian, et al., 2009). In addition, the diffraction data confirmed that the core of PrP27-30 adopts a β -solenoid fold, consisting of 4-stacked β -rungs (Figure 1-3.A). The repeating unit size of 19.2 \AA was also found in the diffraction patterns that were obtained from the PrP^{Sc}106 amyloid fibrils (Figure 1-3.B) (Wan et al., 2015). Recently, cryo-EM and subsequent three-dimensional (3D) reconstructions demonstrated that PrP27-30 amyloid fibrils can be formed by two intertwined protofilaments. Furthermore, the low-resolution negative stain-EM and cryo-EM analysis corroborated that the structure of brain-derived PrP27-30 of BSE-L type and GPI-anchorless RML prion fibrils

consists of a 4-rung β -solenoid architecture (Kamali-Jamil et al., 2021; Vazquez-Fernandez et al., 2016).

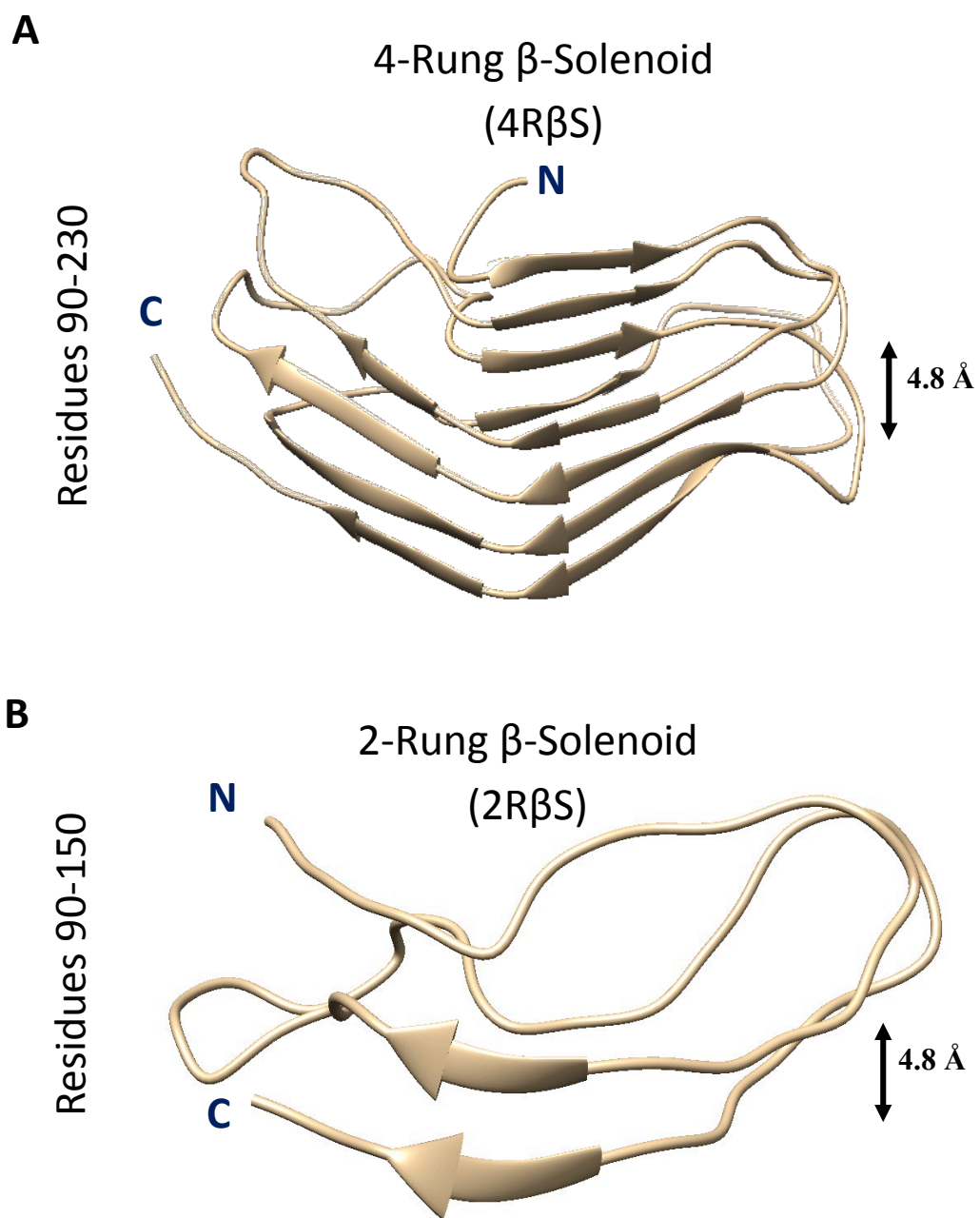


Figure 1-3: 4R β S and 2R β S model of PK-resistant PrP^{Sc}.

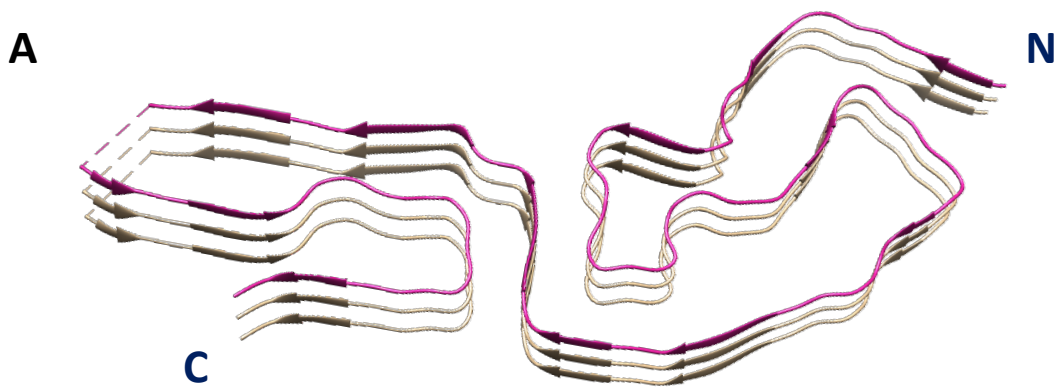
(A) A proposed model of a monomeric subunit within a 4-rung β -solenoid architecture of anchorless RML prion. Spacing across the beta-strand is 4.8 Å and each monomeric subunit of a 4R β S model spans 19.2 Å along the fibril axis (Spagnolli et al., 2019). (B) Molecular dynamic simulation model of the 7kDa A117V-GSS peptide spanning from residues 89-149 forming a 2-rung β -solenoid architecture. The 4.8 Å distance between beta-strands arranged perpendicular to the fibril axis, and the 8.4 Å height of an individual 7kDa PrP is indicated.

1.9.2 Parallel in-register intermolecular beta-sheet structure

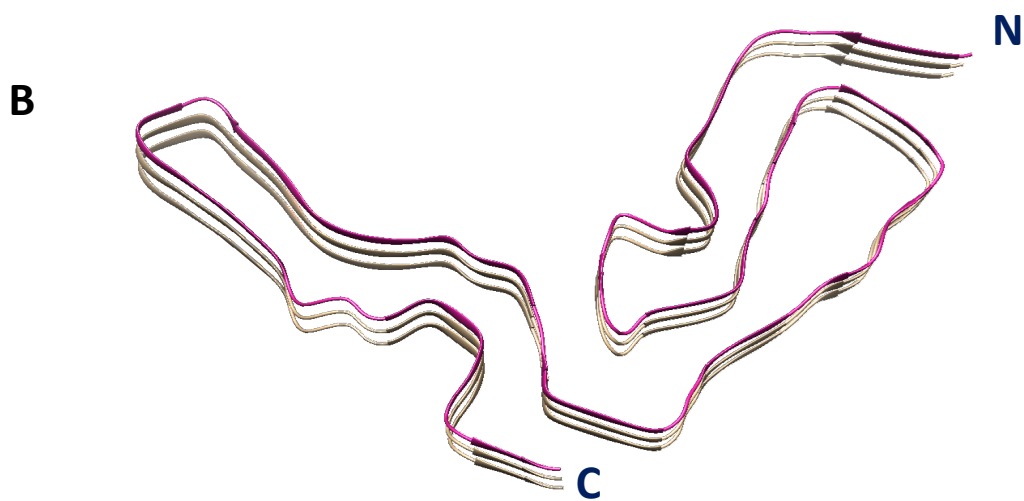
(PIRIBS)

First, ground-breaking electron paramagnetic resonance (EPR) and solid-state NMR (ssNMR) studies of the protease-resistant cores of synthetic recombinant PrP fibrils showed that different recombinant PrP molecules can produce fibrils in which the monomers are stacked parallel and in-register, that is, with the corresponding residues of one monomer aligned immediately adjacent to the corresponding residues of the adjacent monomers (Cobb et al., 2007; Groveman et al., 2014; Tycko, Savtchenko, Ostapchenko, Makarava, & Baskakov, 2010). These proposed structures are consistent with recently reported high-resolution cryo-EM structures of brain-derived hamster 263K prion, a fully infectious *ex vivo* prion, to have the first high-resolution structure (Figure 1-4.A) (Kraus et al., 2021). Since then, the structures of the GPI-deficient (anchorless) (Hoyt et al., 2022) and WT forms of different scrapie prion strains including RML (Figure 1-4.B), ME7 and 22L have also been reported by Manka et al. (Szymon W. Manka et al., 2022a; S. W. Manka, W. Zhang, et al., 2022b). All of these rodent-adapted prions revealed a PIRIBS structures (B. Caughey et al., 2022; Manka, Wenborn, Collinge, & Wadsworth, 2022).

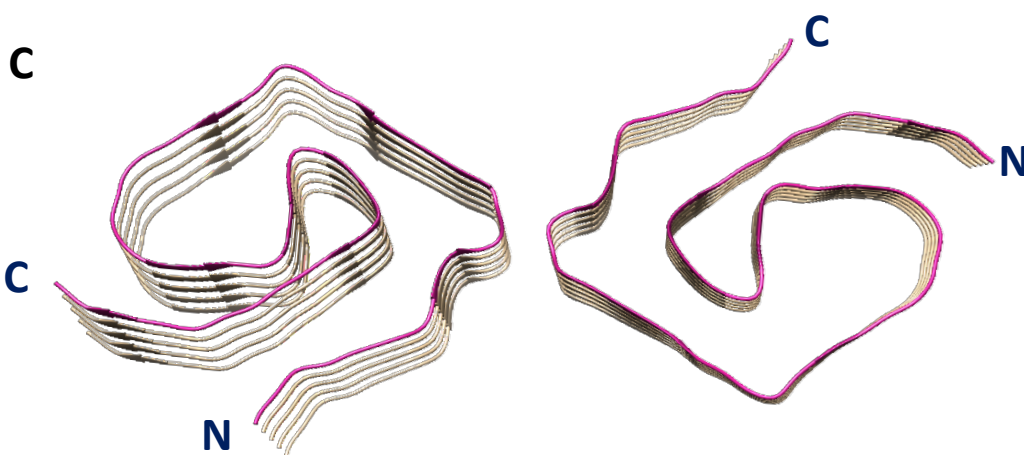
High-resolution structural studies of ex vivo prions and alternative PrP amyloids from the human brain have been extremely difficult to date; nevertheless, cryo-EM structures of prion protein filaments from Gerstmann-Sträussler-Scheinker disease associated with mutation of phenylalanine to serine at *PRNP* position 198 (F198S) have recently been reported to reveal PIRIBS conformation as well (Fig. 1-4.C) (Hallinan et al., 2022).



263K PIRIBS Structure (2021)



RML PIRIBS Structure (2022)



GSS^{F198S} PIRIBS Structure (2022)

Figure 1-4: Recent Cryo-EM PIRIBS structure of PK-resistant PrP^{Sc}.

A monomeric subunit of (A) hamster 263K prions, PDB access code: 7LNA (Kraus et al., 2021) (B) RML prion, PDB access code: 7QIG (S. W. Manka, W. Zhang, et al., 2022), and (C) F198-GSS prion, PDB access code: 7UMQ (Hallinan et al., 2022) all reveal a high-resolution structure of a parallel in-register intermolecular beta-sheet (PIRIBS) or stack architecture. All three strains have a PIRIBS structure however their morphologies differ in the way the beta strands are arranged. (C) F198S-GSS fibrils revealed 2-4 intertwined protofilaments.

1.10 STRUCTURES OF OTHER PATHOGENIC PROTEINS

Recent insights into the structure of PrP^{Sc} have revealed similarities with the structures of pathogenic proteins adopting a parallel in-register β -sheet architecture. This means that each successive layer in the fibril consists of another protein molecule that stacks on top of the preceding one without substantial translation or rotation. These classes of pathogenic amyloids are, A β (1-42) fibrils, tau PHFs, and α -synuclein fibrils, which have been recently solved by cryo-EM with a high-resolution (Fitzpatrick et al., 2017; Yang, Arseni, et al., 2022a; Yang, Shi, et al., 2022b) provides novel insights into the folds of self-propagating amyloids that cause neurodegenerative diseases (Figure 1-5.A-C). However, in all three pathogenic fibrils, a staggered conformation of the subunits was observed in the structures determined by cryo-EM, which resulted in a slight tilt for each layer. In turn, this tilt imparted the fibrils with a 2₁ screw symmetry. The parallel in-register stacking of proteins renders these assemblies very sensitive to charge repulsion wherever charged amino acids are found unless salt bridges neutralize the charge imbalance. While these last three amyloids do not fall under the criteria of a β -solenoid,

they are similar enough to warrant a side-by-side comparison (Flores-Fernandez, Rathod, & Wille, 2018).

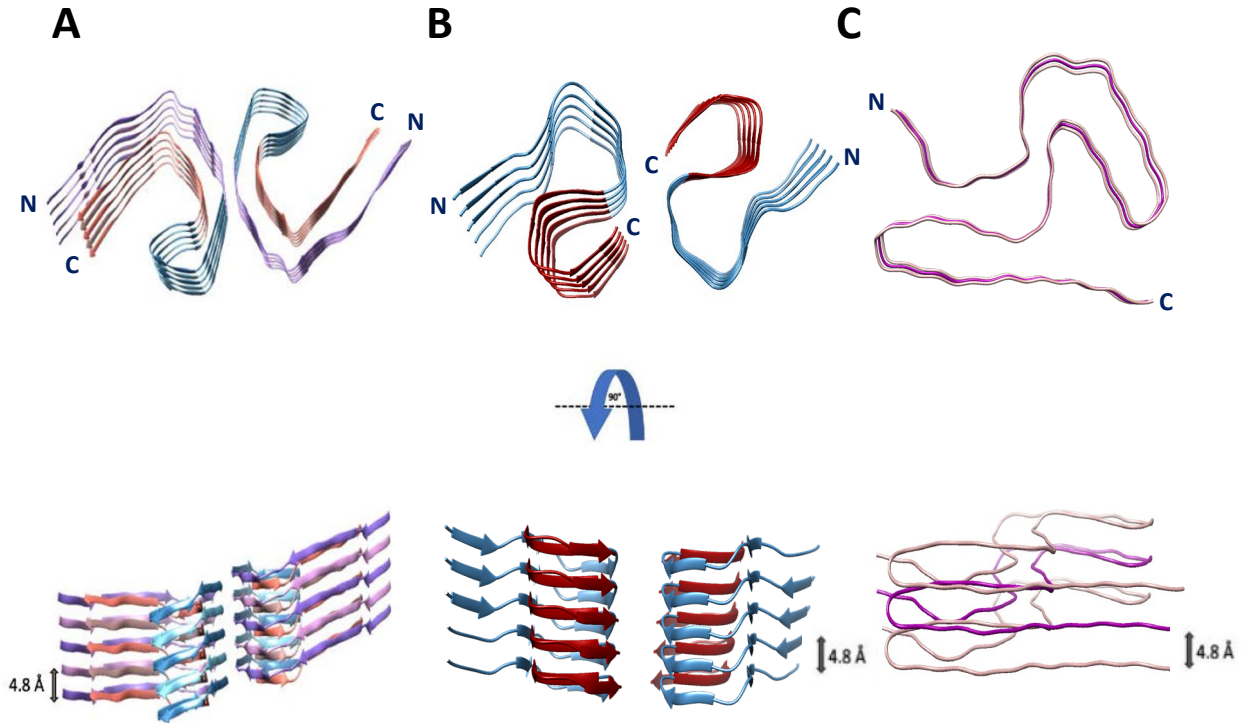


Figure 1-5: PIRIBS structure of other amyloidogenic proteins.

Structures of pathogenic amyloid fibrils **(A)** paired helical filament (PHF) of tau; **(B)** Aβ(1-42); and **(C)** α-synuclein. The fibril cores of these proteins are arranged as parallel in-register β-sheet structures, which are stabilized by hydrophobic interactions, salt bridges, and hydrogen bonds up and down the fibril axis. The axial distance between the stacked protein molecules is $4.8 \pm 0.2 \text{ \AA}$. **(A)** Top and side views of a high-resolution structure of PHFs obtained by cryo-EM. Five successive layers of the tau protein along the fibril axis revealed that the fibril core is composed of two C-shaped subunits (residues 306–378). PDB access code: 5O3L (Fitzpatrick A et al., 2017). **(B)** Top and side views of a high-resolution structure of an Aβ(1-42) fibril type II produced by cryo-EM. The LS-shaped cross-sections of each protofilament reveal a staggered stacking of molecules along the fibril axis. PDB access code: 7Q4M (Yang, Arseni, et al., 2022). **(C)** Top and side views of a high-resolution structure of human α-synuclein determined by cryo-EM. The fibril

core of α -synuclein contains a Greek key motif based on a parallel in-register β -sheet topology (residues 31–100). PDB access code: 8A9L (Yang, Shi, et al., 2022).

1.11 HUMAN IMMUNOGLOBULINS

Antibodies are the primary effector molecules of the immune system, and they are being used as biotherapeutic agents with great effectiveness. The production of an epitope-diverse polyclonal antibody mixture capable of neutralizing invading pathogens or disease-causing substances through binding interference and mediating humoral and cellular effector functions is an important aspect of the adaptive immune response (Oostindie, Lazar, Schuurman, & Parren, 2022). Due to their high specificity and affinity to bind an antigen, antibodies have also become important reagents in the life sciences.

1.11.1 Antibody architecture

Tiselius and Kabat discovered that antibodies were gamma-globulins in 1939 (Tiselius & Kabat, 1939). They were able to separate the various proteins present in serum using Tiselius' recently devised electrophoresis technology, which was awarded the Nobel Prize in Chemistry in 1948, and discovered an increase in gamma-globulins in serum obtained from immunized animals.

Porter and Edelman independently published their findings on the structure of antibodies in 1959 and were given the Nobel Prize in medicine or physiology in 1972. They digested various immunoglobulins and analyzed the physiochemical and biological features of each fragment to determine the structure. Porter discovered three distinct fragments after digesting rabbit gamma-

globulins with the enzyme papain. Two fragments (50 kDa) exhibited high similarity and were able to bind the antigen, resulting in the phrase "fragment antigen binding" (Fab) (Figure 1-6). The third fragment (80 kDa) had no interaction with the antigen and was dubbed the "fragment crystallizable" (Fc) due to its propensity to form crystals easily (Fig. 1-6). Concurrently, Edelman investigated the structure of human and rabbit antibodies using reducing, alkylating, and denaturing agents. He discovered two different chains of 20-24 kDa (Light chain) and 50-60 kDa (Heavy chain) (Edelman, Benacerraf, Ovary, & Poulik, 1961; Edelman & Poulik, 1961). He deduced from the molecular weight of one antibody (150 kDa) that an antibody was made up of two heavy and two light chains linked by disulphide bonds and noncovalent interactions (Figure 1.7.A).

Later Crystallography data of the Fab fragment and a whole intact immunoglobulin supported the proposed structure and showed that a monomeric immunoglobulin molecule is Y-shaped and typically consists of four different protein chains, including two identical heavy chains (HCs) and light chains (LCs) (Davies, Padlan, & Segal, 1975; Poljak, Amzel, Chen, Phizackerley, & Saul, 1975). The HCs are made up of three or four constant domains (CH), depending on the antibody isotype, whereas LCs only have one constant domain (CL). The constant domains compose the Fc area, the hinge region, and the base of the Fab region. the Fab region comprises the variable domains that determine antigen binding specificity and affinity (Diebolder et al., 2014; Vidarsson, Dekkers, & Rispens, 2014).

When examining the amino acid sequences of antibodies, Wu and Kabat discovered extremely variable regions of amino acids in 1970 (Wu & Kabat, 1970). These lengths extend from amino acids 24-34, 50-56, and 89-97 in the light chain and from amino acid residues 31-35, 50-65, and

95-102 in the heavy chain. These sequences, known as complementary-determining regions or CDRs, determine the antibody complementarity (Wu & Kabat, 1970).

Variations in the HC constant domain during an immune response produce five distinct isotypes in humans: IgM, IgD, IgG, IgA, and IgE, with IgG and IgA, further subdivided into subclasses 1-4 and 1-2, respectively. IgG, IgD, and IgE exist as monomers, whereas IgA and IgM (Figure 1-7.B) may have an extra polypeptide J-chain, allowing the production of dimers and pentamers, respectively (Hiramoto et al., 2018; Oostindie et al., 2022).

1.11.2 An abundant class of immunoglobulin: IgG

IgG is the most abundant immunoglobulin class in human serum, which accounts for 10-20% of plasma protein. In decreasing order of abundance, the four subclasses are IgG1, IgG2, IgG3, and IgG4. Each subclass has a distinct profile in terms of antigen binding, complement binding, and IgG binding to Fc receptors (Chatron & Pontet, 1992; Vidarsson et al., 2014).

1.11.3 Engineering a toolbox of recombinant antibody fragments

After deciphering the structure of full-length antibodies, researchers have been interested in engineering and producing additional antibody formats through molecular genetics and DNA technology (Kim, Park, & Hong, 2005; Morrison, Johnson, Herzenberg, & Oi, 1984). The conventional antibodies have been reduced to smaller fragments, such as the Fab fragments and single-chain variable fragments (scFv) (Figures 1-6 and 1-7 C-D). These smaller antibody

fragments have a shorter half-life and greater tissue penetration through the complex antigen structure such as amyloid fibrils (Colcher et al., 1998; Yokota, Milenic, Whitlow, & Schlom, 1992). The Fab domain comprises constant and variable heavy chains linked via a disulphide bond to the light chain and can be obtained by enzymatic digestion of full-length IgG antibody or through recombinant expression in mammalian expression systems or *E.coli*. Similarly, the single-chain variable fragment (scFv), first developed by Huston et al. is composed of the variable domains of the light and heavy chains connected via a polypeptide linker (Huston et al., 1988). This fragment can be easily expressed in bacteria. Belgian researchers discovered another antibody format other than IgG in the early 1990s (Hamers-Casterman et al., 1993). They discovered a heavy chain antibody in Camelidae serum that lacked the light chain and the first constant domain of the heavy chain (HcAb). The antigen is recognized by only one variable domain, known as variable heavy homodimers (VHH). Three CDRs create the antigen binding site within the VHH. The VHH domain is known as a nanobody and is easily expressed in *E. coli* (Figures 1-6 and 1-7.E). The nanobody is tiny (12-15 kDa), penetrates deeper into tissues, and has the same binding affinity as the HcAb (Hamers-Casterman et al., 1993).

1.11.4 How are antibodies generated?

Target-specific monoclonal antibodies (mAbs) are regularly generated via hybridoma technology discovered by Köhler and Milstein or biopanning employing recombinant antibody libraries (Clackson, Hoogenboom, Griffiths, & Winter, 1991; Marks et al., 1991).

B-cells from animals are extracted several weeks after being immunized with the antigen for the formation of hybridoma antibodies. Immortalized hybridoma cells are produced by fusing B-cells with a myeloma cell line. Each hybridoma cell generally secretes a single species of immunoglobulin G (IgG), which is utilized in binding assays such as Enzyme-Linked Immunosorbent Assay (ELISA) to select for cell lines producing antigen binders (El Debs, Utharala, Balyasnikova, Griffiths, & Merten, 2012; Suter, Bruggen, & Sorg, 1980). Since antibody production and affinity maturation take place *in vivo* as part of the animal's immunological response, these mAbs can have high specificity and affinity (Berek, Griffiths, & Milstein, 1985).

Biopanning using recombinant antibody libraries eliminates many of the difficulties of the hybridoma antibody generation (Chao et al., 2006). These libraries are created by cloning synthetic or naive Fabs, single-chain variable fragments (scFvs), or nanobodies (Nbs) (Figure 1-7. C-F) onto phage or yeast display vectors. Several rounds of antigen-binding selection by solid-phase or flow cytometry are used to enrich antibodies. Biopanning settings can be chosen to achieve optimal antibody-antigen binding interactions (Senatore et al., 2020). The phage display technology can help unveil hidden epitopes that would otherwise be masked by conventional monoclonal antibodies (Senatore et al., 2020).

These days using hybridoma technology has been followed by the development of standardizable, high-yield recombinant antibody discovery, production, and purification platforms, ushering in a new era of antibody-based medicines and biomedical research (Kohler & Milstein, 1975).

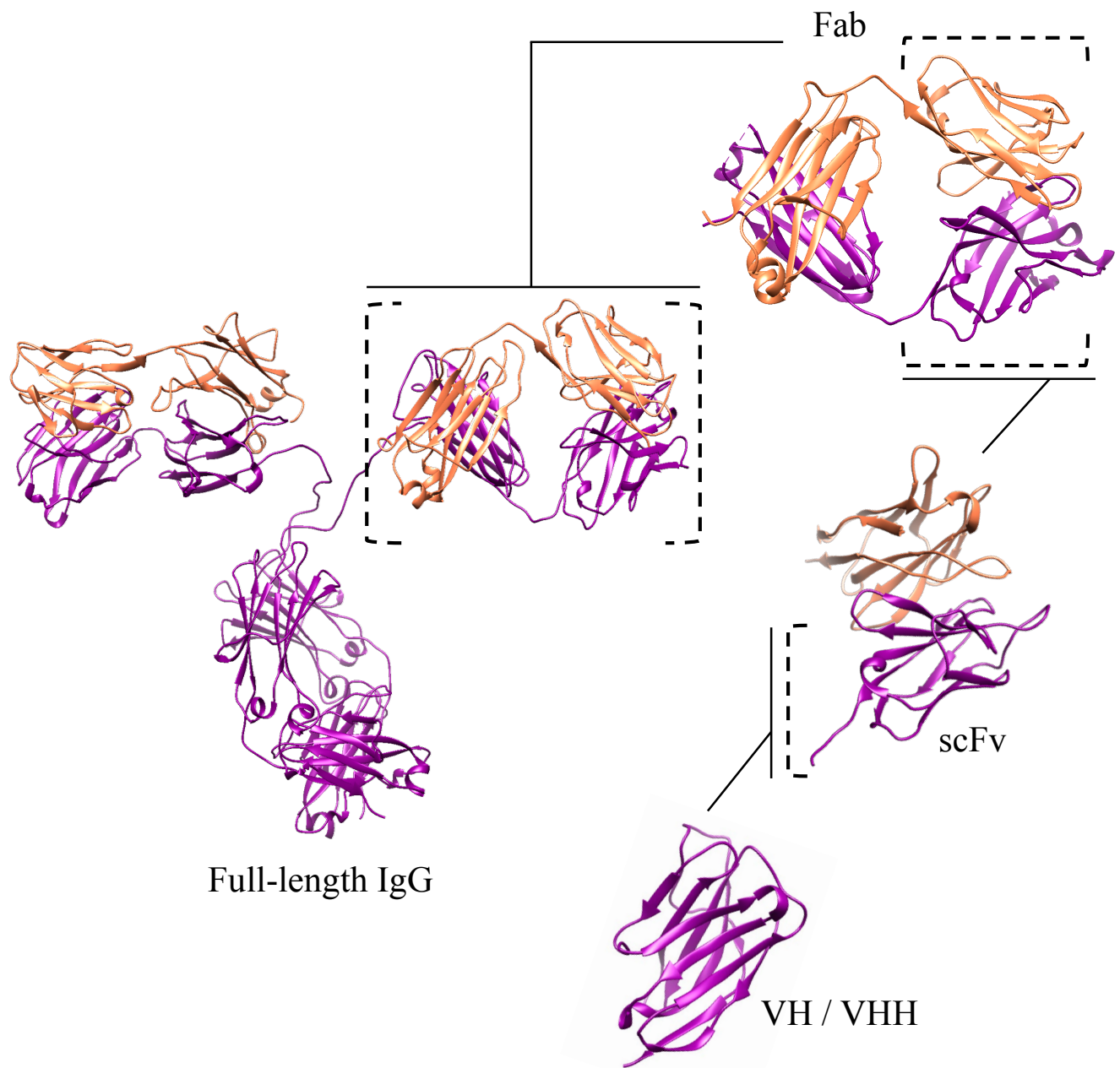


Figure 1-6: Overview of the ribbon structure of full-length and fragment antibodies.

Ribbon diagrams of full-length IgG and fragment molecules. Structures were obtained from the Protein Data Bank (Fab-1IGT, scFv-5VH3, VHH-3R0M). Heavy chains are shown in magenta and light chains are shown in carol. Fab: Fragment antigen-binding; scFv: single chain variable fragments; VH/VHH: heavy chain variable domain fragment

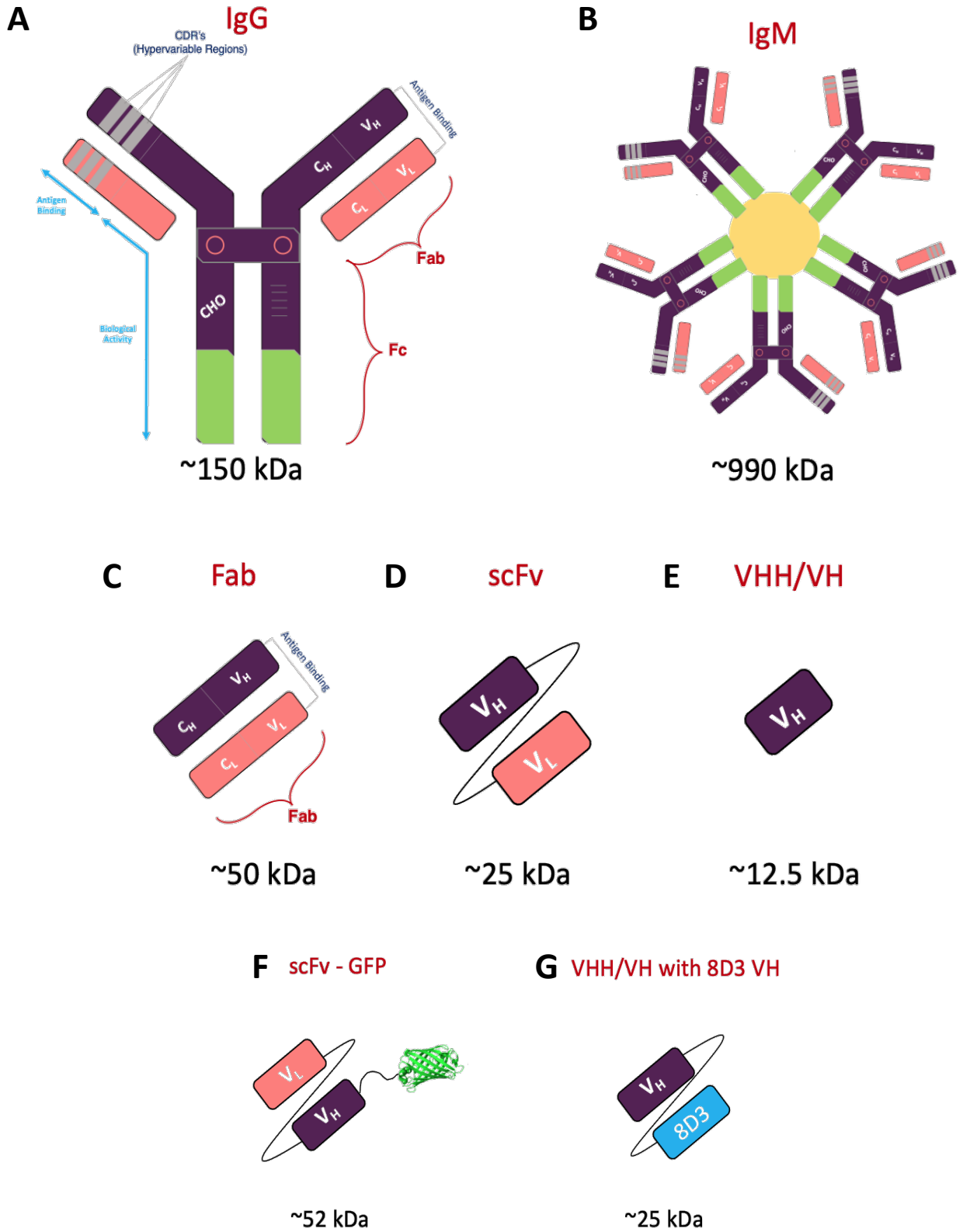


Figure 1-7: Schematic representation of IgG, IgM and its smaller antibody derivatives.

(A) The full-length IgG is composed of four strands of which two light chains and two heavy chains. (B) Full-length IgM antibody in its pentameric form, consisting of a total of ten heavy and light chains. The antigen binding sites consist of the complementarity determining regions (CDRs) and are part of the variable domains of the antibody (highlighted in grey). Smaller engineered fragments of the conventional IgG are the (C) Fab domain and (D) the single chain variable fragment (scFv). (E) Single domain antibodies also known as Nanobodies are the smallest antibody fragments generated exclusively by camelids and sharks. (F) Enhanced GFP protein fused with an scFv at the C-terminus. (G) Fusion of variable heavy chain nanobody with the variable heavy chain of mouse transferrin receptor mAb for delivery of therapeutic protein to the brain through receptor-mediated transcytosis. Heavy or light chains are depicted in purple or peach, respectively. CDR segments are highlighted in grey.

1.12 ROLE OF ANTIBODIES IN PRION DISEASES

Neurodegenerative diseases, including transmissible spongiform encephalopathy (TSEs), Alzheimer's disease (AD), and Parkinson's disease (PD), are a considerable public health issue affecting tens of millions of patients (Collins, Insel, Chockalingam, Daar, & Maddox, 2013; G. Miller, 2009). A hallmark of neurological disorders is the presence and accumulation of misfolded neuronal protein aggregates (Soto, 2003; Stopschinski & Diamond, 2017). Uncovering the structural details of PrP^{Sc} and determining how it differs from PrP^C will provide us with a better understanding of the pathogenesis of prion diseases. The use of PrP antibodies in the structural investigation of the pathogenic isoform PrP^{Sc} will not only shed light on PrP^{Sc} structure but may also be useful therapeutically. This can be achieved with the use of an array of antibodies against many different and unique epitopes of PrP^C, (N-terminal flexible tail, the truncated N-terminal, C-terminal globular domain) providing valuable tools for the prion research (Chapter 2) (P. K. Baral, Swayampakula, Aguzzi, & James, 2015; P. K. Baral et al., 2012; Lindell, 1985). With the help of anti-PrP monoclonal antibodies, Sonati *et al.*, reported that antibodies directed against PrP globular domain can be neurotoxic, suggesting that the N-terminal flexible tail mediates toxicity (Sonati et al., 2013). There are other types of antibodies that recognize both PrP^C and PrP^{Sc}, from sera and CSF and have shown the ability to disrupt the PrP fibrils (Wei et al., 2012). A major advancement in prion diagnostics would be the creation and utilization of antibodies designed to uniquely target the PrP^{Sc} species and not PrP^C. Most existing PrP antibodies recognize both PrP^C and PrP^{Sc}, or only PrP^C, or only PrP^{Sc} under denatured conditions, or differ in their reactivity to PrP^C and PK-cleaved PrP^{Sc} as they recognize epitopes at the truncated PrP site (90-120) (Kascsak et al., 1987; Peretz et al., 1997). Recent

developments in the Wille lab led to the generation of PrP^{Sc}-specific antibodies that only react with infectious PrP material and have a conformational epitope (Chapter 3). Such an antibody could have enormous value as a therapeutic reagent capable of promoting clearance of PrP^{Sc} from tissues, and as investigational tools for characterizing PrP^{Sc} in molecular studies (Colcher et al., 1998).

1.12.1 Antibodies and structure of prion protein

Antibodies are often utilized in structural biology to aid in the determination of high-resolution structures of antibody-antigen complexes due to their capacity to facilitate crystal packing of difficult targets and act as a fiducial marker to aid in particle orientation in electron microscopy (EM) by immunogold labelling. Recombinant Fabs of POMs 1 and 6 anti-prion antibodies (Polymenidou et al., 2008) recognizing distinct epitopes within the prion protein have been widely used to understand the molecular mechanism of the misfolding prone regions of recombinant human and mouse prion protein using X-ray Crystallography (P. K. Baral, Swayampakula, Aguzzi, & James, 2018; P. K. Baral et al., 2012). The current challenge for developing prion therapeutics is finding tight-binding monoclonal antibodies that are also safe for in-vivo administration. Structural research on anti-prion antibodies linked to PrP^C and PrP^{Sc} molecules will provide critical insights in this regard by elucidating the structural features responsible for the tighter interaction and play a key role in the design of therapeutic products against prion diseases.

1.12.2 Antibodies in direct detection of prions

PrP^{Sc} has been used as a universal diagnostic marker for prion diseases. As PrP^{Sc} derives from the misfolding of PrP^C, these two isoforms are always present together in tissue samples. In order to selectively detect PrP^{Sc} using anti-prion antibodies, a common strategy has been to treat samples with a proteinase-K enzyme that digests PrP^C but produces a characteristic proteinase-resistant core, PrP 27-30. Attempts have been made to capture PrP^{Sc} in its conformational state that obviates the use of proteinase-K as a discriminating reagent. However, there has always been a need for an epitope retrieval step by denaturing the sample with 8M guanidine hydrochloride since there are only a couple of antibodies that only recognize PrP^{Sc} in its native conformational state (Fang et al., manuscript in preparation). There have been attempts to develop diagnostic assays that can detect the disease-associated agent, PrP^{Sc}, without using proteinase-K digestion. This rapid assay allowed one-step capture of the PrP^{Sc} molecule using a europian-labelled anti-Pr P^C antibody targeting the N-terminal region of the PrP^{Sc} (Barnard et al., 2007). This rapid assay showed to distinguish between levels of disease-associated PrP isolated from brain and lymphoid tissues from TSE positive and negative cattle and sheep (Barnard et al., 2007). However, a major advance in prion diagnostics would be the creation and use of conformational PrP^{Sc}-specific antibodies engineered for one-step capture to react with native PrP^{Sc} and not with PrP^C. Such antibodies would have enormous value as tools for biomedical research and therapeutic agents capable of promoting the clearance of PrP^{Sc} from tissues.

1.12.3 Antibodies as passive immunotherapeutic tools

Active and passive immunotherapy that promotes the clearance of abnormal aggregates could be used to treat diseases caused by improper protein aggregation (Aguzzi & O'Connor, 2010). So far, there has been no treatment available to cure the development of prion diseases; nevertheless, any disruption in the pathogenic conversion process of PrP^C to PrP^{Sc} at the neuronal level could potentially prevent the progression of these diseases (White et al., 2003). One of the therapeutic options investigated for the treatment of prion diseases has been the use of anti-prion monoclonal antibodies (Figure 1-8) as a passive immunization agent that could potentially decrease PrP^{Sc} accumulation by disrupting the vicious pathological cycle of the PrP^C-to-PrP^{Sc} conversion (Reimann et al., 2016). Anti-prion monoclonal antibodies attach to the PrP^C molecule and stabilize it in its native shape by strong binding, preventing any unfavourable conformational changes (Reimann et al., 2016; Sanz-Hernandez et al., 2021). In parallel, several *in vitro* and *in vivo* trials with anti-prion monoclonal antibodies have been found to lower the amount of scrapie prion (Feraudet et al., 2005; White et al., 2003). The utility of conformational PrP^{Sc}-specific antibodies (YEG Sc-G1) compared to antibodies recognizing PrP^C and PrP^{Sc} molecules would be a better choice for developing successful immunotherapy for prion diseases as described in Chapter 3 of this thesis (Figure 1-8). Targeting the pathogenic isoform would aid in interfering with PrP^{Sc} trafficking, promoting degradation, or inhibiting PrP^{Sc} from interacting with PrP^C molecules (Figure. 1-7.G).

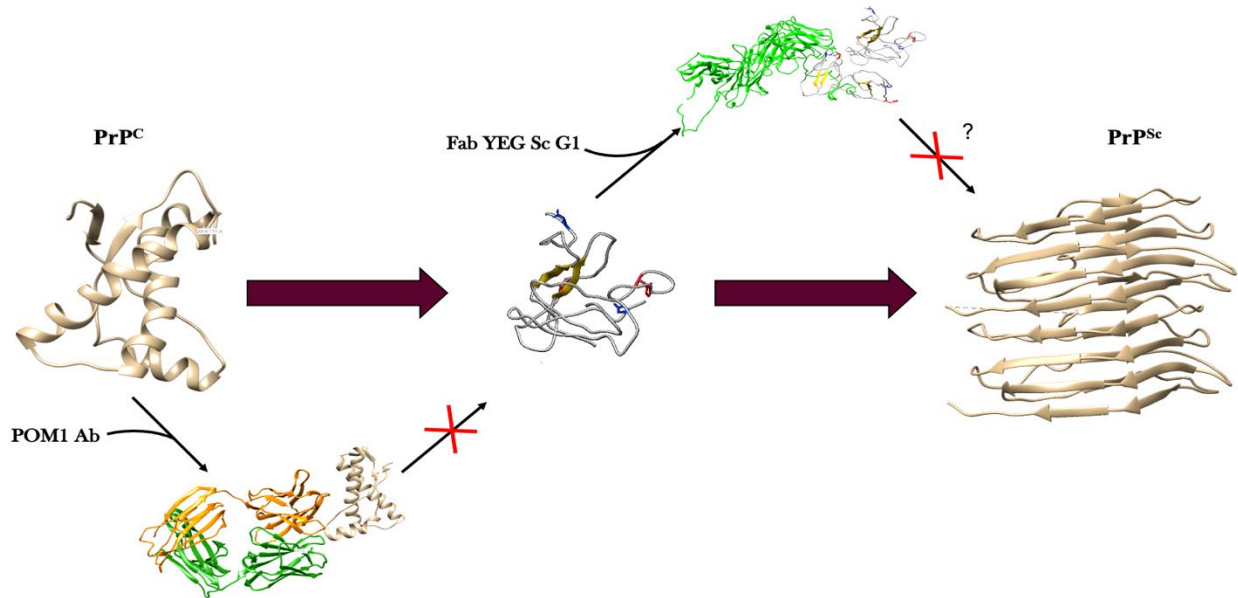


Figure 1-8: Schematic representation of anti-PrP antibody clearance using PrP^C and PrP^{Sc}-specific antibody.

A model showing the utility of anti-PrP antibodies that recognize both PrP^C and PrP^{Sc} such as POM antibodies interfere with the misfolding of the HuPrP^C. POM1 binds to α -helices H1 and H3 and suppresses the accumulation of misfolding intermediate that leads to amyloid formation. Our conformational PrP^{Sc}-specific antibody, YEG Sc-G1 offers an alternate approach of directly targeting the misfolded aggregates only to prevent the accumulation of aggregates and formation of amyloid fibril.

1.13 AIM AND THESIS OUTLINE

The key process behind prion diseases is the conversion of PrP^C into the PrP^{Sc} isoform. The molecular mechanism that causes this change remains long elusive. In this process, anti-PrP antibodies represent one of the strategies for the diagnosis and treatment of prion diseases.

Several studies, in-vitro and in-vivo are performed to understand the structure, pathogenesis and treatment of prion diseases using a wide range of anti-PrP antibodies of which most recognize various epitopes within PrP^C or both PrP^C and PrP^{Sc}.

The research outlined in this thesis aimed to develop a pipeline to produce recombinant humanized antibody fragments for prions derived from phage display technology and hybridoma clones. In the following sections, we highlight the broad utility of anti-PrP antibodies for structural studies with a particular emphasis on PrP^{Sc}-specific recombinant antibody fragments.

In this thesis, we report for the first time a conformational PrP^{Sc}-specific antibody and its engineered smaller antibody derivatives, YEG Sc-G1 monoclonal antibody. The overall objective was to create a toolbox of recombinant antibody fragments that can be used in a wide range of immunoassays for the characterization of infectious prions, such as structural analysis of infectious prion amyloid fibrils by immunogold labelling and electron microscope (Chapter 2), one-step labelling of infectious prions using PrP^{Sc}-specific fluobody (Fig. 1-7.F) and employing PrP^{Sc}-specific antibody (Chapter 3) to analyze different conformational folds adopted by the synthetic GSS-A117V using a time-dependent folding immunoassay (Chapter 4).

Chapter 2 reports the expression and purification of recombinant humanized antibody fragments targeting four main regions of PrP, charged cluster 1 region (CC1), hydrophobic region (HR),

charged cluster 2 region (CC2) and globular domain (GD). Anti-PrP antibody fragments targeting the very N-terminus (Fab 3), truncated N-terminus (Fab 69) and the C-terminus (Fab 29) were extensively characterized and performed higher level structural analysis with purified RML, BSE-L and CWD prion using immunogold labelling.

In **Chapter 3**, I report the development of engineered PrP^{Sc}-specific antibody fragments and small antibody derivatives conjugated with either green fluorescent protein, cell-penetrating linker, as well as the design of bispecific antibodies as a potential therapeutic tool for prion diseases (Fig. 1-7.C-G).

Using our novel conformational PrP^{Sc}-specific antibody, I asked if we could use this specific tool to determine the heterogeneity observed in the crude PrP sample as well as different folds adopted during the protein misfolding events until the protein reached its final stabilized amyloid fibril conformation. To answer that, **Chapter 4** describes the in-vitro refolding of the synthetic 7kDA A117V GSS peptide by creating a time-dependent folding immunoassay using our novel antibody. The folds were analyzed based on the orientation of the epitope, which showed a drift in structure from 2-rung-beta solenoid confirmation to a fibril conformation of the GSS-A117V peptide.

Chapter 5 provides a general discussion of the most important results obtained in this thesis and elaborates on the future perspectives of the work.

Chapter 2: Characterizing Select Epitopes of
PrP using Humanized Recombinant Anti-PrP
antibody fragments

2.1 INTRODUCTION

Prion diseases, also known as transmissible spongiform encephalopathies (TSEs), are a large group of rare, inexorably progressive, and fatal neurodegenerative diseases which affect both animals and humans. The cellular prion protein (PrP^C) is best known for its infamous role in prion diseases, where it misfolds and aggregates, resulting in misfolded scrapie prion protein (PrP^{Sc}) causing fatal neurodegenerative diseases (Prusiner, 1982).

PrP^C is a cell surface glycoprotein encoded by the *PRNP* gene on the short arm of human chromosome 20. In humans, the newly synthesized and unprocessed PrP^C is approximately 253 amino acid residues. Structural studies of recombinant human PrP^C reveal that the protein adopts its physiological structure with a C-terminal globular domain (121-231) and N-terminal flexible tail (23-120) (Riek et al., 1997). The N-terminal flexible tail consists of two charged clusters; charged cluster 1 (CC1), charged cluster 2 (CC2), the octapeptide repeat region (OR) and the hydrophobic region (HR) whereas, the C-terminal globular domain consists of three α -helices and two small antiparallel β -sheets (Wulf et al., 2017). Additionally, two N-glycosylation sites Asn 181 and Asn 197 (Haraguchi et al., 1989) and an intramolecular disulfide linkage between cysteine residues, 179 and 214 (Turk, Teplow, Hood, & Prusiner, 1988) are located in the globular domain upstream of the sialylated glycosylphosphatidylinositol (GPI) anchor at the C-terminus (Figure 2.1.A) (Glockshuber et al., 1997; Stahl et al., 1992). The physiological function of PrP remains unknown, however, it has been speculated to have a potential role in the cell proliferation (Aguzzi et al., 2008), neuroprotection (Westergard, Christensen, & Harris, 2007) and copper metabolism (Vassallo & Herms, 2003).

While PrP^C and PrP^{Sc} have the same primary structure, they differ both in their biochemical properties, as well as their secondary and tertiary structure. One of the biochemical ways to distinguish PrP^C and PrP^{Sc} is through treatment with proteinase K (PK) enzyme: PrP^C is completely hydrolyzed whereas PrP^{Sc} is partially resistant to PK. The PK-resistant core of PrP^{Sc} spans from residue 89-231 (Prusiner, 1998b). Upon PK treatment, different forms of PrP, which vary in relative molecular mass and result directly from differential cleavage events that are related to their distinct strain properties, can be observed using both Western blotting and immunochemical approaches in an antibody-dependent manner.

Although the structure of recombinant PrP^C has been extensively studied using various biophysical techniques, efforts have been made to decipher the structure of the infectious protein. Previous studies revealed the overall architecture of PrP^{Sc} to be rich in a beta-sheet structure consisting of a 4-rung beta-solenoid structure (4R β S) (Vazquez-Fernandez et al., 2016; Wille, Bian, et al., 2009; Wille et al., 2007). Recently a high-resolution cryo-EM study of brain-derived 263K and anchorless RML prions revealed Parallel In-Register Intermolecular β -sheet Structure (PIRIBS) as the underlying fold for these prion strains (Artikis, Kraus, & Caughey, 2022; Kraus et al., 2021; S. W. Manka, W. Zhang, et al., 2022). This is contrary to the low-resolution brain-derived L-type BSE prion which is in agreement with the 4R β S structure (Kamali-Jamil et al., 2021).

A major aim in the prion field is the development of research tools that are applicable to detect multiple prion strains, have utility in a wide range of immunoassays, and have the potential to be able to discriminate between PrP^C and PrP^{Sc} which may help to better understand the structure of

infectious prion protein, develop a diagnostic test or potential therapeutic agents. This has been achieved by a panel of anti-prion antibodies that have shown to recognize both, PrP^C and PrP^{Sc} in different assays, including but not limited to the anti-PrP antibodies P4 and L42 (Shimizu et al., 2010), 8H4, 6H4 and 15B3 (Korth et al., 1997), 3F4 (Kasczak et al., 1987), 12B2/94B4 and 100B3, T1 and T2 (Shimizu et al., 2010), The SAF/Sha (including Sha31) and BAR-series of antibodies (Feraudet et al., 2005), the “R”-series of antibodies (Jeffrey et al., 2001), POM monoclonals (Polymenidou et al., 2008) and the “ICSM” antibodies (Beringue et al., 2003). All the PrP^{Sc}-specific antibodies claimed by several groups have not been shown to be conformational-specific in recognizing the native PrP^{Sc} only (Biasini et al., 2008). A detailed description of PrP^{Sc}-specific antibodies is discussed in chapter 3.

The Aguzzi lab, one of our collaborators, sought to create a panel of humanized recombinant prion antibody fragments in order to find rare antibodies to weakly antigenic epitopes that were overlooked by conventional screening methods (Senatore et al., 2020). They achieved this by panning a synthetic human antibody phage display library to explore the presence of PrP-binding antibody fragments and performing next-generation sequencing (NGS) of panning outputs after the phage selection (Frenzel, Schirrmann, & Hust, 2016; Ravn et al., 2010). The Fab library was biopanned against full-length recombinant mouse prion protein and further enrichment of Fabs to discover unique epitopes was performed with short PrP peptide, specifically targeting the N-terminus flexible tail, (23-110), two charge cluster regions (50-120) and the C-terminus globular domain (120-230).

In this chapter, I have shown the characterization and potential applications of a panel of novel recombinant anti-PrP Fabs. From the unique collection of 35 humanized fragment antibodies (Fabs), I have successfully expressed and characterized 11 Fabs targeting four main regions of

the prion protein: CC1₂₃₋₅₀ region, OR₅₀₋₉₀ region, CC2₉₀₋₁₂₀ region and GD₉₀₋₂₃₁. Specific focus has been given to Fab 3, Fab 69 and Fab 29 due to the usefulness of their epitope in recognizing the N-terminus, truncated N-terminus and the C-terminus region of PrP, respectively. We have demonstrated the utility of these epitope-specific antibodies using Dot blots, Western blots, indirect ELISA using infectious prion isolates, Histoblots, Immunocytochemistry (ICC) and immunogold labelling using electron microscopy. These new tools provide great resources for prion research designed to increase our understanding of different infected prion agents (PrP^{Sc}) and pathogenesis in natural and experimental systems, as well as offer potential use to 3D characterize high-resolution structures of other infectious prion proteins using cryo-EM.

2.2 EXPERIMENTAL PROCEDURES

2.2.1 Fab Library

The clones of human anti-PrP Fabs were provided to us by our collaborator, Dr. Adriano Aguzzi from the University of Zürich, Switzerland. These humanized anti-PrP Fabs target four main regions of the PrP protein, CC1- Charged Cluster 1 region, OR- Octapeptide repeat region, CC2- Charged Cluster 2 region, and GD- Globular domain. Phage display technology was used to generate the human anti-PrP Fab library, utilizing the synthetic human Fab phagemid library for the phage display selections at the Novartis Institute of BioMedical Research (Senatore et al., 2020). The libraries were constructed to mimic human antibody repertoires by combining frameworks from human germline sequences with diversified HCDR3 (Tiller et al., 2013). Enrichment of PrP Fabs covering a large variety of PrP epitopes was achieved by performing two rounds of biopanning against several recombinant mouse PrP fragments and full-length recombinant mouse PrP (recPrP 23-231) using various washing conditions (Senatore et al., 2020). Each anti-PrP Fab construct consists of kanamycin resistance, M13 origin and a bicistronic expression cassette under a lac promoter with OmpA – light chain followed by PhoA-heavy chain – Flag – 6xHis – Amber stop – truncated pIII (amino acids 231 - 406). Corresponding Fabs were subcloned into the Fab expression vector pPE2.

2.2.2 Expression of selected anti-PrP Fabs

One-shot Top10 competent cells (Invitrogen) were chemically transformed with selected pPE2-Fab plasmids and grown on LB agar/Kanamycin/1% glucose plates to amplify the amount of selected pPE2-Fab plasmid. A few 10 ml sterile tubes, each containing a single and distinct colony were inoculated into 6 ml of 2xYT/Kanamycin/1% glucose pre-culture medium and incubated for 13-16 hours (h) at 37°C, 250 rpm for selection and sequencing of the fab clones. The selected clones were purified using a Qiagen miniprep kit and were used for Sanger sequencing (University of Alberta, Molecular Biology Service Unit), using the following sequencing primers:

VH (5'GATAAGCATGCGTAGGAGAAA-3') and M13Rev (5' - CAG GAA ACA GCT ATG AC - 3').

Clones of the selected pPE2-Fab plasmids with the correct and complete sequence were then transformed with chemical competent BL21(DE3) cells (Invitrogen) and grown on LB agar/Kanamycin/1% glucose plates. A single colony was inoculated into 50 mL of 2xYT/Kanamycin/1% glucose, pH 7.0 pre-inoculation culture medium and incubated for 16 h at 37°C, 250 rpm. 500 mL of 2xYT - expressing medium containing Kanamycin/0.1% glucose, pH 7.0 was inoculated with 50 mL pre-inoculation culture and Fab expression was induced by adding 1mM IPTG followed by incubation overnight at 25°C, 180 rpm. The overnight culture was then centrifuged at 5100 g at 4°C for 50 min and the pellet was frozen at -80°C.

2.2.3 Nickel ion affinity chromatography purification of PrP Fabs

To prepare the cell lysate for Fab purification, the thawed pellet (after protein expression) was resuspended with the cell lysis buffer. 3 ml of lysis buffer was used for 1 g of pellet. The lysis buffer contained: 30mM Imidazole, 50mM NaH₂PO₄, 300mM NaCl, 0.5% Triton x-100 (sigma), 1 mg/ml lysozyme (Roche), 100 U/ml Benzonase (Merck), 1 EDTA- free tab for up to 50 ml of lysis buffer, adjusted pH to 8.0. Incubated the cell lysate at RT for 1 h on the gyratory rocker. The cell lysate was sonicated on the ice at an amplitude of 60% for 30 seconds (s) ON and 30 s OFF for 5 minutes (min). The cell lysate was further incubated at RT for an additional 1 h. The cell lysate was then centrifuged at 16,000 g at 4°C for 1 h and the supernatant was filtered through 0.22 μM Millipore Express® Plus Membrane. Fab purification was achieved via the 6x His-Tag of the C-terminal heavy chain by IMAC using empty PD-10 columns packed with 4 ml of slurry NI-NTA beads (QIAGEN). Briefly, after equilibration of the Ni-NTA column with equilibration buffer (30mM Imidazole, 50mM Na-phosphate buffer, 300mM NaCl, pH 8.0). The bacteria cell lysate was loaded and incubated for 1 h on the gyratory rocker at RT. The cell lysate was then washed with a two-step gradient washing buffer (40mM and 45mM Imidazole with 50mM Na-phosphate buffer, 300mM NaCl, pH 8.0). The Fab was eluted with elution buffer (250mM Imidazole, 50mM Na-phosphate buffer, 300mM NaCl, pH 8.0). Buffer exchange in phosphate-buffered saline (PBS), pH 7.4 was performed using PD-10 columns, Sephadex G-25M (Sigma).

2.2.4 SDS-PAGE gels for Coomassie staining and Western blotting

As quality control measures for the expression and purification of the selected PrP Fab fragments, Fab purification fractions were collected at each step of the purification and run on SDS-PAGE gels which were stained with Coomassie and performed Western blots. Cell lysates of the recombinant Fab, wash fractions and eluted Fab fractions were diluted in 5x SDS loading buffer (250mM Tris, pH 6.8, 10% SDS, 50% glycerol, 0.02% bromophenol blue with 5% 2-mercaptoethanol) and heated at 100°C for 10 min before electrophoresis. The proteins were separated by SDS-PAGE gel electrophoresis using 12% Bis-Tris NuPAGE gels (Invitrogen) and MES running buffer (Invitrogen), run for 20 min at 70 volts followed by 1 h 10 min at 150 volts. The SDS-PAGE gel was rinsed three times, 5 minutes each washed with distilled water and stained with InstantBlue® Coomassie protein stain (abcam) for 30 min and destained with distilled water overnight.

Samples were prepared similarly for Western blotting. After gel electrophoresis, proteins were electrically transferred onto a polyvinylidene difluoride (PVDF) membrane (Millipore) for 1 h 20 min at 110 volts. The blotted membrane is blocked with 5% (w/v) skim milk in Tris-buffered saline solution containing 0.1% Tween 20 (v/v) (TBST), for 1 h at RT and then incubated with primary antibody conjugated to horseradish peroxidase (HRP), anti-human Fab HRP (ab98605) at a 1:5000 dilution, for 2 h at RT. Next, the membranes were washed three times with TBST for 5 minutes each wash. Protein signals were developed by adding ~2 ml ECL chemiluminescent substrate (Pierce™ ECL Plus) and detected by chemiluminescent visualization using ImageQuant (GE Life Science).

2.2.5 PrP peptide library

Mouse PrP-peptide libraries were synthesized by Sigma, USA. The library contained 26 synthetic overlapping peptides that covered the entire mature mouse PrP sequence described in Table 2.2. These peptides were separately synthesized, beginning with peptide no.1 at the N-terminus and ending with peptide no.26 at the C-terminus of PrP. These peptides consisted of 12 amino acid residues, with an overlap of 4 amino acids each to the adjacent peptide. The purity of all of the above peptides was expected to be 90% or higher. As a control, a full-length mouse PrP was used. These peptides were dissolved in dimethyl sulfoxide (DMSO) and PBS at 1 mg/ml.

2.2.6 Enzyme-Linked Immunosorbent Assay (ELISA) for epitope mapping

The epitopes for anti-PrP Fab fragments were screened using an indirect ELISA against the PrP peptide library. ELISA SpectraPlates™ were coated with 5ug/ml mouse PrP peptides and recombinant full-length mouse PrP (rmPrP₂₃₋₂₃₁) diluted in PBS, at 4°C overnight. The plate was washed with PBST containing 0.05% (v/v) Tween-20 (PBST) and was blocked with 5% BSA for 2 h at RT. Purified Fabs in PBST were then incubated for 3 h at RT (1:500 in PBST). After three washes with PBST, bound Fabs were then incubated with a secondary anti-human Fab HRP conjugated antibody (1:5000 in PBST). The plate was incubated for 1 h 30 min RT, followed by three washing with PBST. After washing, the plates were developed with 3,3',5,5'-

Tetramethylbenzidine (TMB) substrate (SurModics) and incubated for 30 min, the reaction was then stopped with 50 μ L of 2N sulfuric acid. The optical density was measured at 450 nm.

2.2.7 Activity assays

2.2.7.1 Dot blotting

The full-length and truncated recombinant prion protein were diluted in PBS to load 5ug per well. The recombinant protein was treated with and without 2% SDS (final concentration). The sample treated with 2% SDS was also boiled at 100°C for 10 min. A nitrocellulose membrane was equilibrated in Tris-glycine (transfer) buffer for 10 min, followed by the recommended assembly of 96-well dot blot apparatus (Bio-Rad). The samples were vacuum-filtered through the membrane, and the wells were rinsed twice with TBS. Then the membrane was treated as outlined for Western blots in section 2.2.10.

2.2.7.2 ELISA using brain homogenates

Untreated 10% RML brain homogenate was used from the prion isolation preparation as described in section 2.2.8 of this chapter. 20% RML brain homogenate was diluted with PBS to make 10% RML brain homogenate. The 10% RML brain homogenate was briefly sonicated using a high-intensity ultrasonic bath at an amplitude of 50% for a total of 1 min; 10 s ON and 30

s OFF. Similarly, mice brains infected with human GSS^{A117V} were homogenized using hand-held UltraMax T18 basic homogenizer for 15 s in cold lysis buffer (LB), 100 pH 8.0 (100 mM NaCl, 0.5% Nonidet P-40, 0.5% sodium deoxycholate, 10 mM EDTA, 100 mM Tris-HCl, pH 8.0) (Cracco et al., 2017) to make 10% BH. The 10% GSS^{A117V} BH was indirectly sonicated using high-intensity ultrasonic bath at an amplitude of 50% with 10 s ON and 30 s OFF for 1 min. An aliquot of 100ug/ml of RML and GSS^{A117V} BH was made using PBS and LB, respectively. Coated the ELISA Microtiter plates with 100ul of BH at 4°C overnight. **NOTE:** If necessary, the plates may be kept in a -80°C freezer sealed with a plate sealer for one-two month before the ELISA is performed. The plate was washed with PBST containing 0.05% (v/v) Tween-20 (PBST) and was blocked with 5% BSA for 2 h at RT. Purified Fabs in PBST were then incubated for 3 h at RT (1:500 in PBST). After three washes with PBST, bound Fabs were then incubated with a secondary anti-human Fab HRP conjugated antibody (1:5000 in PBST). The plate was incubated for 1 h 30 min RT, followed by three washing with PBST. After washing, the plates were developed with 3,3',5,5'-Tetramethylbenzidine (TMB) substrate (SurModics) and incubated for 30 min, the reaction was then stopped with 50 µL of 2N sulfuric acid. The optical density was measured at 450 nm. For data analysis subtract the OD value obtained in a well with all the reagents except any primary anti-PrP Fab (control well) from the OD values measured for each of the analyzed samples with their respective anti-PrP Fabs.

2.2.7.3 Histoblots from RML infected and uninfected mouse brain slices

The Sim Lab provided 8-day old Tga20 mouse pups and prepared the organotypic slice cultures for histoblot analysis. Following the cervical dislocation, the brains were removed from the pups

and hemisectioned. They were sliced into 275 μ M thick coronal sections with a vibratome and placed onto Millicell cell culture inserts (Sigma) in a 6-well plate and cultured with cell culture medium, 50% v/v Hank's MEM, 25% v/v heat-inactivated horse serum, 25% Hanks' balanced salt solution (HBSS) supplemented with 0.5% glucose. Penicillin/streptomycin and glutamax which was added basolaterally. After 7 days of culturing the brain slices, 0.9mL of media containing 100 μ g/ml of infectious RML brain homogenate or normal non-infectious Tga20 brain homogenate was added apically to the slices and allowed to gradually seep through the membrane for 4 weeks. The brain slices were cut out of the millicell insert membrane and transferred onto the nitrocellulose membrane using lysis buffer (0.5% Nonidet P-40, 0.5% sodium deoxycholate, 100mM NaCl, 10mM EDTA, 10mM Tris-HCl, pH 7.8). (Pineau et al., manuscript in preparation) After the slices have transferred to the nitrocellulose membrane, allow the membrane to dry (Taraboulos et al., 1992). Rehydrate the membrane in TBST for 1 h and block the membrane in 5% skim milk in TBST for 1 h. The histoblot was then incubated with anti-PrP antibodies, C2-6, Fab 3, Fab 69 and Fab 29 overnight at 4°C (12-14 h) for cell surface labelling of PrP^C and PrP^{Sc}. After three washes with TBST, bound antibodies were incubated with secondary goat-anti mouse HRP conjugated and anti-human Fab HRP conjugated antibody (1:5000 in TBST) for 1 h 30 mins. After the incubation at RT, the histoblots were washed three times with TBST. Histoblots were developed by adding ~2 ml ECL chemiluminescent substrate (PierceTM ECL Plus) and detected by chemiluminescent visualization using ImageQuant (GE Life Science).

2.2.7.4 Immunohistochemistry using CAD 5 and CAD 5 - RML infected cells

The mouse catecholaminergic neuronal tumour cell line CAD5, (Cath.a, differentiated)/CADRML (a generous gift provided by Dr. Hermann Schätzl from the Prion Research Unit, University of Calgary) were cultured as described previously (Suri, Fung, Tischler, & Chikaraishi, 1993; Walia, Ho, Lee, Gilch, & Schatzl, 2019). The mouse neuronal CAD 5/CADRML infected cells were grown and maintained in Dulbecco's modified Eagle's medium (DMEM; Invitrogen) supplemented with 10% fetal bovine serum (FBS; Invitrogen) with 1% penicillin-streptomycin on standard tissue culture dishes in a humidified 5% CO₂ incubator at 37°C. CAD 5 and CAD RML infected cells were grown on glass coverslips (Fisher) to achieve 85-90% cell confluency before fixing them. The cells were washed once with ice-cold PBS and fixed with pre-chilled methanol (-80°C) for 10 min. The cells were washed twice with ice-cold PBS followed by mild permeabilization using 0.1% Triton X-100 in PBS for 5 mins and rinsed twice with ice-cold PBS. The cells were then blocked with 3% BSA in PBST for 1 h at RT and then incubated with anti- PrP Fabs 3, 69 and 29 overnight at 4°C. Aspirate the primary antibody and washed the cells three times in ice-cold PBS, 5 min each wash. Incubated the cells with the Alexa Fluor 647 – conjugated secondary antibody (abcam) in 1% BSA for 2 h at RT in the dark. The slides were then washed three times with ice-cold PBS for 5 min each in the dark. The excess buffer was decanted and the coverslips were mounted with the ProLongTM Gold antifade mountant with DAPI (ThermoFisher) and air-dried in the dark. The coverslips were then sealed with the slide sealer and air-dried in the dark. The cell surface PrP^C and PrP^{Sc} labelling were visualized by confocal laser scanning microscopy, ZENN Digital Imaging for LSM 700 (Zeiss) and analyzed using ImarisViewer Imaging software 9.8.0.

2.2.8 Isolation of RML prions

Using a previously developed protocol (Safar et al., 1998), infectious RML prions were isolated from the brains of terminally ill RML-infected FVB mice. First, all infected brains were weighed and pooled and homogenized at 20% concentration (w/v) in PBS. Two – four brains were used in separate purification experiments. The 20% brain homogenate was then clarified at 500 x g for 5 min, and the supernatant was collected and added to a new falcon tube with an equal volume of 4% sarkosyl diluted in PBS to make 10% w/v brain homogenate. Then, the sample was aliquoted into 1 ml screw-cap microcentrifuge tubes and subjected to digestion with PK (50 ug/ml) at 37°C for 1 h. The PK treatment reaction was stopped with the addition of 10 mM Phenylmethylsulfonyl Fluoride (PMSF). The process continued by adding 2% sodium phosphotungstic acid (PTA, pH 7.2) (SIGMA) to the aliquots and overnight incubation (16 h) at 37°C. The overnight samples were then centrifuged at 16,000 x g for 30 min and the P1 pellet fraction was obtained and resuspended with 0.2% sarkosyl in PBS. Subsequently, 2% sarkosyl in PBS and 2% PTA were added to the resuspended pellets, and the samples were incubated further at 37°C and centrifuged again at 16,000 x g for 30 minutes to obtain the final pellet (P2, pellet 2 fractions). The final pellet was resuspended with 0.2% sarkosyl in PBS. Samples collected from different steps of the purification were stored at -80°C for future analyses.

In order to generate highly purified RML prion isolates suitable for structural examination via immunogold labelling and electron microscopy, we combined the PTA-precipitation protocol with a sucrose step-gradient centrifugation. In this method, the standard PTA purification was performed until the first pellet (P1) was obtained, and after resuspension with 0.2% sarkosyl in PBS, the pellet 1 was loaded onto a sucrose-step gradient of 40% and 80% sucrose and subjected

to ultracentrifugation at 115,000 x g at 4°C for 16 hours (overnight). Following centrifugation, 500 µL fractions were collected from the top of the ultracentrifugation tube. The bottom of the tube was washed with 100 µl of sucrose buffer (10 mM Tris HCl pH 7, 1mM NaN₃, 0.2% sarkosyl) to recover pelleted proteins and labelled as ‘pellet wash’. All collected samples were stored at -80°C for SDS-PAGE, silver staining and TEM studies.

2.2.9 Silver staining

Samples from the RML PTA purification were mixed with a gel-loading buffer (Bio-Rad) containing 2% (w/vol) SDS and heated at 100°C for 10 minutes before electrophoresis. Samples were then loaded on 12% polyacrylamide gels (Bio-Rad) and run for 60 minutes at 150 volts. The gels were then incubated for 30 minutes at room temperature in fixing solution (50% methanol, 12% acetic acid) and afterwards incubated in SDS removal solution (10% ethanol, 5% acetic acid) for 30 minutes at room temperature. Next, the gels were transferred to Farmer’s solution to enhance PrP staining (containing: 0.15 g potassium ferricyanide, 0.3 g sodium thiosulfate, 0.05 g sodium carbonate) for 2 minutes, and then washed three times in distilled water. Next, the gels were treated with 0.2% (w/v) AgNO₃ for 20 minutes and rinsed briefly in distilled water, followed by 100 ml developing solution (15 g sodium carbonate and 250 µL 30% formaldehyde stock solution). Finally, the development stopped in a solution of 0.2% acetic acid (Wille, Shanmugam, et al., 2009).

2.2.10 Western blotting

Samples were diluted in 5 x SDS loading buffer (250mM Tris, pH 6.8, 10% SDS, 50% glycerol, 0.02% bromophenol blue with 5% 2-mercaptoethanol) and heated at 100°C for 10 min before electrophoresis. The proteins were separated by SDS-PAGE gel electrophoresis using 12% Bis-Tris NuPAGE gels (Invitrogen) and MES running buffer (Invitrogen), run for 20 min at 70 volts followed by 1 h 10 min at 150 volts and blotted electrically onto a polyvinylidene difluoride (PVDF) membrane (Millipore) at 100 volts for 1 hour. The blotted membranes were blocked with 5% (w/v) BSA in Tris-buffered saline solution containing 0.05% Tween 20 (v/v) (TBST), overnight, at 4°C and incubated with anti-PrP antibody, POM17 at a 1:5,000 dilution, anti-PrP Fabs 3, 69 and 29 for 3 hours, at a 1:500 dilution at RT, followed by washing three times for 5 minutes with TBST. Next, the membranes were incubated with anti-mouse IgG – HRP (Bio-Rad) at a 1:10,000 dilution and in TBST for one hour and washed three times for 5 minutes in TBST. Prion protein signals were developed by adding ~2 ml ECL chemiluminescent substrate (PierceTM ECL Plus) and detected by chemiluminescent visualization using ImageQuant (GE Life Science).

2.2.11 Negative Staining electron microscopy

5- μ l drops of purified samples were adsorbed onto freshly glow-discharged 400 mesh carbon coated copper grids (Electron Microscopy Sciences) for 2 min and washed in 1–3 drops of (50 μ l) 0.1M and 0.01M ammonium acetate solutions each. Then, the grids were stained using a freshly filtered 2% solution of uranyl acetate and air-dried after removing the excess

stain with filter paper. The stained samples were examined with a Tecnai G20 transmission electron microscope (FEI Company) operating at an acceleration voltage of 200 kV. Electron micrographs were recorded with an Eagle 4k x 4k CCD camera (FEI Company) (Kamali-Jamil et al., 2021; Wille, Zhang, Baldwin, Cohen, & Prusiner, 1996)

2.2.12 Immunogold labelling

Immunogold labeling of the RML prion fibrils was performed using a combination of anti-PrP antibodies, including Fab fragments Fab 3, Fab 69 and Fab 29, detecting prion protein epitopes at different positions. The Fab fragments were selected from a phage display library as described earlier in section 2.2.1. Fab 3, Fab 69 and Fab 29 react with epitopes within residues $_{23}\text{KKRPKPGGWNTG}_{34, 87}\text{GGWGQGGGTHSQ}_{98}$ and $_{215}\text{TQYERESQAYYD}_{226}$ located at N-, truncated N- and C-terminal regions of the murine prion protein, respectively.

Based on a previously published immunogold labeling protocol (Kamali-Jamil et al., 2021; Vanni et al., 2020; Wille et al., 2007), 5 μl of purified RML samples were adsorbed onto glow discharged formvar/carbon-coated nickel grids (TedPella, Inc.) for ~5 minutes, and washed using three drops (50 μl) of 0.1M and 0.01M ammonium acetate buffer pH 7.4. Samples used for labeling with Fab 69 and Fab 29 antibodies, were treated with 50 μl of 3M urea for 10 minutes, to increase the epitope accessibility.

Incubated with primary antibody (Fabs 3, 69 or 29) for 3 h, rinsed five times with 0.1% BSA in TBS, incubated with a bridging goat F(ab')₂ anti-human IgG F(ab')₂ (Abcam ab98531) for 2 h, rinsed five times again with 0.1% BSA in TBS, incubated with a 5-nm gold-conjugated rabbit

anti-goat IgG (Abcam ab202670) for 2 h, rinsed five times with 0.1% BSA in TBS, twice with TBS alone, and twice with water. Controls were treated identically, except that the primary Fab was omitted. Finally, the grids were rinsed with TBS solution and water, and placed onto two drops of 2% PTA for final staining, air-dried, and stored for EM analysis. The samples were analyzed with a Tecnai G20 transmission electron microscope (FEI Company) operating at an acceleration voltage of 200 kV. Electron micrographs were recorded with an Eagle 4k x 4k CCD camera (FEI Company).

2.3 RESULTS

2.3.1 Generation of the anti-PrP Fab library via phage display technology

Utilizing cutting-edge technologies that combine traditional phage display methodology with next-generation sequencing (NGS), our collaborator Adriano Aguzzi and his team at the University of Zürich in Switzerland created a variety of highly specific, highly affine small antibody derivatives (Fabs) that target the entire surface of the prion protein (Senatore et al., 2020). Generation of specific de-novo antibodies was achieved using commercially available human phage display libraries which can express 10^9 - 10^{11} structurally distinct phages (Kotlan & Glassy, 2009; Liu, Huang, & Jiang, 2002). The Fab library was constructed to mimic repertoires of human antibodies by combining human germline sequences with varied HCDR3 whose design approximated the natural gene sequences in human repertoires as compiled in the IMGT database (Giudicelli et al., 2006). The initial two rounds of the human phage library were biopanned against full-length recombinant mouse prion protein (recPrP₂₃₋₂₃₁). To enrich for Fabs that cover a wide range of PrP epitopes, a third biopanning round was performed against short PrP peptides (23-110), selective for regions of PrP that cover the charge cluster regions (CC1₂₃₋₅₀ and CC2₉₂₋₁₂₀), octapeptide repeat regions and globular domain of PrP to uncover the hidden and hot spot epitopes on PrP (Senatore et al., 2020). This method enables the discovery of rare non-immunodominant epitopes that would be otherwise overlooked by conventional technologies. The Fabs were classified into four different epitope groups based on the results from a

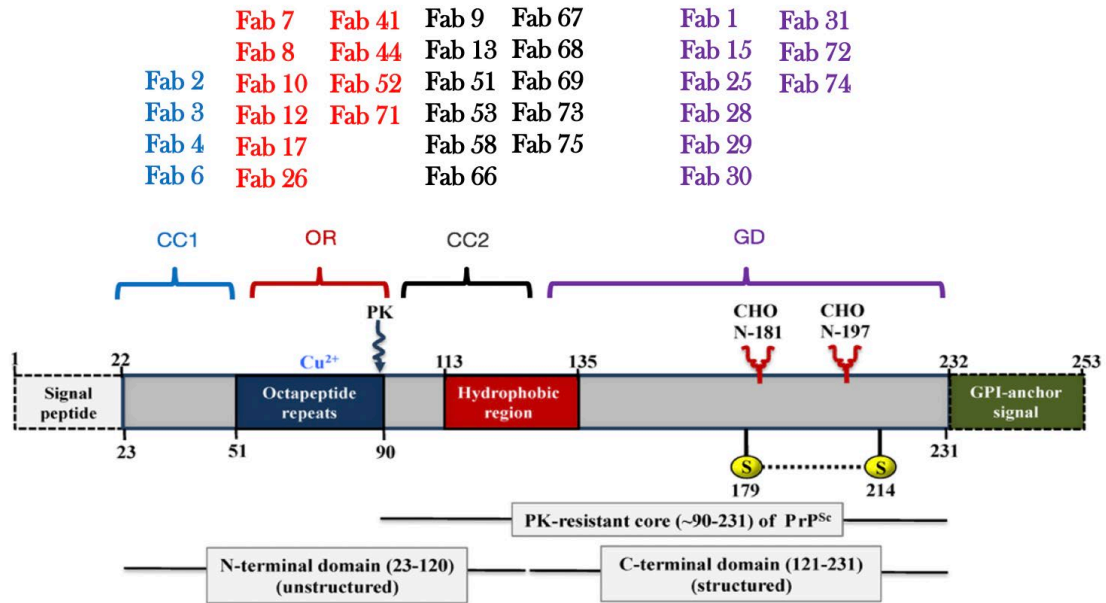
competitive ELISA format (Senatore et al., 2020). A library of 35 successfully biopanned Fabs were sent to us for further characterization of its activity in different biochemical and biophysical assays. From of the 35 Fabs, 4 targeted CC1₂₃₋₅₀, 10 OR₅₁₋₉₁, 11 CC2/HC₉₂₋₁₂₀ and 9 GD₁₂₀₋₂₃₁ (Figure 2-1.A).

2.3.2 Expression and purification of selected anti-PrP Fabs

I developed an efficient protocol to express and purify large-scale quantities of the recombinant anti-PrP Fabs from the Fab library in *E.coli* as soluble and functional Fabs. The design of the Fab constructs was such that the heavy and light chains of the Fab fragments would be expressed in tandem with a 6xHIS-tag at the C-terminus for purification, V_L-C_L-V_H-C_H-6xHis-tag. This would then give the Fabs a molecular weight of 25kDa when separated using SDS-PAGE protein gels. From the library of 35 Fabs, 13 Fabs targeting the four main epitopes on PrP, CC1, OR, CC2 and GD were recombinantly expressed in *E.coli* BL21(DE3) cells and purified using metal-ion affinity chromatography (IMAC) (Figure 2-1.B).

In this chapter I extensively focused on the characterization of the selected anti-PrP Fabs; Fab 3_(CC1: 23-50), Fab 69_(CC2: 92-120), and Fab 29_(GD: 120-231) from the anti-PrP Fab library because of their attractive epitopes targeting the polybasic stretch at the N-terminus, shortened N-terminus, and C-terminus of PrP. (Figure 2-2.A-F).

A



B

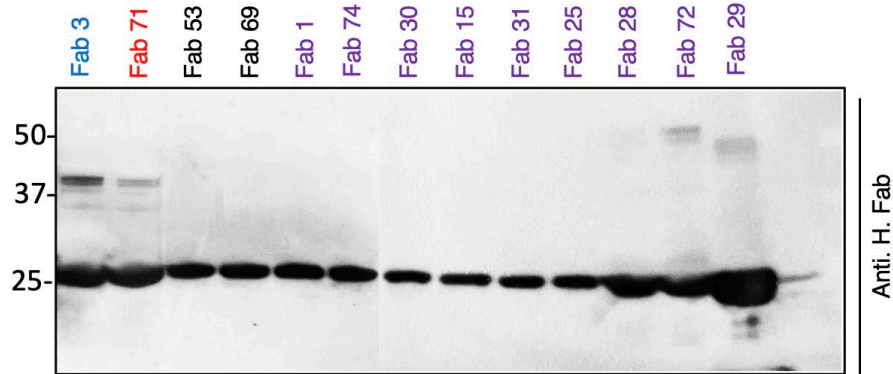
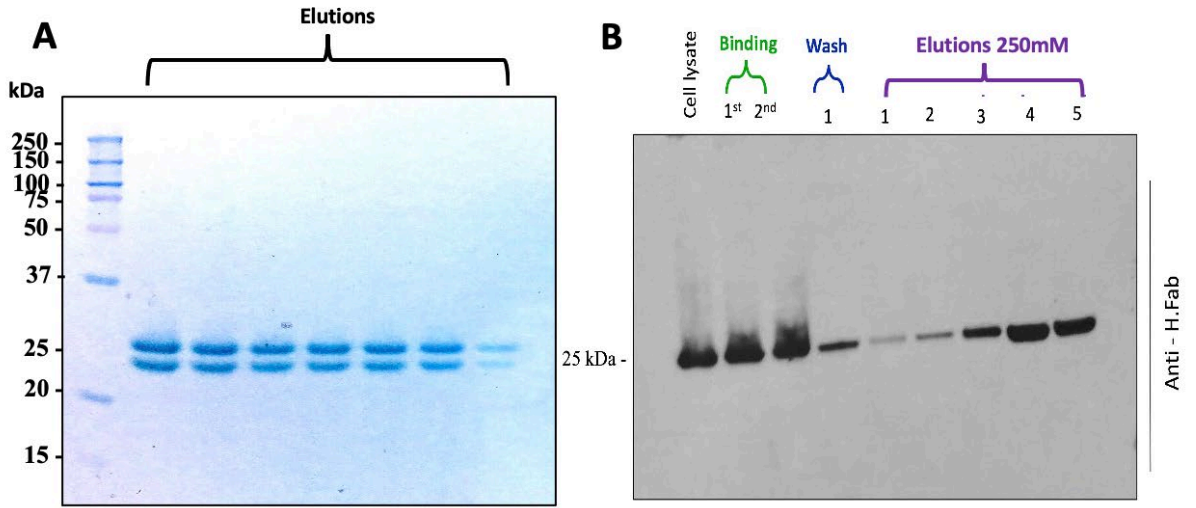


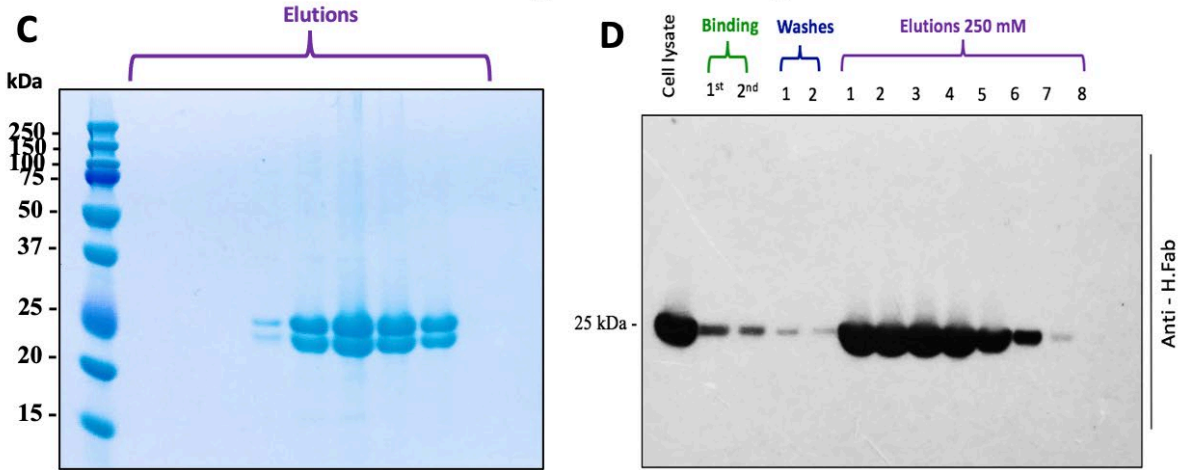
Figure 2-1: PrP Fab library.

(A) Humanized recombinant anti-PrP Fab fragments generated using phage display technology spanning four main regions of the full-length mouse prion protein, CC1₂₃₋₅₀, OR₅₁₋₉₁, CC2₉₂₋₁₂₀, GD₁₂₀₋₂₃₁. (B) Western blot of the successful Fabs that have been recombinantly expressed, purified and performed activity assay to show folding of the PrP Fabs and binding properties to the prion protein.

Fab 3 – Charged Cluster 1 Region



Fab 69 – Charged Cluster 2 Region



Fab 29 – Globular Domain

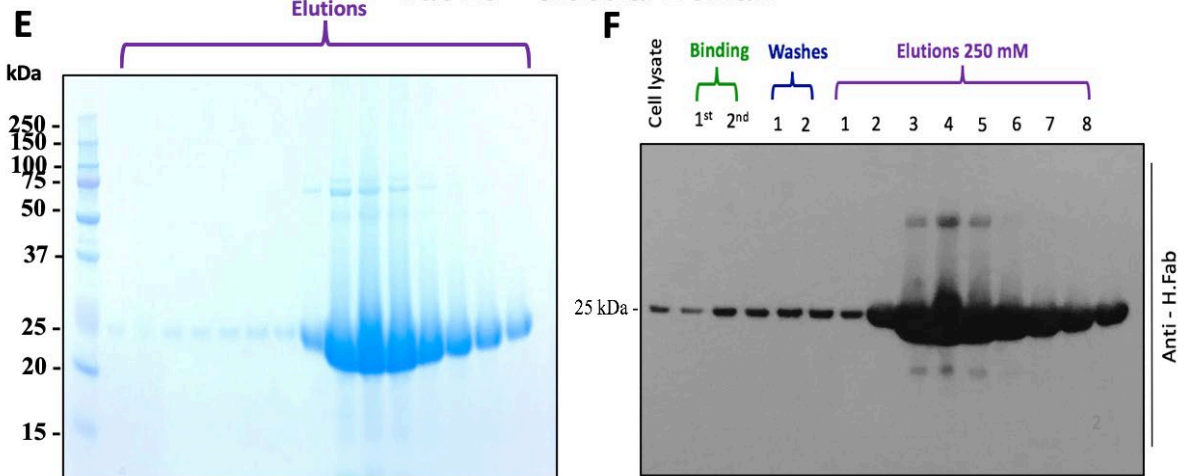


Figure 2-2: Purification of humanized recombinant anti-PrP Fab fragments.

Analysis of recombinant expression in BL21(DE3) cells and IMAC purification via SDS-PAGE coomassie staining (left) and Western blot using anti-human Fab (right) of **(A-B)** anti-PrP mAb Fab3 recognizing the CC1 region of PrP, **(C-D)** anti Prion mAb Fab 69 recognizing the CC2 region of PrP, **(E-F)** anti Prion mAb Fab 29 recognizing the GD of PrP. The Western blot was performed using a secondary antibody, anti-human Fab conjugated to HRP. All recombinant anti-PrP Fabs have a constructed design of VL-CH-VH-CH-6X_{HIS} whereby the light and the heavy chains of the fab fragments are expressed in tandem. Under denaturing conditions Fabs will have a molecular weight of 25 kDa. In cases where the heavy and light chain fragments are observed as two separate bands are due to the difference in the amino acid sequence of each Fab antibody. The top and bottom fragment of the antibody corresponds to heavy and light chains, respectively.

2.3.3 Summary table of expressed and purified anti-PrP Fabs from the Fab library

Table 2-1 summarizes a list of anti-PrP Fabs from the Fab library that have been successfully expressed, purified and further characterized to confirm the epitope and binding behavior of different Fabs to PrP by using a wide range of immunoassays. The activity of these Fabs was measured with a wide range of infectious and non-infectious prion isolates in different assays. Some Fabs showed to have better antigen-antibody recognition under denatured conditions (immunogold labelling), whereas other Fabs either didn't work in a western blot assay (Fab 71, Fab 1 and Fab 15) or showed no signal on the PK-treated RML final pellet after PTA – purification (Fab 29).

Table 2-1: Summary table of characterized humanized recombinant PrP Fabs

Region on PrP	Fabs	E and P	Activity Assay		Epitope Mapping	Immunogold Labelling
			Western Blot	Dot Blot		
CC1	Fab 3	✓	✓	✓	²³ KKRPKPGGWNTG ³⁴	✓
OR	Fab 71	✓	X	✓	⁶³ GWGQPHGGSWGQ ⁷⁴	ND
					⁷¹ SWGQPHGGSWGQ ⁸²	
CC2	Fab 69	✓	✓	✓	⁸⁷ GWGQGGGTHNQW ⁹⁸	✓
	Fab 53	✓	✓	✓	⁹⁵ HNQWNKPSKPKT ¹⁰⁶	✓
GD	Fab 1	✓	X	✓	¹¹⁹ AVVGGLGGYMLG ¹³⁰	ND
	Fab 74	✓	ND	✓	¹⁴³ DWEDRYRENMY ¹⁵⁴	ND
	Fab 30	✓	ND	✓	¹⁵¹ ENMYRYPNQVYY ¹⁶²	ND
	Fab 15	✓	X	✓	¹⁶⁷ QYSNQNNFVHDC ¹⁷⁸	ND
	Fab 31	✓	ND	✓	¹⁶⁷ QYSNQNNFVHDC ¹⁷⁸	ND
	Fab 72	✓	ND	✓	¹⁶⁷ QYSNQNNFVHDC ¹⁷⁸	ND
					¹⁷⁵ VHDCVNITIKQH ¹⁸⁶	
	Fab 29	✓	✓	✓	²¹⁵ TQYQKESQAYYD ²²⁶	✓

Mouse PrP sequence for epitope mapping

E and P: Expressed and Purified

CC1: 23-50 OR: 50-90 CC2: 90-120 GD: 120-230

2.3.4 Epitope mapping of anti-PrP Fabs

Next, I used an indirect ELISA to confirm how the various Fabs interacted with a mouse PrP peptide library and full-length recombinant mouse PrP (23-231) as our positive control. Pure selected Fabs that were expressed and purified were then further characterized by epitope mapping to understand the basis of specificity and to determine which PrP residues play a pivotal role in antigen-antibody recognition. In this chapter, I have shown epitopes of selected Fabs (Table 2-1) and provided a detailed characterization of Fab 3 (N-terminus), Fab 69 (shortened N-terminus) and Fab 29 (C-terminus) (Figure 2-3.A-C). We employed a 12-mer mouse PrP peptide library, spanning residues 23-231 (peptides 1 – 26), with 4 overlapping residues to the adjacent peptide as described on Table 2.2 for our indirect ELISA epitope mapping. This revealed three select linear epitopes on PrP which could be used to understand the misfolding and pathogenesis of prions between strains and gain insight into the different morphologies observed by immunogold labelling with an electron microscope. The binding of Fab 3 was observed to be peaking to immobilized peptides P1, residues 23 – 34 and full-length recombinant mouse PrP, residues 23-231 (Figure 2-3.A), pointing to the KKRPKG polybasic stretch as its epitope. In addition, Fab 69 showed to have the strongest binding with peptide P9, residues 87 – 98 and a weak signal was observed to the adjacent peptide P10, residues 95 – 106 (Figure 2-3.B). This revealed that Fab 69 strongly interacts with truncated N-terminus residues of PrP, THNQW. Fab 29 recognized the sequence TQYERESQAYYD of peptide P 25, residues 214 – 225 and full-length mouse PrP, 23 – 231 (Figure 2-3.C). This epitope is almost at the C-terminus of PrP, upstream of the GPI anchor at the globular domain region.

Table 2-2: Mouse PrP Peptide Library

Number	ID	Name	N-term	Sequence	C-term	MW(Da)
1	A01	23-34	Btn	Mouse	OH	1665.02
2	B01	31-42	Btn	Mouse	OH	1618.82
3	C01	39-50	Btn	Mouse	OH	1525.73
4	D01	47-58	Btn	Mouse	OH	1699.94
5	E01	55-66	Btn	Mouse	OH	1606.81
6	F01	63-74	Btn	Mouse	OH	1592.78
7	G01	71-82	Btn	Mouse	OH	1622.81
8	H01	79-90	Btn	Mouse	OH	1592.78
9	A02	87-98	Btn	Mouse	OH	1623.8
10	B02	95-106	Btn	Mouse	OH	1804.13
11	C02	103-114	Btn	Mouse	OH	1602.98
12	D02	111-122	Btn	Mouse	OH	1252.5
13	E02	119-130	Btn	Mouse	OH	1432.78
14	F02	127-138	Btn	Mouse	OH	1696.18
15	G02	135-146	Btn	Mouse	OH	1856.14
16	H02	143-154	Btn	Mouse	OH	2079.33
17	A03	151-162	Btn	Mouse	OH	1979.29
18	B03	159-170	Btn	Mouse	OH	1871.12
19	C03	167-178	Btn	Mouse	OH	1808
20	D03	175-186	Btn	Mouse	OH	1746.1
21	E03	183-194	Btn	Mouse	OH	1654
22	F03	191-202	Btn	Mouse	OH	1680.88
23	G03	199-210	Btn	Mouse	OH	1805.18
24	H03	207-218	Btn	Mouse	OH	1823.2
25	A04	215-226	Btn	Mouse	OH	1863.06
26	B04	223-234	Btn	Mouse	OH	1727
Rec PrP				Mouse	6xHis	27000

Table 2-2: Mouse PrP Peptide Library. PrP peptides spanning full-length mouse PrP sequence comprising residues, 23-230. Each linear peptide is 12 amino acids long with 4 overlapping amino acids to the adjacent peptide. The mouse PrP peptide library was used for the epitope mapping of recombinant anti-PrP Fabs to elucidate the antigenic determinants and gain insight into its specificity at the molecular level. A fully folded mouse recombinant prion protein was used as a control. The working concentration of each peptide was 1mg/ml.

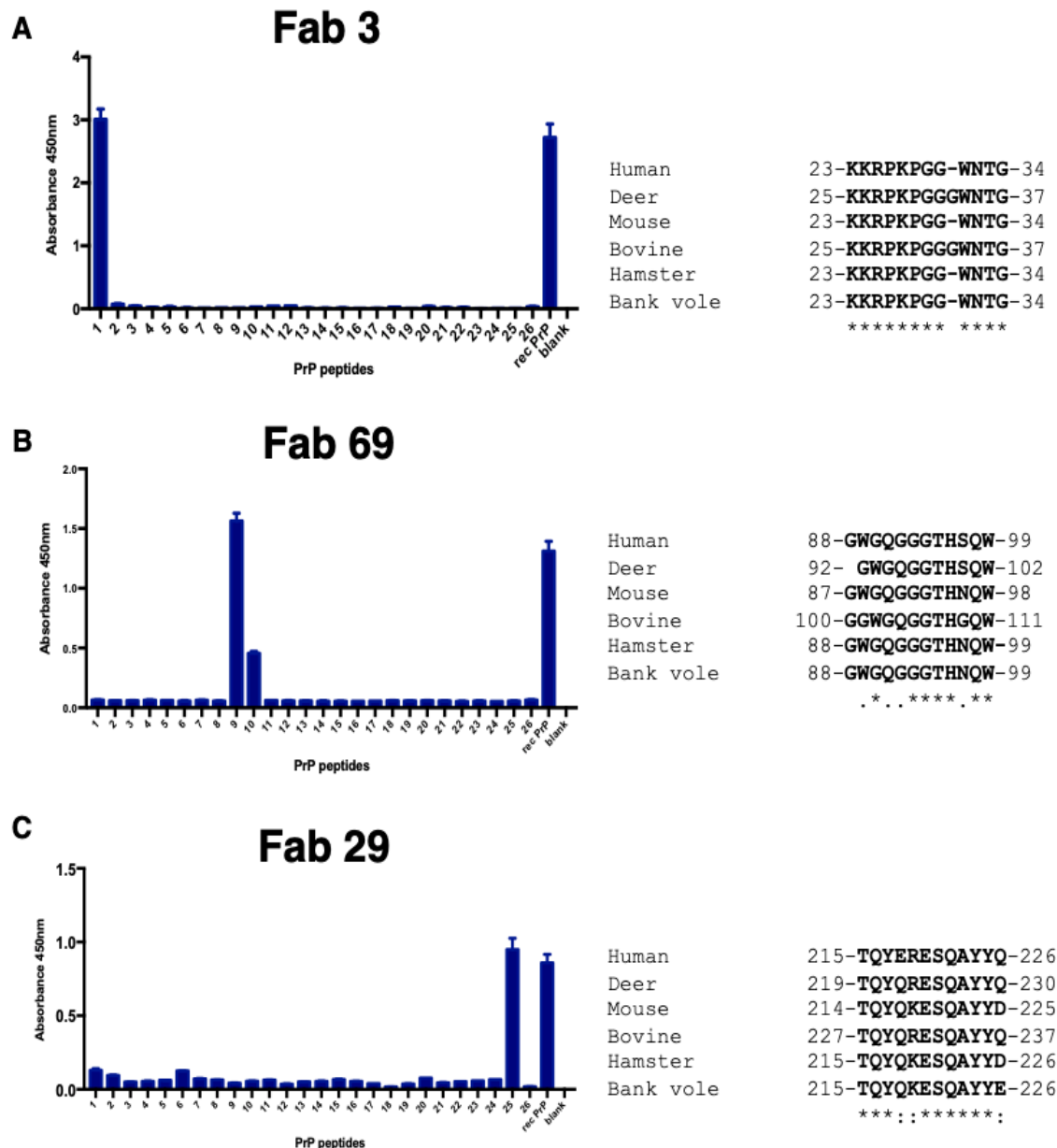


Figure 2-3: Epitope characterization.

Indirect peptide ELISA epitope mapping using an overlapping 12-mer mouse PrP peptide library with recombinant anti-PrP Fabs. To identify linear epitopes, ELISA plates were coated with synthetic overlapping PrP peptides (Table 2-2) that spanned the entire length of PrP (peptides 1 – 26) and fully folded recombinant full-length PrP. ELISA plates were then incubated with Fab fragments and absorbance was read at 450nm (A) Epitope mapping of recombinant Fab 3 revealed the strongest binding with peptide 1, representing amino acid sequence 23 - 34 and FL PrP, 23-

230. **(B)** Epitope mapping of Fab 69 showed the strongest binding to peptide 9, representing amino acid sequence 87 - 98 and FL PrP, 23-230 and **(C)** Fab 29 showed the strongest interaction to peptide 25, representing amino acid sequence 215 – 226 and FL PrP, 23-230. The linear epitope of Fab 3, Fab 69 and Fab 29 are shown and its amino acid sequence similarity with different PrP species.

2.3.5 Epitope confirmation via activity assays

The specificity of the targeted epitope matched the ELISA epitope profiling for all tested Fabs.

The purified Fabs underwent an initial activity assay in a dot blot format to see if they were functional and could detect its antigen both in its native condition and when it was denatured with 2% SDS. Control dot blots were done without incubation with the primary antibody.

Selected Fabs were tested against full-length and truncated recombinant PrP. Fab 3, which recognizes the very N-terminus of PrP showed to bind full-length PrP (23-231) but did not react with truncated PrP (90-230). Whereas, Fabs 69 and 29 reacted with Full length and truncated recombinant PrP since their epitope is at the CC2 region and GD region of PrP, respectively (Figures 2-4.A-B). The PK-resistant core in PrP^{Sc} would also have this Fab 69 and Fab 29 epitope, providing a different method for examining the structural and biochemical properties of prions.

After confirming their activity with recombinant PrP, FL (23-231) and truncated (90-230), we tested the activity of these three Fabs with infectious crude brain homogenates of RML and human GSS^{A117V} prions, which were coated on ELISA plates (Figure 2-4.C).

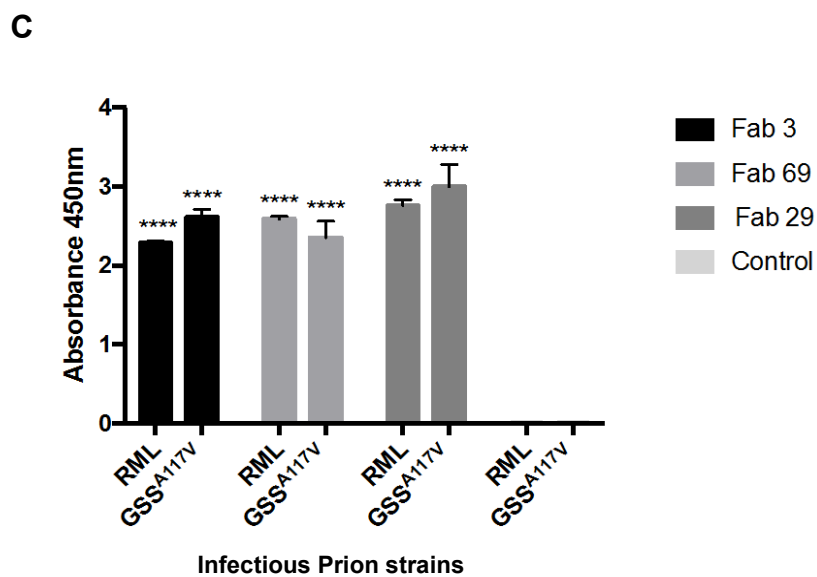
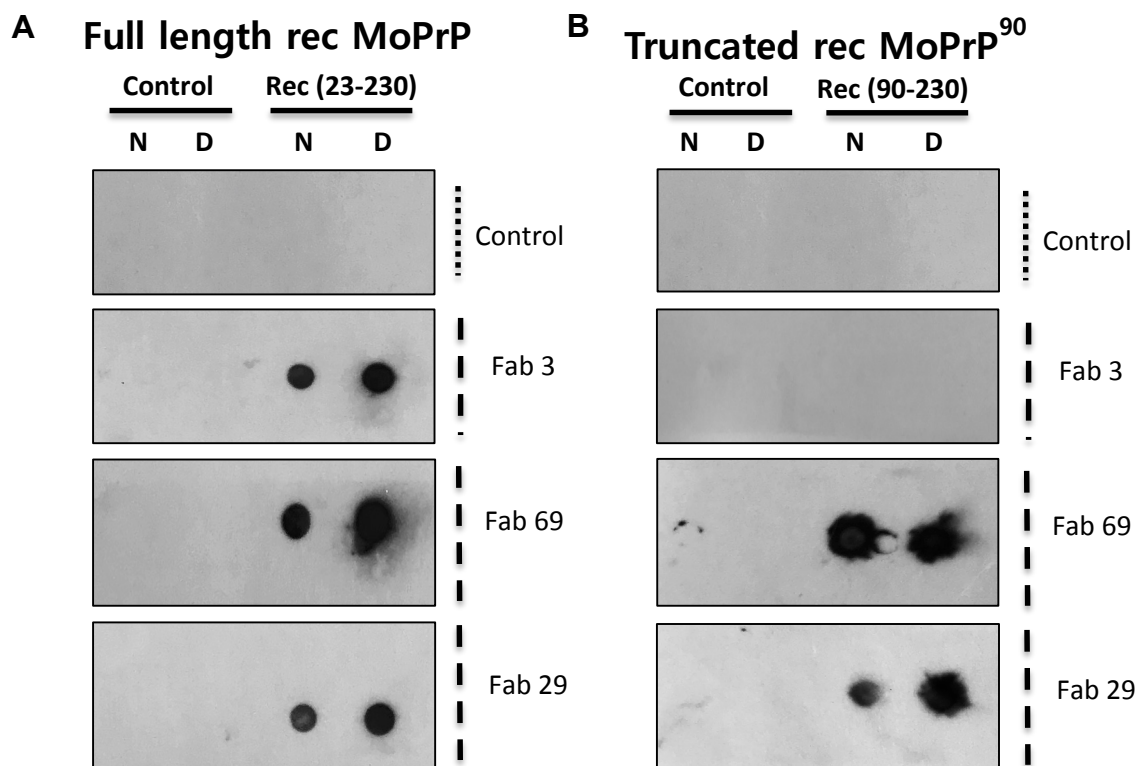


Figure 2-4: Activity Assay.

The fully folded and functional recombinant anti-PrP Fab fragments were tested for their antigen recognition using recombinant PrP and untreated infectious brain homogenate using a Dot Blot and Indirect ELISA assays. Dot blot results show the binding activity of the functional Fab 3₍₂₃₋₃₄₎, Fab 69₍₈₇₋₉₈₎, Fab 29₍₂₁₄₋₂₂₅₎ to **(A)** native and 2% SDS denatured recombinant full-length mouse PrP (23-230), **(B)** native and 2% SDS denatured recombinant truncated mouse PrP (90-230). Control dot blot was only incubated with the secondary anti-human Fab antibody conjugated to HRP **(C)** Functional recombinant PrP Fabs 3₍₂₃₋₃₄₎, 69₍₈₇₋₉₈₎ and 29₍₂₁₄₋₂₂₅₎ were screened in an ELISA assay against untreated infectious RML brain homogenate and human GSS^{A117V} cortex brain homogenate and measurements at OD450 for all infectious prion isolates were higher compared to the control samples which was only incubated with the secondary anti-human Fab antibody. The results shown by the ELISA assays are statistically significant with $p < 0.0001$ for RML and $p = 0.0003$ for GSS-A117V samples using an Ordinary one-way ANOVA, Dunnett's test.

2.3.5.1 Histoblot analysis using anti-PrP Fabs

I immunostained the histoblots with our recombinant anti-PrP Fabs 3, 69 and 29 along with a PrP^C – specific antibody, to detect surface PrP^C and PrP^{Sc} from coronal brain sections of Tga20a uninfected brain and terminally ill Tga20 mice inoculated with RML prions (Figure 2-5.A-H). Our lab has a PrP^C - specific monoclonal antibody, C2-6 which was used in this study. Using this antibody, we see a strong signal of PrP^C accumulation at the periphery of uninfected and infected brain slices (Figure 2-5.A-B). All these anti-PrP Fab antibodies gave a similar staining pattern in the sections of infected RML mice brains (Figure. 2-5.D, F, H) and uninfected Tga20 mice brains (Figure. 2-5.C, E, G). Surface labelling of PrP^{Sc} and PrP^C from the untreated brain slices showed heavy signals in infected RML brain slices when immunoblotted with Fab 3 recognizing the N-terminus (23-34) CC1 region, Fab 69 recognizing residues 87-98 of CC2 region and Fab 29 recognizing the very C-terminal residues 215-226.

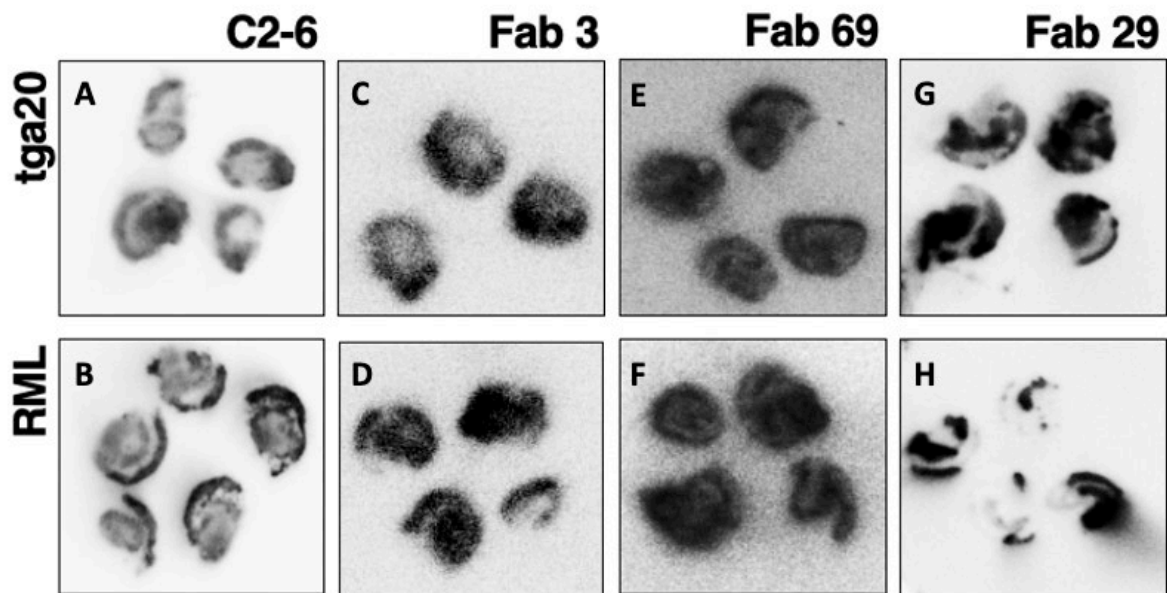


Figure 2-5: Activity assay via Histoblots.

Histoblot analysis shows the anatomical deposition of PrP^C in tga20 (A-D) and PrP^{Sc} in tga20 RML mice brain (E-H). Shown are coronal sections of mouse brain labelled with **(A,B)** PrP^C specific antibody, C2-6, **(C,D)** Fab 3 which targets the very beginning epitope of the CC1 region **(E,F)** Fab 69 which points to CC2 region, and **(G,H)** Fab 29 which targets the very end of the GD. Anti-Mouse HRP secondary antibody used for panels A-B and Anti-Human Fab HRP secondary antibody used for panels C-H.

2.3.5.2 Validation by immunocytochemistry assay

Additionally, utilizing the murine catecholaminergic cell line CAD5 and CAD5 infected with RML prions, I assessed a panel of anti-PrP Fabs' capacity to bind to surface exposed PrP^C and PrP^{Sc} by immunocytochemistry assay and performing Z-stacks on each sample (Z-stack data not shown). The methanol-fixed and semi-permeabilized CAD cells were immunolabelled with Fabs 3, 69 and 29, and examined using immunofluorescence confocal microscopy. In comparison to uninfected CAD5 cells expressing murine WT-PrP^C, Fab 3, Fab 69, and Fab 29 recognized RML-infected CAD 5 cells with high fluorescence intensity as they show labelling to both, PrP^C and PrP^{Sc} (Figure 2-7 and Figure 2-8).

Uninfected CAD 5 Cells

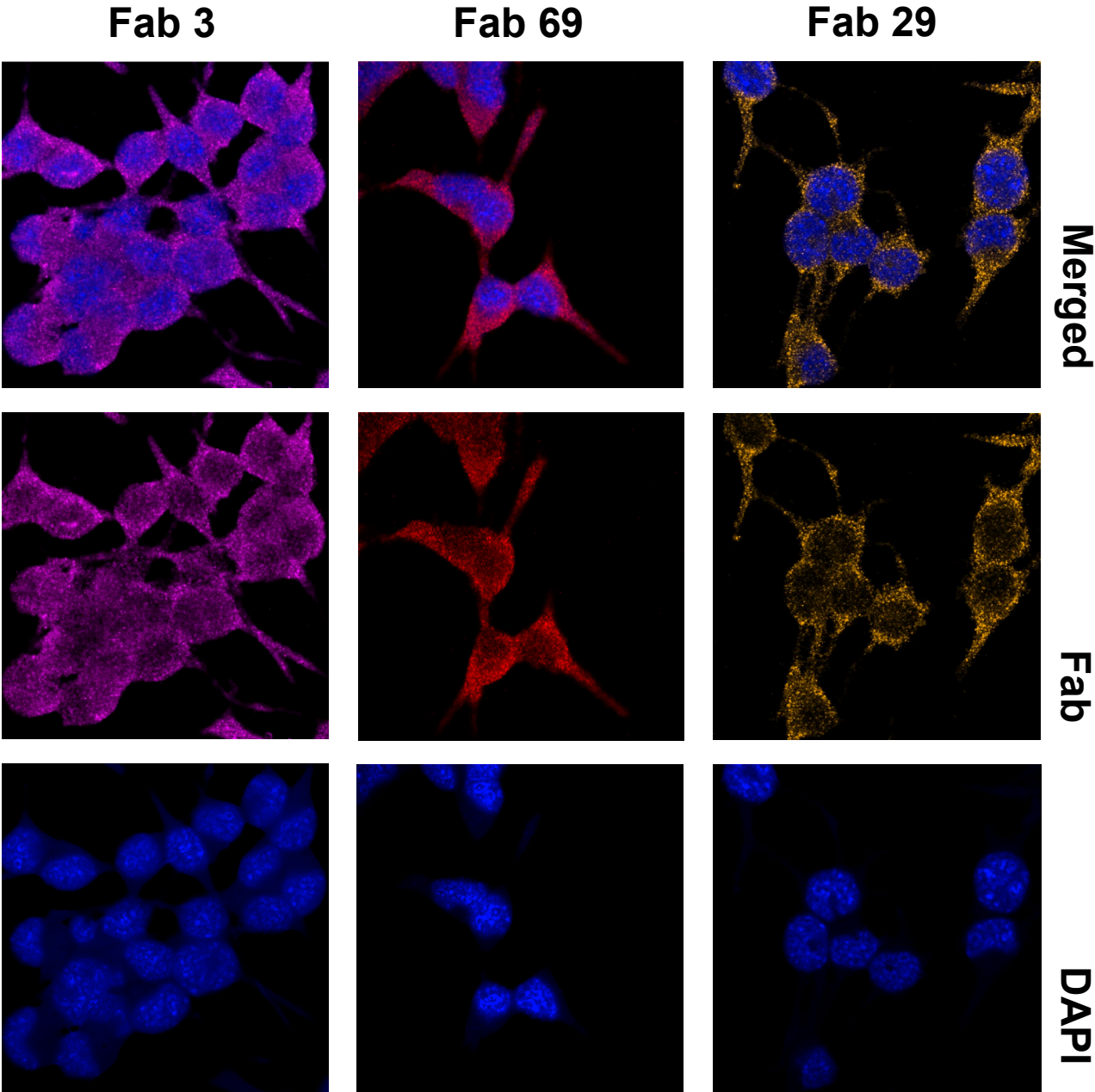


Figure 2-6: Immunocytochemistry of uninfected CAD 5 cells using humanized recombinant anti-PrP Fabs.

Representative immunofluorescence images of methanol-fixed permeabilized uninfected CAD 5 cells with humanized recombinant anti-PrP Fab fragments. We see cell surface labelling of full-length PrP^C with a more diffuse punctae-like form when labelled with **(A)** anti-PrP Fab 3 antibody (purple) that recognizes the polybasic stretch at the very N-terminus within residues 23-34 **(B)** anti-PrP Fab 69 (red) that recognizes residues at the truncated N-terminus within residues 87-98 and **(C)** anti-PrP Fab 29 (gold) recognizing residues 215-226 at the C-terminus of the mouse prion protein. All cells were counterstained with DAPI (blue). Secondary antibody used is anti-human Fab conjugated to AlexaFluor 647. The cells were visualized by confocal laser scanning microscopy. Scale bar = 10 μ M (applied to all images). The cells were cultured by Grant Norman.

RML infected CAD 5 Cells

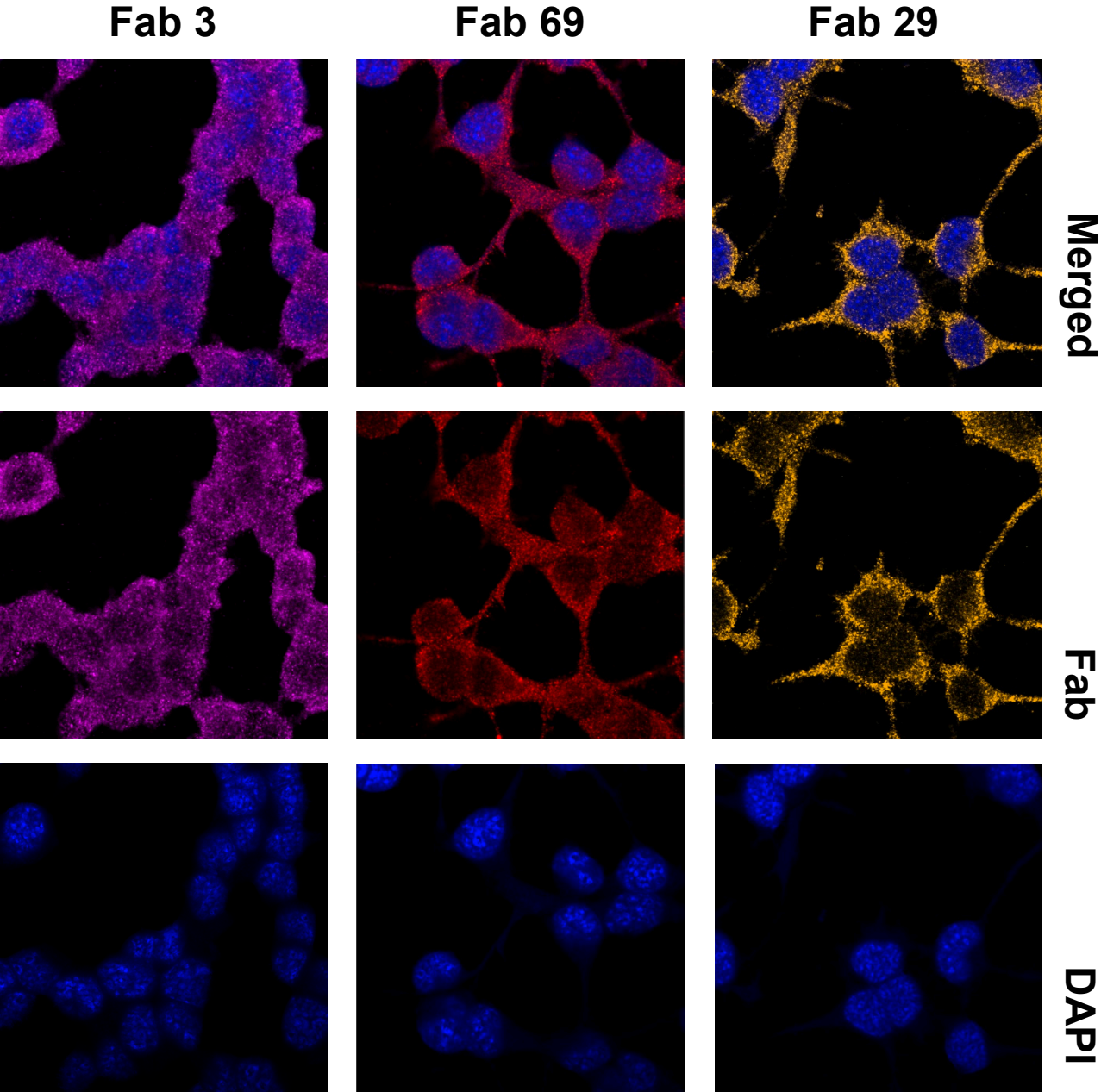


Figure 2-7: Immunocytochemistry of RML infected CAD 5 cells using humanized recombinant anti-PrP Fabs.

Representative immunofluorescence images of methanol-fixed and permeabilized CAD 5 cells infected with RML prions using humanized recombinant anti-PrP Fab fragments. We see an increased fluorescent intensity compared to the uninfected CAD 5 cells, showing labelling of both PrP^C and PrP^{Sc} which is observed in a punctae-like form when labelled with (A) anti-PrP Fab 3 antibody (purple) that recognizes the polybasic stretch at the very N-terminus within residues 23-34 (B) anti-PrP Fab 69 (red) that recognizes residues at the truncated N-terminus within residues 87-98 and (C) anti-PrP Fab 29 (gold) recognizing residues 215-226 at the C-terminus of the mouse prion protein. All cells were counterstained with DAPI (blue). Secondary antibody used is anti-human Fab conjugated to AlexaFluor 647. The cells were visualized by confocal laser scanning microscopy. Scale bar = 10 μ M (applied to all images). The cells were cultured by Grant Norman.

2.3.6 Isolation of RML prions

I then decided to further characterize the selected recombinant and humanized anti-PrP Fab 3, Fab 69 and Fab 29 using immunogold labelling and electron microscopy in order to gain insight into the PrP^{Sc} structure and strain diversity, based on the orientation of the epitopes. I isolated proteinase-resistant PrP^{Sc} from mouse brains with murine-adapted scrapie strain, RML (Wille, Shanmugam, et al., 2009). Additionally, PTA was used in the purification process because studies have shown that it makes it easier to selectively precipitate PrP^{Sc} than PrP^C (Safar et al., 1998; Wille, Shanmugam, et al., 2009). After PTA purification of the RML prions, silver stain and western blot was performed to assess the quality and purity of the sample. I observed signals in the pellet fraction but no protein was found in the supernatant fraction, indicating the samples were of the appropriate purity (Figure 2-8.A). Samples obtained during the purification were

immunoblotted with anti-PrP mAb POM17 and the final pellet (Pellet 2/P2) revealed the characteristic three bands representing un-, mono-, and diglycosylated PrP 27-30 (Figure 2-8.B).

In my study I was interested in labelling RML fibrils with the selected anti-PrP Fabs via immunogold labelling and electron microscopy, we decided to improve the purification process by employing a sucrose step-gradient centrifugation to eliminate superfluous lipids and get a better view of the fibril structure when immunolabelled with our anti-PrP Fabs. For this, a sucrose gradient column (40 percent and 80 percent sucrose) was loaded with the semi-purified P1 pellet from the PTA purification (Figure 2.10.A). This column separates the prion protein from the lipid components and PTA according to their densities. With 1.1 g/ml and 1.4 g/ml solution densities, respectively, the prion protein with a density of 1.2 g/ml was predicted to migrate to the interface between 40 and 80 percent sucrose (Levine et al., 2015). Fractions were taken from the top after ultracentrifugation and subjected to immunoblotting analysis with recombinant Fab 69 (Figure 2-10.B). The top fractions showed strong PrP 27-30 signals and the interface fractions (D), however, PrP 27-30 signal is observed in all fractions. This shows that the RML strain is heterogeneous and has a higher concentration of non-fibrillar aggregates (Bett et al., 2013), whereas the L-type BSE PrP^{Sc} strain has a strong signal in the pellet wash fraction because it naturally forms long fibrillar aggregates in the brain (Kamali-Jamil et al., 2021). The bottom fraction which was the RML pellet wash (H) was used for our immunogold labelling experiments.

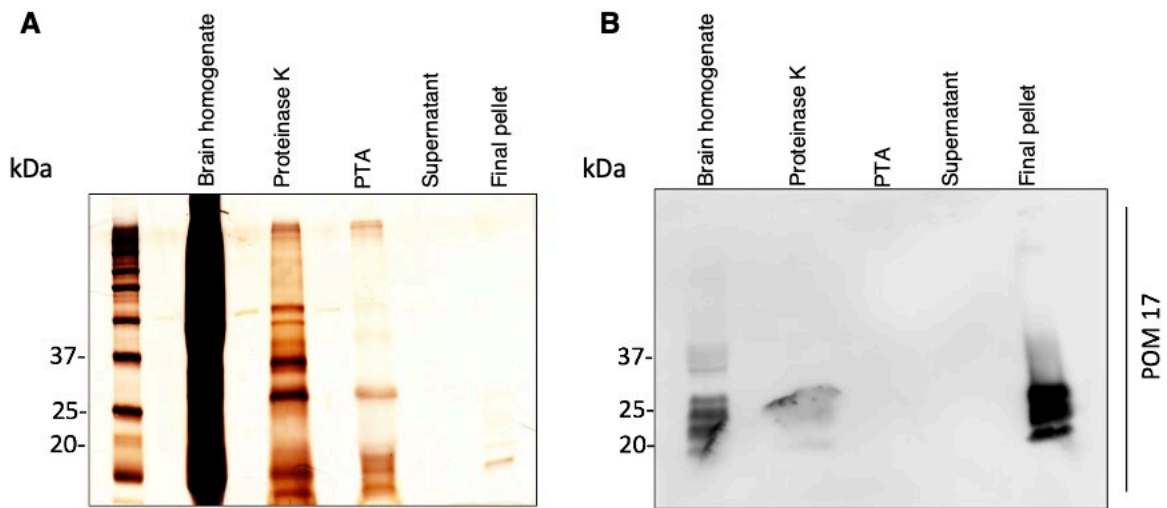


Figure 2-8: Purification of RML Prions.

(A) Silver stain SDS-PAGE gel of samples collected at different steps of RML PTA purification. (B) Western blot of RML prion purification samples using POM 17 anti-prion monoclonal antibody that has an epitope reactivity to helix region of PrP, 144-154. The final pellet shows the typical three bands of the RML prion protein corresponding to di-, mono- and un-glycosylated forms.

2.3.7 The activity of anti-PrP Fabs towards prions

The selected three antibodies with linear epitopes, Fab 3₍₂₃₋₃₄₎, Fab 69₍₈₉₋₉₈₎ and Fab 29₍₂₁₄₋₂₂₅₎ were assessed for their activity under denaturing conditions via western blots (Figure 2-9 A-C). Proteinase K digestion is often used for the diagnosis of prions (PrP^{Sc}), and a method used to eliminate PrP^C (Leffers et al., 2005; Prusiner, 1982). The PK-resistant core spans from residue 90-230, PrP 27-30, which indicates that Fab 3 will not be able to recognize the final pellet as the epitope will be digested upon PK treatment but Fab 69 (Figure 2-9.B) and Fab 29 which are observed in the globular domain will be able to recognize the final pellet. An interesting result was observed when immunoblotted with Fab 29 (Figure 2-9.C), in that it did not recognize the final pellet, suggesting that upon PK treatment there was C-terminal PrP cleavage which resulted in epitope loss, hindering Fab 29 binding. These results are more frequently observed with C-terminal PrP antibodies and have shown not to work in a western blot format (Peretz et al., 1997; Williamson et al., 1998). Fab 69 was also immunoblotted with L-type BSE prions which were also PK digested and PTA purified (Kamali-Jamil et al., 2021). Due to the use of PTA, which enriches PrP^{Sc} (Wille, Shanmugam, et al., 2009), and accessibility of the epitope following PK digestion, I observed a strong signal of un-, mono-, and diglycosylated bands at the final pellet compared to the brain homogenate (Figure 2-9 D).

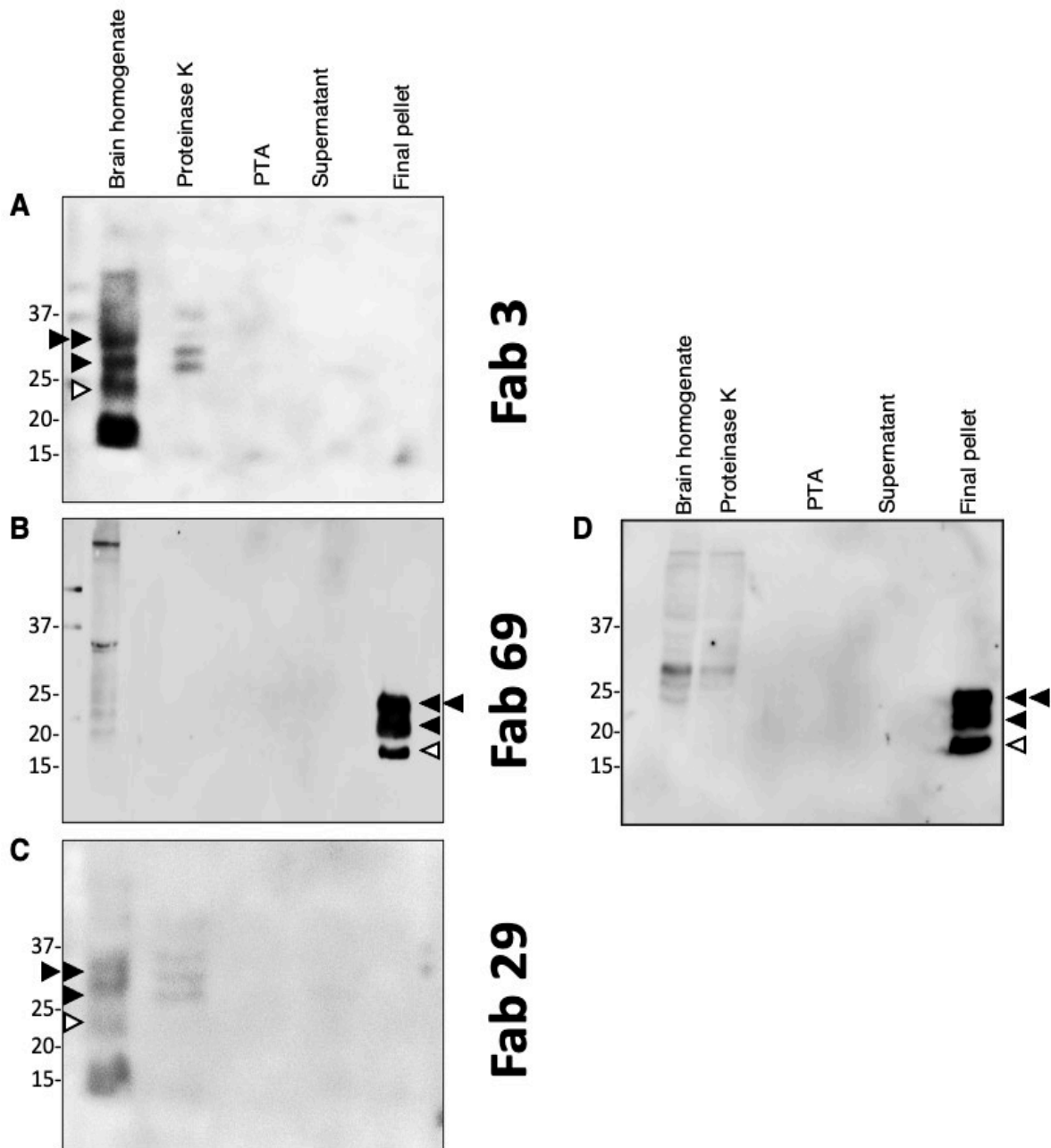


Figure 2-9: Immunoreactivity of recombinant anti-PrP Fabs using purified Prions.

Western blot analysis showing relative immunoreactivities of recombinant anti-prion Fab fragments based on its select epitopes; N-terminal₍₂₃₋₃₄₎, truncated N-terminal₍₈₉₋₉₈₎ and C-terminal₍₂₁₄₋₂₂₅₎ of the prion protein. Shown here are Western blots of the fractions collected at different PTA purification steps of RML prions which are immunoblotted with Fabs 3, 69 and 29

(A) Anti-PrP Fab 3 binds strongly to the polybasic stretch found at the N-terminus of the prion protein and based on its epitope, the typical three bands of RML prion protein corresponding to di-, mono- and un-glycosylated forms (double arrowhead, single arrowhead and open arrowhead, respectively) are seen from the 10% brain homogenate fraction. The Di- and mono- glycosylated bands are observed from PK treated fraction, suggesting incomplete digestion. No bands are detected for the final pellet using Fab 3. **(B, D)** Immunoreactivity of anti-PrP Fab 69 to fraction collected from RML prion purification and L-type BSE prion purification. To both these prion strains, high reactivity using Fab 69 is observed in the final pellet fractions as the epitope is more accessible after the PK treatment. **(C)** A unique banding pattern was observed with anti-PrP Fab 29 that recognizes the C-terminus GD region of PrP. Strong di- and mono- glycosylated bands are observed from the 10% brain homogenate sample and weaker reactivity towards the un-glycosylated band. The final pellet after the PK treatment showed no reactivity to Fab 29. This could be due to the cleavage of the GPI anchor upon PK treatment which results in the loss or truncation of the Fab 29 epitope. All Western blots shown here are from the same prion purification preparation.

2.3.8 Ultrastructure of PTA-Purified RML using electron microscopy

We performed negative stain electron microscopy on all fractions from the PTA purification steps, including pellet 1 (P1), final pellet (P2), and fractions from the sucrose gradient purification, fractions B and H (Pellet wash). Fraction B from the sucrose gradient purification showed to have the strongest signal on the western blot (Figure 2-10.B) and when observed using electron microscopy it showed to have amorphous aggregates, oligomers and only a few intertwined amyloid fibrils were observed in the sample (Figure 2-10.C-F). Electron microscopy analysis of the P1 pellet revealed a dense concentration of fibrillar aggregates, along with some amorphous aggregates and lipid-containing particles, indicating the need for further purification procedures (Figure 2-11. A-D). Negatively stained final pellet (P2) and pellet wash (fraction H) were found to be morphologically heterogenous with amyloid fibrils when studied by EM (Figures. 2-12 and 2-13). Along with single-protofilament fibrils, we saw a significant population of two-protofilament fibrils with helical characteristics. These two-protofilament observations are consistent with earlier studies on the overall structure of the RML fibrils (Sim & Caughey, 2009; Vazquez-Fernandez et al., 2016). These intertwined amyloid fibrils are composed of repeating units of monomeric PrP 27-30 and have a width of ~10nm (C. Terry & Wadsworth, 2019; C. Terry et al., 2016; Vazquez-Fernandez et al., 2016). This observation is not in agreement with the recent brain-derived high-resolution cryo-EM structure of RML prion fibrils revealing a PIRIBS-based structure (S. W. Manka, W. Zhang, et al., 2022). This gives the fibrils a much larger width as each PrP^{Sc} monomer is stacked on top of each other compared to the proposed 4RβS model.

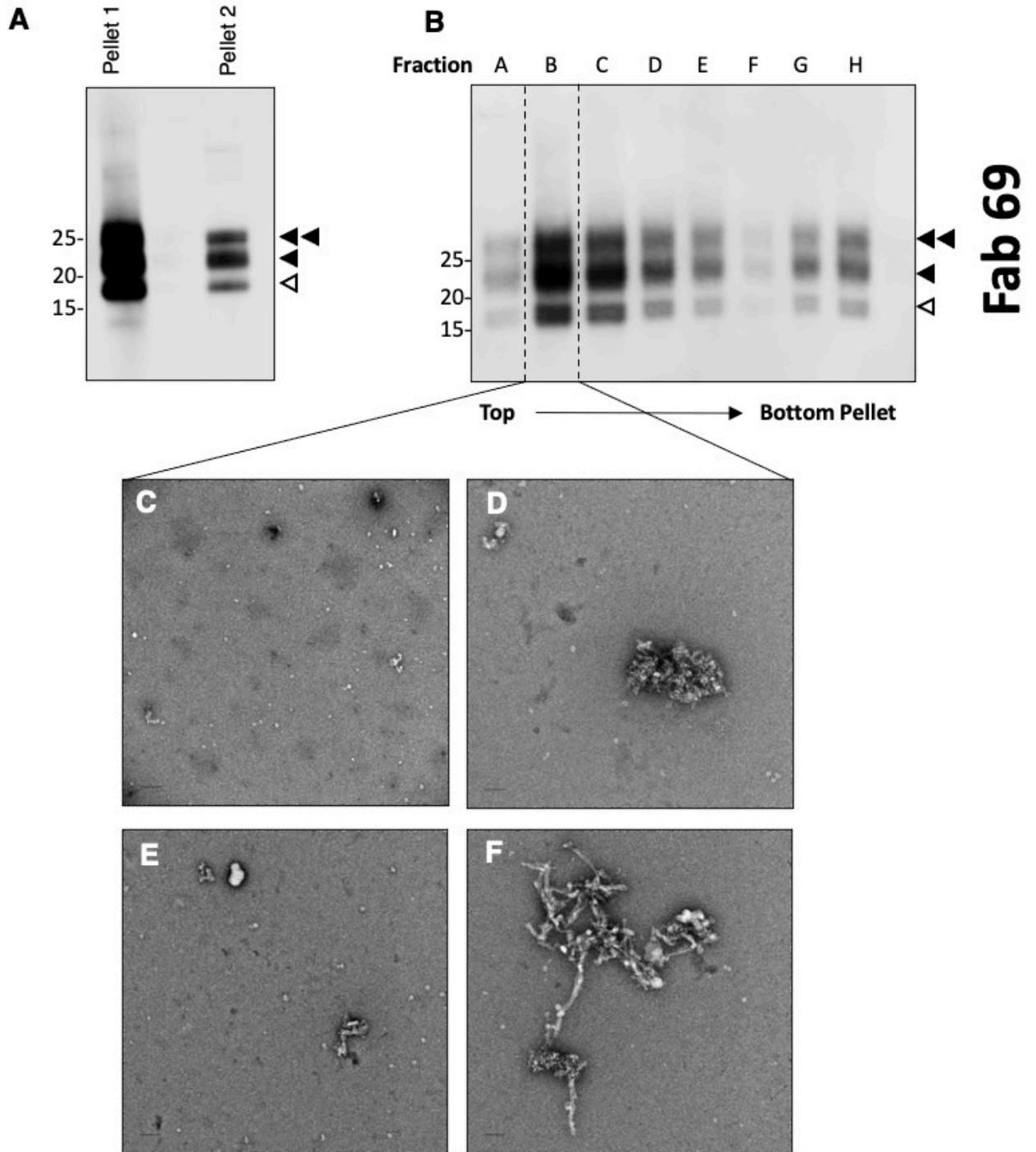


Figure 2-10: Sucrose step gradient purification of RML prions.

(A) Western blot of RML prion purification fractions of PK – digested pellet 1 and pellet 2 (final pellet) show the typical three bands of the RML prion protein corresponding to di- mono- and un-glycosylated forms double arrowhead, single arrowhead and open arrowhead, respectively when immunoblotted with recombinant anti-prion Fab 69. (B) Western blot of the sucrose step gradient fractions. After ultracentrifugation through 40% and 80% sucrose, all fractions were separated based on their densities from the top to bottom (A-G). The pellet wash fraction H was obtained by washing the tube with 100 μ L of sucrose buffer. The western blot was immunoblotted using recombinant anti-prion Fab 69 antibody. Stronger band signals are observed in 40% sucrose, fractions B-D. The di-, mono- and un-glycosylated bands are again indicated by a double arrowhead, single arrowhead, and open arrowhead, respectively. (C-D) Negative stain electron micrographs of sucrose gradient step of top fraction (B) showing heterogeneous morphologies in the fraction. (C) Mostly PrP²⁷⁻³⁰ oligomers and aggregates, (D) Large PrP²⁷⁻³⁰ amorphous aggregates with small oligomers in the background, (E) small oligomers and small aggregates, (F) isolated form of intertwined protofilament fibrils, and fibrillar aggregates. Grids stained with 2% uranyl acetate. Scale bar = 100 nm.

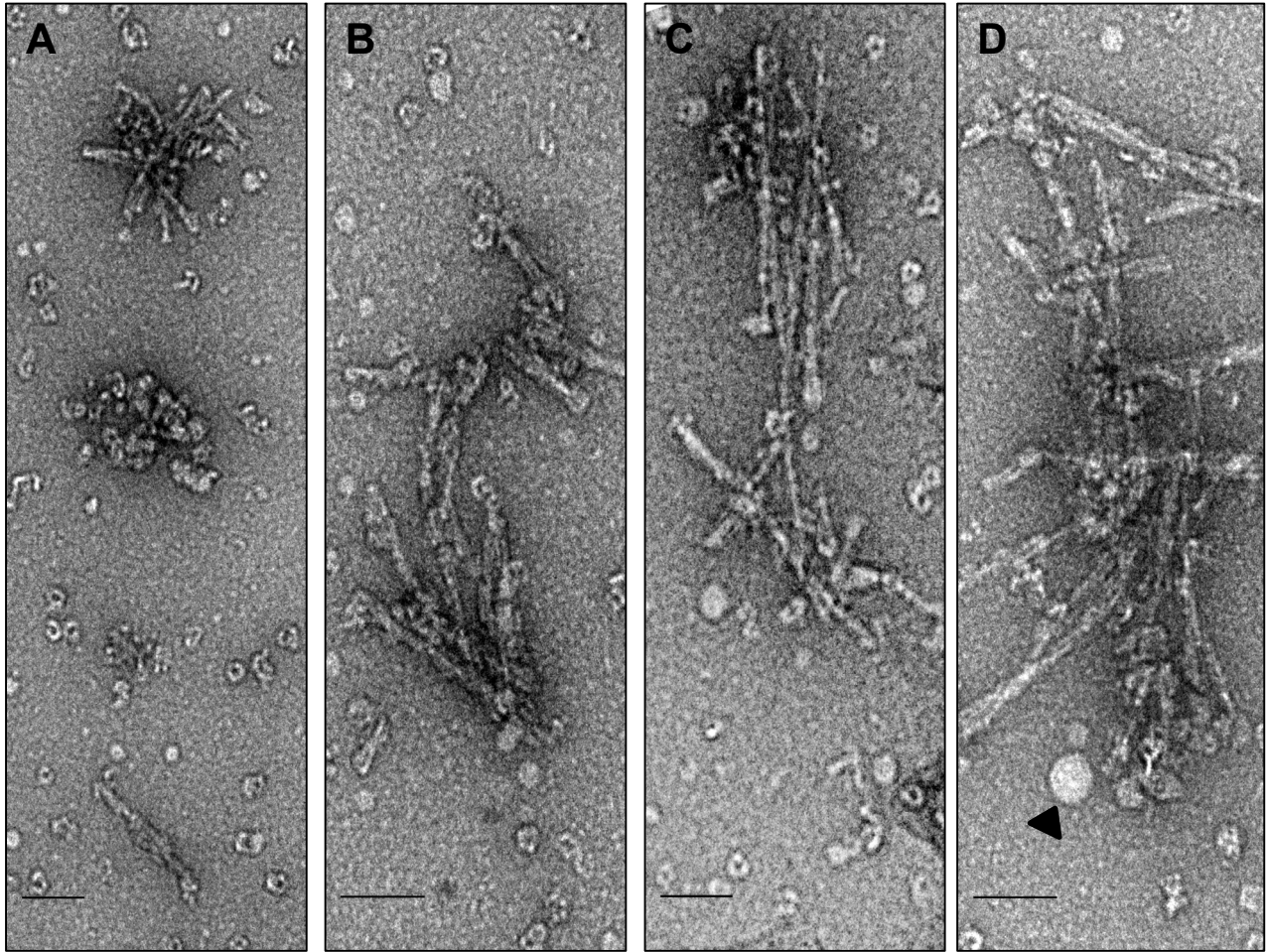


Figure 2-11: Negatively stained electron micrographs of RML Pellet 1.

Representative electron micrographs of pellet 1 RML prion samples showing heterogenous morphologies. **(A)** short aggregated fibrils, oligomers, isolated short protofilament fibril, **(B)** aggregated fibrils, **(C-D)** long aggregated and intertwined fibrils with oligomers in the background. Lipid micelle is shown using black arrowhead. Grids stained with 2% uranyl acetate. Scale bar = 100 nm.

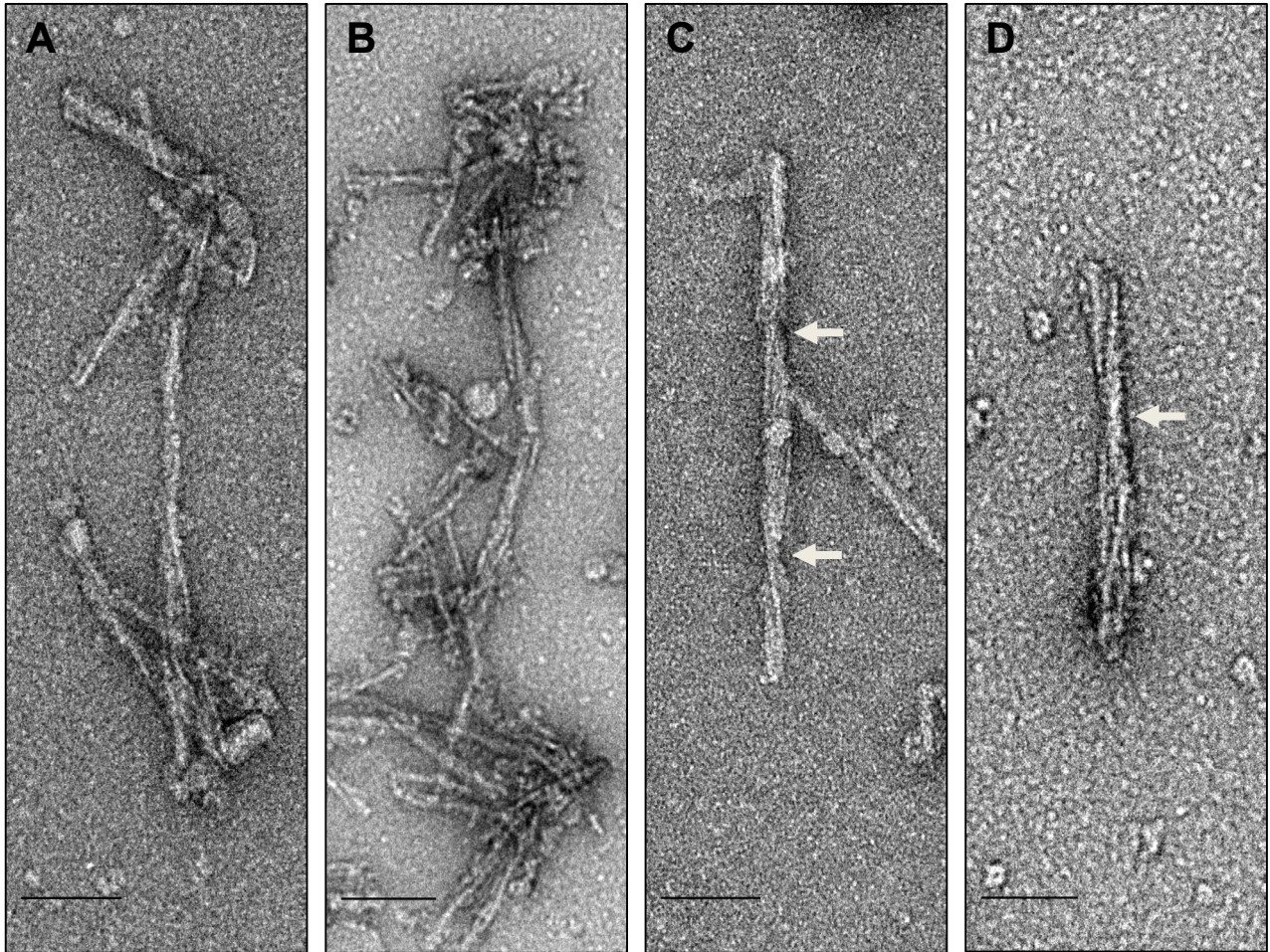


Figure 2-12: Negatively stained electron micrographs of RML Pellet 2.

Representative electron micrographs of pellet 2 RML prion samples showing distinct morphologies. **(A)** intertwined protofilaments, **(B)** aggregated fibrils, **(C-D)** two – protofilament fibrils. The crossover regions for selected two-protofilament fibrils are shown using white arrows. Grids stained with 2% uranyl acetate. Scale bar = 100 nm.

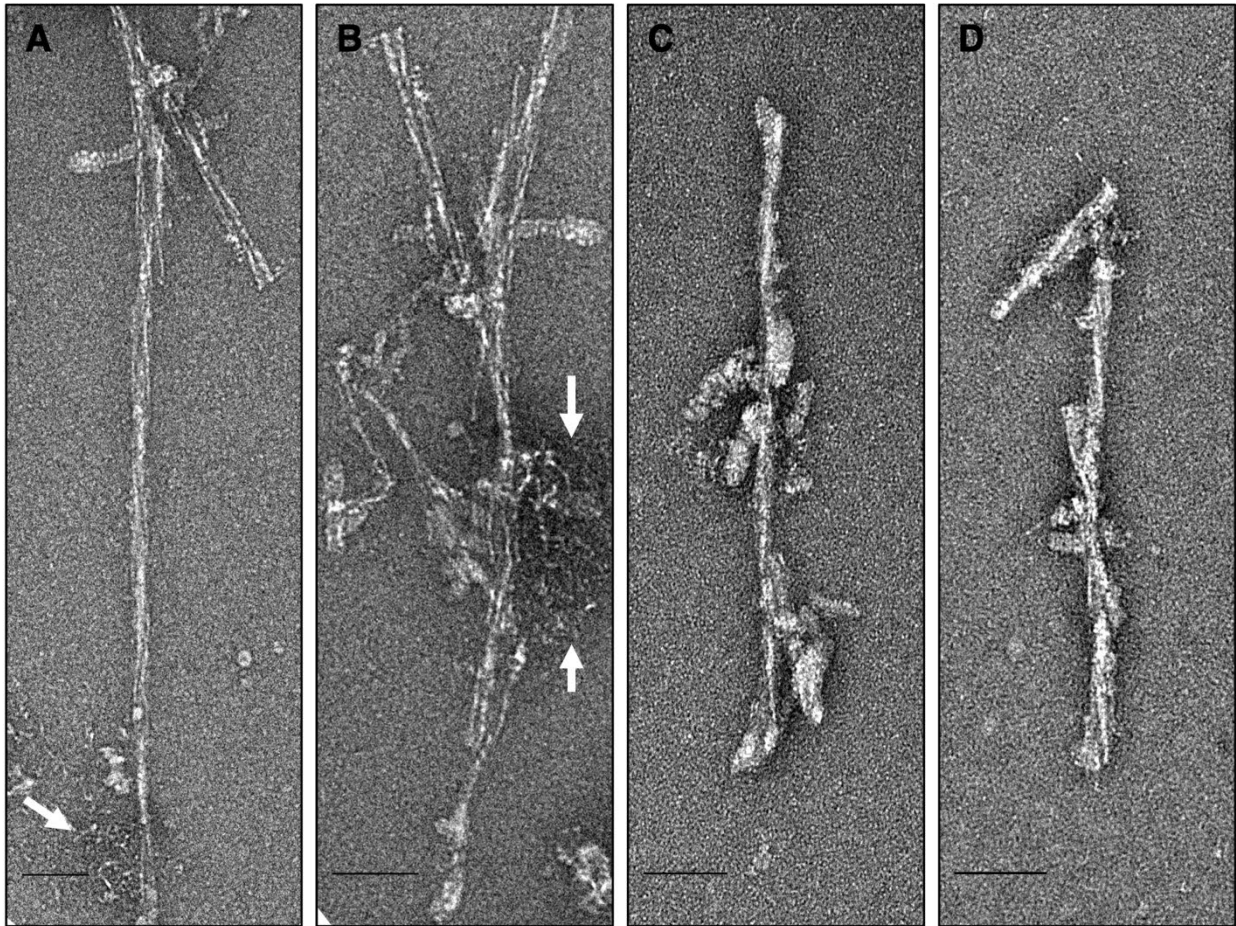


Figure 2-13: Negatively stained electron micrographs of RML Pellet Wash.

Representative electron micrographs of pellet-wash RML prion samples showing distinct morphologies. **(A-B)** two-prot filament fibrils and amorphous aggregates next to the fibrils are shown using the white arrows, **(C-D)** one – prot filament fibrils. Grids stained with 2% uranyl acetate. Scale bar = 100 nm.

2.3.9 Immunogold Labelling of RML, BSE and CWD fibrils using anti-PrP Fabs

We were interested in using an alternate approach to decipher the structure of infectious prion fibrils by using our recombinant anti-PrP Fabs. This would provide us with information on the orientation of the epitopes in these fibrils and verify that the observed morphologies observed by EM are indeed generated by the polymerization of PrP 27-30 monomers. I selected three unique Fabs targeting linear epitopes located at the hotspot regions of the prion protein, covering the full-length 23-230, truncated PrP 27-30 and C-terminal epitopes. Fab 3, which detects an epitope within residues $_{23}\text{KKRPKPGGWNT}_{34}$ located at the polybasic (CC1) region at the very N-terminus of the full-length prion protein, Fab 69, which binds an epitope within residues $_{87}\text{GWGQGGGTHNQW}_{98}$ the truncated N-terminus of prion protein (CC2) and Fab 29 which uncovers an epitope within residues $_{214}\text{TQYQKESQAYYD}_{225}$ near the very C-terminus of the prion protein (GD). Anti-PrP Fab 3 produced the best immunogold labelling when the sample was in its native state, whereas Fab 69 and Fab 29 produced the best immunogold labelling when the purified samples underwent an epitope retrieval step using a denaturing agent, urea, suggesting that these epitopes are less accessible in the native state.

In this chapter I have used semi-purified and sucrose step-gradient purified RML prion fibrils, L-type BSE prion fibrils (Kamali-Jamil et al., 2021) and CWD fibrils (Amidian et al., manuscript in preparation) as shown by the negatively stained electron micrographs (Figure 2-14. A-C) to show the labelling of our recombinant anti-PrP Fabs in different prion fibrils morphology using electron microscopy.

Semi-purified RML fibrils containing full-length PrP^{Sc} were decorated with Fab 3 and PK-digested RML fibrils, PrP 27-30 were decorated with Fab 69 and Fab 29 followed with a secondary anti-human Fab antibody and a tertiary antibody conjugated to 5nm gold particles (Figures 2-15, 2-16 and 2-17. A-C). Control experiments were run in parallel without the use of the primary anti-PrP Fab fragments, which showed no or very rare presence of gold particles, demonstrating the specificity of the immunogold labelling (Figure 2-15, 2-16 and 2-17. D).

In another attempt at immunogold labelling with our recombinant anti-PrP Fabs I used a different animal prion strain, L-type BSE prions. The structure of L-type BSE prions has been previously characterized (Kamali-Jamil et al., 2021) using electron microscopy which showed to have single – and two- protofilament fibrils with a width of ~20nm (Figure 2-14.B) in agreement with the morphologies observed in RML structural studies (Vazquez-Fernandez et al., 2016). Both one- and two-protofilament fibrils of L-type BSE prions were decorated with Fab 69 which detects an epitope within residues ₁₀₀GWGQGGTHGQW₁₁₀ near the N-terminus of truncated bovine PrP 27-30, and Fab 29, which binds an epitope within residues ₂₂₇TQYQRESQAYY₂₃₇ near the very C-terminus of bovine PrP. A secondary anti-Fab antibody and a tertiary antibody bearing 5nm gold particles were used to mark the labelled Fab fragments (Figures 2-18. A-C and 2-19. E-G). In parallel, control experiments without the primary Fab fragments showed no or very little presence of the gold particle, proving the specificity of the immunogold labelling (Figures 2-18.D and 2-19.H).

I employed another animal prion strain, Chronic Wasting Disease (CWD) Prions to broaden the activity and specificity of our recombinant Fabs with various prion isolates. Tg33 Mice expressing deer prion protein were inoculated with CWD prions. CWD prion fibrils were isolated and their morphology and structure were characterized which showed to have multiple

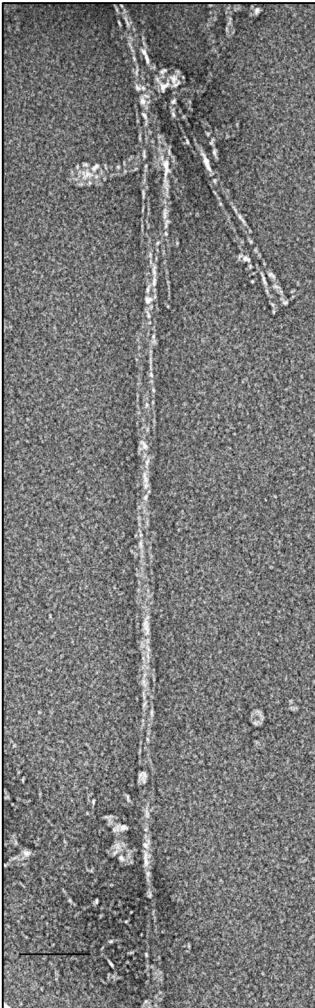
intertwined protofilaments in a fibril with a diameter of ~35nm (Figure 2-14.C) (Amidian et al., manuscript in preparation). We studied the activity of recombinant Fab 3, Fab 69 and Fab 29 with PK-digested and PE-digested purified CWD samples via western blot (data not shown). Fab 3 showed a strong signal with PE-digested samples and no signal was observed in PK-digested samples as expected since the epitope of Fab 3 is within residues 25-37 of the deer prion protein. However, Fab 69 showed the typical three bands, un-, mono- and diglycosylated bands in PE-digested and PK-digested CWD samples since the epitope of Fab 69 is within residues 92-102 of the deer prion protein. Fab 69 also showed a strong banding pattern to the diglycosylated PK-digested CWD sample. Similar results were observed in the RML sample when immunoblotted with Fab 29. Fab 29 has an epitope at the very C-terminus within residues 219-230 of the deer prion protein and it showed a signal for PE-treated samples but not for PK-digested samples which is in agreement with the RML results suggesting loss of epitope after PK cleavage (Kosmac et al., 2011; Peretz et al., 1997). We then confirmed the existence of N- and C-terminus in PE-treated purified CWD fibril via immunogold labelling with Fab 3 that detects the positively charged residues at the very N-terminus within residues $_{25}\text{KKRPKPGGGWNTG}_{37}$ and Fab 29 that has an epitope located upstream of the GPI anchor in the globular domain of the deer prion protein within residues $_{219}\text{TQYQRESQAYYQ}_{230}$ (Figures 2-20 and 2-21. A-B). Fab 3 did not detect PK-digested CWD fibrils but was recognized by Fab 29, this indeed confirms that PK-digested fibrils are composed of multimers of PrP 27-30 monomers and PE-digested are composed of full-length PrP^{Sc} CWD monomers (Figures 2-20 and 2-21.C-D).

A

RML



10 nm

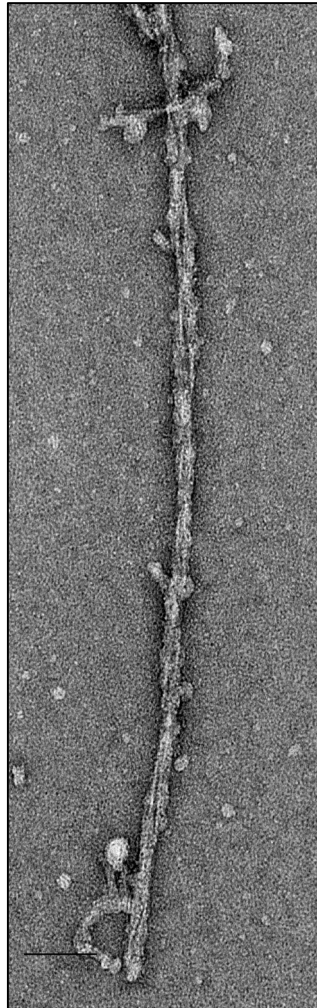


B

BSE - L



20 nm



Dr. Raziieh Kamali Jamil

C

CWD



35 nm



Sara Amidian

Figure 2-14: Negatively stained electron micrographs of Animal Prions.

Different fibrils morphologies shown by the representative 3D reconstructed models and electron micrographs of different animal prions. **(A)** RML prion fibrils, **(B)** L-type BSE prion fibrils, **(C)** CWD prion fibrils. The 3D cross sections of L-BSE and CWD were provided by Dr. Razieh Kamali – Jamil and Sara Amidian, respectively.

Fab 3²³⁻³⁴

Semi Purified RML Prions

RML



10 nm

Fab 3

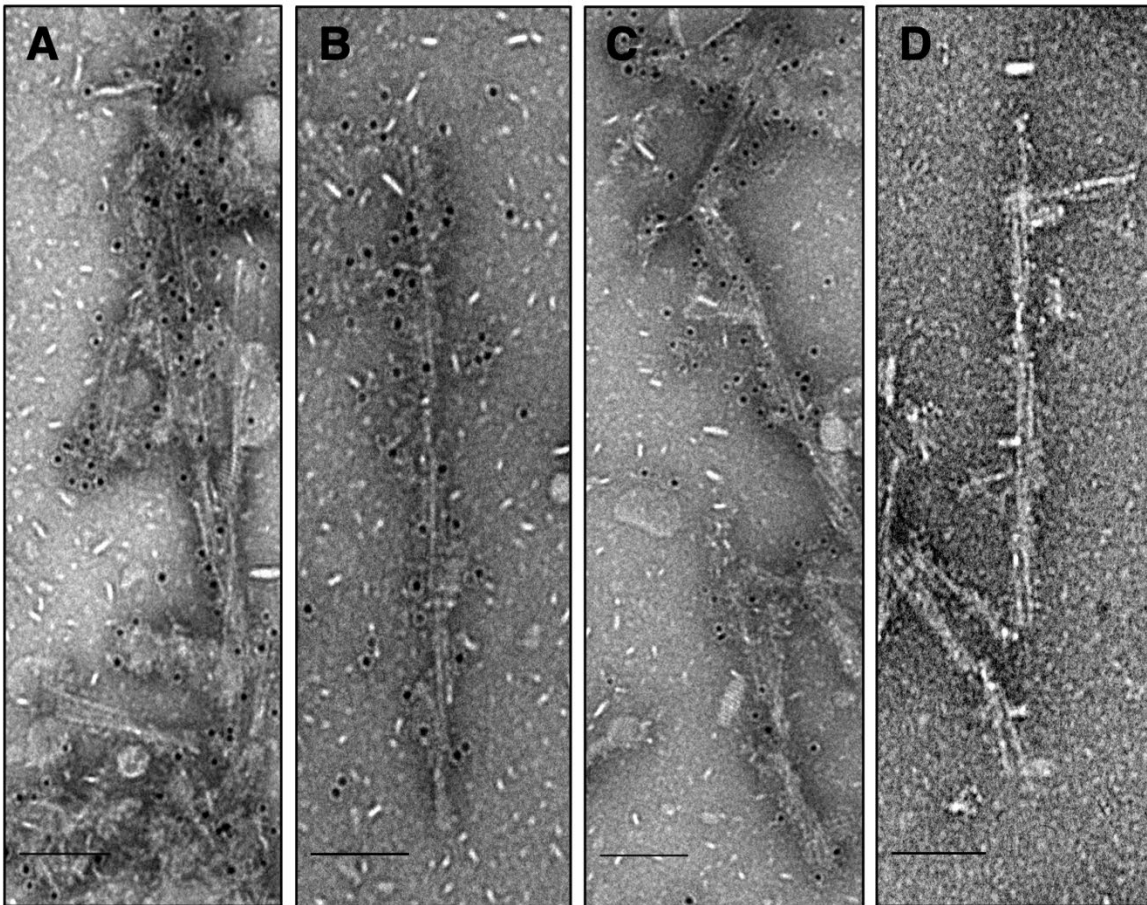
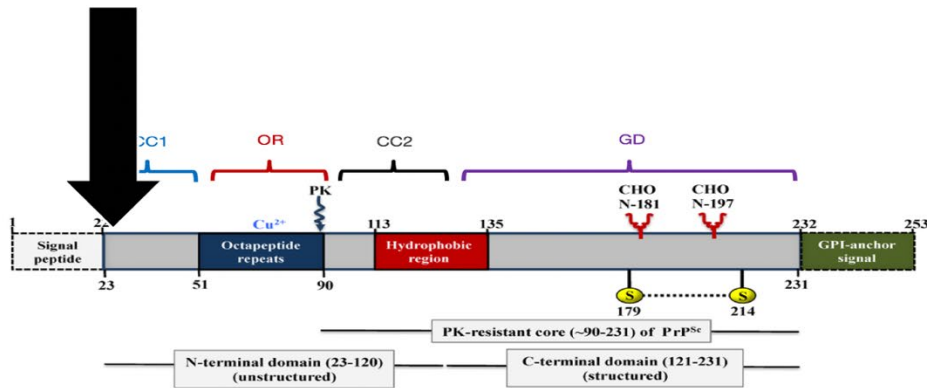


Figure 2-15: Immunogold electron microscopy of semi-purified RML fibrils with recombinant Anti-PrP Fab 3 antibody.

Decoration of semi-purified RML fibrils which includes **(A)** fibrillar aggregate, **(B-C)** two protofilament amyloid fibrils with anti-PrP Fab 3 and a 5nm gold-conjugated ternary detection system. Anti-PrP Fab 3 recognizes an epitope within residues 23 - 34 at the very N-terminal flexible tail, CC1 region of PrP **(D)** No specific labelling was observed in the grids with no primary antibody. Secondary antibody used is goat anti-human fab with tertiary antibody against goat conjugated to 5nm gold. Scale bar = 100 nm.

Fab 69 89-98

PK treated RML Prions

RML



10 nm

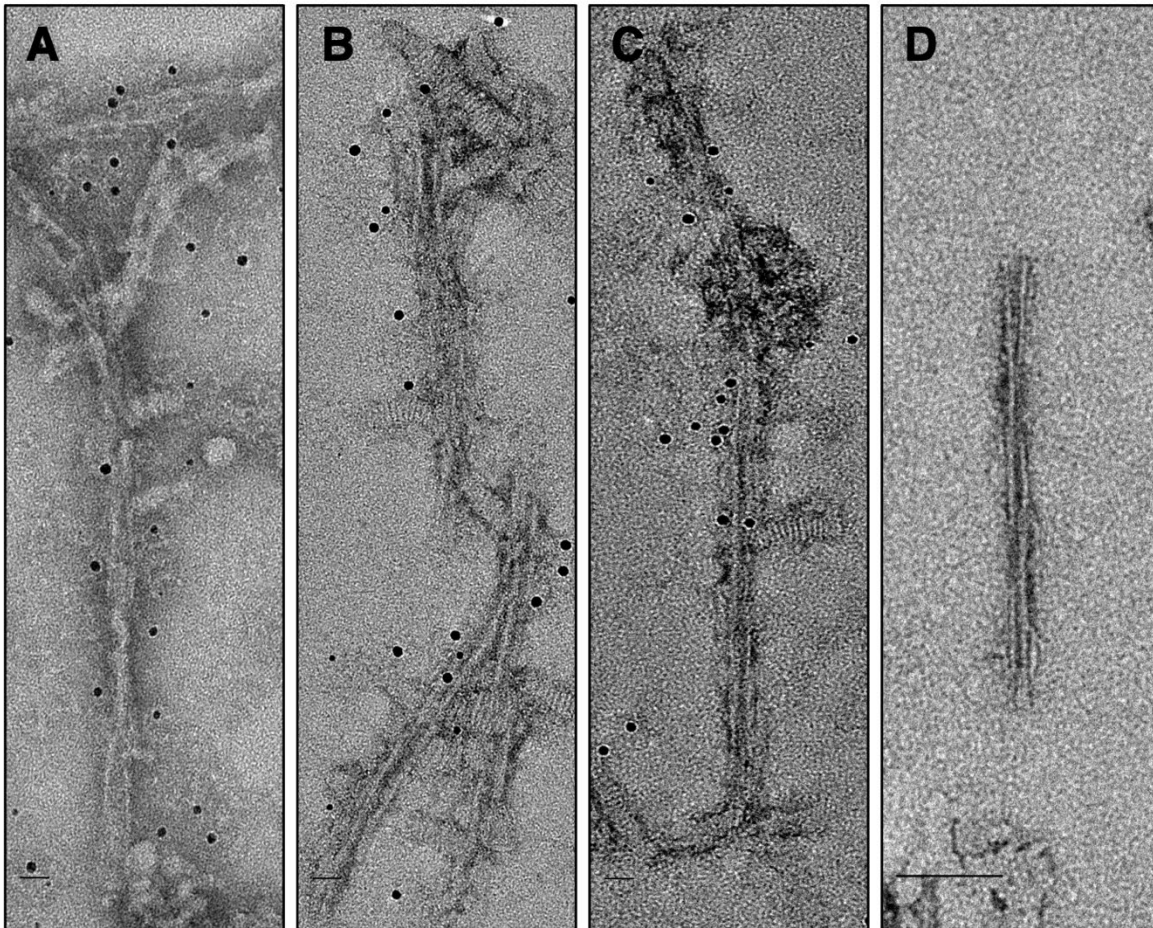
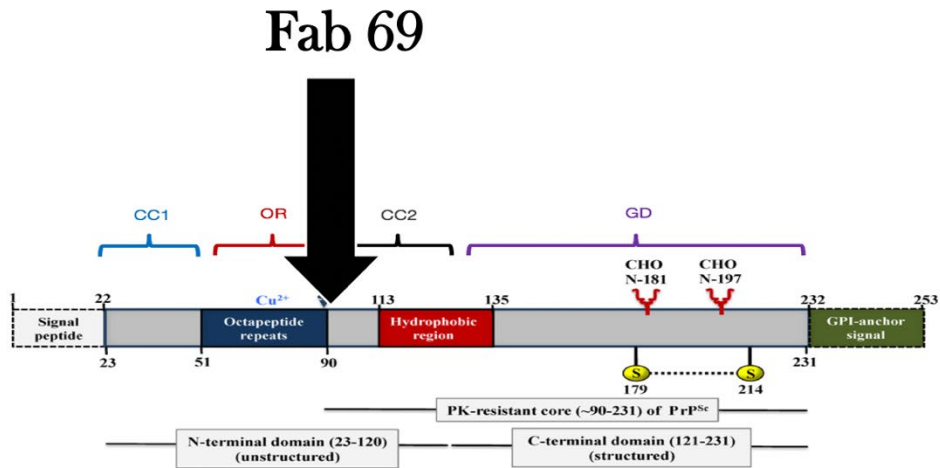


Figure 2-16: Immunogold electron microscopy of semi-purified RML fibrils with recombinant anti-PrP Fab 69 antibody.

Decoration of purified RML fibrils which includes **(A)** fibrillar aggregate, **(B-C)** two- protofilaments fibrils with anti-PrP Fab 69 and a 5nm gold conjugated ternary detection system. Anti-PrP Fab 69 has an epitope between residues 87 and 98 at the CC2 region of PrP. **(D)** No specific labelling was observed in the grids with no primary antibody. Scale bar = 100 nm.

Fab 29 214-225

PK treated RML Prions

RML



10 nm

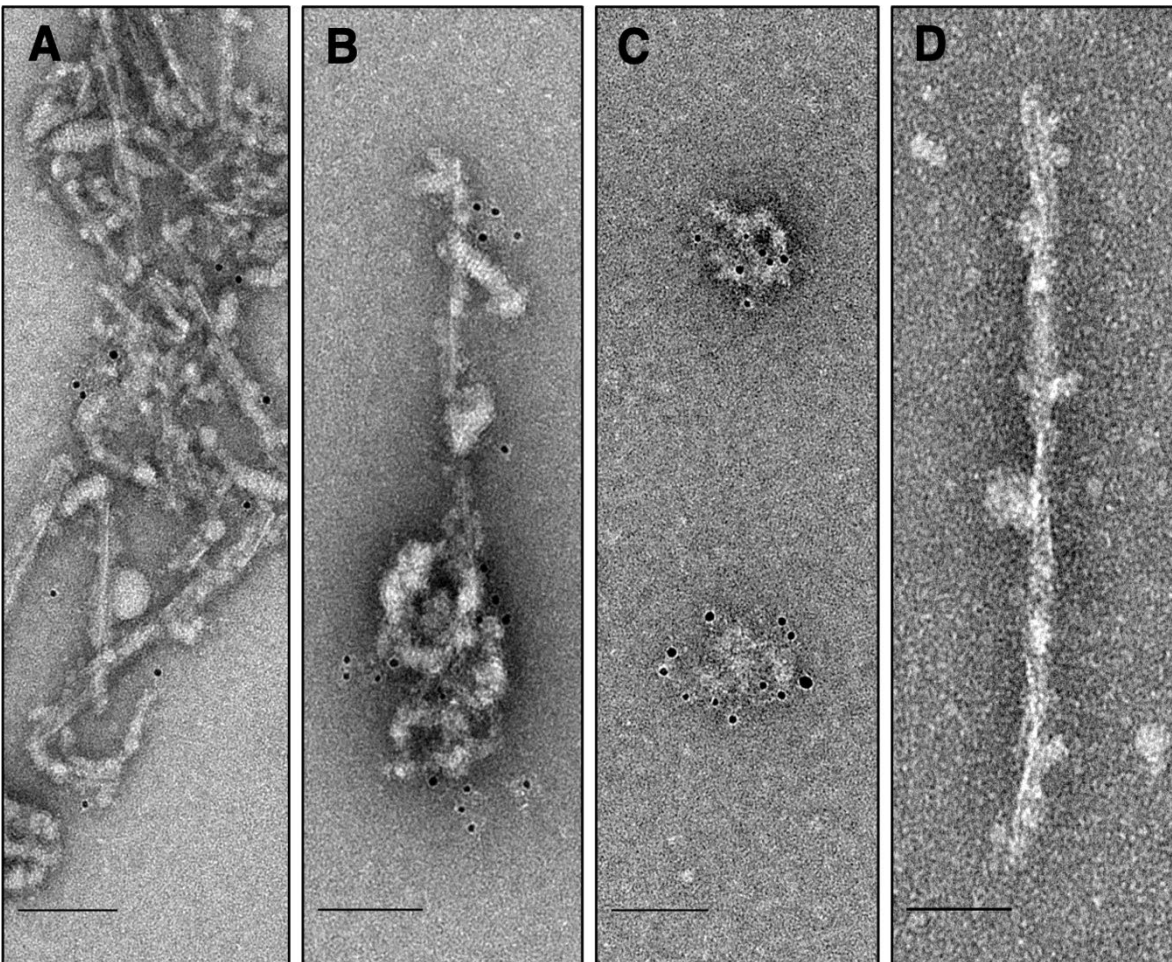
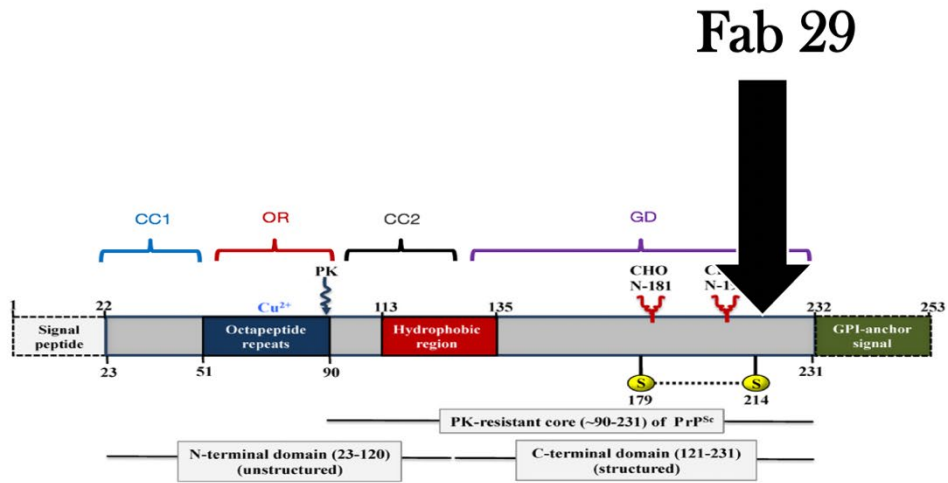


Figure 2-17: Immunogold electron microscopy of semi-purified RML fibrils with Anti-PrP Fab 29 antibody.

Decoration of purified RML fibrils which includes **(A)** fibrillar aggregate, **(B)** oligomeric aggregate and one-protofilament fibril and **(C)** large amyloid aggregates with anti-PrP Fab 29 and a 5nm gold conjugated ternary detection system. Anti-PrP Fab 29 has an epitope between residues 214 and 225 at the GD region of PrP. **(D)** No specific labelling was observed in the grids with no primary antibody. Scale bar = 100 nm

Fab 69 100-110

PK treated BSE-L Prions

BSE - L



20 nm

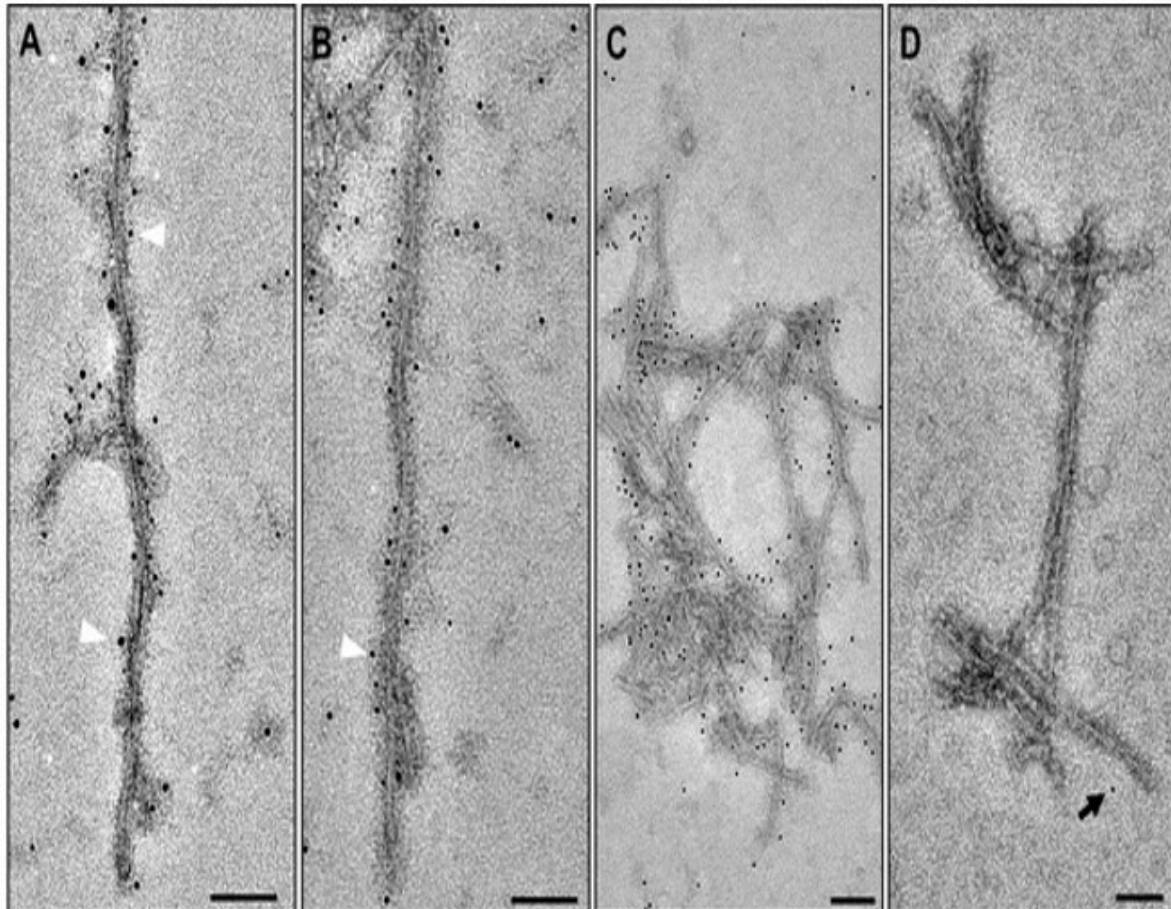
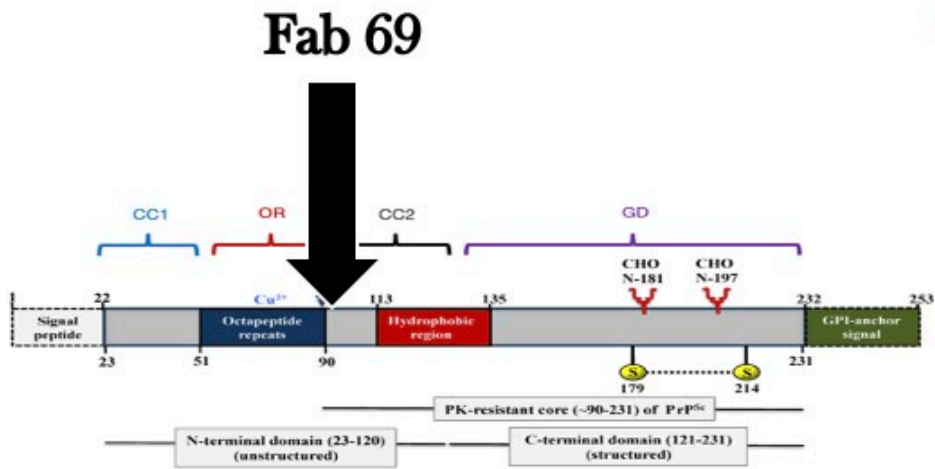


Figure 2-18: Immunogold electron microscopy of purified L-type BSE fibrils with Anti-PrP Fab 69 antibody.

Decoration of different fibrillar assemblies, including **(A)** two-protofilament, **(B)** one- protofilament, and **(C)** fibrillar aggregates, with Fab 69 and a 5nm gold – conjugated ternary detection system. White arrowheads highlight a few gold particles along the fibrils. **(D)** Grids that were incubated without primary antibody showed only rare gold particles (black arrow), demonstrating the specificity of the Fab 69 labeling. Scale bar = 100 nm.

Fab 29²²⁷⁻²³⁷

PK treated BSE-L Prions

BSE - L

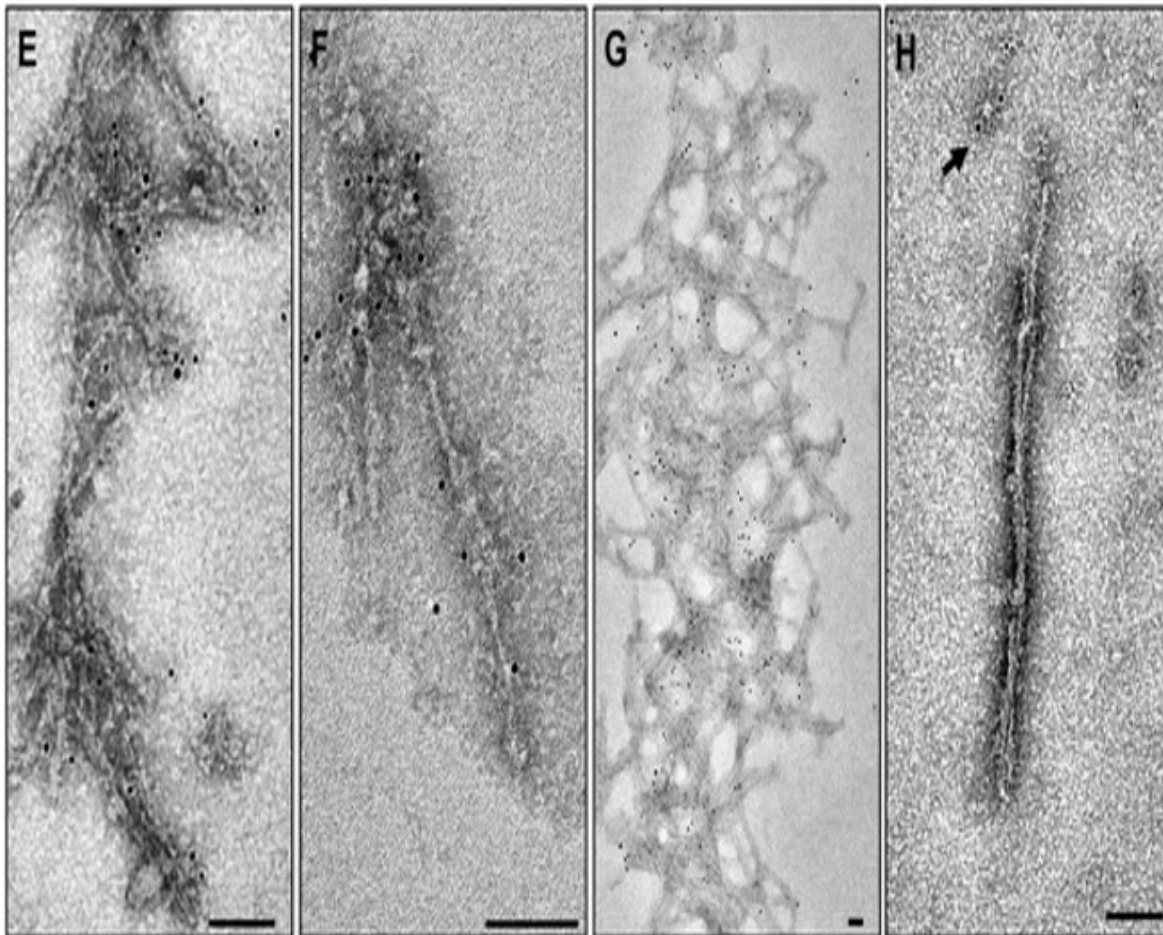
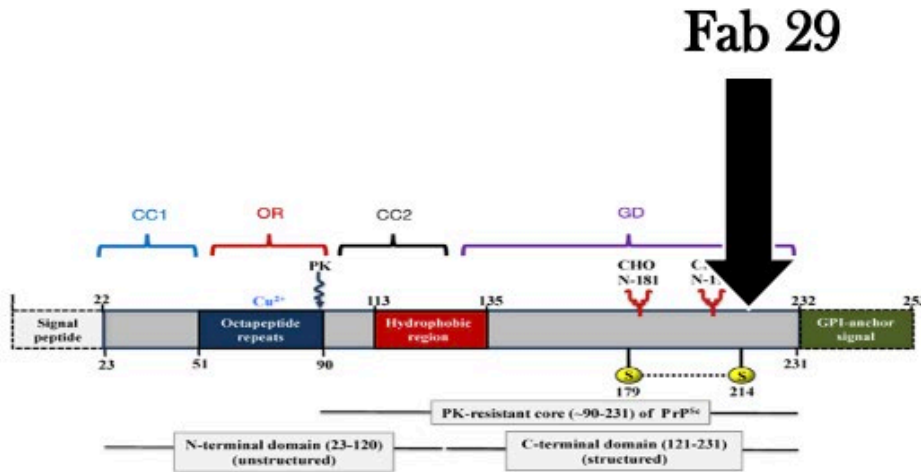
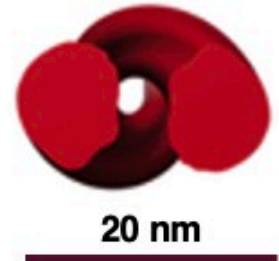


Figure 2-19: Immunogold electron microscopy of purified L-type BSE fibrils with Anti-Prion Fab 29 antibody.

Immunogold labeling of **(E)** two-protofilament, **(F)** one-protofilament, and **(G)** aggregates of L-type BSE fibrils with Fab 29 and a 5 nm gold conjugated ternary detection system. **(H)** No specific labeling was observed in the grids with no primary antibody. Scale bar = 100 nm.

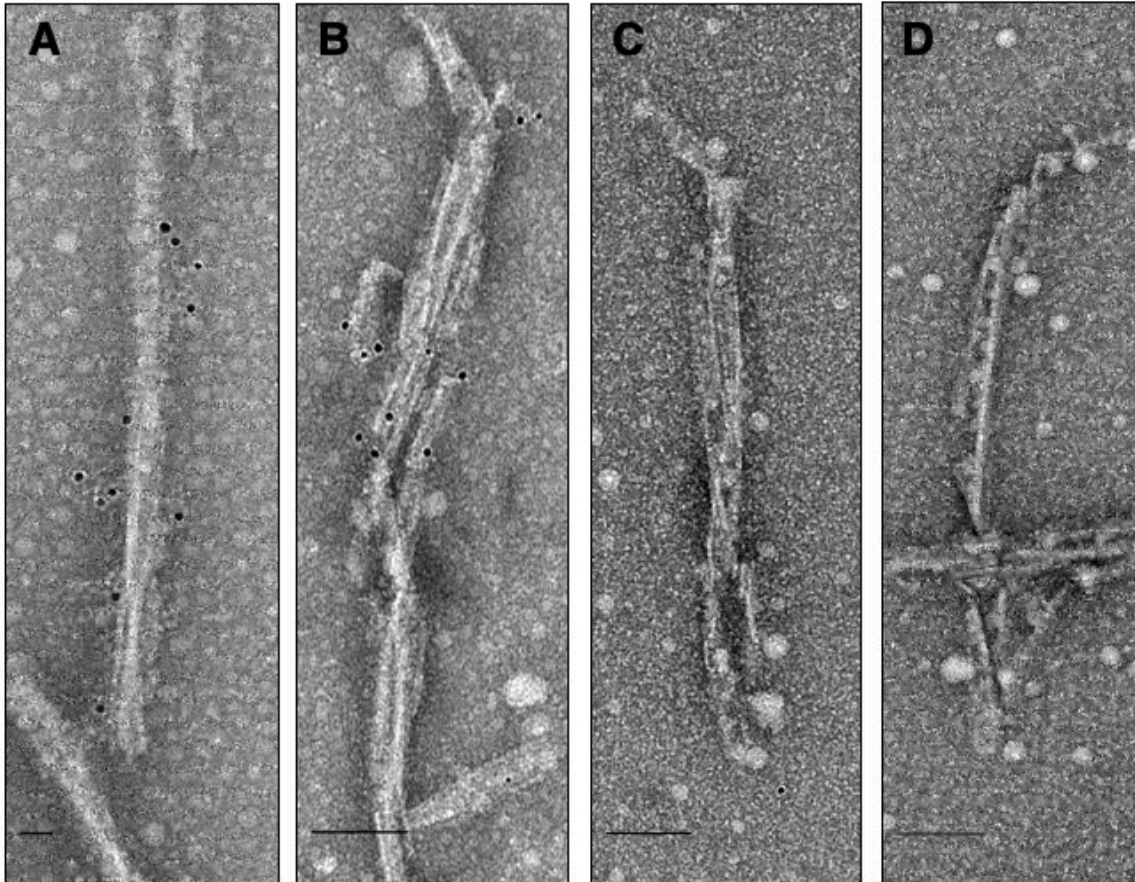
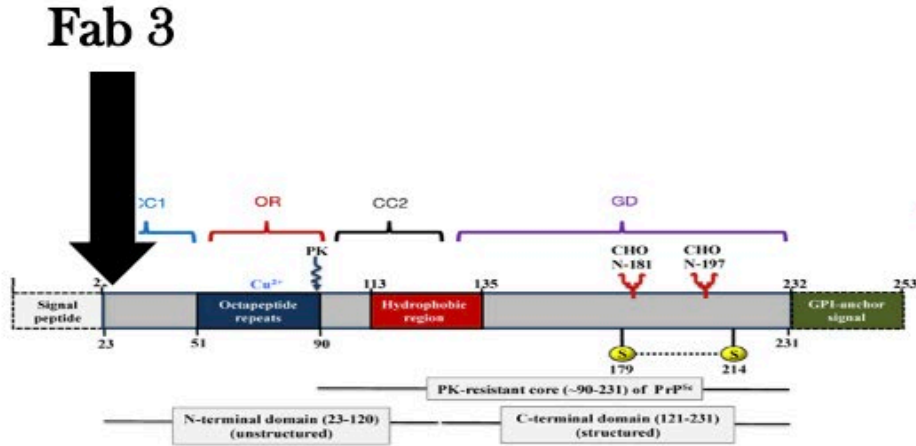
Fab 3²⁵⁻³⁷

CWD Prions

CWD



35 nm



PE treated

PK treated

Figure 2-20: Immunogold electron microscopy of purified CWD fibrils with Anti-Prion Fab 3 antibody.

Immunogold labelling of **(A-B)** PE treated CWD fibrils with anti-PrP Fab 3, **(C-D)** PK treated CWD fibrils. Anti-PrP Fab 3 recognizes an epitope between residues 25 and 37 of the flexible tail at the CC1 region of PrP, hence no specific labelling was observed in the grids with PK treated CWD fibrils. Scale bar = 100 nm.

Fab 29 219-230

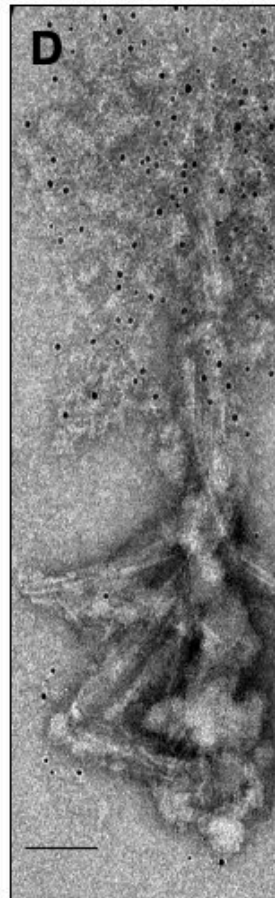
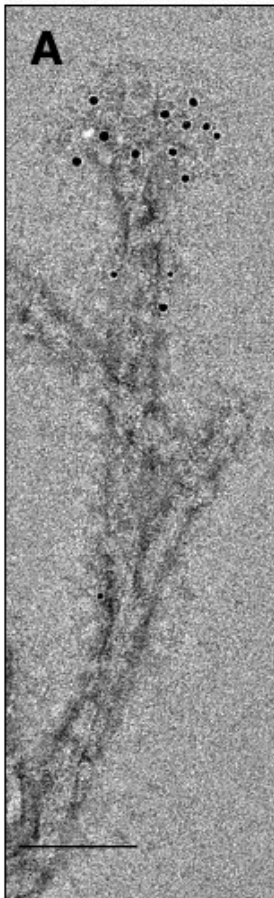
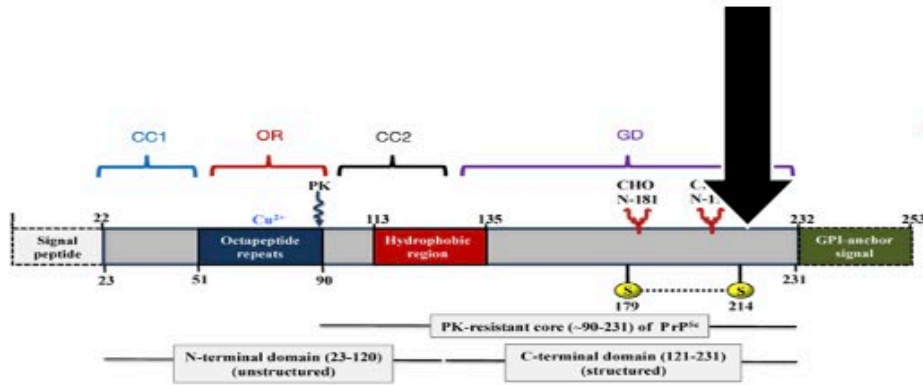
CWD Prions

CWD



35 nm

Fab 29



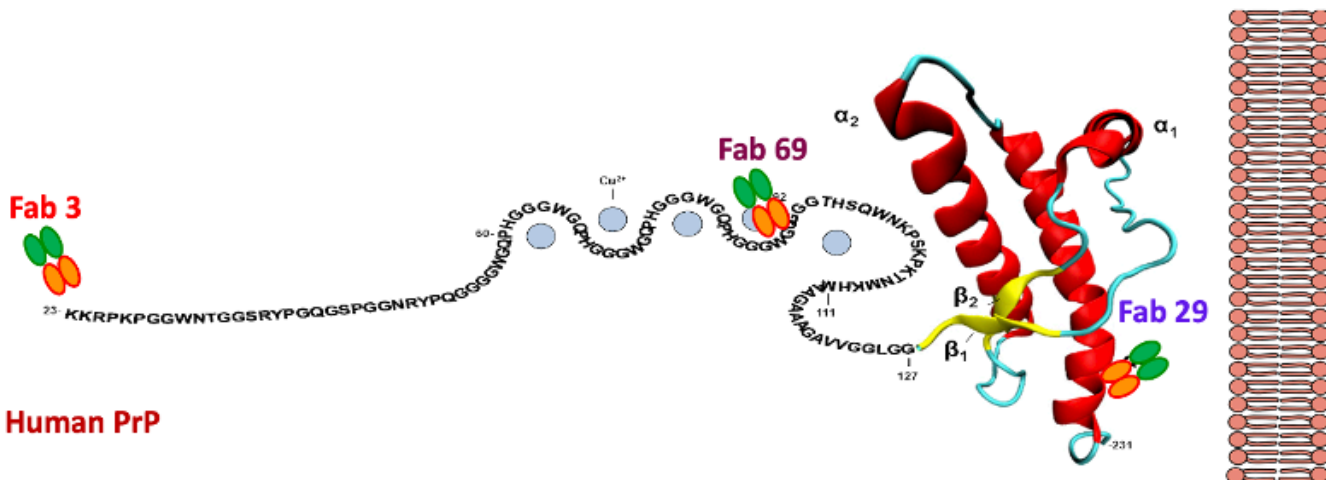
PE treated

PK treated

Figure 2-21: Immunogold electron microscopy of purified CWD fibrils with Anti-Prion Fab 29 antibody.

Immunogold labelling of **(A-B)** PE treated CWD fibrils with anti-PrP Fab 29, **(C-D)** PK treated CWD fibrils and aggregates. Anti-PrP Fab 29 recognizes an epitope between residues 219 and 230 at the GD region of PrP. Scale bar = 100 nm.

A Pr^{PC} Structure



Human PrP

23- KKRPKPGG WNTIGGSRYPG QGSPGGNRYP PQGGGGWQPHG HGGGWGQPHG -70

71- GGWQPHGGG WGQPHGGGWG QGGGTHSQWN KPSKPKTNMK HMAGAAAAGA -120

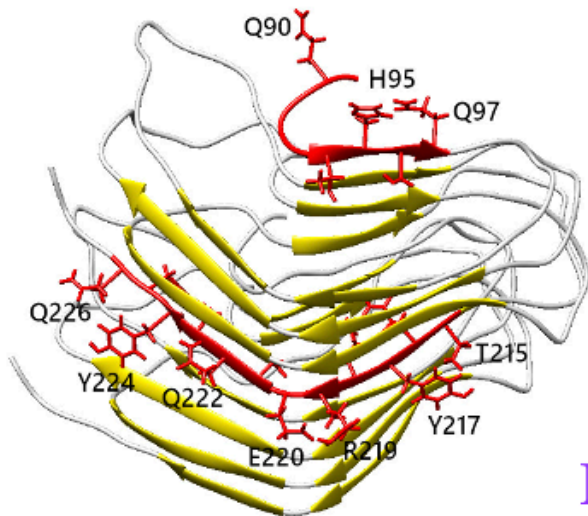
121- VVGGLGGYML GSAMSRPIIH FGSDYEDRYR RENMHRYPNQ VYIRPMDEYS -170

171- NQNNFVHDCV NITIKQHTVT TTTKGENFTE TDVKMMERVV EQMCITQYER -220

221- ESQAYYQRGS -230

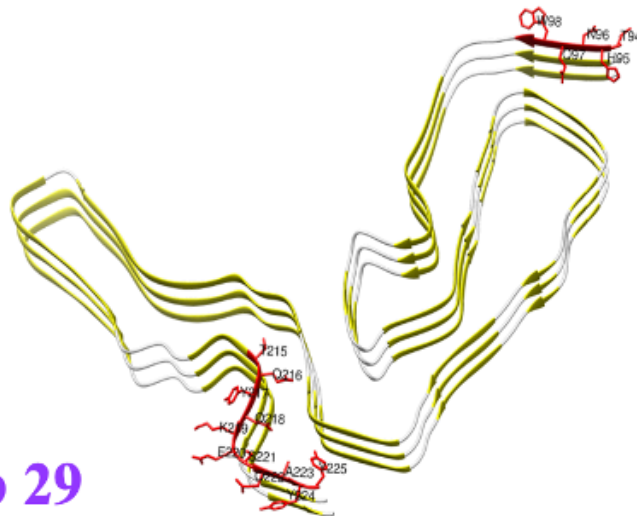
Image adapted from Giachin G., et al, molecules 2013, 18.

Fab 69



B 4RβS PrP^{Sc} Model

Fab 69



Fab 29

C RML PrP^{Sc} PIRIBS Structure

Figure 2-22: Epitope orientation of humanized anti-Prion Fabs in PrP^C structure, dimeric 4R β S PrP^{Sc} model and 263K PrP^{Sc} PIRIBS structure.

(A) PrP is a GPI linked cell surface glycoprotein, shown are the orientation of humanized recombinant anti-PrP Fabs 3, 69 and 29 in PrP^C structure. Epitope mapping amino acid sequences of represent human PrP sequence. Fab 3 recognizes the polybasic stretch of PrP at the CC1 region pointing to the minimal epitope ₂₃KKRPPKPG₂₉, Fab 69 recognizes sequence ₈₇GGWGQGGGTHSQ₉₈ at the C-terminal of the flexible tail, at the CC2 region of PrP. This epitope is closer to the octapeptide repeat region as shown. Fab 29 has an epitope ₂₁₅TQYERESQAYYD₂₂₆ at helix-3 of the globular domain of PrP closer to the GPI anchor. (B) Representative dimeric version of the 4-rung beta solenoid (4R β S) PrP^{Sc} model of human PrP 27-30. The 4R β S model shows the orientation of the epitopes of Fabs 69 and 29. In 4R β S residues of Fab 69; Q90, H95 and Q97 are surface exposed found on the loop and beta strand and has an easy access to antigen – antibody recognition. As animal and human prions may have different structural morphologies, this epitope's uniqueness can be useful in analyzing the N-terminal of PrP 27–30. The fourth rung of the PrP^{Sc} monomer shows the orientation of the Fab 29 epitope on the 4R β S model, with surface-exposed residues T215, Y217, R219, E220, Q222, Y224, and Q226. Comparatively orientation of these epitopes in (C) RML PrP^{Sc} parallel in-register intermolecular β -sheet structure (PIRIBS) is comparable to the orientation in 4R β S PrP^{Sc} Model. Epitope of Fab 69 in the PIRIBS structure has residues T95, H96 and N97 which are surface exposed and Fab 29 has residues Y218, E219, E221, Q223, Y225 and Y226 which are surface exposed. Protein Data Bank access code: 7QIG.

2.4 DISCUSSION

In this study, I further characterized the humanized recombinant antibody fragments, Fabs from the PrP Fab library that were developed by our collaborators, Aguzzi Lab (Senatore et al., 2020). Our collaborators used a human phage display technology to screen a library of synthetic human antibodies, which is distinct from earlier methods in a number of ways (Adamson et al., 2007; Flego et al., 2007). To find antibodies for every region of PrP, they first increased the amount of PrP antigens rather than using a single PrP fragment for panning. Second, they deep-sequenced the panning outputs, which is a technique that enhances the discovery of incredibly rare antibody clones. As a result, they were able to produce anti-PrP Fabs with a wide range of specificities. Along with the 35 Fabs discovered by ELISA screening, hundreds of other rare Fab that hit against less antigenic PrP epitopes were also discovered (Senatore et al., 2020). The objective of this research was to create a high-resolution map of neuroprotective epitopes in order to find potent immunotherapeutics. I utilized these Fabs as tools to characterize the isolated RML, L-type BSE, and CWD fibrils as well as human GSS^{A117V} oligomers (described in chapter 4) via immunogold labelling and electron microscopy (Kamali-Jamil et al., 2021; Vanni et al., 2020). These anti-PrP antibody fragments were bacterially expressed as Fabs which are typically more stable and less susceptible to dimerization than scFv (Arndt, Muller, & Pluckthun, 2001). This enabled us to produce 11 soluble anti-PrP Fabs which target four main epitopes on PrP; CC1 region (23-50), OR region (51 -90) CC2 region (91-120) and GD region (121-230) (Figure 2-1.B). I analyzed the relationship between the anti-PrP Fabs' epitope and its functional activity using various biochemical and biophysical assays. In this chapter I have focused on three linear

epitope anti-PrP Fabs: Fab 3, Fab 69 and Fab 29 due to the attractiveness of their epitope, which targets the very N-terminus of PrP, truncated N-terminus and very C-terminus of PrP.

Kinetic measurements of the anti-PrP Fabs were measured by our collaborators using surface plasmon resonance (SPR) and affinity maturation. All tested Fabs had K_{DS} (determined by SPR as K_{off}/K_{on} ratio) to recPrP₂₃₋₂₃₁ in the 10-100nM range with quick dissociation rate constants ($k_{off} > 10^{-3}$) [S^{-1}] (Senatore et al., 2020).

Previously developed PrP mAbs faced an issue of self-tolerance which inhibits the synthesis of anti-PrP antibodies in WT animals (Polymenidou et al., 2004). Anti-PrP monoclonal antibodies have therefore primarily been created in PrP-deficient animals (Polymenidou et al., 2008; Prusiner et al., 1993) or by phage display (Williamson et al., 1996), and they primarily target immunodominant PrP epitopes in the central region and GD of PrP (Williamson et al., 1998). It is rare to find anti-PrP antibodies in a human repertoire. According to (Porter, Porter, & Cox, 1973), prions do not generate antibody responses. This is most likely because B cells that react to PrP^C, whose primary amino acid sequence is identical to PrP^{Sc}, are negatively selected (Polymenidou et al., 2004). When WT mice were given recombinant PrP as an immunization, N-terminal epitope antibodies were not produced, and the majority of antibodies identified recombinant PrP in ELISA but not native PrP^C on cell membranes. However, I found most of our expressed anti-PrP Fabs did show to recognize cell surface PrP^C via histoblot (Figure 2-5) and immunocytochemistry assay (Figure 2-6).

Our N-terminus epitope Fab 3₍₂₃₋₃₄₎, which binds to polybasic stretch at the CC1 region, ₂₃KKRPK₂₇, has been demonstrated to label surface-exposed PrP^C and PrP^{Sc} and bind with high-affinity to semi-purified RML tangled fibrils as well as PE-digested CWD prion fibrils in the

native state. However, Fab 3 has failed to demonstrate specific immunolabelling when the purified fibril has been treated with the denaturing agent. Similarly, truncated N-terminus epitope Fab69₍₈₇₋₉₈₎, which binds the CC2 region at the rodent PK cleavage site, occurring around residue 89 (Vazquez-Fernandez et al., 2012), ₈₇GWGQGGGTHNQW₉₈ has labelled surface PrP^C and PrP^{Sc} via histoblots and immunofluorescence cell staining, as well as decorated with 5nm-gold particles PK-digested RML amyloid fibrils (Figure 2-16), L-type BSE fibrils (Figure 2-17) with Fab 69 via immunogold labelling. The samples showed more favorable immunolabelling when the epitope was retrieved using a denaturing agent. A positive labelling should have a gold particle within 25nm from the PrP fibrils or aggregates.

Our C-terminus anti-PrP Fab 29₍₂₁₄₋₂₂₅₎, binds the very C-terminal epitope, upstream to the GPI anchor at the globular domain region. It has been shown to have a linear epitope within residues ₂₁₄TQYQKESQAYYD₂₂₅. We employed this antibody to verify the fibril conformation of PrP 27-30 RML fibrils, L-type BSE fibrils, as well as PE and PK digested CWD fibrils consisting of C-terminus in each PrP monomers along the fibril polymerization. Intriguing results were observed with PK-treated RML and CWD fibrils showing more gold labelling around the PrP^{Sc} amyloid aggregates and less labelling on the fibrils. From this observation, we reasoned that PK cleaves off some C-terminal residues near the GPI-anchor resulting in a lost or truncated epitope and abolishing the reactivity of the Fab 29 antibody to the amyloid fibrils (Altmeppen et al., 2015). Alongside we speculated that proteolytic cleavage of extracellular PrP molecules might be resulting in the shedding of PrP (shed PrP/sPrP) which could make it difficult for PrP to be detected by our Fab 29 antibody (Altmeppen et al., 2015). In order to detect the shed PrP in our PK-cleaved sample, I would employ the shed PrP-specific antibody and allow reliable detection of the shed PrP through Western blotting (Mohammadi et al., 2022). I would speculate the

molecular weight of the shed PrP to be slightly lower due to the lack of GPI-anchor and a strong predominance of the diglycosylated PrP band (Linsenmeier et al., 2018).

When comparing how the Fab 69 and 29 epitopes are oriented in the PrP^{Sc} 4RβS model (Spagnolli et al., 2019) and RML PIRIBS structure (Artikis et al., 2022; Kraus et al., 2021), we find that the Fab 69 epitopes are surface exposed in the shortened N-terminus region at the start of the PK resistant core in both models (Figures 2-22.B-C). While the first four residues of Fab 29 epitope ₂₁₄TQYQ₂₁₈ are surface exposed in the 4RβS model, they are hidden in the Greek key topology of the 263K PIRIBS structure.

Other than EST123 antibody from the Prusiner lab (Peretz et al., 1997), antibodies targeting the N-terminus CC1₂₃₋₅₀ region of the prion protein are rare and, to our knowledge haven't been used for structural analyses via immunogold labelling and EM. BAR210 is one of the rare N-terminus commercial monoclonal antibody that has shown to recognize residues ₂₆KRPKPGGGW₃₄ of Ovine prion protein (Feraudet et al., 2005). Epitope characterization showed that mAb BAR210 does not recognize murine PrP but has a strong affinity to Ovine PrP. Other commercial full-length antibody that targets the same region (CC2) as Fab 69 is monoclonal antibody 12B2 at the truncated N-terminus within residues ₉₃WGQGG₉₇ Ovine prion protein (McCutcheon et al., 2014). Similarly, mAb Pri917 that was raised against synthetic human PrP peptide has been shown to recognize an epitope similar to Fab 29 at the very C-terminus of the prion protein within residues ₂₁₆TQYERE₂₂₁ (Feraudet et al., 2005).

In conclusion, this chapter details the production, extensive characterization and application of a panel of anti-prion protein recombinant Fab fragment antibodies that were developed using phage display technology. The benefits of employing Fabs over full-length antibodies include

their ability to penetrate deeply into amorphous aggregates like PrP^{Sc} and the ability to produce them in *E.coli* for a fraction of the cost of hybridoma antibody synthesis (Simmons et al., 2002). Recombinant antibodies can also be engineered to have additional functions including tags for direct protein detections or crossing the blood-brain barrier for therapeutic purposes (detailed description in chapter 3). The development of recombinant Fab fragment antibodies against the entire PrP epitope area offers new resources for understanding how prions cause neurodegeneration in either cell, animal or structural models.

Chapter 3: Engineering and Characterizing
Humanized PrP^{Sc} – Specific Recombinant
Antibody Fragments as Tools for Prion Disease

3.1 INTRODUCTION

Scrapie in sheep and goats, bovine spongiform encephalopathy (BSE) in cattle, and Creutzfeldt-Jakob disorders (CJD) in humans are forms of prions diseases, which are lethal neurological diseases, characterized by the accumulation of a pathogenic, aberrant isoform of the prion protein, known as PrP^{Sc}, in the central nervous system (Prusiner, 1998b). PrP^{Sc} is generated from the host-encoded cellular prion protein, PrP^C, by post-translational modifications such as the conformational modification (Prusiner, 1998a). Although the intricacies of the mechanisms involved in the initial conversion and subsequent replication of PrP^{Sc} are still unknown, this conversion process is thought by some to represent the fundamental molecular event in prion disease pathogenesis.

PrP^{Sc} is the only unambiguous prion disease marker discovered to date and many of the currently available diagnostic tests rely on its detection. Many studies use limited proteinase-K (PK) digestion to discriminate between PrP^C and PrP^{Sc}, a method which totally degrades PrP^C but leaves the PrP^{Sc} N-terminally shortened proteinase-resistant core (PrP 27-30) intact composed of residues ~90-231 (Safar et al., 1998). Reagents capable of distinguishing between PrP^C and PrP^{Sc} under native conditions, without the need for PK treatment, would be highly advantageous.

To date, there have been several reports on the development of monoclonal (mAb) and polyclonal (pAb) antibodies against PrP molecules. The majority of these are anti-PrP antibodies that detect linear or discontinuous PrP^C epitopes, such as mAb 3F4, and react with PrP^{Sc} pretreated with a denaturant such as mAb 6H4 (Kasczak et al., 1987; Peretz et al., 1997; Williamson et al., 1996). Nevertheless, several antibodies have been reported over the past years

to be specific for PrP^{Sc} as have been described in Table 3-1. However, the use of these antibodies outside of the laboratories in which they were produced has thus far been limited (Biasini et al., 2008; Curin Serbec et al., 2004; Korth et al., 1997; Polymenidou et al., 2008).

In addition to the described PrP^{Sc}-specific antibodies, here we report novel PrP^{Sc}-specific monoclonal antibodies that have shown to have a discontinuous epitope and recognize native PrP^{Sc} only, namely YEG Sc-G1, YEG Sc-M63 and YEG Sc-M18 monoclonal antibodies (Fang et al., manuscript in preparation). The specificity of mAb YEG Sc-G1 revealed reactivity towards PrP^{Sc} under native conditions and does not react with PrP^C or denatured PrP.

Additionally, it reacts with all 12 strains of PrP^{Sc} tested (Figure 3-1.A-B).

The availability of a panel of PrP^{Sc}-specific antibodies is indispensable for the analysis of the biochemical and structural properties of PrP^{Sc}, as well as therapeutics for prion diseases (Heppner et al., 2001). The modular nature of antibodies, both structurally and functionally, allows for the generation of smaller antigen-binding fragments such as fragment antigen binding (Fab), the single-chain variable fragment (scFv), and single-domain antibodies (VHH), through molecular cloning and antibody engineering. Under ideal circumstances, these fragments retain their targeting specificity of whole monoclonal antibodies (Holliger & Hudson, 2005).

Engineered recombinant antibodies are classified into two types. The first type of antibody molecule is a chimeric antibody. In this, the rodent-derived residues from the variable domain (VH and VL region) of the antibody are fused to the human constant region, resulting in a chimeric rodent/human antibody that retains its binding affinity while being designed to reduce the immunogenicity of the murine molecule (Boulianne, Hozumi, & Shulman, 1984; Morrison et al., 1984). The second class of antibodies generates humanized antibodies in which rodent-derived complementary-determining regions (CDRs) are grafted onto human antibody

frameworks, effectively retaining antigen-binding capacity (Heppner et al., 2001; P. T. Jones, Dear, Foote, Neuberger, & Winter, 1986; Riechmann, Clark, Waldmann, & Winter, 1988). The humanization of antibodies can result in a significant reduction in immunogenicity.

The production of monoclonal antibodies through the mouse hybridoma technology described by Köhler and Milstein (Kohler & Milstein, 1975) was a significant milestone for the generation of monoclonal antibodies for biomedical and research use. This technology allows the fusion of antibody-producing spleen cells from mice immunized with prion-vaccine, YEG Vacc 14R1 with immortal myeloma cells (Kohler & Milstein, 1975). Polymerase chain reaction (PCR) was used to amplify immunoglobulin heavy (VH) and light chain (VL) from cDNA of positive hybridoma clones YEG Sc-G1, M63, and M18, which expressed immunoglobulin IgG2b and IgM monoclonal antibodies (mAb) recognizing all strains of native PrP^{Sc} only. The CDRs of these PrP^{Sc}-specific antibodies were loop grafted into their specific antibody fragments. I focused on engineering and generating various smaller antigen-antibody fragments which can be used on their own for structural analyses of prions or can be linked to other molecules to generate a myriad of possibilities for bispecific, multi-specific or multifunctional molecules (Figure 3-2). For direct detection of prions, conjugated scFv with an enhanced green fluorescent protein (eGFP) was developed. In order to cross the blood-brain barrier (BBB), scFv was fused with an advanced linker, cell-penetrating peptide (CPP) (Skrlj et al., 2013) and a bispecific nanobody was linked to a molecular trojan horse, mAb 8D3 (Pardridge & Boado, 2012) for receptor-mediated transcytosis, as therapeutic tools for passive immunotherapy of prion diseases.

Table 3-1: List of reported PrP^{Sc}-specific antibodies

Year	Authors	Antibody name	Class	Host	Antibody type	Epitope	Target	Tested application	Comments
Unpublished	Fang <i>et al</i>	YEG Sc G1	IgG-2b	Mouse	Monoclonal Antibody	Conformational His 110, Asp 146	PrP ^{Sc}	DB, ELISA, IHC, IMG, WB	Doesn't react with denatured PrP ^{Sc}
Unpublished	Fang <i>et al</i>	YEG Sc M18 & M63	IgM	Mouse	Monoclonal Antibody	Conformational	PrP ^{Sc}	DB, ELISA, IHC, IMG, WB	Doesn't react with denatured PrP ^{Sc}
2011	Tayebi <i>et al</i>	PRIOC	IgM	Mouse	Monoclonal Antibody	Conformational	PrP ^{Sc}	ELISA, IP, IFI, WB	(+) denaturant with PrP ^{Sc}
2010	Ushiki-Kaku <i>et al</i>	3B7	IgG-2a	Mouse	Monoclonal Antibody	Conformational	PrP ^{Sc}	ELISA, IP	Doesn't react with denatured PrP ^{Sc}
2010	Ushiki-Kaku <i>et al</i>	3H6	IgG-2b	Mouse	Monoclonal Antibody	Conformational	PrP ^{Sc}	ELISA, IP	Doesn't react with denatured PrP ^{Sc} ; Hamster PrP ^{Sc} , CWD
2010	Ushiki-Kaku <i>et al</i>	2C4	IgG-2b	Mouse	Monoclonal Antibody	Conformational	PrP ^{Sc}	ELISA, IP	Doesn't react with denatured PrP ^{Sc}
2010	Ushiki-Kaku <i>et al</i>	1B12	IgG-2b	Mouse	Monoclonal Antibody	Conformational	PrP ^{Sc}	ELISA, IP	Doesn't react with denatured PrP ^{Sc}
2009	Horiuchi <i>et al</i>	6H10	IgG-2b	Mouse	Monoclonal Antibody	Conformational	PrP ^{Sc}	ELISA, IHC, IP, WB	Doesn't react with denatured PrP ^{Sc}
2009	Jones <i>et al</i>	P1.1	IgM	Mouse	Monoclonal Antibody	Conformational	PrP ^{Sc}	IHC, IP, WB	(+) denaturant
2007	Spinner <i>et al</i>	6D11	IgG-1	Mouse	Monoclonal Antibody	⁹⁶ QWNK ¹⁰⁰	PrP ^{Sc}	ELISA, IHC, WB	(+) denaturant, reacts with recPrP
2007	Solforosi <i>et al</i>	IgG 19-33	IgG	293HEK	Monoclonal Antibody	¹⁸ LGLCKRKP ²³ GGWNT ³³	PrP ^{Sc}	IHC, IP, CS	(+) denaturant with PrP ^{Sc}
2004	Moroncini <i>et al</i>	IgG 89-112	IgG	CHO cells	Monoclonal Antibody	⁸⁹ WGQGGGTHSQWNKPSKPKTNMKHM ¹¹²	PrP ^{Sc}	IP, WB	(+) denaturant with PrP ^{Sc}
2004	Moroncini <i>et al</i>	IgG 136-158	IgG	CHO cells	Monoclonal Antibody	¹³⁶ RP ¹⁵⁸ IIHFGSDYEDRYREN ¹⁵⁸ MHRYP ¹⁵⁸	PrP ^{Sc}	IP, WB	(+) denaturant with PrP ^{Sc}
2004	Serbec <i>et al</i>	V5B2	IgG	BALB/c	Monoclonal Antibody	²¹⁴ CITQYQRESQAYY ²²⁶	PrP ^{Sc}	DB, ELISA, IHC, IP, WB	Doesn't react with denatured PrP ^{Sc}
2003	Paramithiotis <i>et al</i>	C2	IgG	Rabbit	Polyclonal Antibody	¹⁴⁹ YYR ^{151, 162} , YYR ¹⁶⁴	PrP ^{Sc}	IP, WB	(+) denaturant with PrP ^{Sc}
2003	Paramithiotis <i>et al</i>	1A12, 17D10	IgM	BALB/c	Monoclonal Antibody	¹⁴⁹ YYR ^{151, 162} , YYR ¹⁶⁴	PrP ^{Sc}	ELISA, IP, WB	(+) denaturant with PrP ^{Sc}
1997	Korth <i>et al</i>	15B3	IgM	Mouse	Monoclonal Antibody	¹⁴² GSDYEDR ^{148, 162} , YYRPVDQYS ^{170, 214} , CITQYQRESQAYY ²²⁶	PrP ^{Sc}	IP, WB	(+) denaturant with PrP ^{Sc}

CHO, Chinese Hamster Ovary

CS, cell staining

DB, Dot blot

IFI, Immunofluorescent imaging

IHC, Immunohistochemistry

IMG, Immunogold labelling

IP, Immunoprecipitation

WB, Western blot

Note: Epitope sequences correlate to human prion sequences.

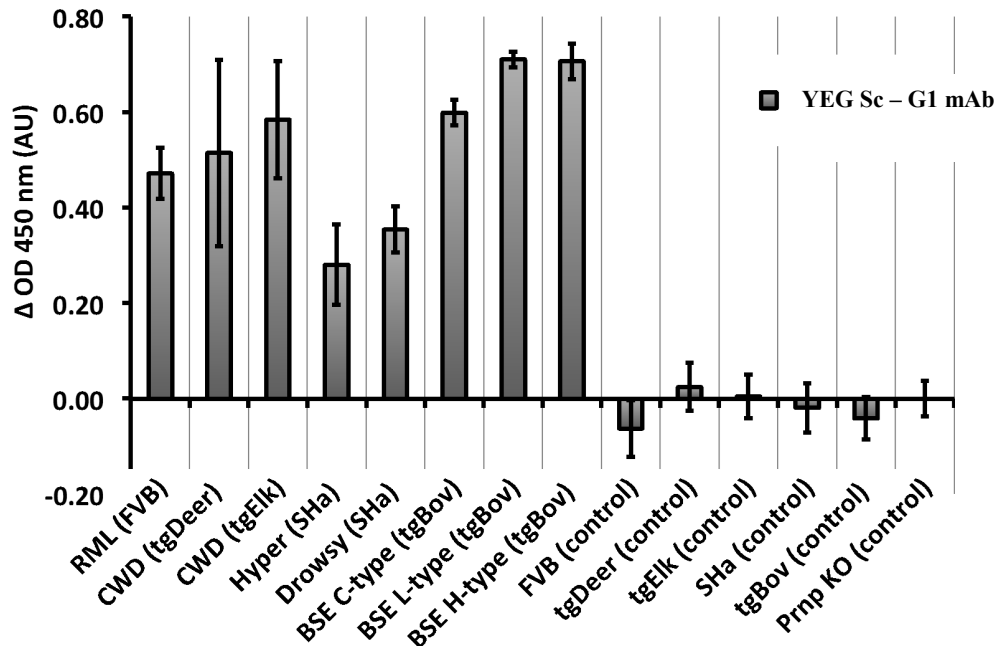
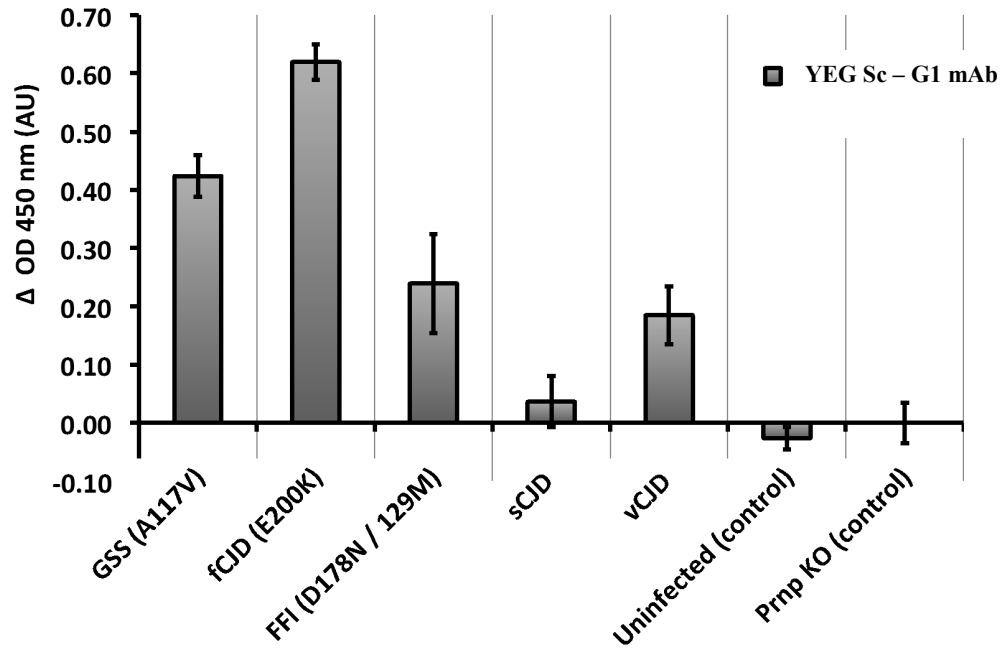
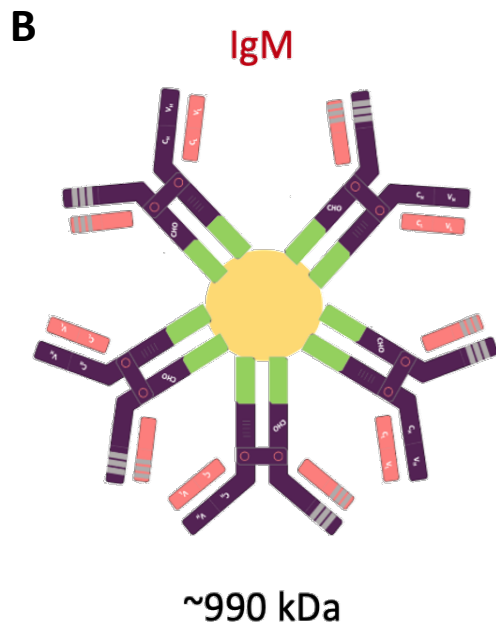
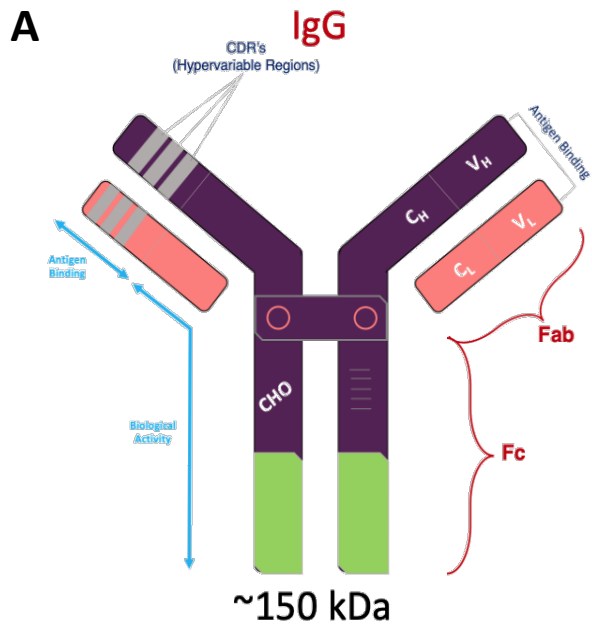
A**B**

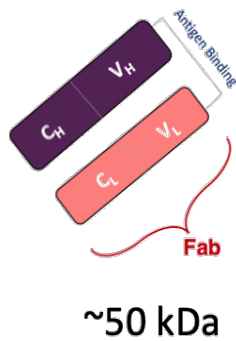
Figure 3-1: YEG Sc – G1, a PrP^{Sc}-specific monoclonal antibody reacts with native PrP^{Sc} only.

The PrP^{Sc} - specific monoclonal antibody is a product of an immune response elicited from the 14R1 (PrP^{Sc}) vaccine that is currently an ongoing project in the Wille lab (Fang et al., manuscript in preparation). The monoclonal antibody YEG Sc – G1 was generated from the 14R1-immunized mice using standard hybridoma technology (Milstein reference to add). **(A)** Competitive ELISA results using the monoclonal antibody YEG-Sc-G1 (IgG) screening crude brain homogenates from prion-infected mouse, transgenic mouse, or hamster brains, as well as uninfected control brain homogenates. When prion-infected brain homogenates were compared to non-infected control samples, there was a distinct difference in the ELISA signal (plotted as Δ OD 450 nm). YEG Sc – G1 recognized prions from various isolates, including sheep scrapie (RML), chronic wasting disease (CWD), transmissible mink encephalopathy (Hyper & Drowsy), and bovine spongiform encephalopathy (BSE all three isolates: C-type, L-type, H-type). **(B)** Similarly, YEG Sc – G1 monoclonal antibody was tested using crude brain homogenates derived from patients, prion-infected and non-neurologic brain homogenates. Consistently, the prion-infected brain homogenates produced a clear difference in ELISA signal (plotted as Δ OD 450 nm) as compared to the non-neurologic control samples. YEG Sc-G1 recognized prions from human isolates based on Gerstmann-Sträussler-Scheinker syndrome (GSS A117V mutation), familial Creutzfeldt-Jakob disease (fCJD E200K mutation), fatal familial insomnia (FFI D178N mutation on the codon 129M background), sporadic Creutzfeldt-Jakob disease (sCJD), and variant Creutzfeldt-Jakob (vCJD, which is bovine spongiform encephalopathy transmitted to humans). These graphs were provided by Dr. Xinli Tang (Unpublished data).

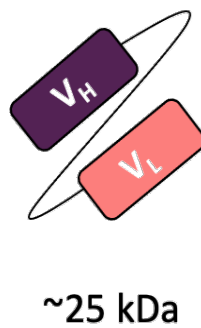
In this chapter, I have shown the generation, characterization and potential applications of a panel of novel-engineered recombinant PrP^{Sc}-specific antibody fragments. From the unique collection of 20 humanized PrP^{Sc}-specific antibody fragments (Table 3-4), we successfully expressed and purified 12 antibody fragments, of which some were further characterized based on their folding. Specific focus was given on IgG-derived antibody fragments, as IgG is the most abundant antibody found in the human body. We have demonstrated the utility of these epitope-specific antibodies using ELISAs with infectious prion isolates, immunogold labelling using electron microscopy, immunocytochemistry assay, and immunoprecipitation. The binding interaction of these engineered antibodies was validated with comparative computational modelling and simulations. These new tools provide valuable resources for prion research designed to increase our understanding of the different conformations adopted during the misfolding events based on the orientation of the epitopes, as well as potential therapeutic tools for combating prion diseases.



C **Fab**



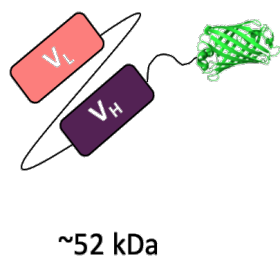
D **scFv**



E **VHH/VH**



F **scFv - GFP**



G **VHH/VH with 8D3 VH**



Figure 3-2: Conventional and recombinant antibody compounds that have been developed against the prion protein.

Schematic representation of full-length IgG, IgM and its antibody fragment derivatives with their respective molecular weight as tools for structural analyses, research diagnostics and therapeutics for prions. **(A)** Depiction of full-length IgG (conventional IgG) antibody that is composed of two pairs of variable and constant heavy and light chains and fragment crystallizable (Fc) portion, linked with disulfide bridge. A variable domain of the conventional antibody that binds to the specific antigen is composed of the sequence on the variable heavy and the variable light chain while each of these sequences is composed of three complementary determining regions (CDRs). **(B)** Full-length IgM in its pentameric form. **(C)** Engineered antibody fragments developed from full-length conventional IgG and IgM including the antigen-binding fragment (Fab), **(D)** A single-chain antibody fragment (scFv) and **(E)** Single – domain antibody fragment: heavy chain variable domain fragment (VHH). **(F)** Enhanced GFP protein fused with an scFv at the C-terminus. **(G)** Fusion of variable heavy chain nanobody with the variable heavy chain of mouse transferrin receptor mAb for delivery of therapeutic protein to the brain through receptor-mediated transcytosis. Heavy or light chains are depicted in purple or peach, respectively. CDR segments are highlighted in grey.

3.2 EXPERIMENTAL PROCEDURES

3.2.1 Cell lines and generation of hybridomas

The immunization of mice with 14R1 and the formation of the hybridoma cells was performed by Dr. Xinli Tang in the Wille lab. Design and generation of 14R1, which is the PrP^{Sc} vaccine/antigen for another ongoing project in the lab titled “Rationally designed vaccine candidates for Chronic Wasting Diseases” was performed by Dr. Andrew Fang in the Wille lab (Fang et al., manuscript in preparation). Myeloma cell lines (Kearney, Radbruch, Liesegang, & Rajewsky, 1979) were used for the generation of the hybridomas by the chemical fusion with the extracted splenocytes from immunized mice with 14R1. Cells were maintained in Iscove’s modified Dulbecco’s Minimal Medium (Invitrogen) containing NaHCO₃, and glutamine and supplemented with 10% fetal bovine serum (Atlanta Biologicals) at 37°C with 5% CO₂.

3.2.2 RNA isolation and cDNA synthesis

The total RNA isolation and cDNA synthesis was adapted from the manufacturer’s protocol using the SuperscriptTM III CellsDirect cDNA synthesis kit (Invitrogen). 10⁷ hybridoma cells expressing positive IgG clones 61D8, 63G4, IgM18 and IgM63 were provided by Dr. Xinli Tang for total RNA extraction. The hybridoma cells were centrifuged at 200 g, for 5 min at 4°C. The cell pellet was resuspended in 1mL ice-cold 1x PBS (Gibco) to wash the cells and centrifuged at 200 g for 5

min at 4°C, this process was done three times. After the final wash, the cells were resuspended in 500 µL 1x PBS. To synthesize cDNA from the hybridoma cells, the Invitrogen SuperScript™ III CellsDirect cDNA Synthesis System Kit was used. In a sterile PCR tube, 10 µL of resuspension buffer, 1 µL of RNaseOUT™ (40 U/ µL) and 2 µL of hybridoma cells, resuspended in 1X PBS, were added and incubated at 75°C for 10 min. Thereafter, 5 µL of DNase I (1 U/µL) and 1.6 µL of 10X DNase I buffer were added and together incubated for 5 min at room temperature. 1.2 µL of EDTA (25 mM) was added, followed by incubation at 70°C for 5 minutes. From there, 2 µL of Oligo(dT)₂₀ (50 mM) and 1 µL of dNTPs (10 mM) were added and incubated at 70 °C for 5 min followed by incubation on ice for 2 minutes. 6 µL of 5X RT buffer, 1 µL of RNaseOUT™ (40 U/µL), 1 µL of SuperScript™ III RT (200 U/µL) and 1 µL of DTT (0.1 M) were subsequently added and incubated at 50°C for 50 minutes immediately followed by an 85°C incubation for 5 minutes to inactivate the reaction. Finally, 1 µL of RNase H (2 U/µL) was added and incubated for 20 minutes at 37°C to degrade any remaining RNA in RNA-DNA hybrid structures. The synthesized cDNA was stored at -20°C until needed. A list of primers is shown in Table 3-2.

3.2.3 In silico primer design

The PCR primers were created by examining and aligning >200 immunoglobulin gene nucleotide sequences from the International ImMunoGeneTics information system (IMGT) (<http://www.imgt.org>), the National Center for Biotechnology Information (NCBI) (www.ncbi.nlm.nih.gov/gene/), and the UniProt Consortium (<http://www.uniprot.org/>). Immunoglobulin gamma heavy and kappa light chain sequences for each immunoglobulin

subgroup were aligned using Clustal Omega (<http://www.ebi.ac.uk/Tools/msa/clustalo/>) and consensus sequences > 65% at each nucleotide position were used when defining each primer.

Table 3-2: Primer sequences for mouse immunoglobulin PCR amplification and sequencing

DNA	Variable Chain	Direction	Primer Name	Primer Sequence
IgG	Heavy Chain	Reverse	IgG1	5'-gga aga tct ATA GAC AGA TGG GGG TGT CGT TTT GGC-3'
IgG	Heavy Chain	Reverse	IgG2A	5'-gga aga tct CTT GAC CAG GCA TCC TAG AGT CA-3'
IgG	Heavy Chain	Reverse	IgG2B	5'-gga aga tct AGG GGC CAG TGG ATA GAC TGA TGG-3'
IgG	Heavy Chain	Reverse	IgG3	5'-gga aga tct AGG GAC CAA GGG ATA GAC AGA TGG-3'
IgM	Heavy Chain	Reverse	IgM	5'-gga aga tct GAC ATT TGG GAA GGA CTG ACT CTC-3'
IgG/IgM	Heavy Chain	Forward	MH-1	5'-ctt ccg gaa ttc SAR GTN MAG CTG SAG SAG TC-3'
IgG/IgM	Heavy Chain	Forward	MH-2	5'-ctt gaa ttc SAR GTN MAG CTG SAG TCW GG-3'
IgG/IgM	Light Chain	Forward	MK	5'-ff gag ctc GAY ATT GTG MTS ACM CAR WCT MCA-3'
IgG/IgM	Light Chain	Reverse	KC	5'-ggt gca tgc GGA TAC AGT TGG TGC AGC ATC-3'
Fab Vector	—	Reverse	HuCAL	5'-GAT AAG CAT GCG TAG GAG AAA-3'
Fab Vector	—	Reverse	M13	5'-CAG GAA ACA GCT ATG AC-3'

3.2.4 PCR amplification of variable regions

The protocol was adapted and optimized from New England BioLabs Q5® High-Fidelity DNA Polymerase. Despite the use of alternative polymerases, the Q5® High-Fidelity DNA Polymerase showed to be superior in comparison. First, a PCR reaction tube was loaded with 0.5 μ M of forwarding primer and 0.5 μ M of the reverse primer. Different primers were employed depending on whether the amplification was for the heavy or light chain of IgG or IgM. (Table 3-2). In addition to primers, 1X Q5 reaction buffer, 200 μ M of dNTPs, 1 Unit of Q5® High-Fidelity DNA polymerase and 1 μ g of synthesized immunoglobulin cDNA, used as template DNA, were added. Finally, DNase-free water (Invitrogen) was added up to a final volume of 50 μ L prior to the amplification of DNA by PCR. For light chain amplification, the reaction mixtures were first denatured in the Thermocycler at 98°C for 3 minutes. A total of 40 gradient temperature cycles were employed for primer annealing of the light chain, starting at 98°C for 10 seconds, 65°C for 15 seconds, 63.6°C for 15 seconds, 59.5°C for 15 seconds, and lastly 72°C for 30 seconds. The final elongation required a two minutes incubation at 72°C, followed by an infinite incubation at 4°C. Temperatures differed depending on whether the light or heavy chain was being amplified, hence the heavy chain necessitated a separate set of temperatures for successful PCR. The heavy chain reactions were first denatured at 95°C for 3 minutes. To determine whether the DNA had been successfully amplified, the PCR product was run for 30 minutes at 135 V on 1.2% agarose (0.72 g agarose, 60 mL 1X TAE, 6 μ L ethidium bromide) in 1X TAE (40 mM Tris-acetate, 1 mM EDTA, pH 8.3). The amplified cDNA of antibody variable region products appeared between 350-400 base pairs. The one KbPlus DNA Ladder (Invitrogen) was used as the standard.

3.2.5 PCR product clean-up and gel extraction

The PCR products were purified using two methods, the first using the QIAquick PCR product clean-up as described by the Purification Kit protocol (Qiagen) followed by gel extraction and the DNA was purified using the QIAquick gel extraction kit (Qiagen). The PCR clean-up was performed with a 5:1 ratio of the PCR product and the diluent. The final PCR product was then on a 1.2% agarose gel (0.72 g agarose, 60 mL 1X TAE, 6 μ L ethidium bromide) in 1X TAE, for 30 minutes at 135 V. The bands observed at \sim 400 bp were cut from the gel and purified using the protocol described by the QIAquick Gel Extraction Kit protocol. Quantification of DNA was performed using a Nanodrop and measuring absorbance at 260 nm, using DNase-free water as a blank.

3.2.6 Sequencing of antibody variable regions

Purified PCR product samples were prepared using 200 ng of DNA, 0.25 μ L of corresponding 10 μ M forward or reverse primer, and DNase-free water to a final volume of 10 μ L. The primer sequences are listed in Table 3-2. These samples were sent to the Sanger DNA Sequencing Service to be sequenced at the University of Alberta, Molecular Biology Service Unit.

The ExPASy translation tool (<http://web.expasy.org/translate/>) and the GenBank database were used to build and test the sequences for proper translation (www.blast.ncbi.nlm.nih.gov). To determine the percent identity of the IgBLAST reference sequences for light and heavy chains,

the final DNA sequence for each antibody variable region was submitted to IgBLAST with default parameters and the mouse was selected as the organism for the query sequence. The DNA sequences were also run via IMGT/BlastSearch using the default parameters to determine their percent identity to the IMGT reference sequences.

The IMGT/V-Quest tool (www.imgt.org/IMGT_vquest/vquest) was used to find the framework and complementarity determining regions (CDRs) (Lefranc, 2014). Contaminating transcripts are variable region (VR) sequences that have been fully transcribed and translated into full immunoglobulin proteins and have 100% similarity to previously reported sequences. The CDRs were validated further by employing the Kabat numbering technique to read the nomenclature of residue positions as well as to determine the three CDRs from variable heavy and variable light chains. (Martin, 1996). Aberrant sequences are those that lack a fully transcribed or translated VR sequence due to premature stop codons, are missing conserved VR motifs, or are non-specific PCR results.

3.2.7 Designing of PrP^{Sc}-specific Fabs, scFv and nanobodies

After decoding the rodent CDRS from the PrP^{Sc} - specific antibody clones, I aligned them with human full-length antibodies from the GenBank database to see how the CDRs and framework varied. I used the human Fab framework from the anti-PrP Fabs as described in chapter 2, to graft the mouse-derived CDRs of PrP^{Sc}-specific antibodies to create recombinant humanized/chimeric antibody fragments (Y. F. Zhang & Ho, 2017). In this chapter, I have discussed the designs and engineering of various antibody fragments specific to the misfolded

and infectious isoform of PrP from the CDR sequences derived from mouse full-length IgG and IgM antibodies.

Multiple synthetic genes codon-optimized for *E. coli* expression encoding the various human antibody fragments (Fabs, scFv, scFv – eGFP, VHH/nanobody) with a His tag at the C-terminus were purchased from BioBasic DNA Technologies (Markham, Ontario).

3.2.8 Cloning of variable region amplicons

3.2.8.1 Engineered antibody fragments

The various antibody fragment constructs DNA came lyophilized from BioBasic. Each construct DNA was resuspended in ultra-filtered water to a concentration of approximately 100ng/ μ L, as per the company's instructions. The constructs were given in a pUC57 vector containing an ampicillin resistance gene. HindIII and XbaI restriction cut sites were inserted for ligation with a human Fab vector as described in chapter 2. The sequences within HindIII and XbaI contain the heavy and light chain CDR sequences along with the antibody fragment framework and a His tag at the C-terminus of the antibody fragment.

The engineered antibody fragments in the pUC57 vector were chemically transformed in One-shot Top10 competent cells (Invitrogen) and grown on LB agar/Ampicillin/1% glucose plates to amplify the amount of selected insert antibody plasmid. Individual colonies of the TOP10 cells were grown in cultures of 5 mL of 2YT medium containing 1% glucose and 5 μ L of 100 mg/mL

ampicillin and incubated at 250 RPM, 37°C for 16-18 hours. The selected clones were purified using a Qiagen miniprep kit. DNA concentration was determined using a Nanodrop, blanking with sterile water and measuring absorbance at 260 nm.

3.2.8.2 Digestion and ligation

I used the same vector, pPE2-Fab plasmid as described in chapter 2 for cloning our engineered antibody fragment inserts for expression in *E.coli*. A double restriction digest was done with 1000 ng of engineered antibody fragments (insert), and a human pPE2-Fab plasmid (vector), using the restriction enzymes HindIII and XbaI (Invitrogen) to excise the DNA fragments. The digested DNA was run on a 1.2% agarose gel in 1X TAE buffer for 30 minutes at 135 V to isolate the DNA. The excised DNA fragments (insert and vector) of interest were purified using the QIAquick gel extraction kit. The inserts of antibody fragments, such as Fab G1 were ligated to the human pPE2-Fab vector through sticky ends using a 1:1 ratio (insert (ng) : vector (ng)) and 1 U of T4 DNA ligase (ThermoFisher Scientific). The ligated reactions were then chemically transformed in One-shot Top10 competent cells (Invitrogen) and grown on LB agar/Kanamycin/1% glucose plates to amplify the amount of successfully ligated engineered antibody clones. Individual colonies of the TOP10 cells were grown in cultures of 5 mL of 2YT medium containing 1% glucose and 5 µL of 100 mg/mL ampicillin and incubated at 250 RPM, 37 °C for 16-18 hours. The selected clones were purified using a Qiagen miniprep kit and were used for Sanger sequencing (University of Alberta, Molecular Biology Service Unit) using the following sequencing primers:

VH (5'GATAAGCATGCGTAGGAGAAA-3') and M13Rev (5' - CAG GAA ACA GCT ATG AC - 3').

The sequences derived from the same *E. coli* transformation and corresponding to a specific chain from a specific antibody (Parent antibody, IgG and IgM) were then aligned using Clustal Omega to verify for antibody chain sequence consensus.

3.2.9 Antibody expression and purification

The engineered humanized PrP^{Sc} – specific Fabs, scFv's, nanobodies and their antibody fragment conjugates were expressed and purified as soluble folded proteins using the same protocol as previously described in Chapter 2, sections 2.2.2 and 2.2.3.

3.2.10 SDS-PAGE Gel for Coomassie staining and Western blotting

Samples for Coomassie staining and Western blotting were prepared as described in the previous Chapter 2, section 2.2.4. Immunoblotting of Fabs was performed using anti-human Fab conjugated to HRP (ab98605) at 1:5000 dilution and scFv's and with their conjugates along with nanobodies (VHHG1) were immunoblotted with anti-His tag monoclonal antibody conjugated to HRP (MAB050H) at 1:5000 dilution. Anti-His tag antibody was also used for immunoblotting fractions from immunoprecipitation assay as described in section 3.2.15.

3.2.11 Enzyme-Linked Immunosorbent Assay (ELISA) for epitope mapping

To determine the precise epitope of PrP^{Sc}-specific antibodies, revert mutants of 14R1 antigen/vaccine candidate were created and produced by Dr. Andrew Fang in the Wille Lab. The 14R1 revert mutants comprised constructs A, B, C, D, E, F, G, H, 1G, 2G and HG whose amino acids were either vertically or horizontally reverted back to the original amino acid sequence of Het-s scaffold protein used for creating 14R1 vaccine. An indirect enzyme-linked immunosorbent assay (ELISA) was performed against revert mutants of 14R1 antigen/vaccine for screening key epitopes for anti-PrP^{Sc} Fab fragments. ELISA SpectraPlates™ were coated with sonicated 5 µg/ml of 14R1 revert mutants diluted in PBS, at 4°C overnight. We also coated 0.5 µg 14R1 as a positive control and 0.5 µg Het-2s scaffold protein as our negative control. The plate was washed with PBS containing 0.05% (v/v) Tween-20 (PBST) and was blocked with 5% BSA for 2 h at RT. Purified Fabs in PBST were then incubated for 3 h at RT (1:500 in PBST). After three washing with PBST, binding Fabs were detected by anti-human Fab HRP conjugated antibody (1:5000 in PBST). After 1 h 30 min incubation at RT, followed by three washing with PBST. After washing, the plates were developed with 3,3',5,5'-Tetramethylbenzidine (TMB) substrate (SurModics) and incubated for 30 min, the reaction was then stopped with 50 µL of 2N sulfuric acid. The optical density was measured at 450 nm.

3.2.12 Activity assay

3.2.12.1 Indirect ELISA

Indirect ELISAs were used to determine recombinant PrP^{Sc}-specific antibody fragments' folding and binding specificity. ELISA SpectraPlates™ plates provided by Dr. Andrew Fang were coated with 14R1 vaccine/antigen and then blocked with 5% BSA in 0.05% (v/v) Tween-20 (PBST) for 1 h. The rest of the indirect ELISA procedure was performed as previously described in section 3.2.11, except Fab G1, Fab M18 and Fab M63 were used as primary antibodies with a 1:500 dilution.

Similarly, indirect ELISA with infectious untreated RML and GSS^{A117V} brain homogenates was performed using recombinant Fab G1 antibody to determine the folding and binding specificity of the purified Fab G1 as previously described in Chapter 2 section 2.2.7.2.

3.2.12.2 Two-step indirect competition ELISA

Two-step indirect competition ELISA was performed to determine the folding and binding specificity of the single chain (scFv) and single-domain/nanobody (VHH) PrP^{Sc}-specific antibody fragments. ELISA plates were coated with 14R1 vaccine/antigen and then blocked with 5% BSA in PBST for 1 h. Plates were incubated with scFv's and VHH-G1 for 3 h at room temperature. Plates were rinsed four times with 0.05% PBST and then incubated with mouse-

derived full-length YEG Sc-G1 for 1.5 h at room temperature. Plates were rinsed four times with 0.05% PBST and then incubated with rabbit anti-mouse antibody conjugated to HRP (BioRad) for one hour at room temperature. Plates were rinsed five times with 0.05% PBST. After washing, the plates were developed with 3,3',5,5'-Tetramethylbenzidine (TMB) substrate (SurModics) and incubated for 30 min, the reaction was then stopped with 50 μ L of 2N sulfuric acid. The optical density was measured at 450 nm.

3.2.13 Immunogold labelling

Immunogold labeling on the PTA purified and PK-digested pellet 2 (PK_P2) and sucrose step gradient purified (pellet wash) RML prion fibrils was performed as previously described in chapter 2, sections 2.2.8 and 2.2.12 using PrP^{Sc}-specific monoclonal antibodies, YEG Sc – G1 (full-length, hybridoma-derived), Fab YEG Sc – G1 (recombinant) and Fab YEG Sc – M63 (recombinant). These PrP^{Sc}-specific antibodies are produced in the Wille lab and have been shown to recognize a discontinuous epitope in native PrP^{Sc} only.

The recombinant Fab and full-length YEG Sc – G1 monoclonal antibodies have a structural epitope whereby it recognizes the exposed residues H110 and Asp146 at the β -arc region of the 4R β S model of the infectious prion protein, PrP^{Sc}. Similarly, the recombinant Fab YEG Sc – M63 monoclonal antibody recognizes exposed residues Asn103 and Asp143 of the 4R β S model under native conditions only.

Based on a previously published immunogold labeling protocol (Kamali-Jamil et al., 2021; Vanni et al., 2020; Wille et al., 2007), 5 µl of purified RML samples were adsorbed onto glow discharged formvar/carbon-coated nickel grids (TedPella, Inc.) for ~5 minutes, and washed using three drops (50 µl) of 0.1M and 0.01M ammonium acetate buffer pH 7.4. Following the washing steps, the grids were stained with 2 drops of freshly filtered 2% sodium phosphotungstic acid (PTA), pH 7.2, then blocked for 90 minutes with 0.3% bovine serum albumin (BSA) in Tris-buffered saline (TBS: 50 mM Tris-HCl, 150 mM NaCl, pH 7.4). Labelling of RML samples with Fab and full-length YEG Sc-G1 and YEG Sc-M63 monoclonal antibodies was performed under the native state for 3 h, rinsed five times with 0.1% BSA in TBS, incubated with a bridging goat F(ab')₂ anti-human IgG F(ab')₂ (Abcam ab98531) for 2 h, rinsed five times again with 0.1% BSA in TBS, incubated with a 5-nm gold-conjugated rabbit anti-goat IgG (Abcam ab202670) for 2 h, rinsed five times with 0.1% BSA in TBS, twice with TBS alone, and twice with water. Controls were treated identically, except that the primary Fab was omitted. Finally, the grids were rinsed with TBS solution and water, and placed onto two drops of 2% PTA for final staining, air-dried, and stored for EM analysis. The samples were analyzed with a Tecnai G20 transmission electron microscope (FEI Company) operating at an acceleration voltage of 200 kV. Electron micrographs were recorded with an Eagle 4k x 4k CCD camera (FEI Company).

3.2.14 Immunocytochemistry assay

CAD 5 and CAD 5 – RML cells were provided by Grant Norman from Dr. Valerie Sim's lab at the Centre for Prions and Protein Folding Disease, University of Alberta, as described in Chapter

2 section 2.2.7.4. The cells were washed once with ice-cold PBS and fixed with pre-chilled methanol for 10 min. The cells were washed twice with ice-cold PBS followed by mild permeabilization using 0.1% Triton X-100 in PBS for 5 mins and rinsed twice with ice-cold PBS. The cells were then blocked with 3% BSA in PBST for 1 h at RT and then incubated with respective antibodies as shown in Table 3-3 overnight at 4°C. Aspirate the primary antibody and washed the cells three times in ice-cold PBS, 5 min each wash. Incubated the cells with the respective secondary antibodies conjugated to Alexa Fluor in 1% BSA for 2 h at RT in the dark. The slides were washed three times with ice-cold PBS for 5 min each in the dark. Excess buffer was decanted and the coverslips were mounted with the ProLong™ Gold antifade mountant with DAPI (ThermoFisher) and air dried in the dark. The coverslips were then sealed with the slide sealer and air dried in the dark. The cell surface PrP^C and PrP^{Sc} labelling were visualized by confocal laser scanning microscopy, ZENN Digital Imaging for LSM 700 (Zeiss) and analyzed using ImarisViewer Imaging software 9.8.0.

It is important to note that the quality of data from fixed samples can vary depending on the sample type. Our protocol is expected to be compatible with a wide range of cell and tissue types, but not all. Cell and tissue types that are extremely delicate and difficult to separate (e.g., organoids, solid tissue or other neuronal cells) may necessitate extra optimization to aid in preservation.

Table 3-3: List of antibodies used for ICC assay

	Antibody name	Dilution	Catalogue #	Company/Source
1	YEG Sc - G1	1/1000	G1	Wille lab / Dr. Tang
2	Fab G1	1/250	G1	Wille lab / this thesis
3	scFv G1 - GFP	1/500	G1	Wille lab / this thesis
4	GFP (control)	1/1000	N/A	Wille lab / this thesis
5	Anti- Ganglioside GM1	1/1000	ab23943	Abcam
6	Anti-CD90/Thy-1	1/1000	ab3105	Abcam
7	SAF83	1/1000	189765	Cayman chemicals
8	Fab 3	1/1000	Chapter 2	Aguzzi lab
9	Anti-Mouse Alexa 594	1/1000	A-11005	Thermofisher
10	Anti-Rat Alexa 555	1/1000	ab150158	Abcam
11	Anti-Human IgG (H+L) Alexa 647	1/1000	A-21445	Thermofisher

3.2.14.1 Thresholding

Raw confocal images were analyzed using ImarisViewer Imaging software 9.8.0 and a threshold was applied to infected and uninfected immunofluorescence images collected at the same gain. This means that every pixel below a certain gray level was converted to zero. This removed the background so that only PrP^{Sc}-punctae are visible.

3.2.15 Immunoprecipitation assay

We developed an immunoprecipitation method using our recombinant humanized PrP^{Sc} – specific antibody fragments, Fabs and scFv, and 14R1 vaccine/antigen as our pull-down protein of interest. 14R1 vaccine/antigen was provided to us by Madeleine Fleming from the Wille lab. The immunoprecipitation protocol was adopted from the PierceTM Protein L Magnetic beads manufacturer's protocol (ThermoFisher Scientific) and was optimized to our antibody and antigen of interest.

In all instances, the protein of interest for the immunoprecipitation experiment was fibrillized 14R1. The PrP^{Sc} vaccine 14R1 is expressed in *E.coli*, purified using an IMAC purification system and eluted at low pH. The desalted sample is then fibrillized by increasing the pH to 7.5 using 3 M Tris and stored at room temperature with 1 mM sodium azide.

For each reaction mixture, 50 µl of protein L magnetic beads were washed gently with binding/wash buffer (Tris-buffered saline containing 0.05% Tween-20) and placed the tube on a

magnetic rack to discard the supernatant. All the wash steps in this assay were performed three times unless otherwise stated. Different dilutions of either recombinant Fab G1 or scFv G1 were created in separate reaction tubes and diluted with binding buffer to a final volume of 500 μ l. The antibody was incubated with the protein L magnetic beads overnight with continuous rotation at 4°C. A mixture containing a 1:1 ratio of fibrillized 14R1 antigen was formed with bovine serum albumin (BSA) to create a mixture and incubated overnight at 4°C with continuous rotation. The coated antibody to bead was then mixed with 150 μ l of the 14R1:BSA mixture and diluted with 350 μ l of binding buffer. The antigen-antibody mixture was incubated overnight at 4°C with continuous rotation to form a complex. After the incubation, the tube was placed on the magnetic rack to pulldown the beads containing the bound complex with the antibody and remove the supernatant post immunoprecipitation (after complex fraction). The beads were washed three times using wash buffer (Tris-buffered saline containing 0.05% Tween-20), and the supernatant was collected for Western blot analysis as wash fraction. The complex was eluted by adding 200 μ l of elution buffer (0.1 M glycine, pH 2.0) and incubated for 20 mins at room temperature with occasional mixing. Neutralization buffer (1 M Tris, pH 8.5) was added to the elution tubes. The beads were then resuspended in wash buffer for western blot analysis. Electrophoresis and western blotting were then performed as previously described in section 3.2.10, except that the blots were developed using ECL Plus reagent (GE Biosciences). Anti-his tag conjugated to HRP was used for western blot analysis.

Similarly, a different antigen complex was created to specifically pull down 14R1 by mixing it with 5% uninfected PrP^C brain homogenate at 1:1 ratio. The immunoprecipitation assay was performed as described above. The western blot analysis was performed using the SAF 83 antibody that recognizes residues 126-164 of the mouse prion protein.

3.2.16 Homology modelling of antibody fragments

Modelling, molecular docking and molecular dynamic simulation of various PrP^{Sc}-specific antibody fragments and docked with the 4RβS human PrP^{Sc} model were performed by Dr. Luda Dorosh at the Wille lab. In all systems, the C-terminal and N-terminal extremities of all peptides were kept charged ($-\text{COO}^-$ and $-\text{NH}_3^+$), whereas all other titratable amino acids were assigned their canonical states at pH 7.4 with the PropKa implementation in Chimera (Sondergaard, Olsson, Rostkowski, & Jensen, 2011).

3.2.16.1 Homology modeling of Fab G1, scFv G1 and Nano G1 and preparing of huPrP^{Sc} conformer for simulations

The FASTA-formatted sequences of constructs Fab G1 (~50kDa), scFv G1 (~25kDa), and Nano G1 (~12.5kDa) were submitted to the homology modelling online tool Phyre2 (Kelley, Mezulis, Yates, Wass, & Sternberg, 2015). About 200 templates were generated for each construct, from which the template with the best confidence (100%), coverage, and ID % was chosen to build the final models. The template for Fab G1 was based on the protein data bank (PDB) (Berman et al., 2000) entry 4H88 (T. N. Baral, MacKenzie, & Arbabi Ghahroudi, 2013). Obtained Fab G1 structure lacked N-terminal (chain B ¹ACVGENHMKQSTIALALLPLLFTPVTKA²⁸) and C-terminal (chain B ²⁴⁹KSEFDYKDDDDKGAPHHHHHH²⁶⁹) residues which were consequently built using Biovia Discovery Studio software as random coils.

Modeled scFv G1 structure was based on PDB entry 2KH2 (Wilkinson et al., 2009). Missing

residues ¹⁴¹TIALALLPLLFTPVTKAQVQLVES¹⁶⁴ and ²⁷⁵VSSHHHHHH²⁸³ were built in Biovia Discovery Studio software as random coils. Nano G1 structure was built on PDB entry 4PFE. Missing residues ¹ACVGENHMKQSTIALALLPLLFTPVTKA²⁸ and ¹⁴⁹HHHHHH¹⁵⁴ were built in Discovery Studio.

3.2.16.2 Homology modeling of scFv G1 conjugated to eGFP

Construct consisting of part antibody G1: scFv G1 tagged with Green fluorescent protein scFv-YEG Sc-G1-mEGFP (~59.7kDa) was built via online homology server Phyre2. EGFP sequencing identified PDB entry 5FGU (Moon, Krahn, Lu, Cuneo, & Pedersen, 2016) as a base structure, 2KH2 for scFv, then multiple domains were linked in “intensive mode”. This mode produced model of collapsed eGFP with scFv, so it was corrected in VMD.

3.2.16.3 Homology modeling of human four–rung beta solenoid (4RβS) model (huPrP^{Sc})

The coordinates of the 4-rung β-solenoid (4RβS) model for mouse scrapie PrP sequence 89-230 (mouse numbering, 90-231 human) were uploaded (Spagnolli et al., 2019), mouse to human mutations applied in Accelrys VS software.

3.2.17 Molecular dynamics simulations of modelled systems for stabilization

All modelled antibodies Fab G1, scFv G1, Nano G1, and all huPrP^{Sc} conformers have been subjected to minimizations, equilibrations and production molecular dynamics (MD) simulations using the GROMACS 2018.3 package (Van Der Spoel et al., 2005). OPLS-AA (Optimized Potential for Liquid Simulation, All Atom) forcefields were used for protein, urea, and ions, and SPC/E (Simple Point Charged Extended) water forcefields (Jorgensen & Tirado-Rives, 1988). Systems Fab G1, scFv, Nano G1, and 4RβS were solvated in a periodic rectangular water box and Cl⁻ or Na⁺ ions were added to electro-neutralize the systems. Minimizations with gradual release of restraints and equilibration procedures are described previously (Mercer et al., 2018). The production MD simulations, and the last equilibration step, were conducted at a temperature of 310 K and a pressure of 1 atm with isotropic pressure coupling (NPT ensemble), with Verlet cut-off neighbour searching, Particle-Mesh Ewald treatment of electrostatics, twin-range cut-off for Van der Waals, V-rescale temperature coupling, and Parrinello-Rahman pressure coupling algorithms. 40ns NPT equilibration/production was executed on the huPrP^{Sc} model to stabilize its mutated mouse → human conformation. 30ns production was used on Fab G1, and 20ns production MD was used on scFv G1, and Nano G1 to make constructed terminal parts more compact. Final stable conformations were extracted from trajectories and prepared for docking: water molecules and neutralizing ions were stripped. huPrP^{Sc} showed high stability of initial β-sheets. Modeled flexible termini in antibodies folded closer to the antibody body, making the systems more compact.

3.2.18 Docking and Analysis tools and following simulations of docked systems

Representative conformations from the production MD trajectories were used as templates for protein-antibody docking using Cluspro server (Desta, Porter, Xia, Kozakov, & Vajda, 2020). where for Fab G1/scFv's/Nano G1 option antibody was chosen. The top ten docking models (with the highest docking energy) were chosen for the following structural analysis: hydrogen bonds (using Chimera scripts), and an inspection of antibody orientation for different modes (Pettersen et al., 2004). Snapshots from trajectories and graphical representations of models were done with Chimera or Discovery Studio.

3.2.19 Following MD simulation of docked complexes

To confirm the stability of docked complexes and test the formation of HBs in solution, production simulations of the constructs were conducted at 310 K temperature and at a pressure of 1 atm with isotropic pressure coupling (NPT ensemble) for 150ns for each system, 1 fs time step. To mimic the major condition of the experiment 0.137 M of NaCl was added to the water solution. Hydrogen bond evolution along 150 ns MD trajectory was calculated in Chimera using MD/Ensemble analysis tool (Pettersen et al., 2004).

3.3 RESULTS

3.3.1 Antibody variable region sequence identification workflow

The progressive technique for identifying variable regions of PrP^{Sc}-specific monoclonal antibody clones is depicted in a workflow diagram (Figure 3-3.A). The establishment of a clonal antigen-binding immunoglobulin-producing hybridoma cell line is the first step in identifying the variable regions of the monoclonal antibody. The genetic material for subsequent PCR amplification of the heavy chain and light chain of the immunoglobulin variable regions is contained in the cell line. Amplified PCR products are extracted from the agarose gel, purified and the DNA is sequenced before being translated into primary protein structures for each monoclonal antibody's variable regions heavy and light chain. Kabat numbering was used to identify the three CDR of the heavy and light chain variable regions (Martin, 1996). Once the CDRs were decoded, they were grafted on an existing human Fab fragment with a 6x His tag at the C-terminus of the antibody fragment construct for purification using IMAC chromatography and cloned into shuttle vector for expression in *E.coli* (Figure 3-3.B).

3.3.2 PCR amplification of the immunoglobulin variable regions

In order to elucidate the primary structure of the positive IgG (Figure 3-3) and IgM (Figures 3-4 and 3-5) clones of the PrP^{Sc}-specific antibodies derived from the Chronic Wasting Disease vaccine project led in the Wille lab (Fang et al., manuscript in preparation), I obtained cDNA

from the hybridoma cells expressing the variable regions and amplified the cDNA using universal mouse immunoglobulin heavy and light chain primers (Coloma, Larrick, Ayala, & Gavilondo-Cowley, 1991; Ward, Schneider, Kreissig, Hammock, & Choudary, 1993) as detailed in Table 3-2.

Optimal PCR conditions were standardized for each PCR primer set for IgG and IgM antibodies. PCR primer sets designed for amplification of all the IgG isotypes variable heavy chain, were sufficient for the detecting of single DNA bands of predicted molecular weight for both the IgG antibody clones, 61D8 and 63G4 respectively (Figure 3-4.A-B). However, a different IgG light chain primer set was used for successful PCR amplification of the variable light chain, which resulted in a single DNA band at the predicted molecular weight (Figure 3-4.C). The two IgG antibody clones, 61D8 and 63G4 were from two independent mice cohorts immunized with the PrP^{Sc} vaccine 14R1. Similarly, cDNAs corresponding to IgM 63 and IgM 18 antibody clones were successfully PCR amplified with a heavy chain IgM primer set and was sufficient for the detection of a single DNA band (Figures 3-5.A and 3-6.A). Alongside, the IgM primer set was used for successful PCR amplification of the variable light chain of IgM 63 and IgM 18 antibody clones with a single DNA band at the predicted molecular weight (Figures 3-5.B and 3-6.B).

The immunoglobulin gamma-1 (IgG1) heavy chain with a kappa (κ) light chain represents the most abundant antibody isotype found in nature and produced by hybridoma cell lines (Johnson & Wu, 1997; Thiebe et al., 1999). For this reason, I focused on our IgG antibody clones, 61D8 and 63G4, PCR amplified them with IgG1, IgG2A, IgG2B, and IgG3 primers along with a mixture of heavy chain primers and we successfully got amplification of the cDNA using all the IgG primer mixture (Figure 3-4.A-B).

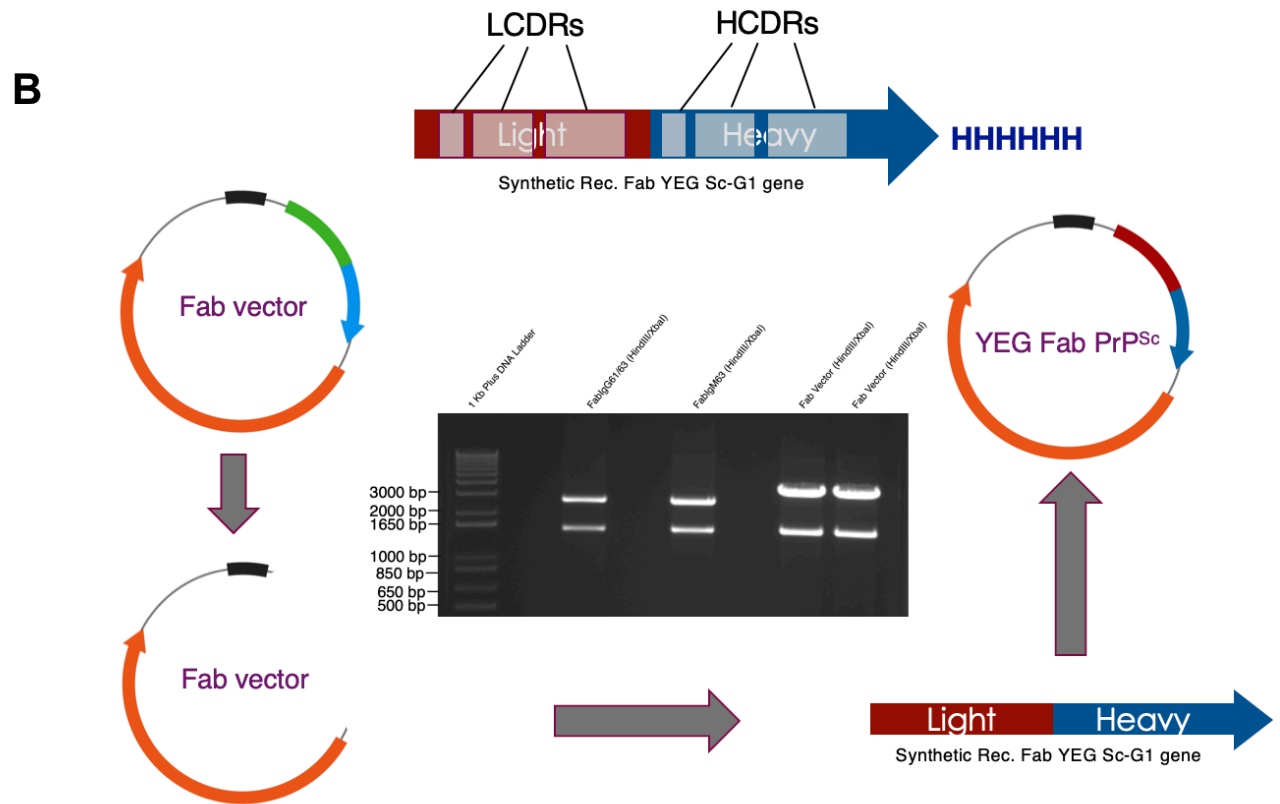
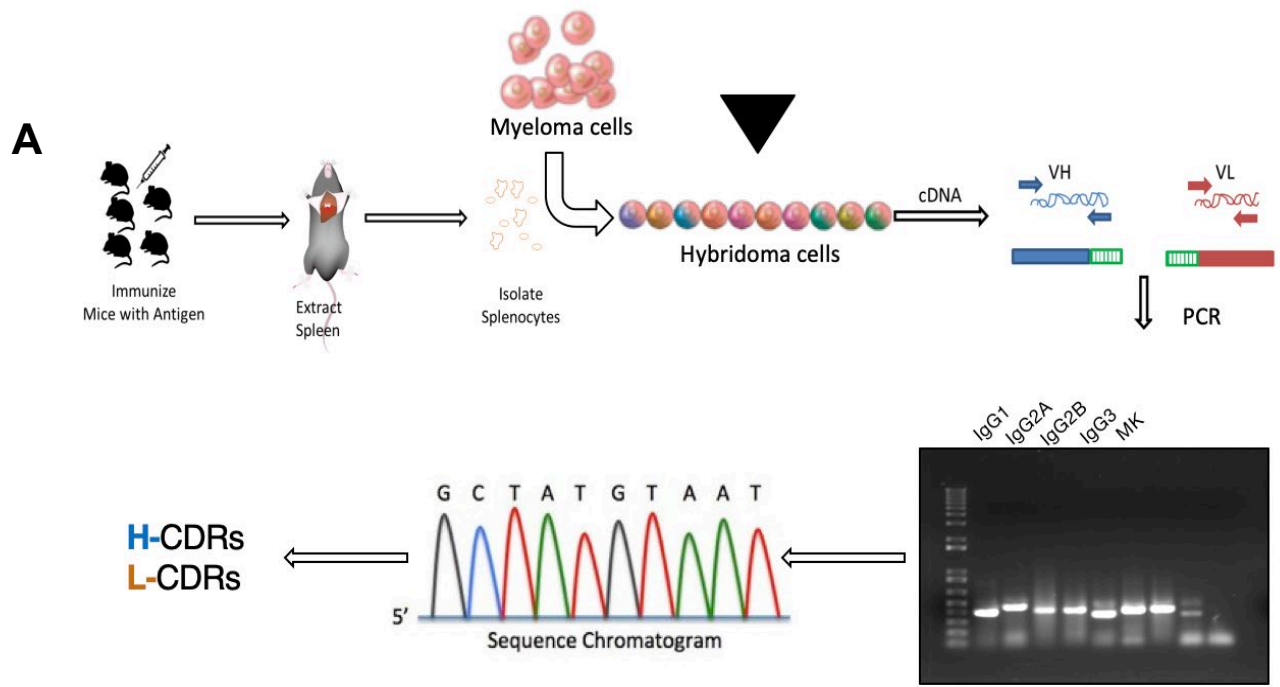


Figure 3-3: Schematic representation of engineering different PrP^{Sc} – specific antibody fragments currently in our research toolbox.

(A) Mice injected with PrP^{Sc} – vaccine (14R1), elicited an immune response to the vaccine for prions. The spleen is extracted from the mice at the end of the vaccine trial and the splenocytes were fused with myeloma cells to form mature hybridoma cells which are then grown in a selective culture medium and clones are grown from single parent cells on microtiter wells. The antibodies secreted by the different clones were then assayed for their ability to bind 14R1, PrP^{Sc} vaccine/antigen using indirect ELISA. The black arrowhead represents where my workflow began with hybridoma cells, followed by mRNA isolation and synthesis of cDNA by the retro-transcription system using the Superscript cDNAIII kit. The cDNA is amplified with different heavy chain primers and light chain primers. DNA sequences were analyzed and VH and VL CDRs are identified based on the primary protein structure of the antibody. **(B)** Mouse-derived variable heavy (VH) and variable light (VL) CDRs were grafted onto a human Fab and other antibody fragments framework with a 6xHis tag at the C-terminus for nickel affinity purification. The Fab gene was double digested and cloned into a Fab vector which can then be transformed and expressed in *E.Coli*.

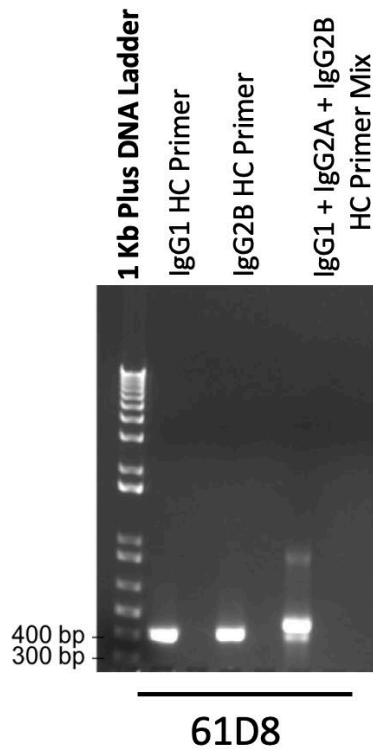
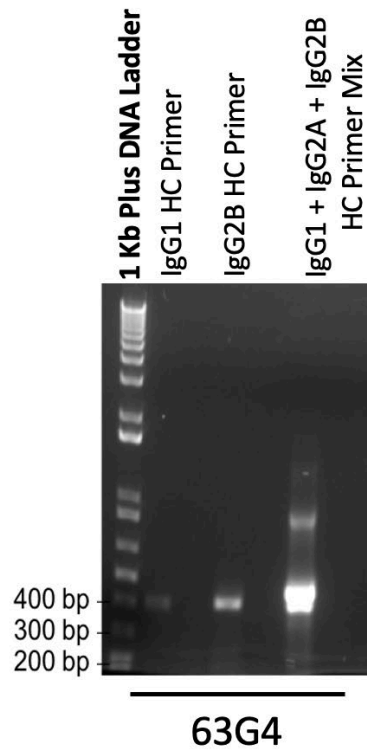
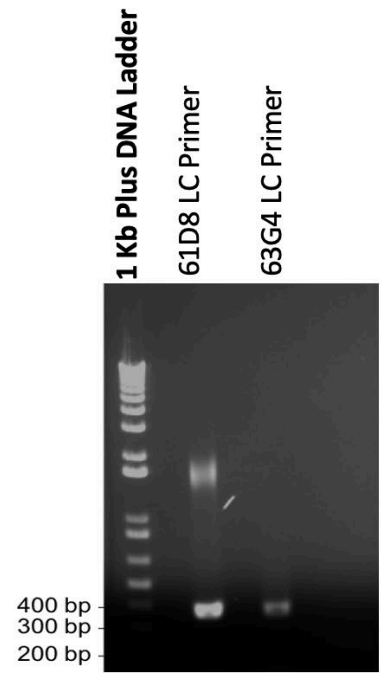
3.3.3 DNA sequence analysis

Following RT-PCR, we purified the RT-PCR products with a PCR clean-up kit and further purified the amplicons by agarose gel extraction and directly Sanger sequencing to determine the variable region sequences of the heavy and light chain from the IgG and IgM antibodies. The identified nucleotide sequences for the heavy chain and light chain variable regions from IgG antibody clones, 61D8 and 63G4 (data not shown) as well as IgM antibody clones, IgM 63 and IgM 18 (data not shown) were translated into protein sequences. The protein sequence data from both IgG and IgM antibody clones were compared by Blastp program to those deposited in the NCBI protein database and were determined to be a unique (Lagnel, Tsigenopoulos, & Iliopoulos, 2009). The heavy chain and light chain variable region sequences for each hybridoma were submitted to IMGT VQUEST to align framework regions and define three unique CDR regions. The Kabat numbering scheme was also used to verify the three CDR of the heavy and light chain variable regions (Martin, 1996).

The primary structure of the 61D8 antibody was determined from cDNA that was prepared from the 61D8-expressing hybridoma cells. The nucleotide sequence was translated into the respective protein sequence and the complementarity determining regions (CDRs) were identified based on the conserved sequences that frame both the heavy and light chain CDRs. A second monoclonal antibody (63G4) that was generated independently from another immunized mouse was found to have an identical primary structure, indicating the prominence of the epitope and the reproducibility of the immune response using the 14R1 antigen (Figure 3-4.D-E). We also performed Clustal Omega multiple sequence alignment (not shown) of the constant regions from all subclasses of mouse IgG (IgG1, IgG2a, IgG2b, and IgG3) using sequences available on

IMGT. Based on the sequence alignment from our PCR products amplified sequences and IgG subclass sequences, we concluded that our IgG monoclonal antibody was indeed an IgG2b subclass.

Similarly, I was able to elucidate the primary structure of IgM 63 and IgM 18 from cDNA that was prepared from their respective hybridoma cells. The nucleotide sequence was translated into the respective protein sequence and unique variable heavy and light chain CDRs of IgM 63 (Figure. 3-5.C-D) and IgM 18 (Figure. 3-6.C-D) were identified.

A**B****C****D**

Heavy Chain

Antibody	HCDR1	HCDR2	HCDR3
61D8	GYSFTSYWMH	MIDPSDSETKLNQQFKD	GKMGGRFYFDY
63G4	GYSFTSYWMH	MIDPSDSETKLNQQFKD	GKMGGRFYFDY

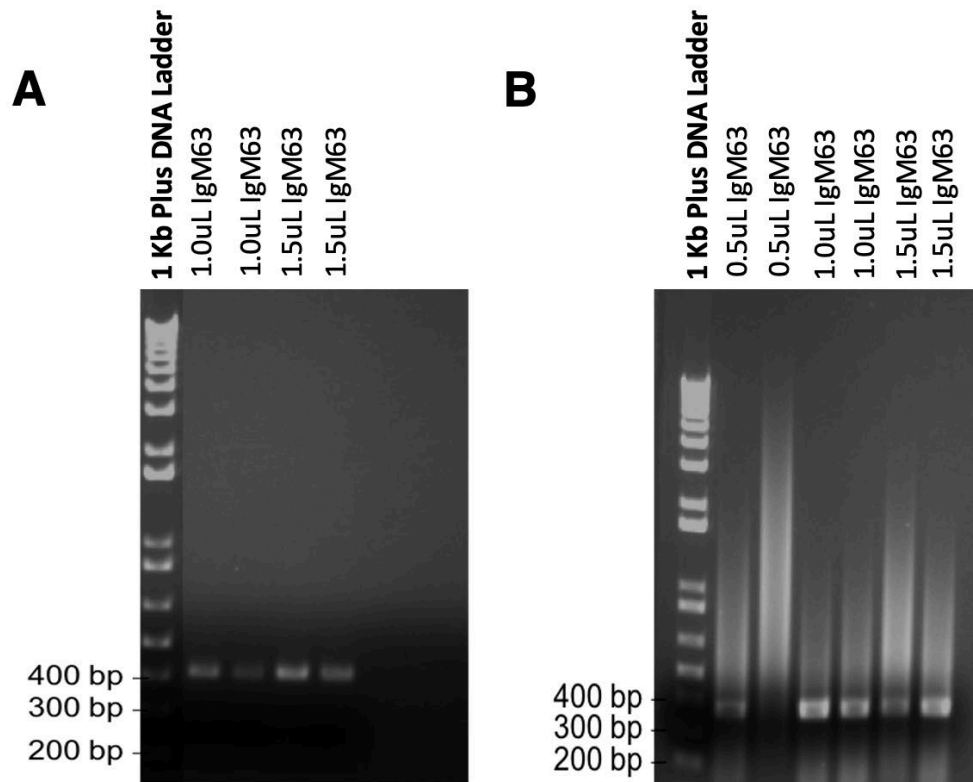
E

Light Chain

Antibody	LCDR1	LCDR2	LCDR3
61D8	KASQDVGTAVV	WASTRHT	QQFSSYPYT
63G4	KASQDVGTAVV	WASTRHT	QQFSSYPYT

Figure 3-4: PCR amplification of full-length heavy chain and light chain of monoclonal antibodies IgG-61D8 and IgG-63G4 cDNA (1 µg/µL).

Among other positive hybridoma clones generated from the same immunization, two IgG clones showed strongest reactivity with the antigen (14R1) namely 61D8 and 63G4. (A-B) Here we have shown the PCR amplification of the heavy chain and light chain cDNA of the two IgG clones, 61D8 and 63G4 derived from two separate mouse immunized with 14R1 to decode the primary structure of these antibodies and analyze its complementarity determining regions (CDRs). Reactions were made using different heavy chain reverse IgG primers (IgG1, IgG2A, IgG2B) at 0.5 µM and all reactions consisted of 0.5 µM of MH-1 and 0.5 µM MH-2 as heavy chain forward primer. DNA bands observed at ~ 400 bp were sent for nucleotide sequencing. (C) Light chain of both the clones were made using 0.5 µM of MK light chain forward primer and 0.5 µM of KC light chain reverse primer. Bands were observed at ~375 bp were sent for DNA sequencing (D-E) The primary structure of the 61D8 antibody was identified using cDNA synthesized from 61D8-expressing hybridoma cells. The nucleotide sequence was translated into the corresponding protein sequence, and the complementarity determining regions (CDRs) were discovered based on the conserved sequences that frame both the heavy and light chain CDRs. The primary structure of a second monoclonal antibody (63G4) generated independently from another immunized animal was found to be identical, confirming the prominence of the epitope and the reproducibility of the immune response employing the 14R1 antigen.



C Heavy Chain

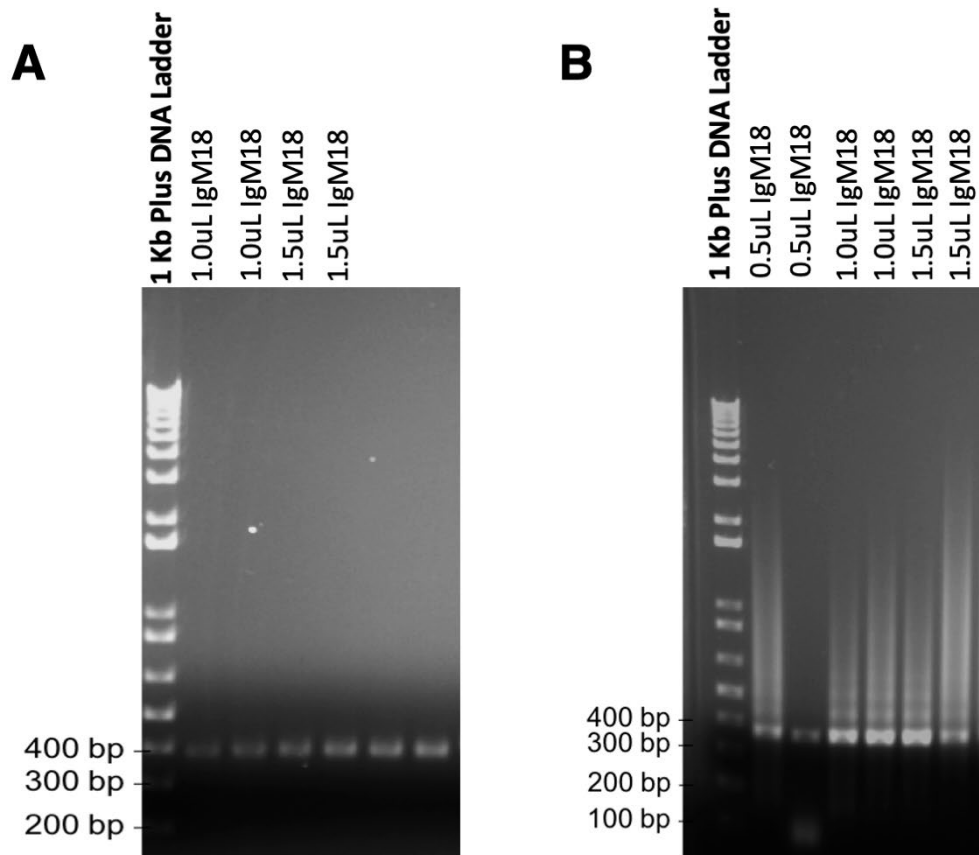
Antibody	HCDR1	HCDR2	HCDR3
IgM 63	GYTFTSYWMH	RIDPNSGGTKYNEKFKS	THYSYYSYDVRFAY

D Light Chain

Antibody	LCDR1	LCDR2	LCDR3
IgM 63	RASQSISNNLH	YASQSIS	QQSNSWPLT

Figure 3-5: PCR amplification of heavy chain and light chain of monoclonal antibody IgM63 cDNA (YEG Sc-M63) (1 µg/µL).

A total of twelve monoclonal antibodies (IgG and IgM) derived from the same immunization studies were discovered to exhibit the same specificity for native PrP^{Sc} as YEG Sc – G1. **(A-B)** Here we have shown the PCR amplification of the heavy chain and light chain cDNA of the IgM63 clone. Reactions were made using IgM heavy chain reverse primer at 0.5 µM and all reactions consisted of 0.5 µM of MH-1 and 0.5 µM MH-2 as heavy chain forward primer. DNA bands observed at ~ 400 bp were sent for nucleotide sequencing. **(C)** Light chain of the IgM63 clone was amplified in a reaction mixture containing 0.5 µM of MK light chain forward primer and 0.5 µM of KC light chain reverse primer. Bands observed at ~375 bp were sent for DNA sequencing **(D-E)**. The primary structure of the M63 antibody was identified using cDNA synthesized from IgM63-expressing hybridoma cells. The nucleotide sequence was translated into the corresponding protein sequence, and the complementarity determining regions (CDRs) were discovered based on the conserved sequences that frame both the heavy and light chain CDRs.



C Heavy Chain

Antibody	HCDR1	HCDR2	HCDR3
IgM 18	YTFTSYWMN	MIHPSDSETRLNQKFKD	DRYYFDY

D Light Chain

Antibody	LCDR1	LCDR2	LCDR3
IgM 18	RASGNIHNYLA	NAKTLAD	QHFWSPTPT

Figure 3-6: PCR amplification of heavy chain and light chain of monoclonal antibody IgM18 cDNA (YEG Sc-M18) (1 µg/µL).

A total of twelve monoclonal antibodies (IgG and IgM) derived from the same immunization studies were discovered to exhibit the same specificity for native PrP^{Sc} as YEG Sc – G1. **(A-B)** Here we have shown the PCR amplification of the heavy chain and light chain cDNA of the IgM18 clone. Reactions were made using IgM heavy chain reverse primer at 0.5 µM and all reactions consisted of 0.5 µM of MH-1 and 0.5 µM MH-2 as heavy chain forward primer. DNA bands observed at ~ 400 bp were sent for nucleotide sequencing. **(C)** The light chain of the IgM18 clone was amplified in a reaction mixture containing 0.5 µM of MK light chain forward primer and 0.5 µM of KC light chain reverse primer. Bands observed at ~375 bp were sent for DNA sequencing **(D-E)**. The primary structure of the M18 antibody was identified using cDNA synthesized from IgM18-expressing hybridoma cells. The nucleotide sequence was translated into the corresponding protein sequence, and the complementarity determining regions (CDRs) were discovered based on the conserved sequences that frame both the heavy and light chain CDRs.

3.3.4 Engineering a toolbox of PrP^{Sc}-specific antibody fragments

Historically, a great deal of effort has been devoted to developing antibodies that specifically recognize PrP^{Sc} but not PrP^C, as such antibodies would have enormous diagnostic and experimental value. Most existing antibodies recognize both PrP^C and PrP^{Sc}, or only PrP^C (Korth, Streit, & Oesch, 1999; Peretz et al., 1997). Nevertheless, several antibodies have been described during the past 10 years that are reported to be specific for PrP^{Sc}, Table 3-1. However, they are not known to have a conformational epitope recognizing native PrP^{Sc} but rather recognize linear PrP epitopes (Biasini et al., 2008).

The modular nature of antibodies, both structurally and functionally, allows for the generation of smaller antigen-binding fragments whereby separate domains can be extracted through biochemical or genetic means (Kipriyanov & Le Gall, 2004). I have employed recombinant DNA technology to create a wide range of PrP^{Sc}-specific antibody toolbox composed of a wide range of recombinant humanized antibody fragments for prion diseases. Table 3-4 provides a complete list of all engineered PrP^{Sc} – specific antibody fragments grafted with CDRs derived from full-length IgG and IgM clones into a human antibody framework (P. T. Jones et al., 1986). These PrP^{Sc}-specific antibody fragments can be employed as research tools for purifying and structural characterization of PrP^{Sc} in molecular investigations (chapter 4), as well as tools for prion disease therapeutics by promoting PrP^{Sc} clearance from tissues. In this chapter, I have focused on engineering antibody derivatives and their conjugates from the IgG clone such as Fab G1, scFv G1 conjugated with GFP and VHH G1/nanobody as IgG is the most abundant immunoglobulin class in human serum (Dall'Acqua, Cook, Damschroder, Woods, & Wu, 2006).

Table 3-4: Recombinant antibody fragment derivatives of YEG Sc, PrP^{Sc} – specific monoclonal antibody

Recombinant Humanized YEG Sc Antibody Fragments												
Construct #	Construct	Vector	Cloning Sites	Signal Peptide	C-terminus MYC tag	C-terminus HIS tag	Linker (GGGS)	MW kDa	PI	Soluble	Inclusion	Stop Codon
1	Fab G1	Fab 69	Xho1/HindIII	OmpA/PhoA	X	6 x HIS	N/A	52.5	8.68	✓	X	✓
2	Fab M18	Fab 69	Xho1/HindIII	OmpA/PhoA	X	6 x HIS	N/A	52.4	8.56	✓	X	✓
3	Fab M63	Fab 69	Xho1/HindIII	OmpA/PhoA	X	6 x HIS	N/A	53.1	8.66	✓	X	✓
4	scFv G1	Fab 69	Xho1/HindIII	OmpA/PhoA	X	6 x HIS	(GGGS) ₄	31	9.05	✓	X	✓
5	scFv G1 - CPP	Fab 69	Xho1/HindIII	OmpA/PhoA	X	6 x HIS	CPP Linker	34	8.62	✓	X	✓
6	scFv G1 - mEGFP	Fab 69	Xho1/HindIII	OmpA/PhoA	X	12 x HIS	(GGGS) ₄ + (GGGS)	59.2	7.2	✓	X	✓
7	scFv G1	Fab 69	Xho1/HindIII	OmpA/PhoA	✓	6 x HIS	(GGGS) ₄	33.8	9.27	✓	X	X
8	scFv G1 - CPP	Fab 69	Xho1/HindIII	OmpA/PhoA	✓	6 x HIS	CPP Linker	35	9.69	✓	X	X
9	scFv G1 - mEGFP	Fab 69	Xho1/HindIII	OmpA/PhoA	✓	12 x HIS	(GGGS) ₄ + (GGGS)	62.2	7.79	X	✓	X
10	scFv G1 - mEGFP - CPP	Fab 69	Xho1/HindIII	OmpA/PhoA	✓	12 x HIS	CPP + GGGS	63	8.88	X	✓	X
Without the stop codon and PhoA signaling peptide												
11	scFv G1	Fab 69	Xho1/HindIII	OmpA	X	6 x HIS	(GGGS) ₄	30	9.41	N/D	N/D	X
12	scFv G1 - CPP	Fab 69	Xho1/HindIII	OmpA	X	6 x HIS	CPP Linker	33	8.94	N/D	N/D	X
13	scFv G1 - mEGFP	Fab 69	Xho1/HindIII	OmpA	X	12 x HIS	(GGGS) ₄ + (GGGS)	58.6	8.1	Partial	Partial	X
14	scFv G1	Fab 69	Xho1/HindIII	OmpA	✓	6 x HIS	(GGGS) ₄	31.5	9.09	N/D	N/D	X
15	scFv G1 - CPP	Fab 69	Xho1/HindIII	OmpA	✓	6 x HIS	CPP Linker	34.3	8.64	N/D	N/D	X
16	scFv G1 - mEGFP	Fab 69	Xho1/HindIII	OmpA	✓	12 x HIS	(GGGS) ₄ + (GGGS)	59.8	7.16	N/D	N/D	X
17	VHH G1	Fab 69	Xho1/HindIII	OmpA	X	6 x HIS	N/A	16.8	9.73	✓	X	X
18	VHH G1	Fab 69	Xho1/HindIII	OmpA	✓	6 x HIS	N/A	18.3	9.2	N/D	N/D	X
19	VHH G1 + 8D3	Fab 69	Xho1/HindIII	OmpA	X	6 x HIS	(GGGS) ₄	31.2	9.06	✓	X	X
20	VHH G1 + 8D3	Fab 69	Xho1/HindIII	OmpA	✓	6 x HIS	(GGGS) ₄	32.6	8.56	N/D	N/D	X

3.3.5 Design of PrP^{Sc}-specific Fabs

Fab agents are the oldest class of monoclonal antibody fragments that have been widely used in biomedical research and therapeutics. Here we show the design and engineering of recombinant PrP^{Sc} – specific Fab fragments (Figure 3-7) through motif grafting, whereby the rodent IgG and IgM CDRs are loop grafted onto an existing human variable domain and constant region framework, as previously described in chapter 2. PrP^{Sc}-specific Fab fragments have an N-terminus OmpA signaling peptide for periplasmic expression and a 6x his tag at the C-terminus of the protein for Ni-NTA affinity purification.

The synthetic gene consisting of the Fab G1, M63 (Figure 3-8.A) and M18 (Figure 3-8.B) constructs were synthesized by BioBasic DNA Inc, Markham Ontario. These genes were double digested using restriction enzymes, HindIII and XbaI and were successfully cloned into a Fab expressing vector (as previously described in chapter 2) for recombinant expression and purification (Figure 3-8.A-B).

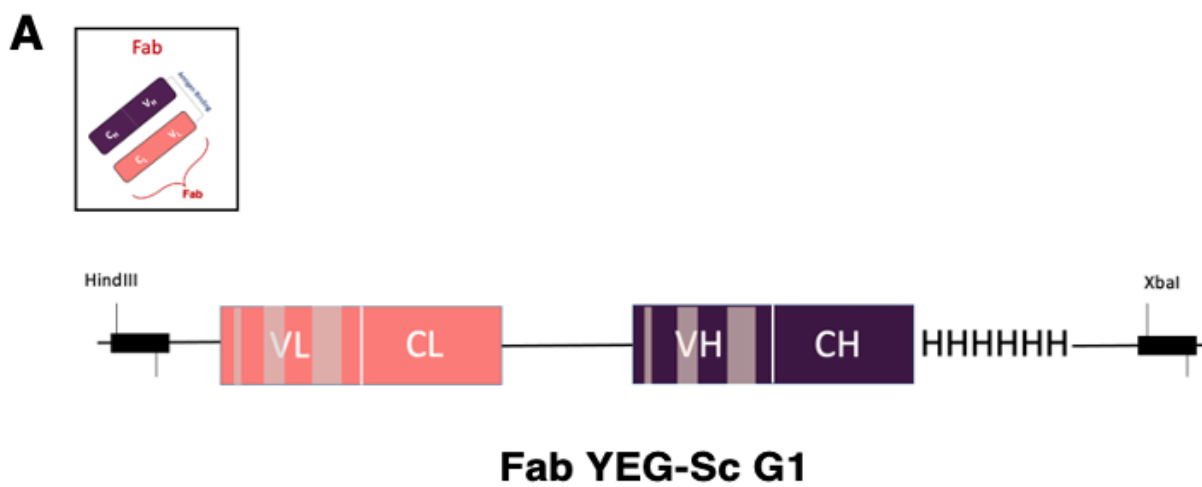


Figure 3-7: Design of recombinant PrP^{Sc} – specific Fabs.

(A) Schematic representation of engineered humanized recombinant antigen-binding fragment antibody (**Fab YEG Sc-G1**). Cartoon depicting the design of human Fab framework with component sequences of variable light chain with constant light chain (purple) and variable heavy and constant heavy chain (peach). The light and heavy chains are expressed in tandem with a 6xHis tag fused at the C-terminus of a constant heavy chain for purification by the Ni-NTA column. Similar, constructs for Fab IgM 63 and Fab IgM 18 were created by inserting specific rodent CDRs of the respective IgM antibodies into a human Fab framework to create recombinant Fab YEG Sc – M63 and M18.

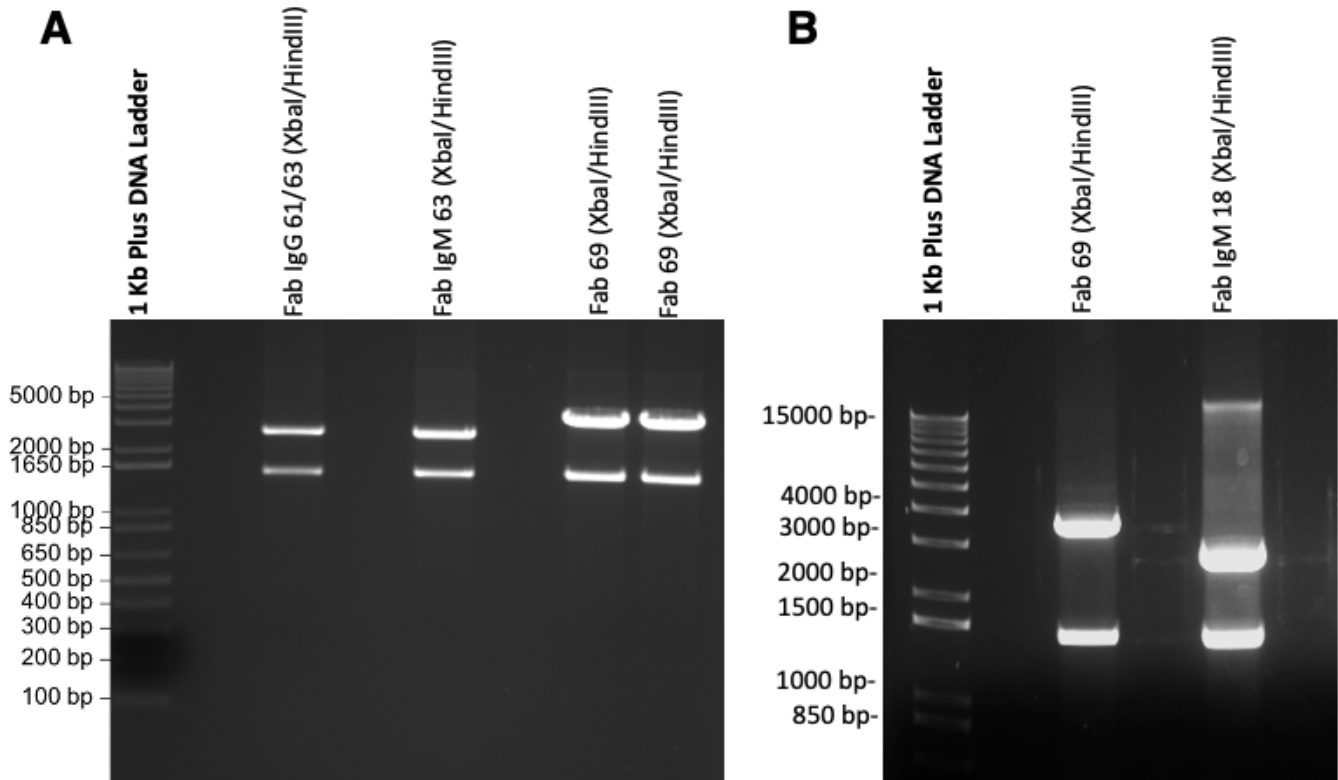


Figure 3-8: Double restriction digest of recombinant Fab G1, Fab M63 and Fab M18 constructs and human Fab vector.

(A-B) Insert Fab plasmids were incubated with the *Xba*I and *Hind*III restriction enzyme which yields two bands whereby the ~1650 bp band corresponds to the human Fab constructs (insert) and the band at ~2900 bp corresponds to the construct vector. The Fab insert is then ligated with the Fab 69 human vector corresponding band at ~4000 bp. These excised fragments were subsequently ligated to generate a human recombinant Fab monoclonal antibody that would elicit the antibody features of the full-length mouse PrP^{Sc}-specific antibodies.

3.3.6 Expression and purification of selected PrP^{Sc}-specific antibody fragments

An efficient methodology for the successful expression and purification of large quantities of recombinant anti-PrP Fabs in *E. coli* as soluble and functional Fabs was previously developed and described (Chapter 2). The same procedure was used to successfully express PrP^{Sc}-specific recombinant Fab G1, Fab M63, and Fab M18 (Figure 3-9.A-B) (S1). The design of the Fab constructs was such that the heavy and light chains of the Fab fragments would be expressed in tandem with a 6xHIS-tag at the C-terminus for purification, V_L-C_L-V_H-C_H-6xHis-tag. This would then give the Fabs a molecular weight of ~25 kDa when separated using SDS-PAGE protein gels. In this chapter, we focused on the characterization of two anti-PrP^{Sc}-specific Fabs, Fab G1 and Fab M63, and analyzed their activity in several immunoassays such as immunogold labelling, immunoprecipitation of the PrP^{Sc} vaccine/antigen, and immunocytochemistry. G1 indicates IgG clone antibody, and M63 represents IgM63 clone antibody.

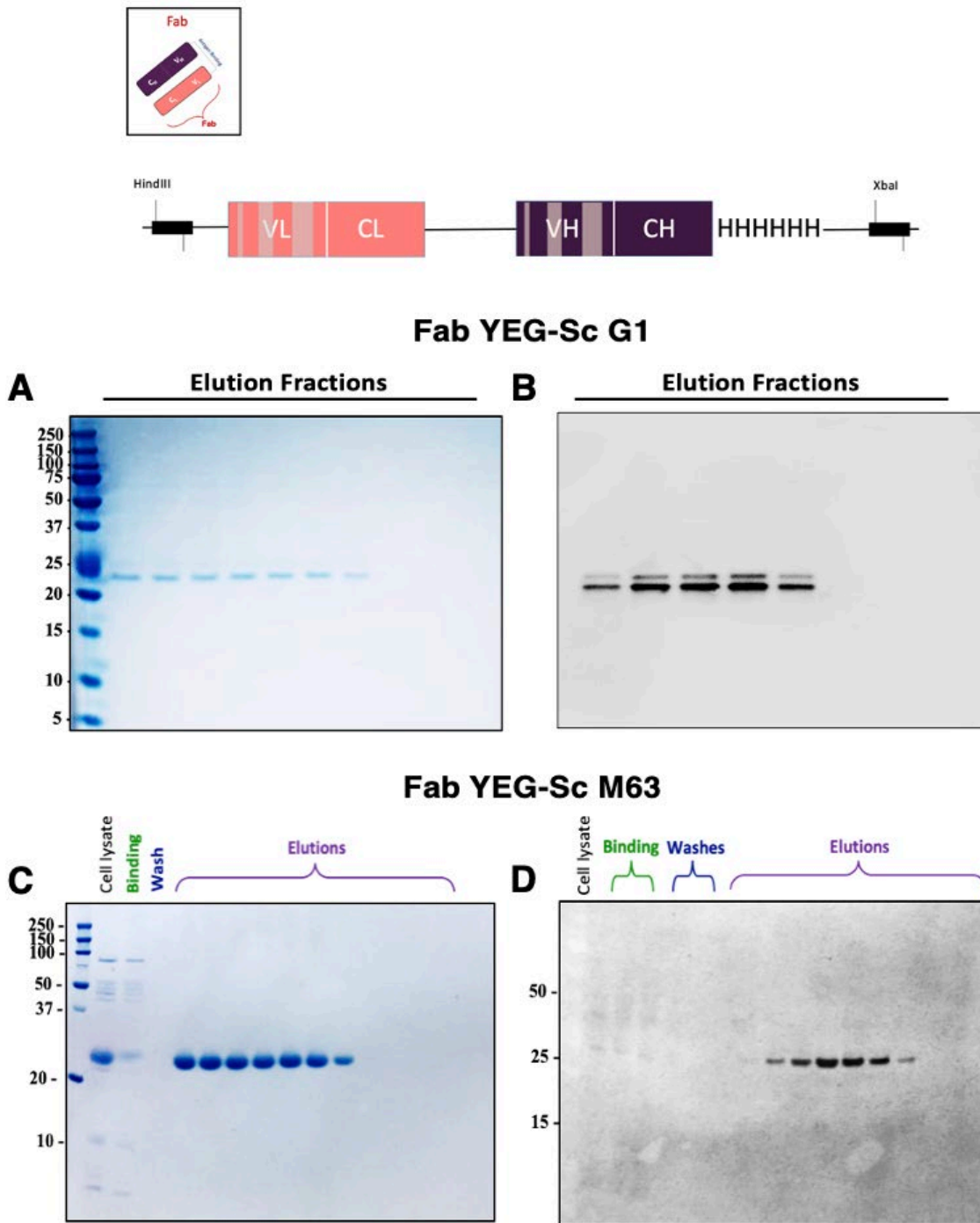


Figure 3-9: Expression and purification of recombinant PrP^{Sc} – specific Fabs.

Expression and purification of recombinant PrP^{Sc} – specific Fab fragments. Analysis of recombinant expression in BL21(DE3) cells via IMAC purification via SDS-PAGE Coomassie

staining (left) and western blot using anti-human Fab (right) of **(A-B)** PrP^{Sc} specific YEG Sc - G1 and **(C-D)** PrP^{Sc} specific YEG Sc - M63. All recombinant PrP^{Sc} Fabs have a construct design of VL-CH-VH-CH-6X_{HIS} whereby the light and the heavy chains of the fab fragments are expressed in tandem. Under denaturing conditions Fabs will have a molecular weight of 25 kDa. In cases where the heavy and light chain fragments are separately noticed is due to the difference in the amino acid sequence of each Fab antibody. The top and bottom fragment of the antibody corresponds to heavy and light chain, respectively.

3.3.7 Epitope mapping of YEG Sc – G1, M18 and M63

Next, we used an indirect ELISA to confirm how the PrP^{Sc}-specific Fabs interacted with revert-mutants of the 14R1 vaccine/antigen and the unmodified 14R1 vaccine/antigen as positive control and unmodified Het-2s scaffold protein of PrP^{Sc} vaccine/antigen (Fang et al, manuscript in preparation). The project on developing the 14R1, a PrP^{Sc} vaccine for Chronic Wasting Disease and other prions was led by Drs. Andrew Fang and Holger Wille.

The light bulb idea for developing the PrP^{Sc} vaccine was from the structure of HET-s consisting of a 2-rung beta solenoid structure (Wasmer et al., 2008). HET-s is a fungal prion protein from *Podospora anserina*, unrelated to any vertebrate protein and therefore was used as a scaffold for prion vaccine in the Wille lab. A four-rung β -solenoid construct of HET-s, termed HET-2s, was created through duplication and by using an optimized linker comprised mainly of glycine residues. Using HET-2s as a scaffold, our lab created a prion vaccine, 14R1, by replacing the surface residues of HET-s with those predicted to be on the surface of the 4-rung beta solenoid model of PrP^{Sc} (Fang et al, manuscript in preparation).

Fang and colleagues created a wide range of revert-mutants to determine the key residues involved in forming the antigen-antibody complex of 14R1-derived antibodies. For each of the constructs, two of the amino acids originally inserted to mimic the structure of PrP^{Sc} were reverted to the original HET-s sequence (Wasmer et al., 2008). Since 14R1 is based on a duplicated version of HET-s (218-289), the reversion mutations were applied to both halves of 14R1 (Figure. 3-10). Constructs A-D and 1G to HG reverted amino acids along vertical columns

(Figure 3-10. A and C). Whereas constructs E through H reverted amino acids along horizontal rows (Figure 3-10.B).

The epitope mapping using the 14R1 revertant mutants with Fab G1 revealed construct A and 2G, with residues His 110 and Asp 146 playing a key role in forming the antigen-antibody complex (Figure 3-11.A). This was shown by the indirect ELISA whereby the Fab G1 recognized most of the constructs, including the positive control, unmodified 14R1 but showed significantly less binding to the constructs A and 2G. His 110 and Asp 146 are placed at the β -arc region of the 14R1 as well as on the 4R β S model of PrP^{Sc} (Spagnolli et al., 2019). When both these residues are replaced with Gly, as represented by construct 2G, abolishes the antibody binding revealing its role as part of the Fab YEG Sc – G1 PrP^{Sc} specific antibody epitope. These epitope mapping results were in agreement with the epitope mapping results with full-length YEG Sc – G1 monoclonal antibody (Figure 3-11.B). The full-length YEG Sc – G1 has a bivalent property as it has two fragment antigen binding sites (Fabs) while the Fab has monovalent antigen binding properties which are concurrent with our ELISA OD 450 measurements (Oostindie et al., 2022).

We also performed epitope mapping of our engineered IgM PrP^{Sc} – specific Fab fragments, Fab M18 and Fab M63 using revertant mutants of 14R1 (Figure 3-12). The ELISA results with Fab M18 revealed more than one epitope for Fab M18 (Figure 3-12.A), showing the ability to recognize multiple epitopes on the 4R β S model of PrP^{Sc}, residues Asn 103 and Asp 143 (construct C) and Asp 146 and His 110 (construct 2G) as the key residues for the Fab M18 PrP^{Sc} – specific antibody epitope. Comparatively, Fab IgM 63 showed less binding to construct C (residues, Asn 103 and Asp 143) compared to the rest of the construct and the positive control, unmodified 14R1 (Figure 3-12.B).

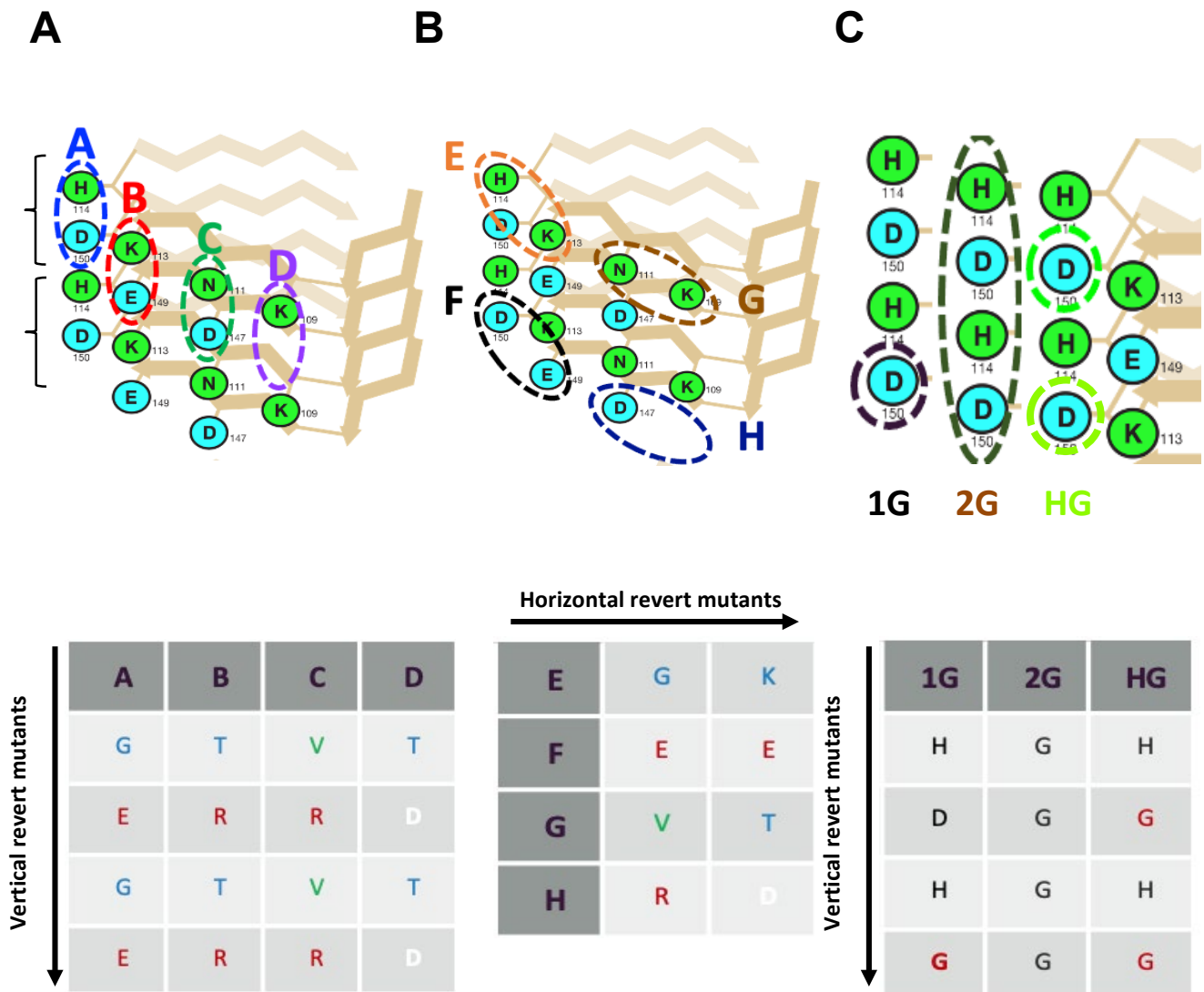


Figure 3-10: 14R1 revert mutants to identify the core epitope of Fab G1.

To determine the precise epitope of YEG Sc – G1 and other 14R1-derived antibodies, revertant mutants of the 14R1 antigen/vaccine candidate were created by Andrew Fang (Fang et al., manuscript in preparation) and was used for epitope mapping. Two of the amino acids originally inserted to mimic the structure of PrP^{Sc} were reverted to the original HET-s sequence pairwise either **(A, C)** vertically or **(B)** horizontally in each of the constructs (Wasmer et al., 2008). Because 14R1 is based on a duplicated version of HET-s (218-289), reversion mutations were performed on both halves of 14R1 (shown in black brackets).

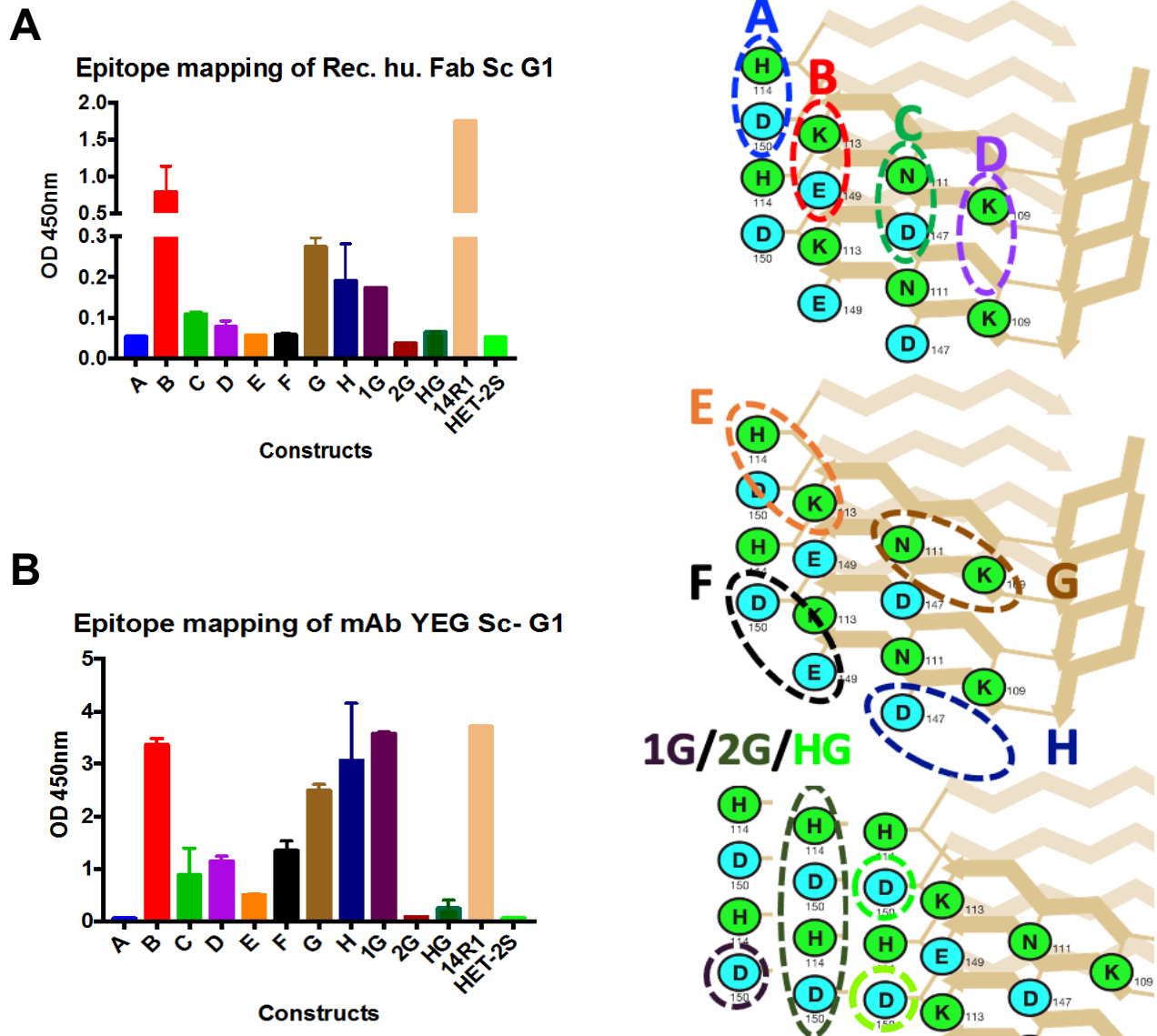


Figure 3-11: Epitope mapping of recombinant Fab YEG Sc G1 and full-length mouse-derived YEG Sc G1 using 14R1 revert mutants to identify the core epitope of Fab G1.

To determine the precise epitope of YEG Sc – G1 and other 14R1-derived antibodies, revertant mutants of the 14R1 antigen/vaccine candidate were created by Andrew Fang and used for epitope mapping. The ELISA results show that both the (A) recombinant Fab and the (B) full-length YEG Sc-G1 monoclonal antibody recognizes most revertant mutants of 14R1 (B, D, F, G, and H) as well as 14R1. The revertant mutant “A” and “2G” abolishes the antigen-antibody interaction in Fab and full-length YEG Sc–G1 binding, demonstrating the significance of the His and Asp residue at the B-ark region as part of the YEG Sc-G1 PrP^{Sc}- specific antibody epitope.

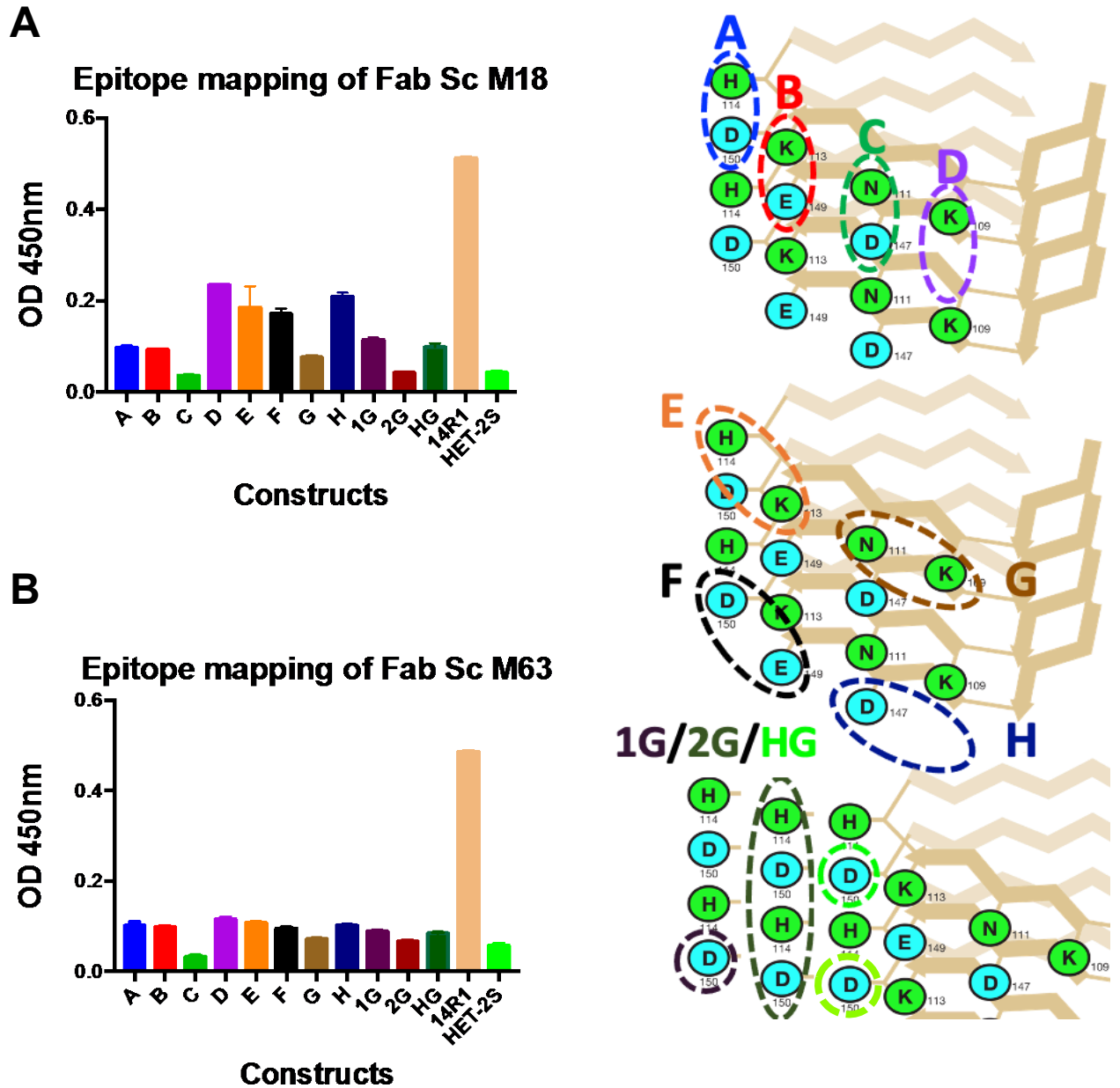


Figure 3-12: Epitope mapping of recombinant Fab M18 and Fab M63 using 14R1 revert mutants to identify the core epitope of Fab M18 and Fab M63.

Epitope mapping using the 14R1 revertant mutants to identify the amino acids that form the core epitope of recombinant Fab IgM 18 and Fab IgM 63. The indirect ELISA results indicate that most revertant mutants (A, B, D, E, F, G, H, and HG) of 14R1 are equally well recognized by the recombinant (A) Fab M18 and (B) Fab M63. In contrast, the revertant mutant “C” and “2G”

abolished antigen-antibody interaction with recombinant Fab M18 and revertant mutant “C” abolished its binding to recombinant Fab M63 antibody, demonstrating the significance of the Asn 103 and Asp 143 residue as part of the YEG Sc – M18 and M63 PrP^{Sc}-specific antibody epitope.

3.3.8 Epitope confirmation via activity assays

The specificity of the targeted epitope matched the ELISA epitope profiling for all tested Fabs.

The initial activity of the purified and fully folded recombinant PrP^{Sc} Fabs was done using an indirect ELISA assay against coated 14R1 amyloid fibrils, PrP^{Sc} vaccine/antigen (Figure 3-13.A).

All the engineered Fabs recognized its antigen, 14R1 showing that the engineering of the Fabs was successful. Based on the earlier epitope mapping results showed that our antibody has a discontinuous epitope and can only recognize the antigen 14R1/PrP^{Sc} in its native condition.

After confirming its activity with the PrP^{Sc} vaccine/antigen, 14R1. We tested the activity of these three Fabs with infectious crude brain homogenates of RML and human GSS^{A117V} prions, which were coated on ELISA plates (Figure 3-13.B).

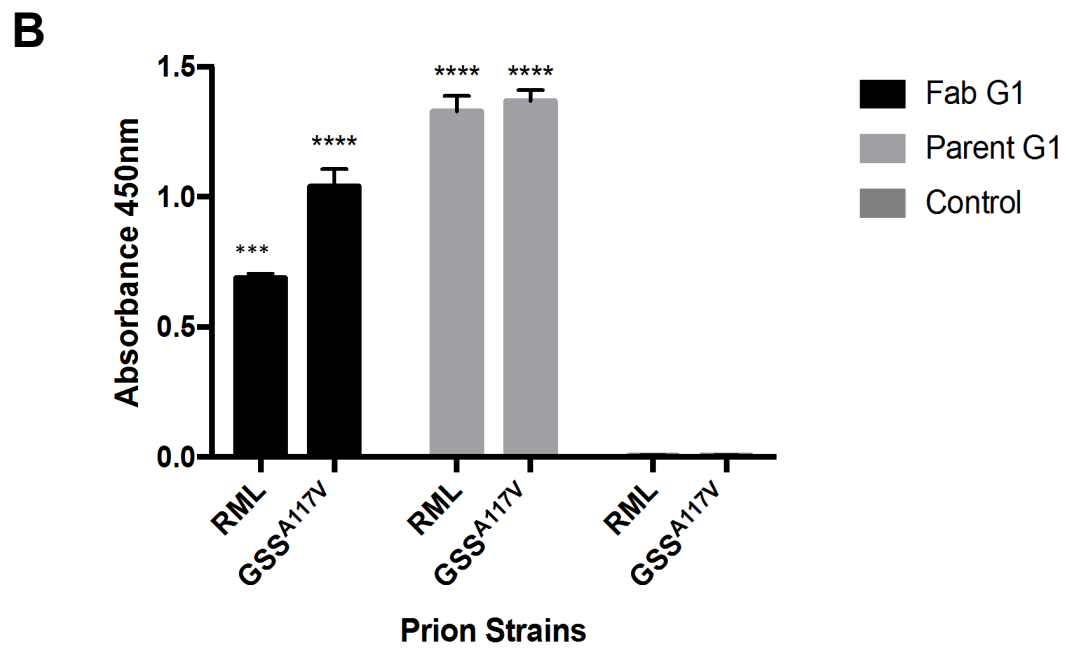
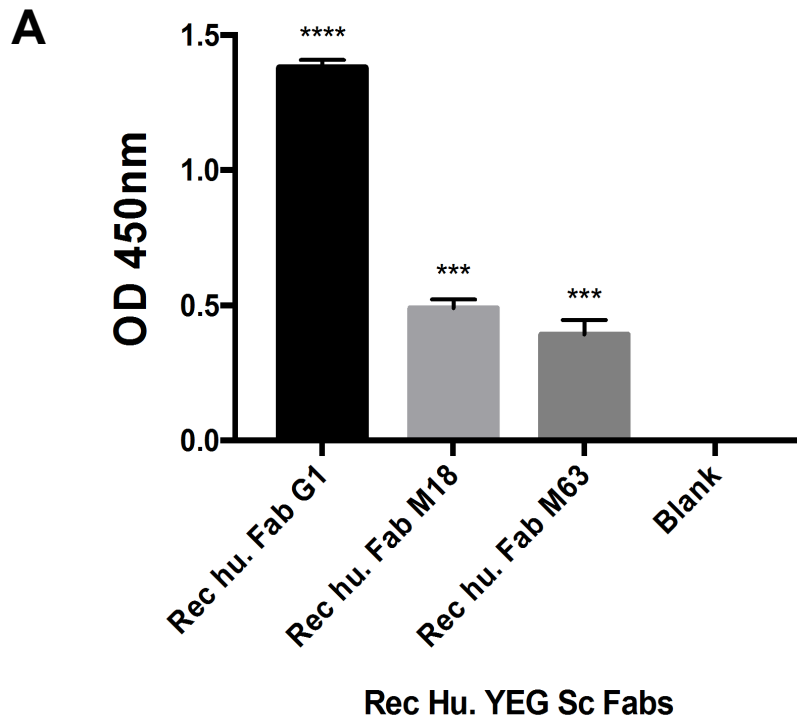


Figure 3-13: Activity assay of Fab G1 towards PrP^{Sc} – vaccine/antigen (14R1) and prions.

The fully folded and functional recombinant PrP^{Sc}-specific Fab fragments were tested for antigen recognition using an indirect ELISA assay with 14R1 antigen and infectious brain homogenates.

(A) Indirect ELISA results indicate binding of recombinant PrP^{Sc}-specific fragment antibodies to 14R1 antigen with the highest antigen-antibody interaction with the recombinant Fab G1 from the IgG clone. **(B)** The recombinant Fab G1 and the full-length G1 monoclonal antibodies were screened in an ELISA assay against untreated infectious RML brain homogenate and human GSS^{A117V} cortex brain homogenate and measurements at OD450 for all infectious prion isolates were higher compared to the control samples which was only incubated with the secondary anti-human Fab antibody.

(A) The data presented are statistically significant compared with the blank ($p < 0.0001$) **(B)** RML $p = 0.0001$ and GSS-A117V $p = 0.0002$ using One-way ANOVA, Dunnett's test on prism 7.0 graphpad.

3.3.9 Comparative *in silico* modelling and docking of Fab G1

Computational modelling was performed on the structure of the Fab G1 antibody by Dr. Luda Dorosh from the Wille lab to understand the folding of the engineered antibody fragment as well as to perform *in silico* binding to the human PrP^{Sc} model. The Fab G1 model was adapted from the Fab structure available in Protein Data Bank (PDB), PDB# 4H88 (Berman et al., 2000) and simulated with the same buffer conditions as used in experimental conditions. The ribbon diagrams of the fragment antibody, showing stabilized representative conformation of the Fab G1 model after 20 ns (Figure 3-14.A-B). The stabilized model of Fab G1 was docked with the human PrP^{Sc} model to observe if hydrogen bonds are formed and more specifically between which key residues. The comparative computational docking and simulation revealed favorable hydrogen bonds between the residues H111 and D147 of the human PrP^{Sc} and the hydrophilic patch of the antibody (Figure 3-14.C). These docking results are in alignment with our experimental epitope mapping results.

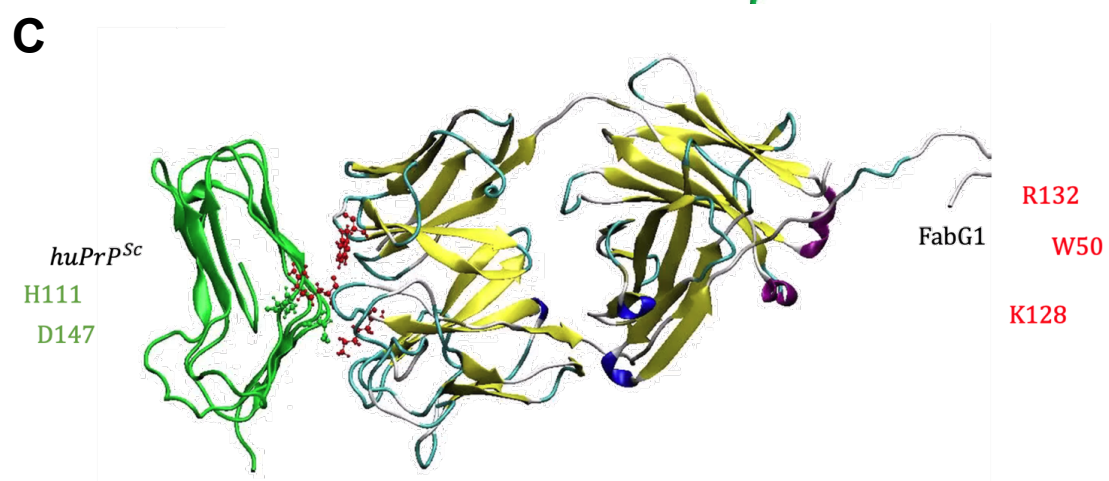
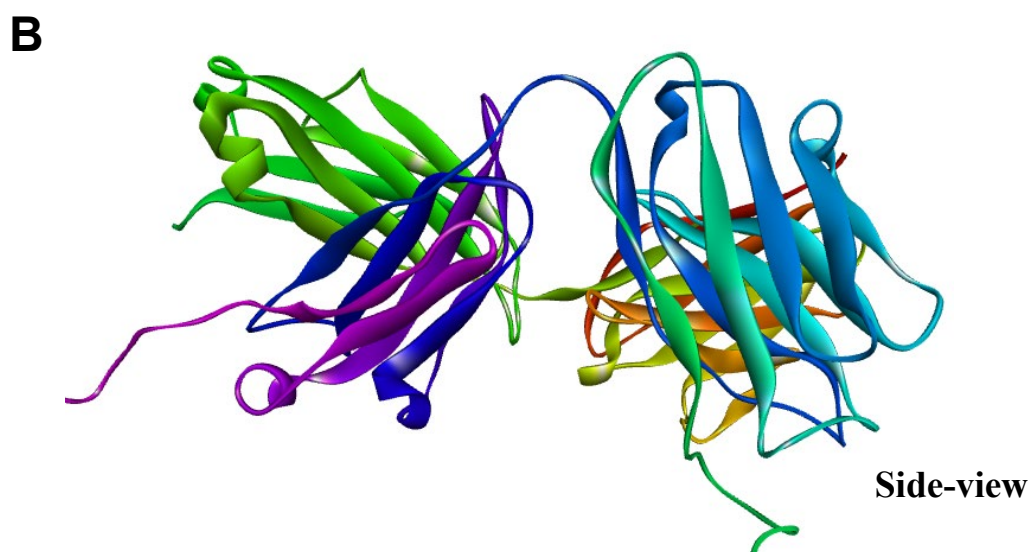


Figure 3-14. Molecular dynamics simulation of Fab G1 and human PrP 27-30 stabilized for 140 ns.

Ribbon diagrams of fragment antibody **(A)** top view and **(B)** side view showing stabilized representative conformation of Fab G1 model after 20ns MD. **(C)** The identical conditions were used as in the wet-lab experiment for molecular docking and the modelling of Fab G1 (shown in yellow beta-strands) with huPrP 90-231 (green beta-solenoidal structure) in AccelrysDS and simulated at 310K for 50. ns. The docked hydrophilic surface of the Fab G1 antibody formed a complex with residues H111 and D147 of the human PrP^{Sc} 4R β S model. These computational results are in alignment with our experimental epitope mapping results showing the importance of the key residues for the antigen-antibody interaction.

3.3.10 Immunogold labelling of RML prions using YEG Sc – G1 and YEG Sc – M63

We were interested in using our PrP^{Sc} – specific monoclonal antibodies, specifically the engineered recombinant Fab YEG Sc - G1 and M63, as well as hybridoma-derived full-length YEG Sc – G1 monoclonal antibodies as an alternate approach to decipher the structure of infectious prion fibrils. This would provide us with information on the orientation of the epitopes in these infectious amyloid aggregates or fibrils and confirm that the morphologies identified by EM are produced by the polymerization of PrP 27-30 monomers. Our recombinant Fab YEG Sc-G1 and mouse-derived full-length YEG Sc-G1 have a discontinuous epitope that recognizes PrP^{Sc} only in its native structure, with key residues H110 and D146 being crucial in antigen-antibody recognition. We employed another PrP^{Sc}-specific Fab M63 antibody that has a

discontinuous epitope and recognizes PrP^{Sc} in its native condition only, with key epitope residues, Asn 103 and Asp 143. The best immunogold was achieved when the sample was in its native state.

In this chapter I have used PK digested and PTA purified and sucrose step–gradient purified RML prion fibrils as previously described and shown in Chapter 2, (Figures 2-12 and 2-13). The large amyloid aggregates of PK_P2 RML prions (PrP 27-30) were decorated with the conformational mouse-derived full-length YEG Sc-G1 monoclonal antibody, recognizing the two pivotal residues, H110 and D146 in their native form followed with a secondary anti-mouse antibody conjugated to 6nm gold particles (Figure 3-15.A-D). In contrast, no antibody decoration occurred in the control samples (Figure 3-15.E), indicating the specificity of the labeling. An interesting observation was made, that the PrP^{Sc}-specific YEG Sc-G1 labeled more specifically to the large aggregates of PrP27-30 and not the long amyloid fibrils, suggestive of different structural morphologies observed between the large aggregates and twisted amyloid fibrils of RML prions. These results are in alignment with the immunogold labeling performed using monoclonal antibody YEG Sc-G1 on purified L-type BSE prions in their native form, indicating its specificity for all infectious prions (Kamali-Jamil et al., 2021).

To determine if the engineered Fabs retain their specificity to RML prions, I performed immunogold labelling with Fab YEG Sc-G1 on PK_P2 fractions and pellet wash samples from sucrose step gradient purification (as described in chapter 2). PK_P2 sample is known to consist of different conformational states of the infectious RML prion protein such as clumps of amyloid fibrils, large and small amyloid aggregates, 2D crystals and the pellet wash sample after the sucrose-step gradient purification is known to have a dense amount of isolated amyloid fibrils (Kamali-Jamil et al., 2021). Fab YEG Sc-G1 decorated the RML PK_PE large fibrillar

aggregates (Figure 3-16.A-B). The epitope of the full-length and Fab YEG Sc-G1 is the same, it has a conformational epitope for native PrP^{Sc} only, recognizing residues H110 and D146 to form an antigen-antibody complex. In contrast, Fab YEG Sc-G1 did not label the isolated amyloid RML fibrils from the pellet wash fraction (Figure 3-16.D-E). This indicates that the long twisted amyloid fibrils in the pellet wash indicate that RML fibrils have a different conformational state compared to the aggregates found in the PK-P2 fraction. In parallel, control experiments without the primary Fab fragment showed no presence of gold particles, proving the specificity of the immunogold labelling (Figure 3-16.C and F). These observations made via immunogold labelling using the conformational antibody is in agreement with the recent cryo-EM structure of the RML amyloid fibrils revealing a Parallel In-Register Intermolecular β -sheet structure (PIRIBS) (Artikis et al., 2022).

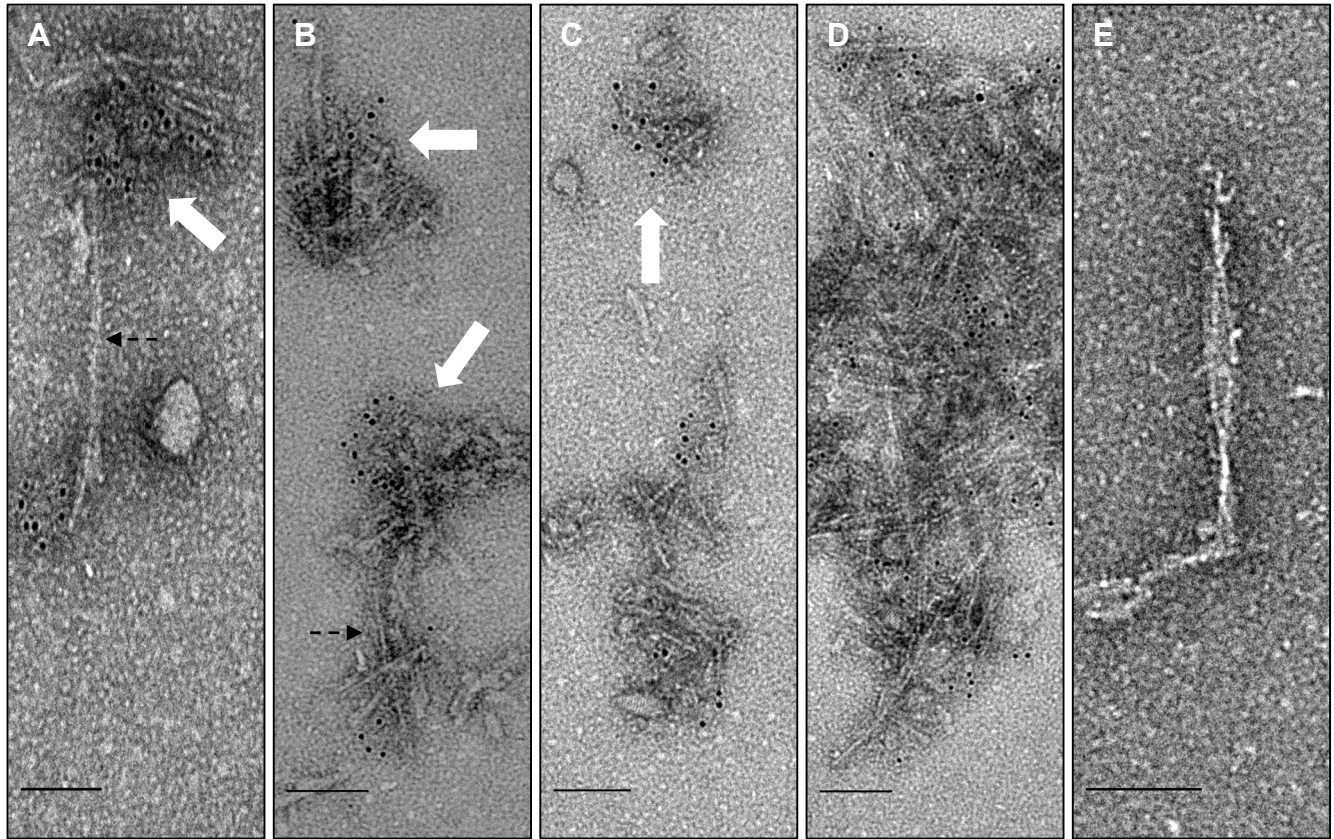


Figure 3-15: Immunogold electron microscopy of purified RML prions with PrP^{Sc}-specific YEG Sc – G1 antibody.

Decoration of the purified PK treated and PTA purified pellet-2 RML fibrillar aggregates (**A-D**) Large fibrillar amyloid aggregates (white filled arrows) were decorated with mouse-derived full-length YEG Sc-G1 (Parent G1) monoclonal antibody and 5nm gold conjugated ternary detection system under native conditions. Long protofilament amyloid fibrils suggestive of PIRIBS structure were not labelled by the YEG Sc – G1 antibody (black dashed arrows). YEG Sc-G1 monoclonal antibody has a discontinuous epitope in which it recognizes the His 110 and Asp 146 residue in a vertical pair epitope orientation in a 4R β S model. In contrast, the antigen-antibody interaction is abolished in a PIRIBS conformation showing no specific labelling of YEG Sc-G1 antibody. (**E**) No specific labelling was observed in the grids with no primary antibody. Scale bar = 100 nm.

PK Pellet-2

PK Pellet-Wash

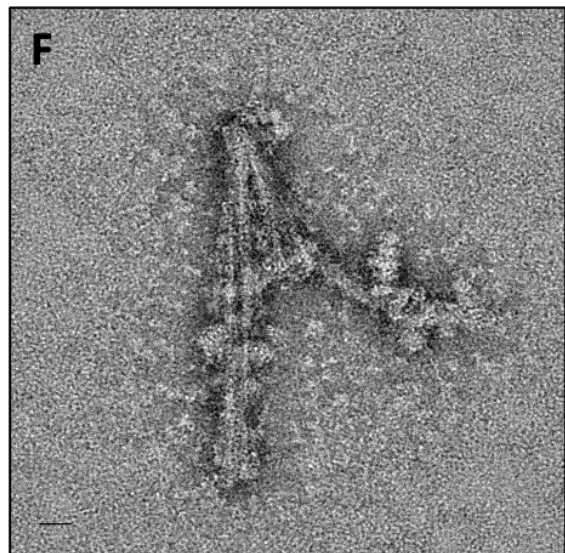
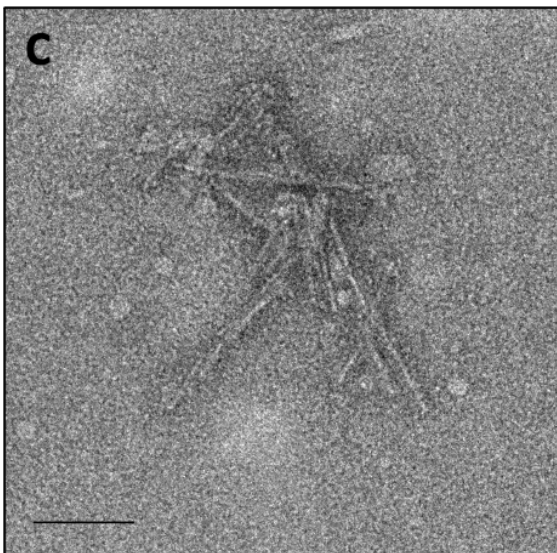
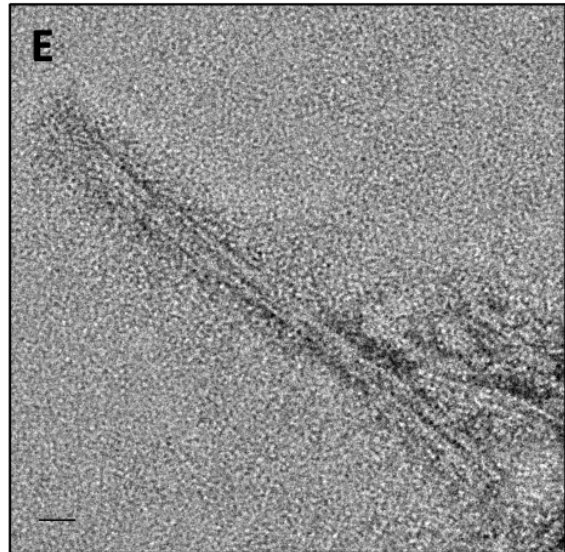
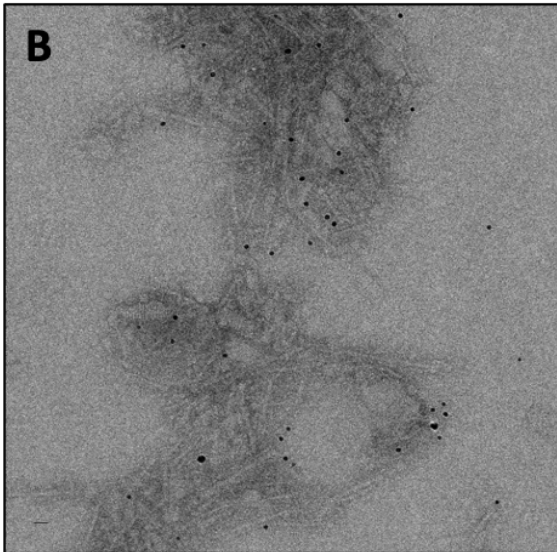
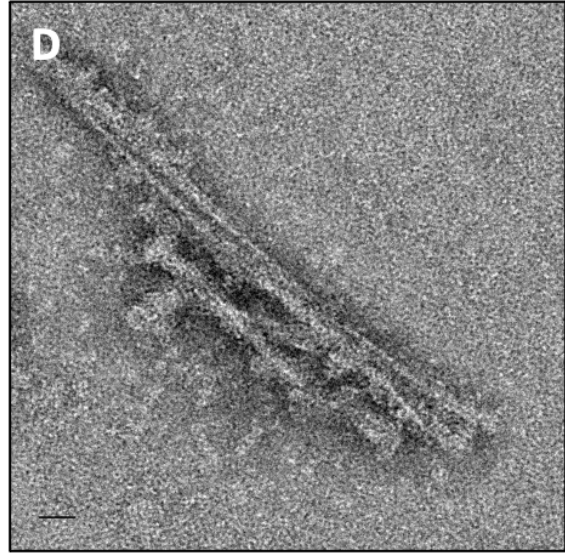
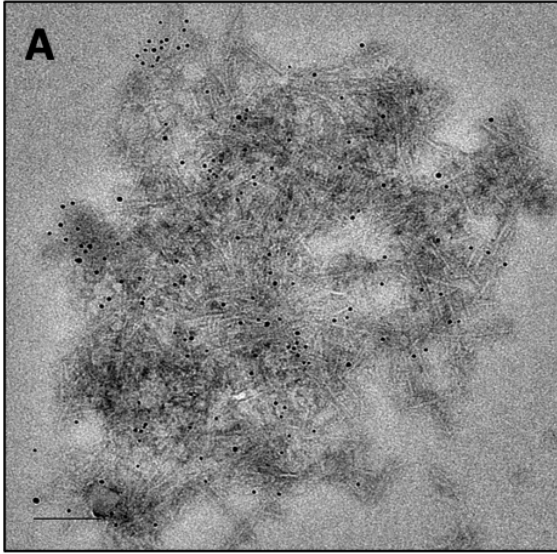


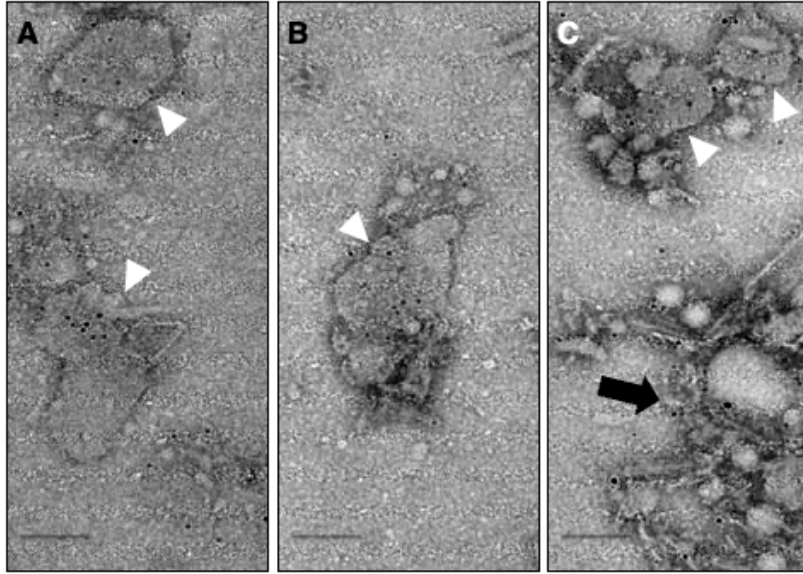
Figure 3-16: Immunogold labelling of recombinant Fab YEG Sc - G1 with purified (P2) and pellet wash RML prions.

Decoration of different fibrillar assemblies, including **(A-B)** PK and PTA, purified pellet-2 RML fibrils consisting of large fibrillar aggregates were labelled with recombinant Fab G1 antibody under native conditions. YEG Sc-G1 monoclonal antibody has a discontinuous epitope in which it recognizes the His 110 and Asp 146 residue in a vertical pair epitope orientation in a $4R\beta S$ model of the infectious prion protein. In contrast, **(D-E)** isolated PK treated and sucrose step purified RML fibrils from the pellet wash sample which showed to consist of many amyloid fibrils (described in chapter 2) did not show any labelling with recombinant Fab G1 antibody. The antigen-antibody interaction is abolished in a PIRIBS conformation due to the orientation of the His 110 and Asp 146 epitope, showing no specific labelling of the YEG Sc-G1 antibody. **(C, F)** No specific labelling was observed in the grids with no primary antibody with these samples. Scale bar for panels A and C = 200 nm, panels B – F = 100 nm.

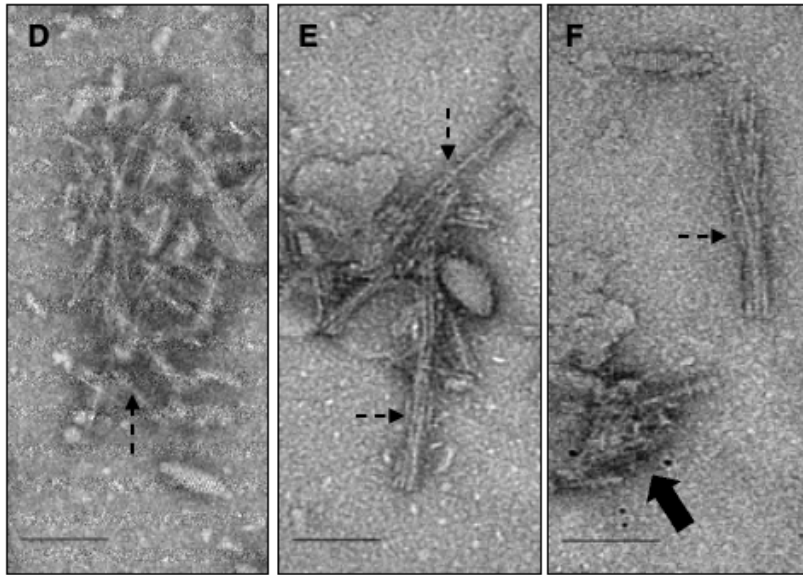
We employed another engineered Fab derived from one of the IgM clones, Fab YEG Sc-M63, to test the activity and specificity with RML prion isolate via immunogold labelling. We observed that this PK_P2 sample consisted of some non-fibrillar particles along with the fibrils, including small two-dimensional crystals. The Fab YEG Sc-M63 antibody showed more specific labelling to the non-fibrillar particles as well as to the two-dimensional (2D) crystals under the native state, represented by the tertiary antibody conjugated to the 5nm gold particles. (Figure 3-17.A-C). This suggests that the 2D crystals are indeed composed of PrP²⁷⁻³⁰ (Wille, Shanmugam, et al., 2009). In contrast, the Fab YEG Sc – M63 did not show any labelling to the amyloid fibrils observed in the PK_P2 sample (Figure. 3-17.D-F) indicating a different conformational is observed in the amyloid fibrils compared to the 2D crystal structure of PrP²⁷⁻³⁰. Control experiments were run in parallel without the use of the primary antibody fragment, which showed no presence of gold particles (Figure. 3-17.G-I). It has been previously reported that the purified fractions showed a dense amount of the prion rods but also contained 2D crystals that appear to be alternative quaternary structures of native PrP²⁷⁻³⁰ and expected to be fully infectious (Wille et al., 2007; Wille, Shanmugam, et al., 2009). Their finding was based on the immunogold labeling experiments with anti-PrP antibodies, R1, R2 and 3F4. Our immunogold labelling of 2D crystals with PrP^{Sc} – specific Fab M63 is in agreement with immunolabeling performed with R1 and R2 monoclonal antibodies that recognize the linear epitope of PrP within residues 225-231 under native conditions (Peretz et al., 1997; Wille et al., 2007). However, another monoclonal antibody 3F4 binds in the region of residues 104-113 (Kanyo et al., 1999; Kacsak et al., 1987), which is accessible in native and denatured PrP^C but buried in PrP^{Sc}, showed labeling to PrP²⁷⁻³⁰ 2D crystals under denatured condition by treating with 2M urea to retrieve the buried epitope (Wille, Shanmugam, et al., 2009). The difference in the labeling of

our conformational antibodies to various conformational states observed in the RML prion sample is probed based on the orientation of the residues H110 and D146 Fab G1 epitope and residues N103 and D143 epitope for Fab M63, which strongly suggests that the amyloid aggregates are composed of the 4R β S (Spagnolli et al., 2019; Wille, Bian, et al., 2009). The residues H110 and D146 are found in a vertical pair-wise orientation in the 4R β S model (Spagnolli et al., 2019) and are surface exposed (Figure 3-18.A), comparatively, the orientation of these residues on the brain-derived RML PIRIBS structure (Artikis et al., 2022) is no longer in the vertical pair-wise orientation but are rather further apart from each other (Figure 3-18.B). Interestingly the epitope residue D146 for Fab M63 is buried inwards of the hydrophobic core in the RML PIRIBS conformation, abolishing the reactivity of our Fab M63 to amyloid fibrils.

2D Crystals PrP27-30



PrP27-30 fibrils



Control

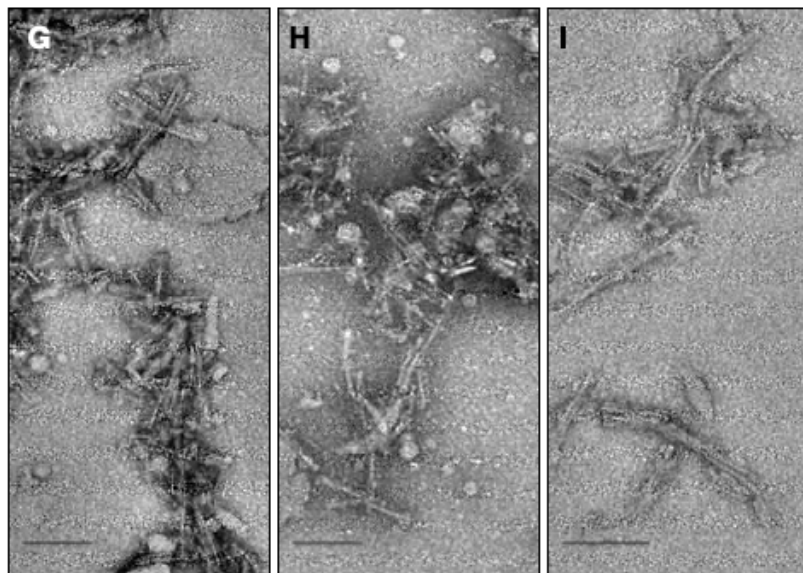
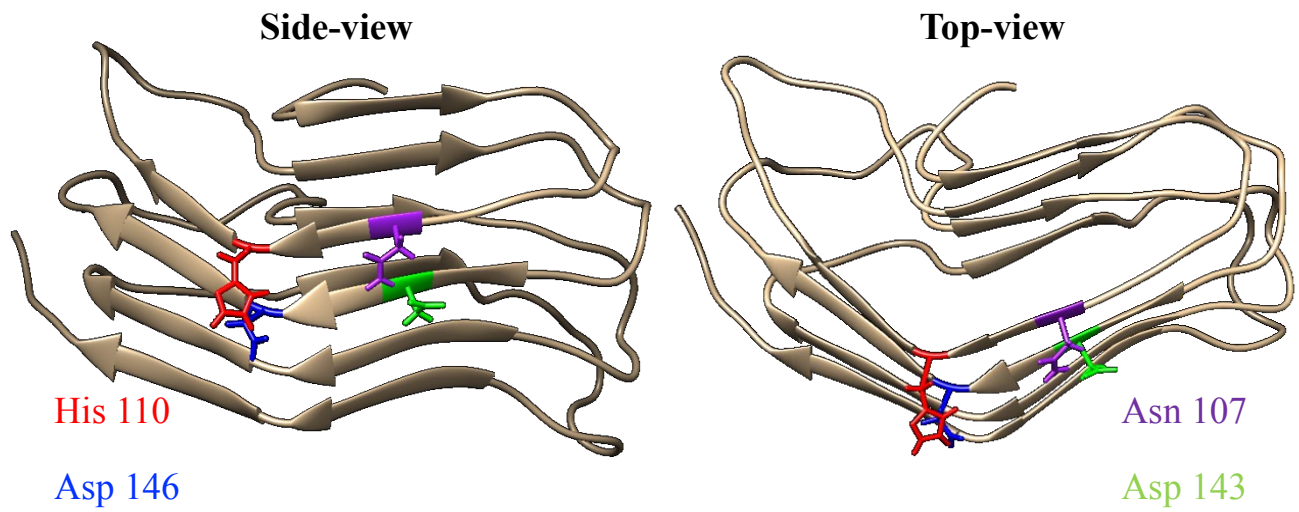


Figure 3-17: Immunogold labelling of recombinant Fab YEG Sc – M63 with PTA purified RML prions.

(A-C) Decoration of two—dimensional crystals (2D) (white arrowheads) and fibrillar aggregates (black filled arrows) of RML PrP 27-30 under native conditions with recombinant Fab YEG Sc-M63 monoclonal antibody. The recombinant Fab YEG Sc-M63 antibody has a discontinuous epitope in which it recognizes the Asn 103 and Asp 143 residues in a vertical pair epitope orientation in a 4R β S model of the infectious prion protein. In contrast, **(D-F)** long protofilament amyloid fibrils consisting of RML PrP27-30 did not show any labelling with recombinant Fab M63 antibody suggestive of PIRIBS configuration of the amyloid fibrils. The antigen-antibody interaction is abolished in a PIRIBS conformation due to the orientation of the epitope residues, Asn 103 which is surface exposed and Asp 143 buried interior of the hydrophobic patch in the PIRIBS RML structure, hence no specific labelling of the YEG Sc-M63 antibody. **(G-I)** No specific labelling was observed in the grids with no primary antibody with these samples. Scale bar = 100 nm.

A Mouse 4R β S Model



B PIRIBS RML Structure

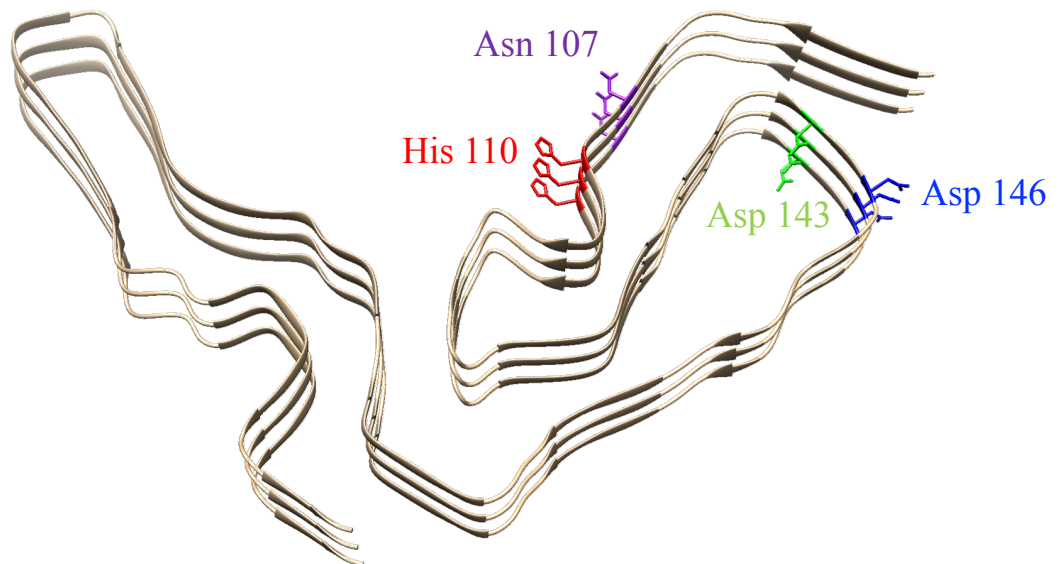


Figure 3-18: Epitope orientation of the mAb YEG Sc-G1 in mouse 4-Rung-Beta Solenoid (4R β S) model and brain-derived RML, Parallel in-Register Intermolecular Beta Sheet (PIRIBS) Structure.

(A) The orientation of monoclonal antibody YEG Sc-G1 and YEG Sc-M63 epitope (full-length and Fab) sits vertically on the beta arc region of rungs 1 and 2 of the mouse 4R β S model. For the antibody to form the complex with its antigen, the epitope must be orientated such that the surface exposed residues H110 and D146 for G1 and Asn 107 and Asp 143 for M63 are in a vertical position and sitting on top of each other of each monomeric PrP^{Sc} on a 4R β S model. (B) In contrast, the cryo-EM structure of brain-derived RML prions revealed a PIRIBS structure. The orientation of the YEG Sc-G1 is found to be on the β -arc region between strands 2 and 3 and strands 5 and 6, H110 and D146 respectively. These residues are surface exposed and facing 180° to each other on a monomeric RML PrP^{Sc} structure. Whereas the orientation of the YEG Sc-M63 epitope on the RML PIRIBS structure is on the β -strands 2 and 5, N103 and D143 respectively. N103 is surface exposed while the residue D143 is facing inwards toward the hydrophobic core.

3.3.11 Immunoprecipitation of fibrillized 14R1 vaccine/antigen

Our PrP^{Sc} monoclonal antibodies have shown to have specificity and affinity towards the misfolded isoform of the prion protein (PrP^{Sc}) only. We took advantage of this tool to further characterize the specificity of monoclonal antibody YEG Sc-G1 and its derivatives for aggregated forms of PrP, we tested the ability of this antibody to immunoprecipitate insoluble prion isolates from infectious brain homogenates (experiments ongoing). In parallel, we tested the specificity of this antibody to immunoprecipitate fibrillized 14R1, PrP^{Sc} vaccine/antigen (mimic structure of 4R β S PrP^{Sc}). Under denaturing condition through Western blotting, we were able to differentiate the monomeric and dimeric insoluble 14R1 antigen when spiked with BSA (1:1) using the PrP^{Sc}-specific Fab-G1 and scFv-G1 (Figure 3-19.A and Figure 3-20.A). In this assay, we tested different antibody dilutions to see the effect of 14R1 affinity towards 14R1, and we observed all the dilutions worked effectively to pulldown the aggregated 14R1 and no bands were observed in wash fractions, showing high specificity for 14R1. To better interpret the banding pattern according to their size, original 14R1, Fab-G1 and scFv-G1 were immunoblotted with an anti-His tag (Figures 3-19.B and 3-20.B).

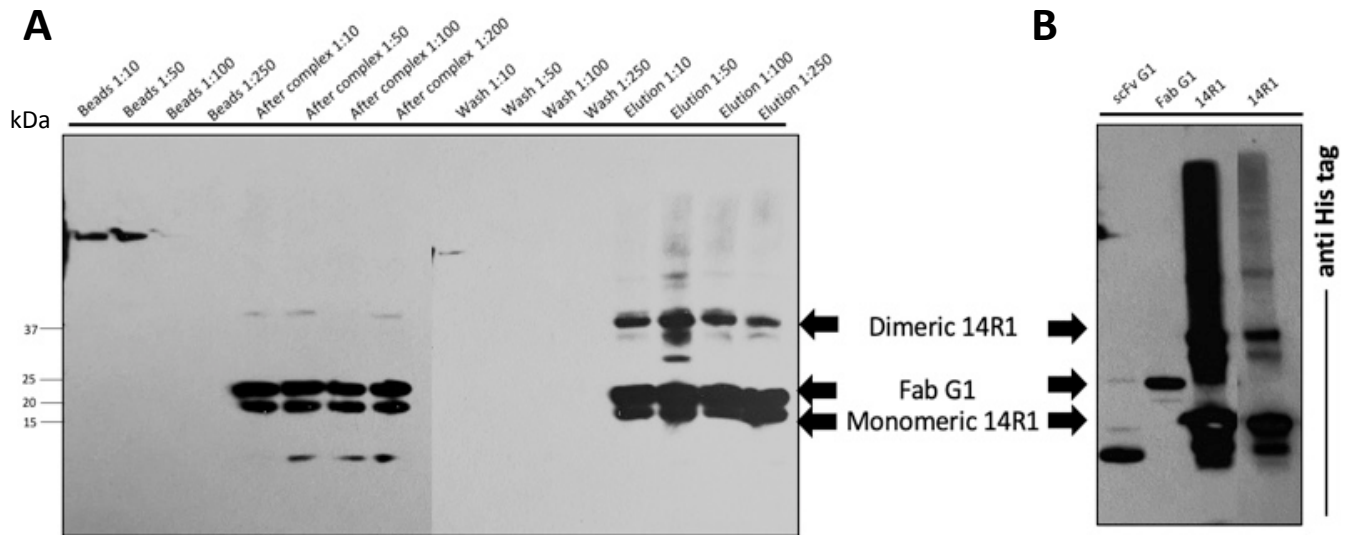


Figure 3-19: Analysis of protein Immunoprecipitated with Fab G1 in a complex with PrP^{Sc} vaccine/antigen 14R1 in its fibrillar conformation.

Immunoprecipitation, as determined by western blotting under denaturing conditions using anti-his tag monoclonal antibody. PrP^{Sc} vaccine/antigen 14R1 in its native fibrillar conformation spiked with bovine serum albumin (BSA) was precipitated using PrP^{Sc}-specific antibody, Fab G1. **(A)** Antibody–bead complex was formed and incubated with a complex consisting of 14R1 (PrP^{Sc} vaccine/antigen) and BSA to mimic crude homogenate. Fractions were collected from all the steps of the CoIP experiment and ran on an SDS-PAGE gel. Strong bands of isolated 14R1 and the signal corresponding to Fab G1 antibody is detected. Dimers of 14R1 were also detected in the elution fraction. After elution, the protein-L beads were resuspended in binding buffer and ran on an SDS-PAGE gel, the western blot showed residual affinity of the antigen-antibody complex with the beads at lower antibody dilution. The wash fraction showed no profound bands of 14R1 antigen showing stronger affinity to the antibody. **(B)** Western blot showing the molecular weights of Fab G1, scFv G1 and 14R1 used for the immunoprecipitation assay using anti-his tag antibody.

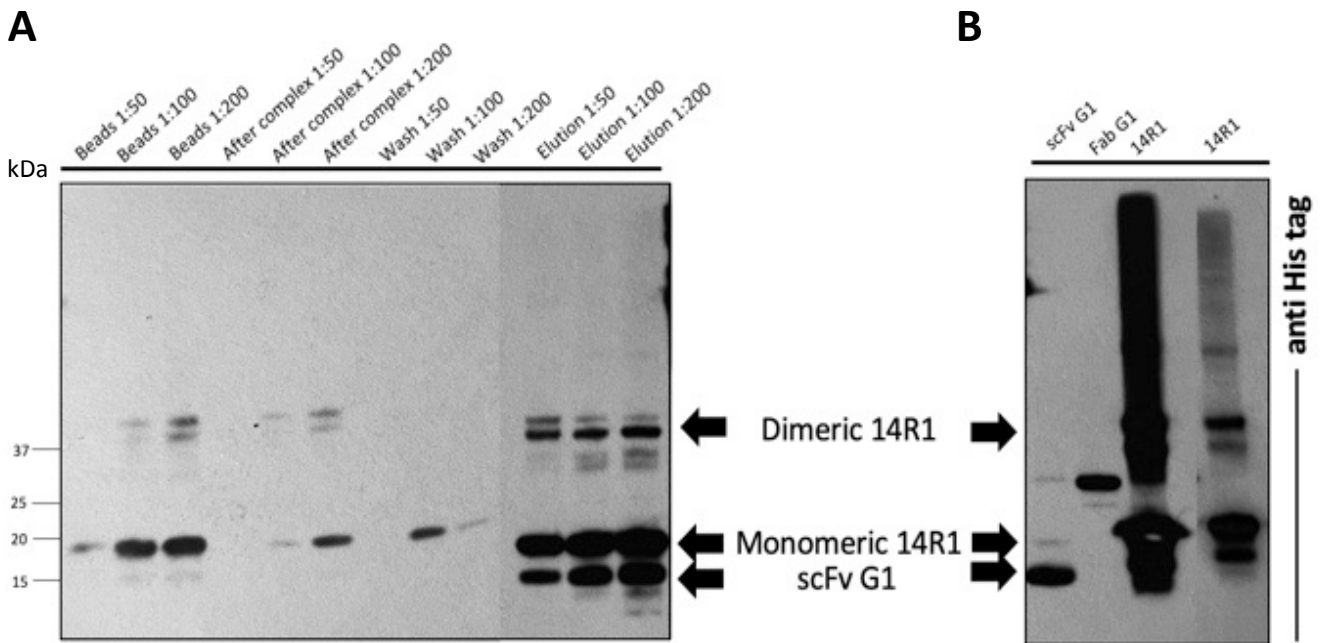


Figure 3-20: Analysis of protein Immunoprecipitated with scFv – G1 in a complex with PrP^{Sc} vaccine/antigen 14R1 in its fibrillar conformation.

Immunoprecipitation, as determined by western blotting under denaturing conditions using anti-his tag monoclonal antibody. PrP^{Sc} vaccine/antigen 14R1 in its native fibrillar conformation spiked with bovine serum albumin (BSA) was precipitated using a PrP^{Sc}-specific antibody, Fab G1. **(A)** Antibody–bead complex was formed and incubated with a complex consisting of 14R1 (PrP^{Sc} vaccine/antigen) and BSA to mimic crude homogenate. Fractions were collected from all the steps of the CoIP experiment and ran on an SDS-PAGE gel. Strong bands of isolated 14R1 and the signal corresponding to the scFv-G1 antibody is detected. Dimers of 14R1 were also detected in the elution fraction at ~ 40kDa. After elution, the protein-L beads were resuspended in binding buffer and ran on an SDS-PAGE gel, the western blot showed residual affinity of the antigen-antibody complex with the beads at higher antibody dilution. The after complex and wash fractions showed 14R1 antigen bands at higher dilutions of scFv antibody showing lower affinity to the antibody. **(B)** Western blot showing the molecular weights of Fab-G1, scFv-G1 and 14R1 used for the immunoprecipitation assay using anti-his tag antibody.

To further validate the specificity of our conformational antibody to be PrP^{Sc} specific and recognize 14R1 in its 4R β S mimic structure of PrP^{Sc}. We immunoprecipitated 14R1 from a complex containing crude brain homogenate of FVB-WT uninfected mice (Figure 3-21). We observed immunoprecipitated aggregated 14R1 in the elution fraction when immunoblotted with an anti-his antibody (Figure 3-21.A) and no 14R1-related band was observed in the wash fraction. The assay also revealed no PrP^C being immunoprecipitated by our PrP^{Sc}-specific Fab-G1 when immunoblotted with SAF 83 monoclonal antibody, which recognizes the central region of PrP within residues 142-164 (Rubenstein et al., 1986). All the unbound PrP^C was found in the wash fraction and after-complex fraction, indicating that our Fab-G1 antibody does not recognize cellular prion protein (Figure 3-21.B).

FabG1 - 14R1 : FVB^{WT}

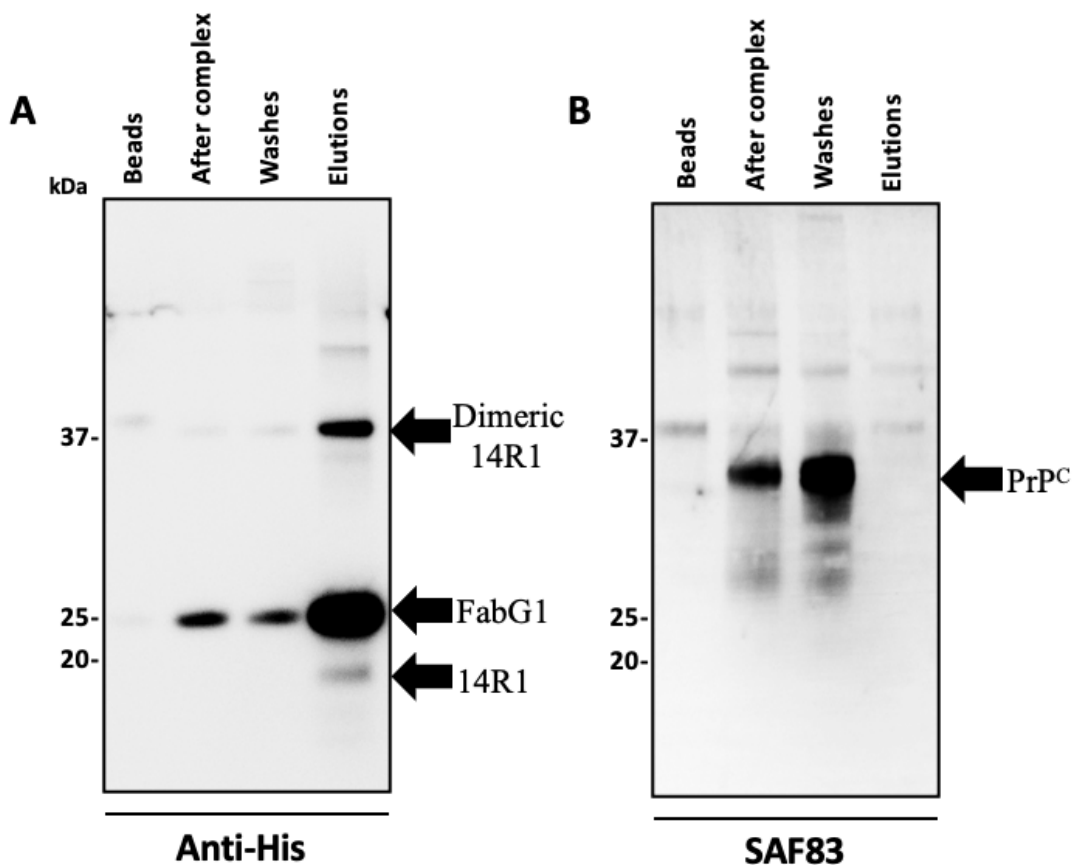


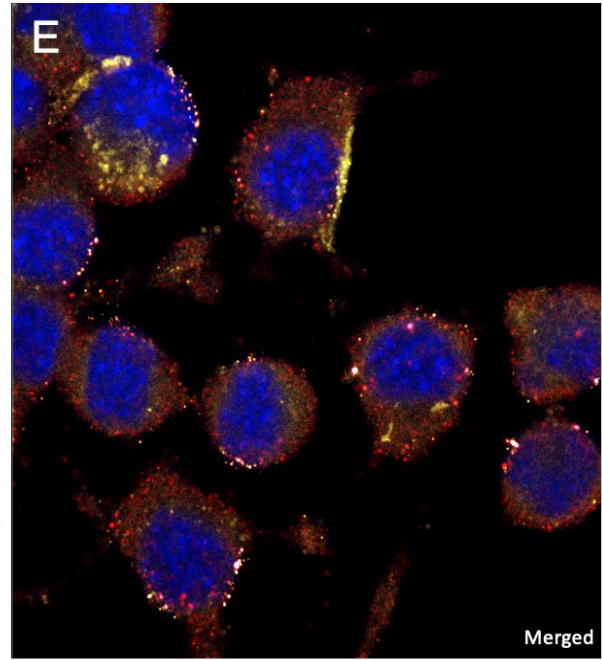
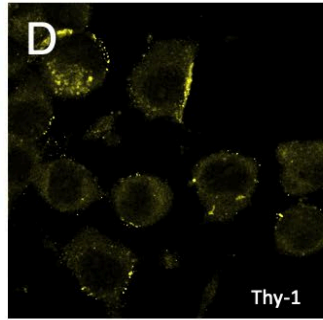
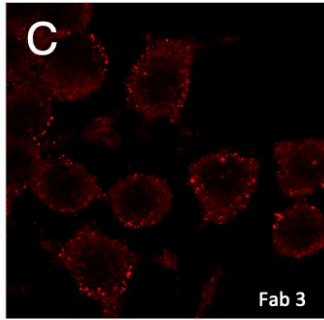
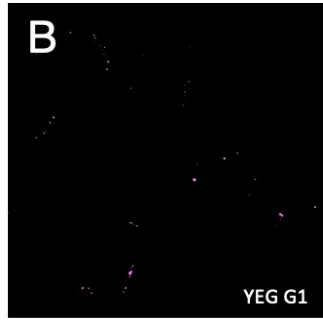
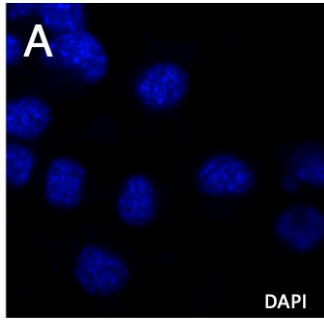
Figure 3-21: Analysis of protein immunoprecipitated with Fab – G1 in a complex with PrP^{Sc} vaccine/antigen 14R1 in its fibrillar conformation and cellular mouse prion protein.

Immunoprecipitation, as determined by western blotting under denaturing conditions using (A) anti-his tag and (B) anti-prion protein SAF83 monoclonal antibodies. PrP^{Sc} vaccine/antigen 14R1 in its native fibrillar conformation with cellular prion protein (PrP^C) was precipitated using a PrP^{Sc}-specific antibody, Fab G1. (A) Antibody–bead complex was formed and incubated with a complex consisting of 14R1 (PrP^{Sc} vaccine/antigen) and cellular mouse prion protein. Fractions were collected from all the steps of the CoIP experiment and ran on an SDS-PAGE gel. Bands of isolated 14R1 and the signal corresponding to Fab G1 antibody were detected. Dimers of 14R1 were also detected in the elution fraction. After elution, the protein-L beads were resuspended in binding buffer and ran on an SDS-PAGE gel, the western blot showed almost perfect elution of the complex. The wash fraction showed no profound bands of 14R1 antigen showing a stronger affinity to the antibody than cellular prion protein. (B) The same western blot probed with an anti-his tag antibody was washed and probed with anti-prion protein SAF 83 antibody to detect PrP^C. PrP^C bands at ~37 kDa were observed in the after complex and wash fractions indicating the specificity of our Fab G1 to only 14R1 PrP^{Sc} vaccine/antigen which is a mimic of the infectious prion protein in its 4RβS structure.

3.3.12 Validation by immunocytochemistry assay

Additionally, utilizing the murine neuroblastoma cell line CAD5 and CAD5 infected with RML prions, we assessed the specificity of our PrP^{Sc}-specific monoclonal antibody, full-length murine-derived YEG Sc-G1 and recombinant Fab YEG Sc-G1 to surface label the misfolded isoform of prion protein in CAD RML infected cells by immunocytochemistry assay. Our YEG Sc-G1 has a discontinuous epitope and recognizes PrP^{Sc} in its native state, specifically residues H110 and D146 when orientated in a vertical pair-wise conformation. On methanol-fixed and semi-permeabilized CAD cells, these PrP^{Sc}-specific antibodies were examined using immunofluorescence. Our YEG Sc-G1 antibodies (full-length and Fab) showed specificity and labelling to RML-infected CAD 5 cells only with higher fluorescence intensity compared to WT-PrP CAD 5 cells (Figures 3-22.G and 3-23.G) and did show less to unspecific labelling to CAD 5 cells expressing murine WT-PrP (Figures 3-22.B and 3-23.B). Both the CAD 5 cells expressing WT-PrP and RML infected were counterstained with anti-prion Fab 3 (Figure 3-22.C, H), which recognizes the polybasic region at the very N-terminus of PrP within residues 23-34 of the mouse prion protein (Chapter 2) and anti-PrP SAF-83 monoclonal antibodies at recognizes the central region of PrP within residues 126-164 of the mouse prion protein (Figure 3-23.C, H). Since PrP is a membrane-bound GPI anchored protein, we stained both the uninfected and infected cells with CD90/Thy-1 monoclonal antibody (Figures 3-22.D, I and 3-23.D, I) to compare the signals observed from PrP^{Sc} and PrP^C labelling with our antibodies to fluorescence signal from the membrane staining. We observed the majority of the PrP^{Sc} and PrP^C labelling around the cell membrane, wherein the PrP^{Sc} labelling was seen in small, diffuse punctae and larger foci, suggesting different stages of replication or aggregation (Figures 3-22.J and 3-23.J).

CAD



CAD RML

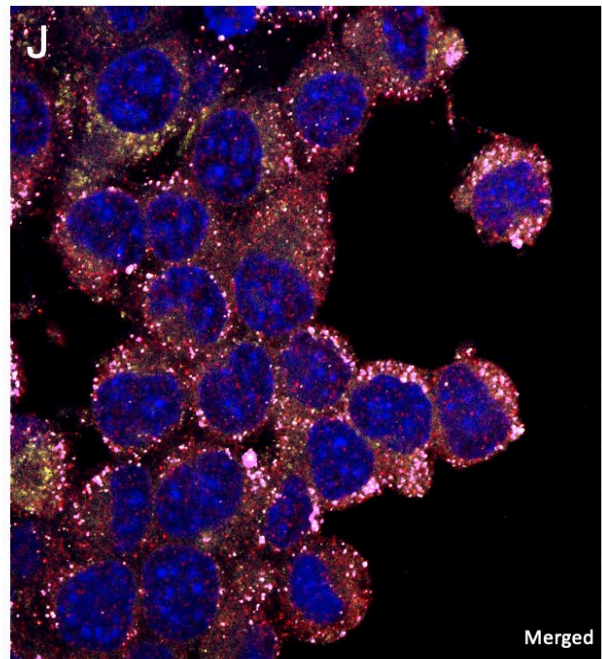
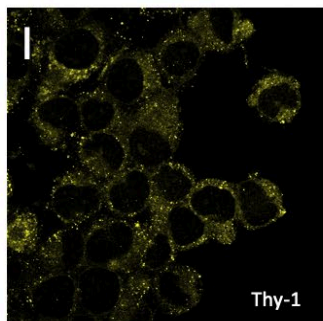
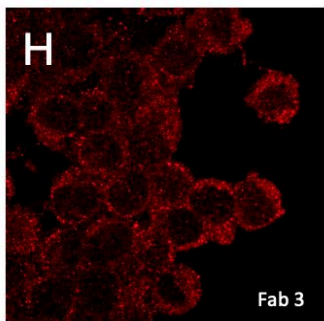
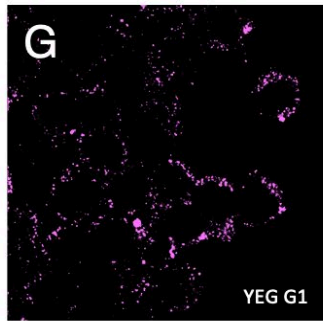
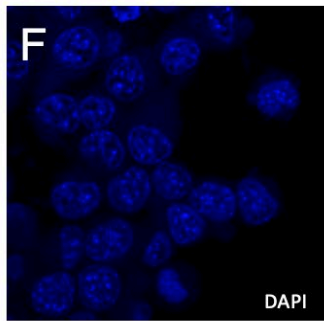
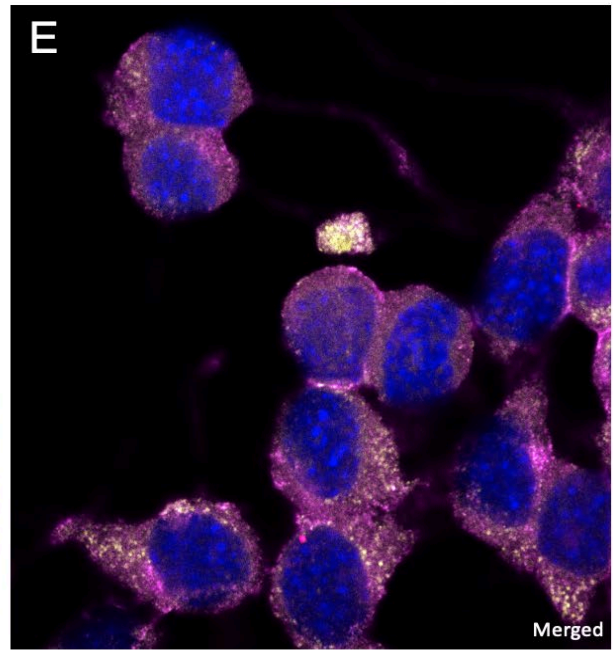
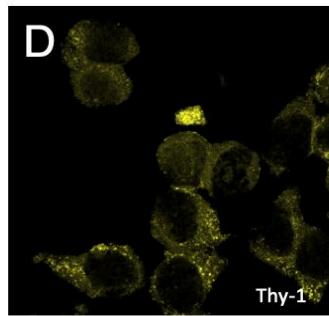
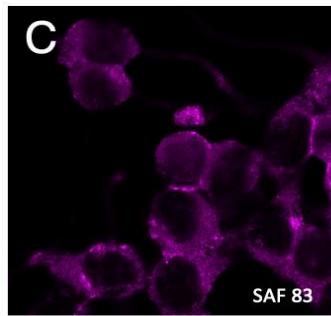
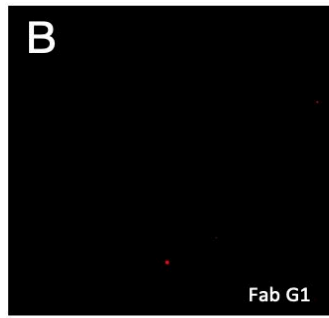
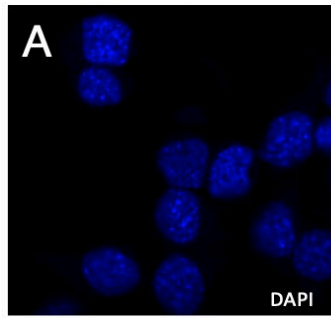


Figure 3-22: Immunocytochemistry of CAD 5 PrP / RML infected cells using mouse-derived full-length YEG Sc – G1.

Representative immunofluorescence images of PrP^C and PrP^{Sc} staining with **(A-E)** uninfected and **(F-J)** infected CAD 5 cells with RML prions. Surface labelled immunofluorescence images of methanol fixed PrP^C and PrP^{Sc} in permeabilized CAD5/CAD5-RML infected PrP cells with **(B,G)** mouse-derived full-length PrP^{Sc}-specific monoclonal antibody, YEG Sc – G1. As previously shown, the YEG Sc-G1 antibody has a discontinuous epitope and recognizes the infectious prion protein only when the epitope residues His 110 and Asp 146 are sitting on top of each other at the beta arc region of the 4RβS model. Labelled PrP^{Sc} is observed in a punctae-like form. **(C,F)** PrP^C and PrP^{Sc} were stained with anti-PrP Fab 3 antibody (red) targeting the N-terminus of PrP within residues 23-34 of mouse prion protein and **(D,I)** Thy-1 monoclonal antibody (yellow) recognizes GPI-linked membrane glycoproteins. **(A,F)** All cells were counterstained with DAPI (blue). The cells were visualized by confocal laser scanning microscopy. Scale bar = 10μM (applied to all images).

CAD



CAD RML

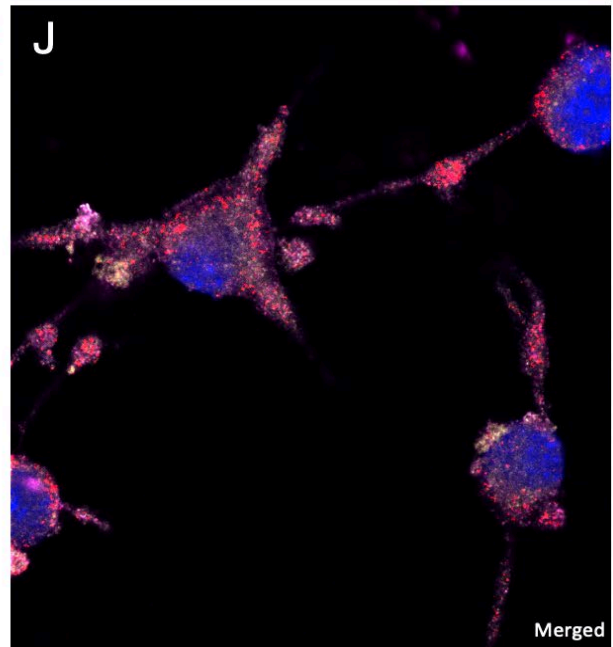
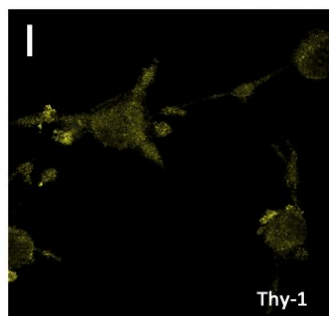
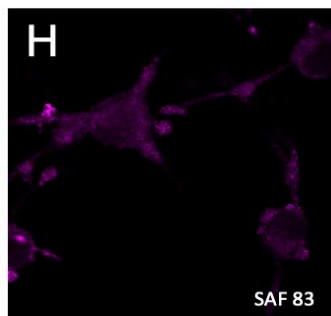
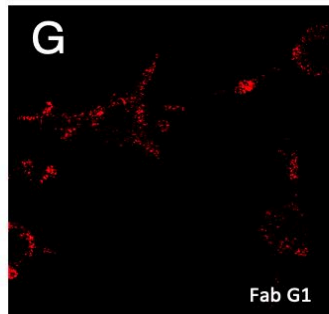
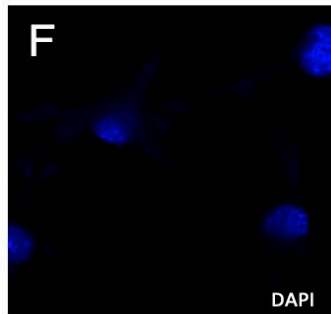


Figure 3-23: Immunocytochemistry of CAD 5 PrP / RML infected cells using recombinant Fab YEG Sc – G1.

Representative immunofluorescence images of PrP^C and PrP^{Sc} staining with **(A-E)** uninfected and **(F-J)** infected CAD 5 cells with RML prions. Surface labelled immunofluorescence images of methanol fixed PrP^C and PrP^{Sc} in permeabilized CAD5/CAD5-RML infected PrP cells with **(B,G)** PrP^{Sc}-specific monoclonal antibody, a recombinant humanized Fab YEG Sc – G1. As previously shown, the Fab YEG Sc-G1 antibody has a discontinuous epitope and recognizes the infectious prion protein only when the epitope residues His 110 and Asp 146 are sitting on top of each other at the beta arc region of the 4RβS model. Labelled PrP^{Sc} is observed in a punctae-like form. **(C,F)** PrP^C and PrP^{Sc} were stained with anti-PrP SAF 83 antibody (red) targeting the central region of PrP within residues 126-164 of mouse prion protein and **(D,I)** Thy-1 monoclonal antibody (yellow) recognizes GPI-linked membrane glycoproteins. **(A,F)** All cells were counterstained with DAPI (blue). The cells were visualized by confocal laser scanning microscopy. Scale bar = 10μM (applied to all images).

3.3.13 Design of single-chain antibody fragments and their conjugates

After successfully designing and characterizing of PrP^{Sc}-specific Fabs, I switched to engineering smaller antibody fragments, single-chain antibody fragments that can now be used in broader assays such as direct detection of prions as well as potential therapeutic tools for prion diseases.

3.3.13.1 Design of PrP^{Sc}-specific single-chain variable fragment

I engineered a PrP^{Sc}-specific single-chain antibody derived from the IgG clone (scFv YEG Sc-G1) of around 25 kDa (less than one-sixth the size of immunoglobulin G) that link an antibody's heavy and light chain variable domains via a flexible glycine-serine rich linker (Gly₄Ser)₄ (Figure 3-24.A). The specificity remains unchanged, despite the reduction in size results in the absence of the complement response that is present with conventional antibodies (Skrlj, Serbec, & Dolinar, 2010). The rodent-derived IgG CDRs were loop grafted onto an existing human variable region framework, as previously described in chapter 2. PrP^{Sc}-specific scFv fragments have an N-terminus OmpA signalling peptide for periplasmic expression and a 6x His tag at the C-terminus of the protein for Ni-NTA affinity purification.

3.3.13.2 Design of PrP^{Sc}-specific single-chain variable fragment with a cell penetratin linker

In order for the PrP^{Sc}-specific scFv-G1 to cross cross the blood-brain barrier (BBB), I designed a similar scFv-G1 as described earlier but modified in that the standard (Gly₄Ser)₄ linker was replaced with a cell-penetrating peptide (CPP) sequence between the variable light and heavy chain (Figure 3-22.B). Although adding a CPP to an antibody fragment is not a novel approach, such peptides were standardly linked to the N- or C-terminus. In our design, we hypothesized that by simply placing it between the variable domains, it would fold similarly to scFv-G1 or even better by not forming dimers due to the hydrophilic CPP linker. The first proof of protein transduction using CPP was revealed in 1988 when the HIV-1 transactivating protein TAT was discovered to penetrate mammalian cells (Green & Loewenstein, 1988).

3.3.13.3 Design of PrP^{Sc}-specific fluobody (scFv G1 – eGFP)

I engineered a recombinant, PrP^{Sc}-specific “fluobody” based on the PrP^{Sc}-specific monoclonal antibody mAb YEG Sc-G1 with the hope to create a tool for the direct detection of prions in their native state. A fluobody is a genetically encoded antibody probe, consisting of an enhanced green fluorescent protein (eGFP) linked to a single chain variable region fragment (scFv) (Figure 3-24.C). This PrP^{Sc}-specific fluobody proved to be a unique tool for visualizing the spatiotemporal dynamics of PrP^{Sc} in RML-infected CAD5 cells. A modified version of PrP^{Sc}-specific fluobody has been designed for future experiments whereby the eGFP is linked in between the variable light and variable heavy chain, known as the PrP^{Sc}-specific flashbody (data not shown) (Movaghar Asareh et al., 2022).

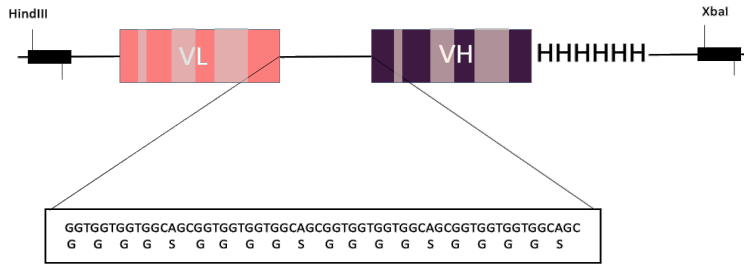
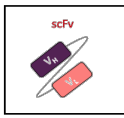
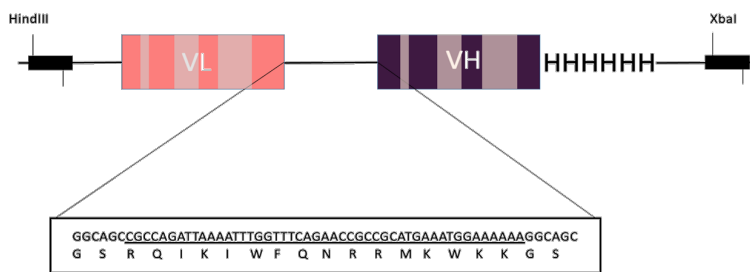
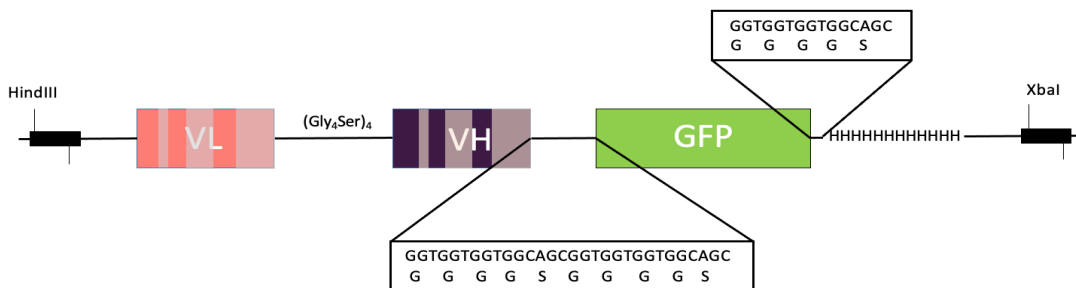
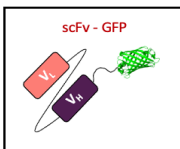
A**B****C**

Figure 3-24: Construct design of single chain antibody fragments and their conjugates.

Schematic representation of engineered humanized recombinant antibody fragments specific to PrP^{Sc}, single chain variable fragment (scFv YEG-Sc G1). The variable domains of both the heavy (purple) and light (peach) chains are responsible for the antigen binding site of the molecule. **(A)** The variable regions of the VL and VH of the antibody is linked by a flexible linker, (Gly₄Ser)₄ **(B)** Bioengineering of scFv-G1 for crossing the blood brain barrier by replacing the standard linker with the cell penetrating sequence (). **(C)** Fusion of green fluorescent protein (green) to scFv-G1 with a 12xHis tag at the C-terminus for purification by Ni-NTA column.

3.3.14 Cloning, Expression and activity of engineered scFv's

The synthetic gene consisting of the scFv-G1, scFv-G1-CPP and scFv G1-GFP (Figure 3-24.A-C) constructs were synthesized by BioBasic DNA Inc, Markham Ontario. These genes were double digested using restriction enzymes, HindIII and XbaI and were successfully cloned into a Fab expressing vector (as previously described in chapter 2) for recombinant expression and purification (Figure 3-25.A-B).

These engineered clones of PrP^{Sc}-specific scFv's were successfully expressed and purified in *E.coli* as soluble and functional Fabs as described earlier in the chapter. The same procedure was used to successfully express PrP^{Sc}-specific recombinant scFv-G1, scFv-G1 CPP (Figure 3-26.A-B), and scFv-G1 GFP (Figure 3-26.C-D).

Two-step competition ELISA results revealed all our engineered and fully folded recombinant scFv's recognized its antigen, fibrillized 14R1 (Figure 3-27.A-C). The specificity of the targeted epitope matched the ELISA epitope profiling for all tested scFv's. This activity assay performed under native conditions also validated that scFv's, despite being small in size and consisting of only variable regions did maintain their epitope specificity for antigen-antibody recognition and was compared to a murine-derived full-length antibody (Gilliland, Luo, Vafa, & Almagro, 2012).

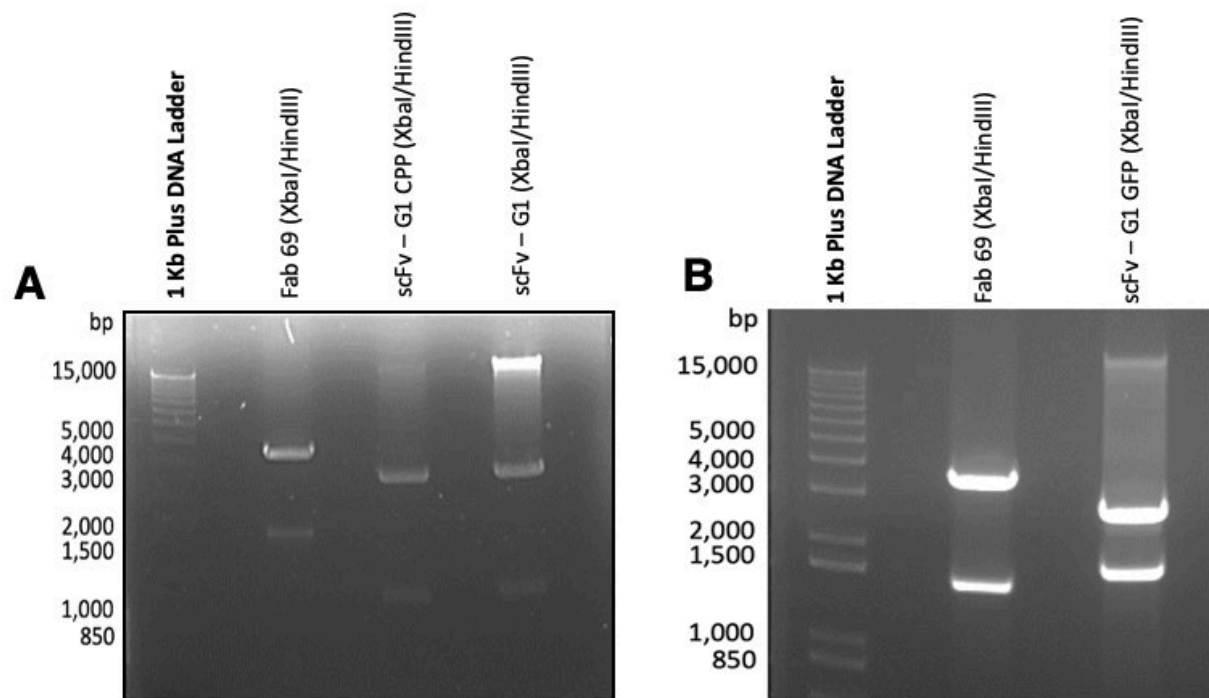


Figure 3-25: Double restriction digest of recombinant single-chain antibody fragments and their conjugates: scFv-G1, scFv-G1 CPP and scFv-G1 GFP constructs and human Fab vector.

(A) Insert scFv plasmids were incubated with the *Xba*I and *Hind*III restriction enzyme which yields two bands whereby the ~1100 bp band corresponds to the human scFv constructs (insert) and the band at ~3500 bp corresponds to the insert vector. The human fab vector at ~4000 bp was ligated with the scFv inserts. These excised fragments were subsequently ligated to generate a human recombinant scFv monoclonal antibodies that would elicit the antibody features of the full-length mouse PrP^{Sc}-specific antibodies. **(B)** scFv G1 – GFP plasmid was incubated with *Xba*I and *Hind*III restriction enzyme, giving two bands, a ~1500 bp corresponding to the insert and a ~2900 bp corresponding to the vector. The scFv-G1 GFP insert was then ligated to the human Fab vector (~4000bp band).

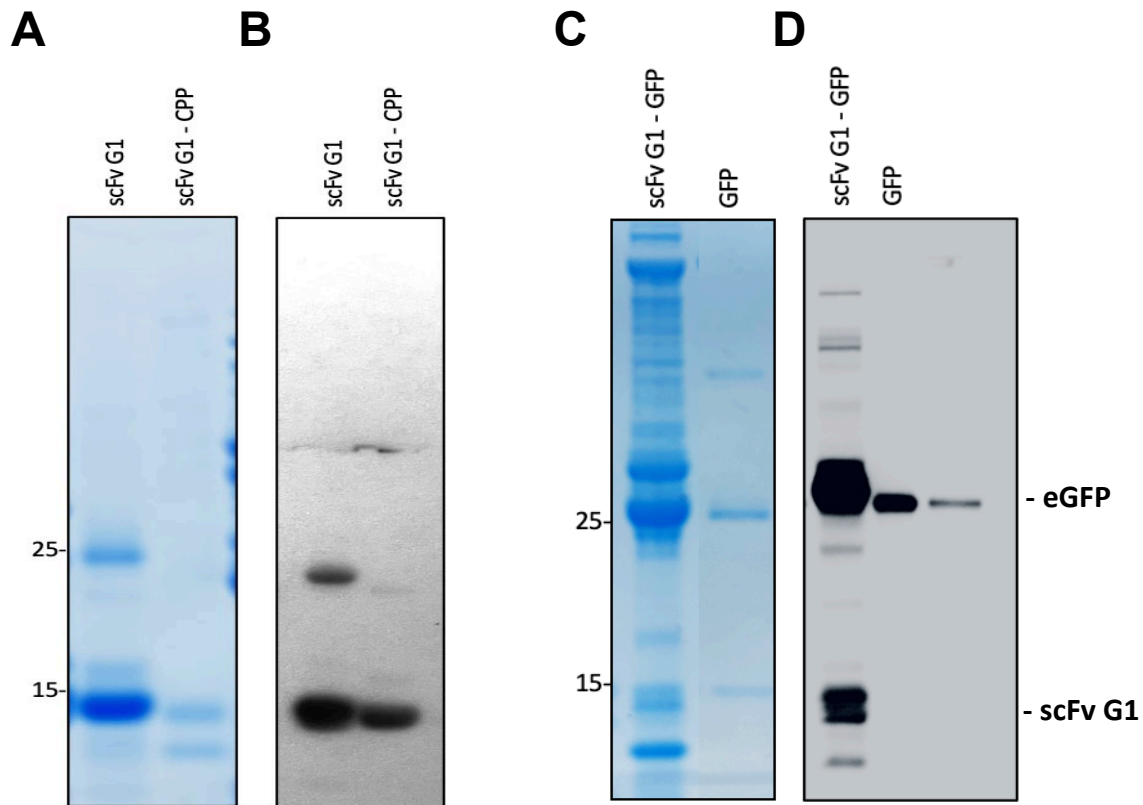
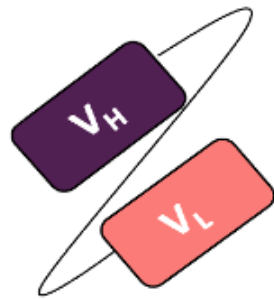
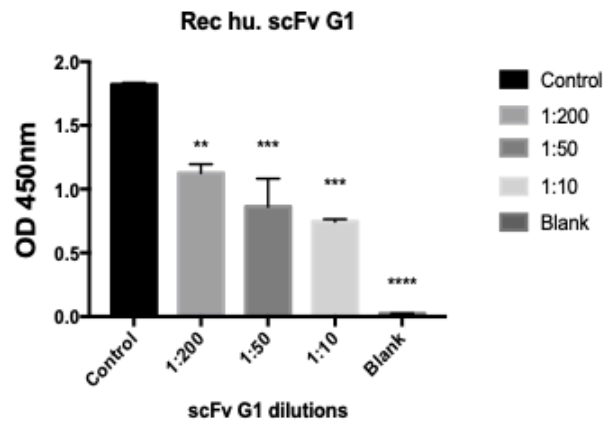
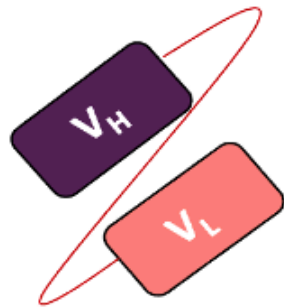


Figure 3-26: Expression and purification of single-chain antibody fragments and their conjugates.

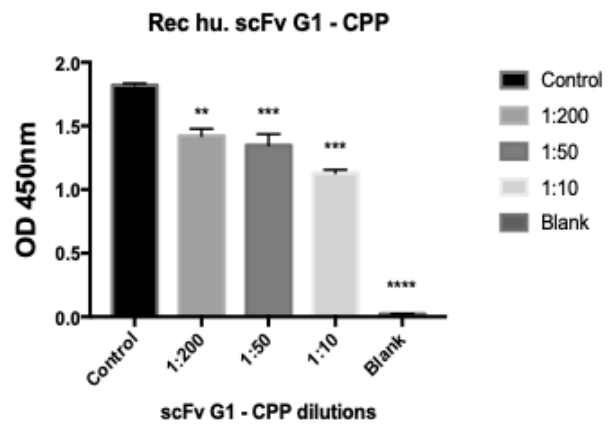
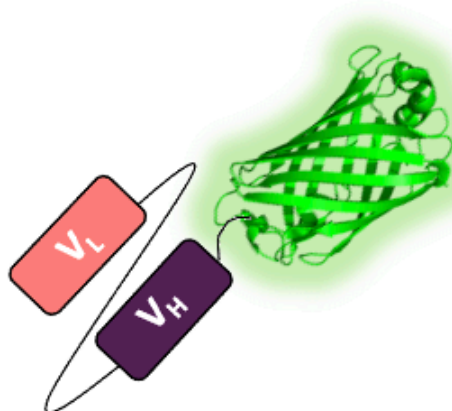
Purification of recombinant PrP^{Sc} scFv fragments and with its GFP conjugate. Analysis of recombinant expression in BL21(DE3) cells via IMAC purification via SDS-PAGE Coomassie staining (left) and western blot using an anti-his tag (right) of **(A-B)** single-chain antibody fragment with regular (GlySer)₄ linker (scFv-G1) and scFv-G1 replaced with a cell penetrating linker (scFv-G1 CPP). Recombinant PrP^{Sc} – specific scFv's fragments are expressed in tandem, and under denaturing conditions, scFv's will have a molecular weight of ~ 15kDa. **(C-D)** Single-chain G1 fused with an enhanced green fluorescent protein (eGFP) and a control unconjugated eGFP. Under denaturing conditions, scFv's - eGFP will have bands at the molecular weight of ~ 15kDa representing the scFv fragment and at ~29 kDa representing the eGFP.

A

scFv G1 ~ 25 kDa

**B**

scFv G1 - CPP ~ 25 kDa

**C**

scFv G1 - GFP ~ 55 kDa

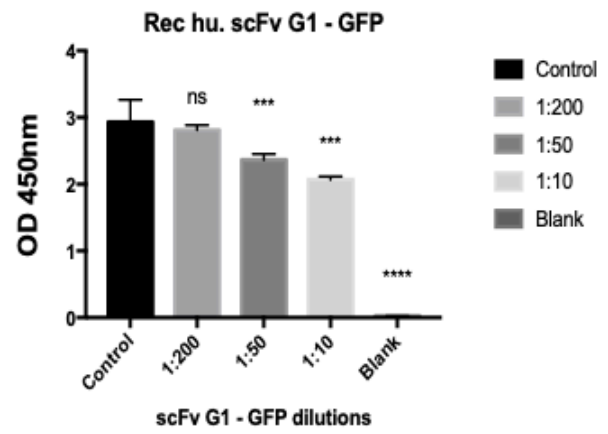


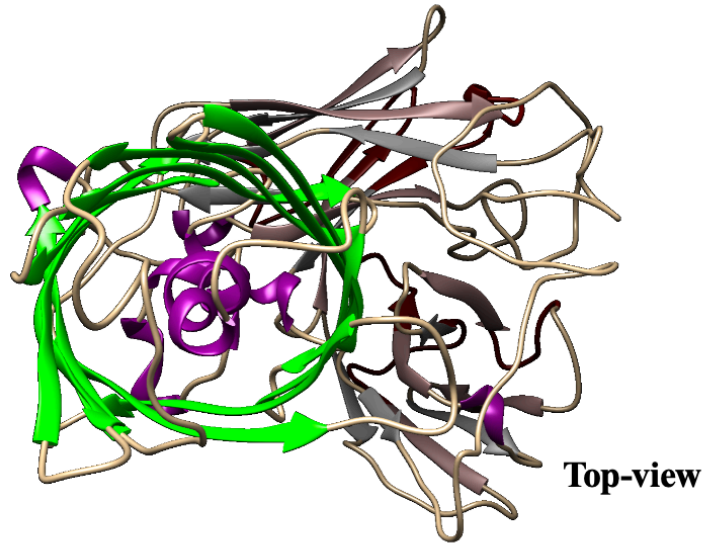
Figure 3-27: Activity assay of single-chain antibody fragments against PrP^{Sc} vaccine/antigen (14R1).

The fully folded and functional recombinant PrP^{Sc}-specific scFv antibody fragments were tested for antigen recognition using a two-step indirect competition ELISA assay with 14R1 antigen. The two-step competition ELISA results indicate the binding of all recombinant scFv – G1 derivatives to the 14R1 antigen. **(A)** scFv – G1 antibody fragment consisting of regular (GlySer)₄ linker shows greater binding to 14R1 at different dilutions compared to the rest of the scFv derivatives. **(B)** scFv – G1 antibody fragment whereby the regular linker between the heavy and the light chain is replaced with the cell penetrating linker and **(C)** scFv-G1 linked to an enhanced green fluorescent protein. Both these derivatives show binding to the 14R1 antigen whose structure mimics the 4RβS model of infectious prion protein. Control well is measured by the omission of primary antibody (scFv), consisting of only secondary antibody (Parent-G1) and tertiary detection system (anti-mouse HRP). The blank well was only incubated with tertiary antibody, anti-mouse. The data presented are statistically significant compared with the control **(A)** p=0.0001, **(B)** p<0.0001, and **(C)** p<0.0001 except for dilution 1:200 was not significant. Statistical analyses were performed using One-way ANOVA, Dunnett's test on prism 7.0 graphpad.

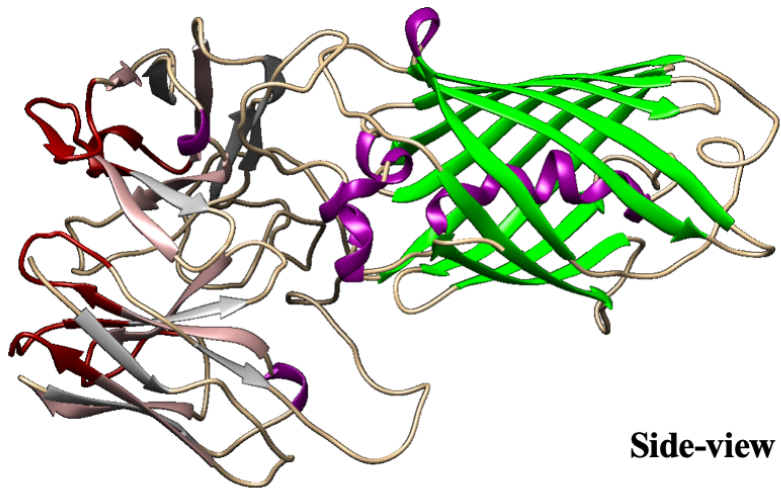
3.3.15 Comparative in silico modelling and docking of scFv G1 and with its eGFP conjugate

Computational modelling was performed on the structure of the scFv G1 linked to enhanced green fluorescent protein antibody by Dr. Luda Dorosh from the Wille lab to understand the folding of the engineered conjugated antibody fragment as well as to perform in silico interaction with the human PrP^{Sc} model. The scFv G1-GFP model was adapted from the scFv structure available in Protein Data Bank (PDB), PDB# 2KH2 (Wilkinson et al., 2009) and eGFP sequencing identified by ODB entry 5FGU (Moon et al., 2016) which was then simulated together with the same buffer conditions as used in experimental conditions. The ribbon diagrams of the fragment antibody show stabilized representative conformation of the scFv G1-GFP model after 20 ns (Figure 3-28.A-B). The stabilized model of scFv G1-GFP was docked with the human PrP^{Sc} model to observe if hydrogen bonds are formed and more specifically between which key residues. The comparative computational docking and simulation revealed favorable hydrogen bonds between the residues H111 and D147 of the human PrP^{Sc} and the hydrophilic residues, D28 and S92 of the scFv G1-GFP antibody (Figure 3-28.C). These docking results are in alignment with our experimental epitope mapping results.

A



B



C

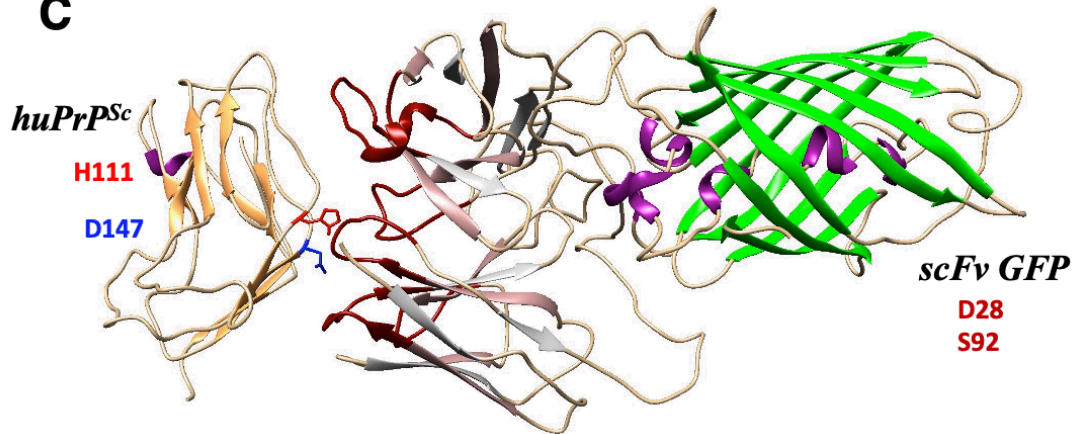


Figure 3-28: Molecular dynamics simulation of scFv-G1 GFP and human PrP 27-30 stabilized for 140 ns.

Ribbon diagrams of single-chain fragment antibody fused with an enhanced green fluorescent protein tag **(A)** top view and **(B)** side view showing stabilized representative conformation of scFv-G1 GFP model after 20ns MD. **(C)** The identical conditions were used as in the wet-lab experiment for molecular docking and the modelling of scFv-G1 GFP (shown in yellow beta-strands) with huPrP 90-231 (green beta-solenoidal structure) in AccelrysDS and simulated at 310K for 50 ns. The docked hydrophilic surface of the Fab G1 antibody formed a complex with residues H111 and D147 of the human PrP^{Sc}-4R β S model. These computational results are in alignment with our experimental epitope mapping results showing the importance of the key residues for the antigen-antibody interaction.

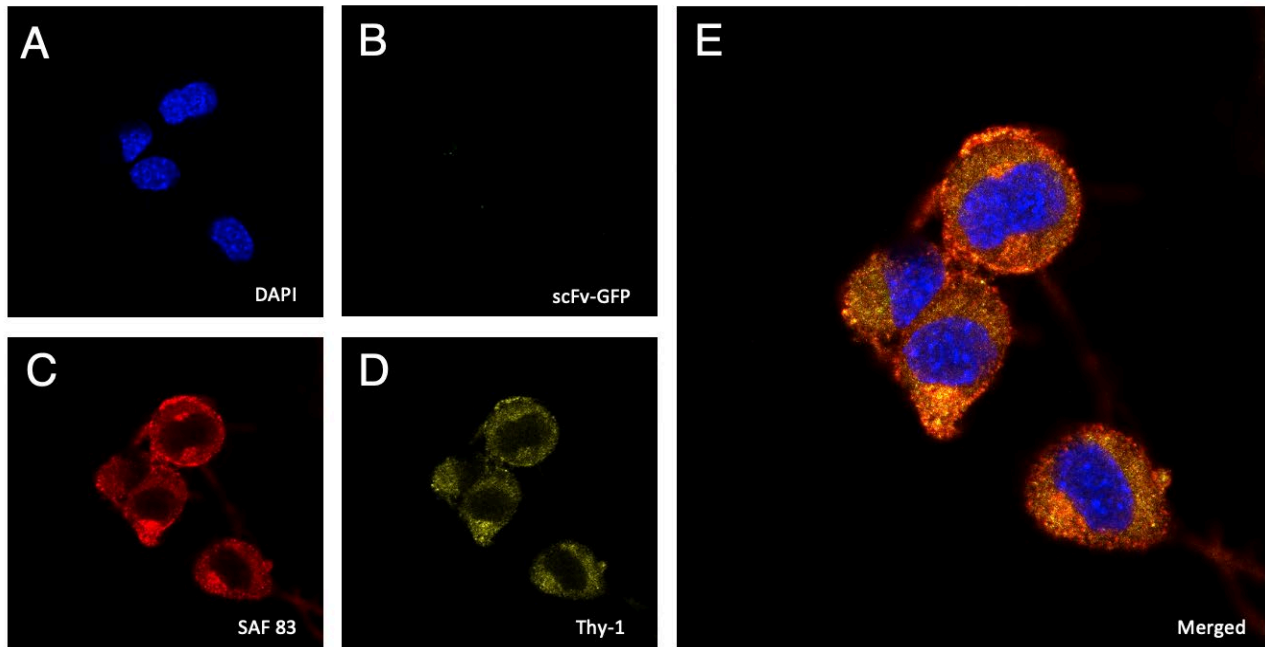
3.3.16 Labelling of native PrP^{Sc} in RML-infected CAD 5 cells using PrP^{Sc}-specific fluobody

Results from a first confocal microscopy study using the PrP^{Sc}-specific fluobody revealed widespread surface labelling of PrP^{Sc} on RML-infected cells (Figure 3-29.G), while uninfected control cells expressing WT murine PrP^C remained completely unlabeled (Figure 3-29.B). PrP^{Sc} was seen in small, diffuse punctae and larger foci. Both the CAD 5 cells expressing WT PrP and RML infected were counterstained with anti-prion monoclonal antibody SAF 83 which recognizes the central region of PrP within residues 126-164 of the mouse prion protein (Figure. 3-27.C, H). Since PrP is a membrane-bound GPI anchored protein, we stained both the uninfected and infected cells with CD90/Thy-1 monoclonal antibody (Figures 3-29.D, I) to compare the signals observed from PrP^{Sc} and PrP^C labelling with our antibodies to fluorescence signal from the membrane staining. We observed the majority of the PrP^{Sc} and PrP^C labelling around the cell membrane, wherein the PrP^{Sc} labelling was seen in small, diffuse punctae and larger foci, suggesting different stages of replication or aggregation (Figures 3-29.J). Additional studies with the fluobody in organotypic slice cultures infected with different prion strains are ongoing.

In order to validate the engineering of our fluobody and the immunofluorescence results shown above, we decided to create a recombinant GFP protein as a control, which was expressed and purified using the same protocol described earlier. GFP staining was performed on both, the uninfected WT-PrP^C cells (Figure 3-30. A-D) as well RML infected CAD cells (Figure 3-30. E-H) and revealed no specific labelling of the GFP protein to the cells (Figure 3-30. B, F). Both the

CAD 5 cells expressing WT-PrP and RML infected were counterstained with anti-prion monoclonal antibody SAF 83 which recognizes the central region of PrP within residues 126-164 of the mouse prion protein (Figure 3-30.C, G). PrP^{Sc} was labelled with higher fluorescent intensity as small, diffuse punctae (Figure 3-30.G) compared to PrP^C labelling with SAF 83 (Figure 3-30.C).

CAD



CAD RML

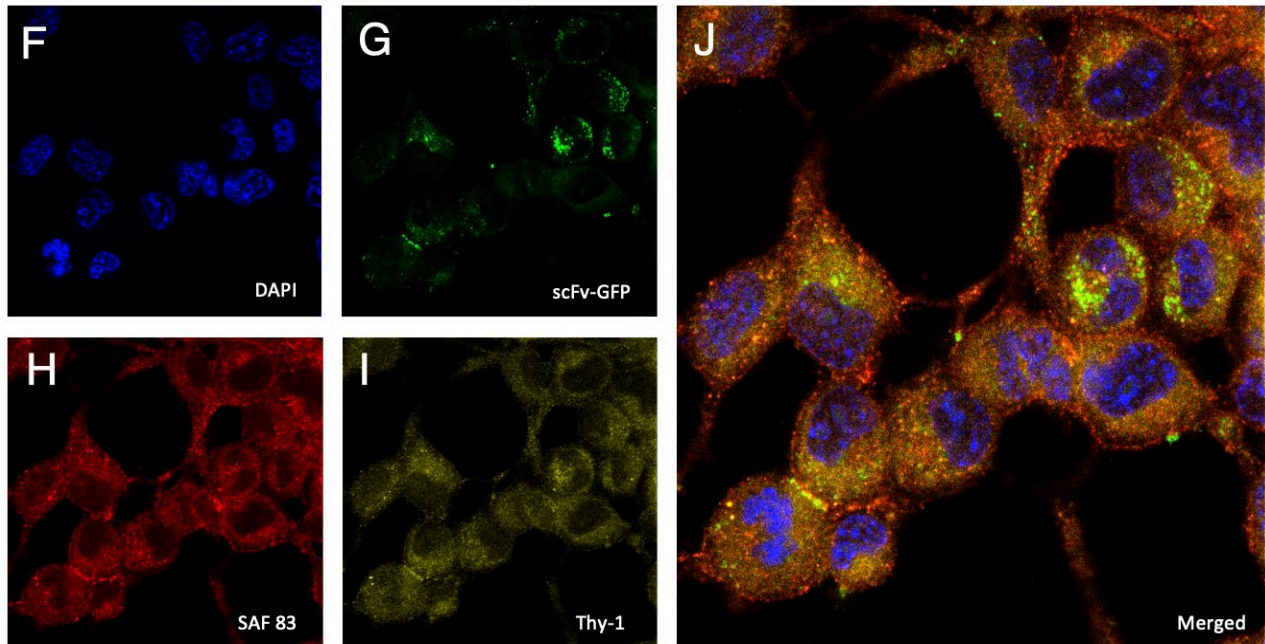


Figure 3-29: Immunocytochemistry of CAD 5 PrP / RML infected cells using recombinant scFv YEG Sc – G1 conjugated to enhanced green fluorescent protein (scFv G1 – GFP).

Representative immunofluorescence images of PrP^C and PrP^{Sc} staining with **(A-E)** uninfected and **(F-J)** infected CAD 5 cells with RML prions. Surface labelled methanol fixed PrP^C and PrP^{Sc} in permeabilized CAD5/CAD5-RML infected PrP cells with **(B,G)** PrP^{Sc}-specific scFv – eGFP monoclonal antibody, a conjugated derivative from the YEG Sc – G1 antibody family. As previously shown, the YEG Sc-G1 antibody has a discontinuous epitope and recognizes the infectious prion protein only when the epitope residues His 110 and Asp 146 are sitting on top of each other at the beta arc region of the 4RβS model. Labelled PrP^{Sc} is observed in a punctae-like form (green). **(C,F)** PrP^C and PrP^{Sc} were stained with anti-PrP SAF 83 antibody (red) targeting the central region of PrP within residues 126-164 of mouse prion protein and **(D,I)** Thy-1 monoclonal antibody (yellow) recognizing the GPI anchor linking the prion protein to the cell membrane. **(A,F)** All cells were counterstained with DAPI (blue). The cells were visualized by confocal laser scanning microscopy. Scale bar = 10μM (applied to all images)

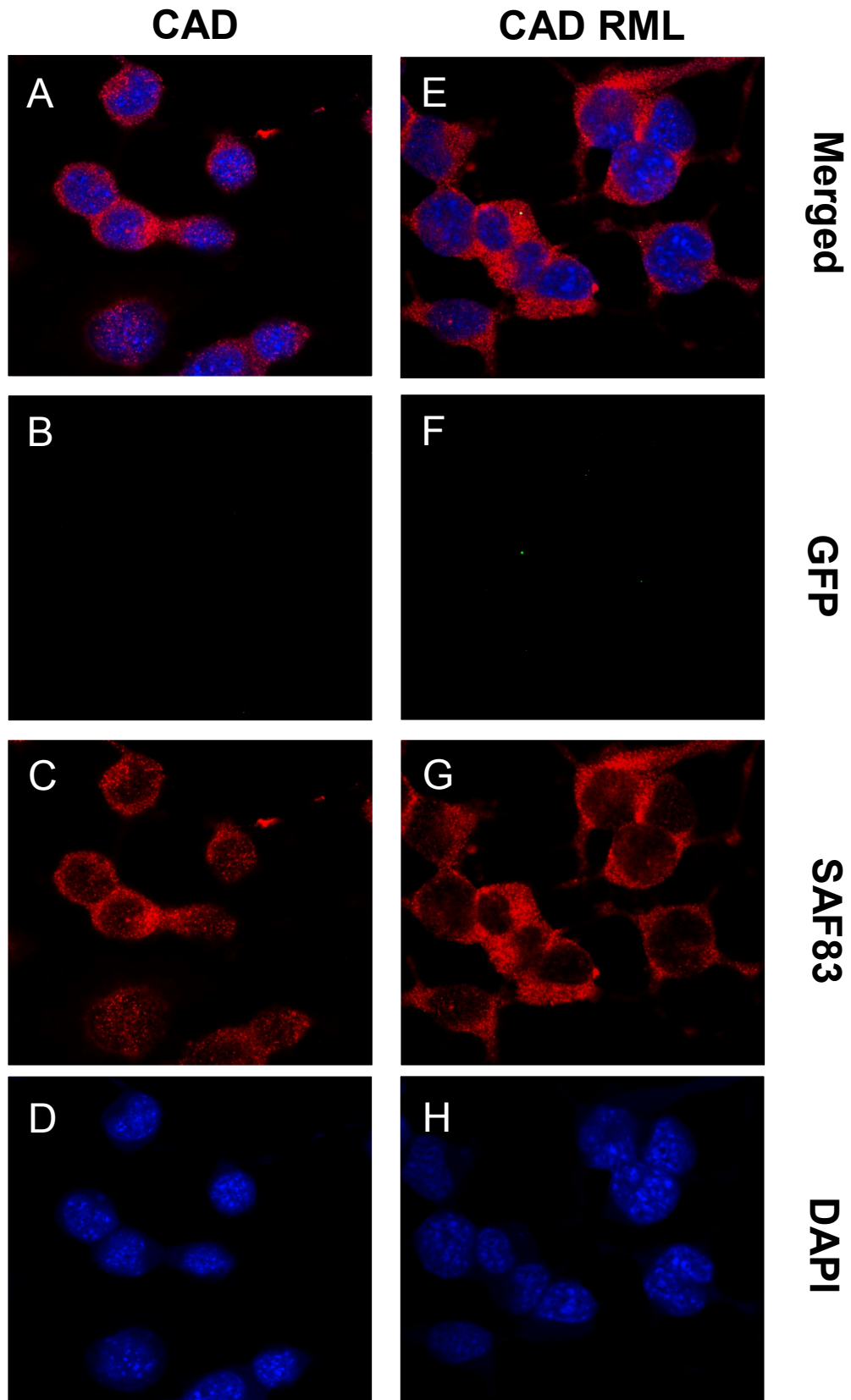


Figure 3-30: Immunocytochemistry of CAD 5 PrP / RML infected cells using recombinant enhanced green fluorescent protein as a control.

Representative immunofluorescence images of PrP^C and PrP^{Sc} staining with **(A-D)** uninfected and **(E-H)** infected CAD 5 cells with RML prions. Surface labelled methanol fixed PrP^C and PrP^{Sc} in permeabilized CAD5/CAD5-RML infected PrP cells with **(B,F)** eGFP protein as a control experiment of the previously shown immunofluorescent staining with scFv-GFP antibody. No specific labelling with eGFP was observed in CAD 5 PrP /CAD RML cells. **(C,G)** PrP^C and PrP^{Sc} were stained with anti-PrP SAF 83 antibody (red) targeting the central region of PrP within residues 126-164 of the mouse prion protein. **(A,H)** All cells were counterstained with DAPI (blue). The cells were visualized by confocal laser scanning microscopy. Scale bar = 10µM (applied to all images)

3.3.17 Design of PrP^{Sc}-specific nanobody

Single domain antibodies or nanobodies (Nbs) are the smallest class of antibody fragments with a molecular weight of ~15 kDa (Desmyter, Spinelli, Roussel, & Cambillau, 2015). They are highly soluble, have a high folding capacity and have easy access to challenging and cryptic epitopes. They recognize their antigen through a single variable domain (VHH). In this chapter, I have described the design, expression and activity assay of engineered PrP^{Sc}-specific single-domain antibody fragments/nanobodies (Figure 3-31.A) and derivatives that are fused with the trojan horse molecules for the delivery across the mouse BBB (Figure 3-31.B).

The variable heavy chain CDRs from PrP^{Sc} IgG clones were successfully loop grafted onto a nanobody framework to engineer PrP^{Sc}-specific nanobodies that are devoid of light chain which will be easier to produce recombinantly in bacteria without folding issues relating to inter-domain interactions. Their biophysical and economic properties (size, affinity, specificity, stability, and production cost) have encouraged antibody engineering of single-domain antibodies for use in research and potential therapeutic candidate (Schumacher, Helma, Schneider, Leonhardt, & Hackenberger, 2018). Nbs can be readily cloned into various formats by fusion of other proteins or peptides, thereby tailoring their utility for certain therapeutics applications to generate bispecific Nbs (Wesolowski et al., 2009).

The synthetic gene consisting of the VHH-G1, and VHH G1-VHH 8D3 (Figure 3-31.A-B) constructs were synthesized by BioBasic DNA Inc, Markham Ontario. These genes were already cloned into their Fab expressing vector (as previously described in Chapter 2) for recombinant

expression and purification by the manufacturer. The cloning was performed using restriction enzymes, HindIII and XbaI.

These engineered PrP^{Sc}-specific scFv's were successfully expressed and purified in *E.coli* as soluble and functional Fabs as described earlier in the chapter. The same procedure was used to successfully express PrP^{Sc}-specific recombinant VHH-G1, and VHH G1-VHH 8D3 (Figure 3-30. A-B).

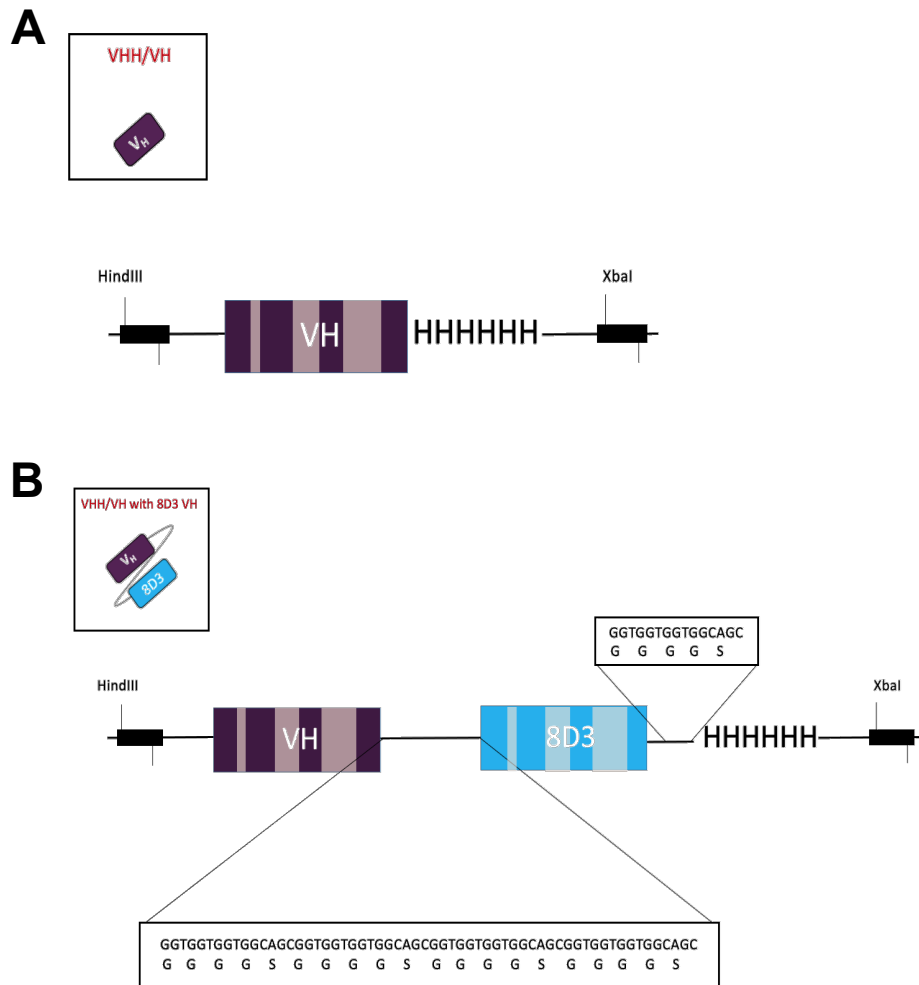


Figure 3-31: Construct design of single domain antibody fragment and their bispecific conjugates.

Schematic representation of engineered humanized recombinant antibody fragment specific to PrP^{Sc}, single domain antibody/nanobody (nano YEG-Sc G1). The nanobody consists of three CDRs from the variable heavy chain region. The construct lacks a light chain and its ability to recognize the antigen is mediated through the variable domain of the heavy chain. **(A)** HCDRs are grafted onto a nanobody framework with a 6xHis tag at the C-terminus for purification by Ni-NTA column. **(B)** Fusion of PrP^{Sc}-nanobody with mAb (8D3) that targets mouse transferrin receptor creating a bispecific nanobody for the transport of therapeutic nanobody across the blood brain barrier (BBB) and to the target in the CNS.

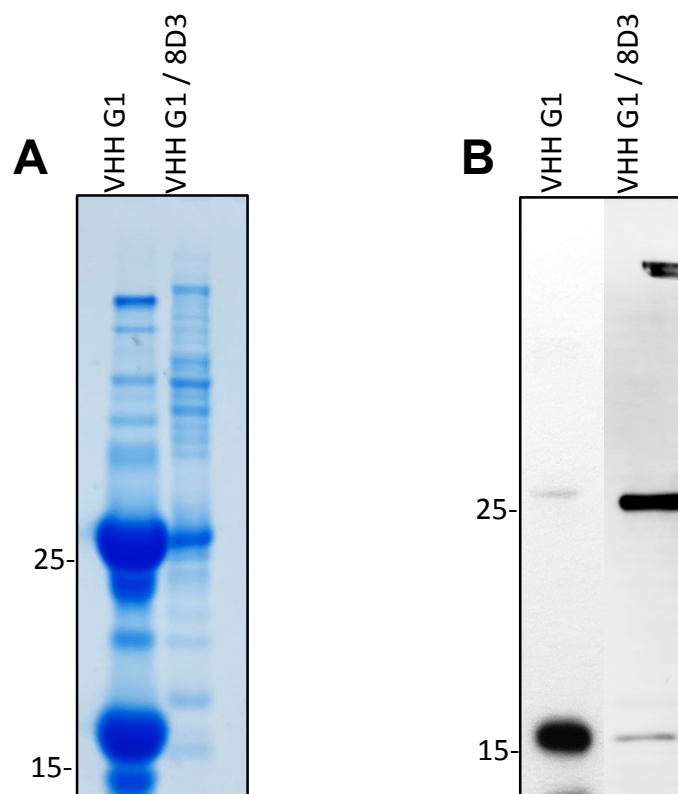


Figure 3-32: Expression and purification of single domain antibody fragments and their conjugates.

Purification of recombinant PrP^{Sc} variable heavy single-domain fragment and with molecular trojan horse conjugate for blood-brain barrier access. Analysis of recombinant expression of VHH G1 and VHH G1-8D3 via (A) SDS-PAGE Coomassie staining (left) and (B) Western blot using an anti-His tag (right) of single-domain antibody fragment VHHG1/nano-G1, represented by the ~16 kDa fragment and corresponding dimer at ~ 30kDa and bispecific nanobody show a band at ~28 kDa, whereby the nano-G1 is fused to a variable heavy chain targeting the transferrin receptor protein, represented by the ~25 kDa band.

3.3.18 The activity of variable heavy chain only

The two-step competition ELISA result revealed that our engineered and fully folded recombinant VHH-G1 recognized its antigen, fibrillized 14R1 (Figure 3-33.A). The specificity of the targeted epitope matched the ELISA epitope profiling. This activity assay performed under native conditions also validated that VHH-G1, despite being small in size and consisting of only variable regions did maintain their epitope specificity for antigen-antibody recognition and was compared to a murine-derived full-length antibody (Gilliland et al., 2012). Further characterization of these recombinant single-domain antibody fragments with infectious prion isolates is ongoing.

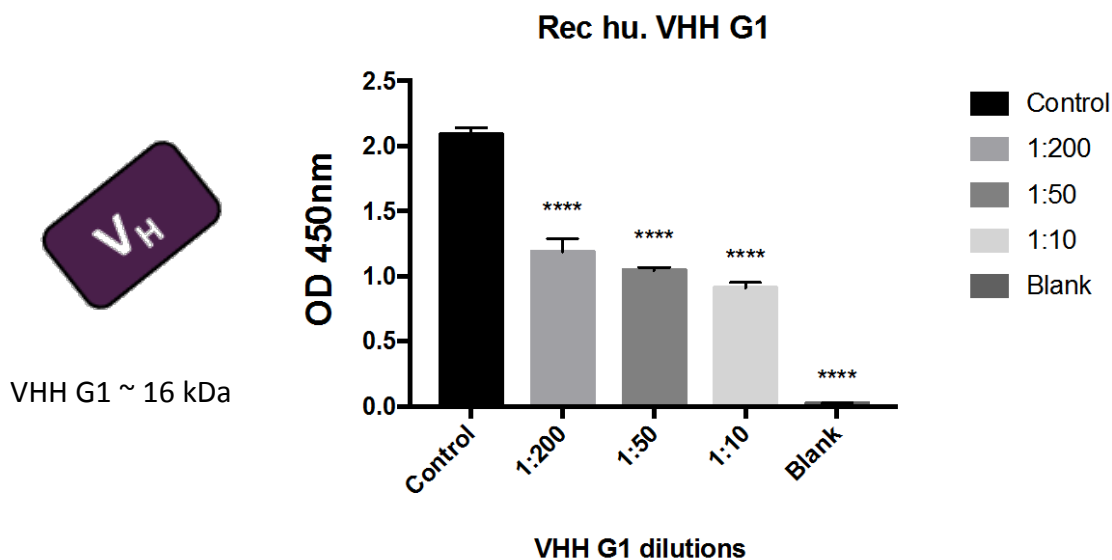


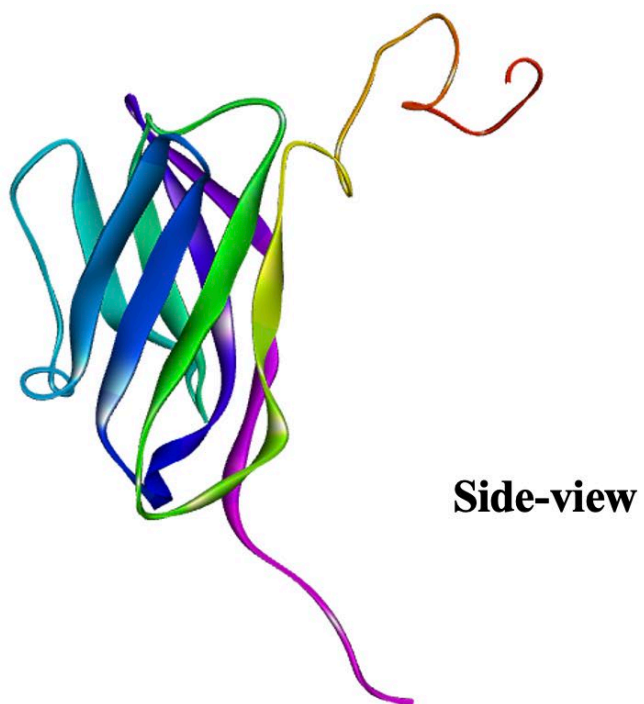
Figure 3-33: Activity assay of variable heavy single domain antibody fragment against PrP^{Sc} -vaccine/antigen (14R1)

The fully folded and functional recombinant PrP^{Sc}-specific VHH-G1 (nanobody) was tested for antigen recognition using a two-step indirect competition ELISA assay with 14R1 antigen. The two-step competition ELISA results indicate the binding of VHH-G1 to the 14R1 antigen whose structure mimics the 4R β S model of infectious prion protein. Control well is measured by the omission of primary antibody (VHH-G1), consisting of only secondary antibody (Parent-G1) and tertiary detection system (anti-mouse HRP). The blank well was only incubated with tertiary antibody, anti-mouse. The data presented are statistically significant compared with the control ($p < 0.0001$) using One-way ANOVA, Dunnett's test.

3.3.19 Comparative in-silico modelling and docking of VHH-G1 and huPrP^{Sc}

Computational modelling was performed on the structure, single domain antibody fragment by Dr. Luda Dorosh from the Wille lab to understand the folding of the engineered and binding interaction with the human PrP^{Sc} model. The VHH-G1 model was adapted from the VHH structure available in Protein Data Bank (PDB), PDB# 4PFE (Eshaghi et al., 2015) which was then simulated together with the same buffer conditions as used in experimental conditions. The ribbon diagrams of the fragment antibody show stabilized representative conformation of the VHH G1 model after 20 ns (Figure 3-34.A). The stabilized model of VHH G1 was docked with the human PrP^{Sc} model to observe if hydrogen bonds are formed and more specifically between which key residues. The comparative computational docking and simulation after 140 ns revealed favorable hydrogen bonds between the residues H111 and D147 of the human PrP^{Sc} with residues, D136, M78 and W75 of the VHH G1 antibody (Figure 3-34.B). These docking results are in alignment with our experimental epitope mapping results.

A



B

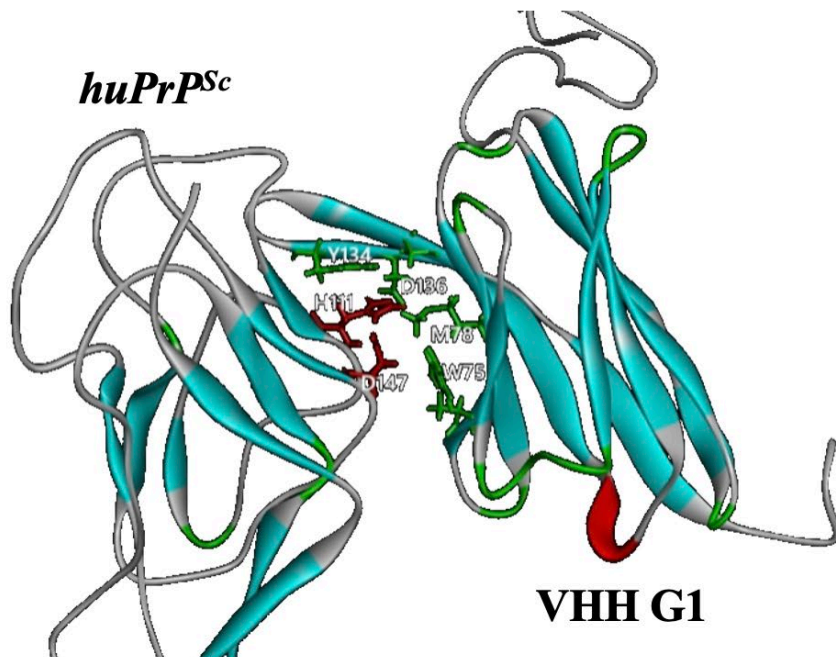


Figure 3-34: Molecular dynamics simulation of VHH G1 and human PrP 27-30 stabilized for 140 ns.

Ribbon diagrams of variable heavy single-domain fragment antibody or nanobody (A) Side view showing stabilized representative conformation of VHH/nano-G1 model after 20ns MD. (C) The identical conditions were used as in the wet-lab experiment for molecular docking and the modelling of VHHG1/nano-G1 (shown in cyan beta-strands) with huPrP 90-231 (green beta-solenoidal structure) in AccelrysDS and simulated at 310K for 50 ns. The docked hydrophilic surface of the Fab G1 antibody formed a complex with residues H111 and D147 of the human PrP^{Sc} 4R β S model. These computational results are in alignment with our experimental epitope mapping results showing the importance of the key residues for the antigen-antibody interaction.

3.4 DISCUSSION

In this chapter, I have focused on engineering recombinant PrP^{Sc}-specific antibody fragments and discuss the generation of chimeric and humanized antibodies from murine-derived full-length IgG and IgM antibodies (Milstein, 2000). These PrP^{Sc}-specific monoclonal antibodies are an immune response from the “Rationally designed, model-based PrP^{Sc} vaccine” project from the Wille lab (Fang et al., manuscript in preparation). My PrP^{Sc}-specific antibodies, YEG Sc-G1 are appealing because they only identify infected prion isolates and do not attach to the cellular form of the prion protein, PrP^C. The YEG PrP^{Sc}-specific monoclonal antibodies have a conformational epitope and recognize the 4RβS model structure of PrP^{Sc}, with key residues His 110 and Asp 146 (YEG Sc-G1) and Asn 103 and Asp 143 (YEG Sc-M63) for strong antigen-antibody interaction. Here I have shown the activity and specificity of our antibodies using a wide range of assays including immunofluorescence assay, immunogold labelling and immunoprecipitation.

In this study, I have used the DNA technology developed by Köhler and Milstein to develop smaller, antigen-binding fragments, derived from our murine-derived PrP^{Sc}-specific full-length antibody clones by first elucidating their primary structures and grafting the CDRs into antibody fragment framework. My PrP^{Sc}-specific antibody toolbox consists of antibody fragments that can be used on their own or linked to other molecules such as eGFP, CPP linker and molecular trojan horse to generate numerous possibilities for bispecific or multifunctional molecules for its utility in structural analyses of prions, direct detection and potential therapeutics. I adopted the recombinant expression and purification protocol as described previously (Chapter 2) to produce functional Fabs, scFvs, and Nanobody. Using diverse biochemical and biophysical techniques,

we investigated the link between the epitope of these completely folded PrP^{Sc} antibody fragments and their functional activity (detailed biophysical study described in chapter 4).

Numerous groups have made efforts in generating PrP^{Sc}-specific antibodies to distinguish PrP^{Sc} from PrP^C. However, a significant number of promising antibodies have shown not to have a discontinuous epitope, that can differentiate the pathogenic (PrP^{Sc}) and the non-pathogenic isoforms in their native form. Rather they have been shown to react with linear epitopes of PrP^{Sc} in a denatured environment including monoclonal antibodies 15B3 (Korth et al., 1997) and 8G8 (Feraudet et al., 2005) and a list briefly described in Table 3-1. While PrP^{Sc}-specific antibodies are desired for their specificity, they have an inherent restriction. Because PrP^{Sc} is a conformationally altered and aggregated version of PrP^C, a true PrP^{Sc}-specific antibody will have epitopes that will be conformation-dependent and/or discontinuous. As a result, one would expect a conformational dependent PrP^{Sc}-specific mAb would fail to react to denatured materials like those used for western blotting. Furthermore, the frequent pre-treatments employed to improve PrP immunostaining with standard PrP antibodies (guanidine treatment, antigen retrieval by hydrolytic autoclaving, and so on) would be expected to disrupt PrP^{Sc}-specific conformational epitopes. The conformational dependent PrP^{Sc}-specific full-length and its smaller antibody derivatives have shown not to work under denaturing conditions such as western blot (data not shown) or when the tissue or cells are fixed with formaldehyde/covalent fixations for immunohistochemistry assays. Additionally, immunogold labelling performed using 3M urea has failed to recognize the epitope of RML prions.

The specificity of our PrP^{Sc} monoclonal antibody, YEG Sc-G1 showed to recognize PrP^{Sc} under native conditions and does not react with PrP^C or denatured PrP. Additionally, it reacts with all strains of PrP^{Sc} tested (12 strains) as shown by the competition ELISA results (Figure 3-1.A-B). Characterization of the YEG mAb Sc-G1 epitope revealed a discontinuous epitope that recognizes PrP^{Sc} in its putative β -solenoid configuration. Specifically, discontinuous residues H110 and D146 appear to play a pivotal role in antigen-antibody recognition. The PrP^{Sc}-specific full-length and Fab YEG Sc-G1 antibody revealed widespread surface labelling of PrP^{Sc} on RML-infected cells, while uninfected control cells remained completely unlabeled. Our engineered scFv antibodies have the advantage of being able to penetrate deep into antigen complexes in cells and tissues due to their small size (Ahmad et al., 2012). Conjugation of the scFv probe with eGFP is a powerful strategy for imaging protein aggregates in living cells or lightly fixed tissues without the need for secondary detection systems. The PrP^{Sc}-specific fluobody promises to be a highly beneficial tool versus regular, linear epitope antibodies due to its strict specificity, selectivity, and affinity for native PrP^{Sc}. Hence, this tool may allow new insights into important physiological phenomena of prion infections in living cells, tissues, and organisms. Specific cell surface labeling of native PrP^{Sc} in RML-infected CAD5 cells using a single-chain fluobody was achieved (Figure. 3-29.J). PrP^{Sc} was seen in small, diffuse punctae and larger foci, suggesting different stages of replication or aggregation. Additional studies with the fluobody in organotypic slice cultures infected with different prion strains are on-going. One drawback might be that the use of extremely cold methanol can deform the cell morphology when surface labelling PrP^{Sc} with the PrP^{Sc}-specific antibody on methanol-fixed cells. Various alcohol and formaldehyde fixation studies on tissues and cells indicated no staining difference

between ice-cold 80% methanol diluted in PBS and formaldehyde fixed tissues. (Alles et al., 2017).

PrP^{Sc}-specific antibodies and their smaller antibody derivatives (Fabs) offer an alternate approach to deciphering the structure of infectious prions based on the orientation of their epitopes. There is an ongoing debate between the previously reported four-rung beta solenoid (4R β S) (Vazquez-Fernandez et al., 2016; Wille, Bian, et al., 2009) structure and recent brain-derived cryo-EM structures revealing a Parallel In-Register Intermolecular β -sheet Structure as the underlying fold of infectious prion protein (Artikis et al., 2022). Due to the attractiveness of our discontinuous epitope PrP^{Sc}-specific antibodies, it was able to distinguish the suggestive 4R β S fold observed in small amorphous aggregates, 2D crystals and clumps of fibrillar aggregates as well as the PIRIBS conformation observed in isolated amyloid fibrils through immunogold labelling and electron microscopy in their native form. Due to the heterogeneity in our samples and in the previous investigations (Kamali-Jamil et al., 2021; Vazquez-Fernandez et al., 2016) suggests that more than one structure could co-exist in the brain of one host. Moreover, RML-infected FVB mice completely lack fibrillar assemblies in the brain (Godsave et al., 2008) and suggestive that PTA purification in the presence of detergent is causative of fibril formation (Levine et al., 2015; Safar et al., 1998).

When comparing how the YEG Sc-G1 and YEG Sc-M63 epitopes are oriented in the PrP^{Sc} 4R β S model (Spagnolli et al., 2019) and RML PIRIBS structure (Artikis et al., 2022; Kraus et al., 2021), we observed that the YEG Sc-G1 epitope residues H110 and D146 are surface exposed at the β -arc region between rungs 1 and 2 in a vertical pair-wise orientation. Similarly, the orientation of YEG Sc-M63 epitope residues N103 and D143 is surface exposed on rungs 1 and 2 of the 4R β S model in a vertical pair-wise orientation (Figure 3-18.A-B). In contrast, the

orientation of these epitopes in the brain-derived RML PIRIBS structure is no longer in a vertical pair-wise confirmation. The orientation of the YEG Sc-G1 is found to be on the β -arc region between strands 2 and 3 and strands 5 and 6, H110 and D146 respectively. These residues are surface exposed and facing 180° to each other on a monomeric RML PrP^{Sc} structure. Whereas the orientation of the YEG Sc-M63 epitope on the RML PIRIBS structure is on the β -strands 2 and 5, N103 and D143 respectively. N103 is surface exposed while the residue D143 is facing inwards toward the hydrophobic core (Figure 3-18.B).

Based on the orientation of the YEG Sc-G1 and M63 epitopes in the 4R β S model and PIRIBS structure, we can study the different folds that are adopted during protein misfolding events in which misfolded prion proteins transition to β -oligomers (β -solenoidal conformation) and form stable amyloid fibrils (PIRIBS conformation) in various prion strains (detailed description on chapter 4).

The discovery of an antibody that binds specifically to PrP^{Sc} from various species opens up a new avenue for directly identifying PrP^{Sc} with and without the use of proteinase K digestion as a criterion and selectively precipitating PrP^{Sc} from infected brain homogenate through immunoprecipitation using YEG Sc-G1 antibody (experiments ongoing). As previously demonstrated by 15B3 and P1:1 PrP^{Sc} specific antibodies, they selectively isolated PrP^{Sc} either after PK digestion, PrP 27-30 (Korth et al., 1997) or failed to immunoprecipitate PK-digested PrP^{Sc} (M. Jones et al., 2009), respectively. This indicates that, despite being claimed as PrP^{Sc}-specific monoclonal antibodies, they tend to recognize selective linear PrP epitopes.

Nevertheless, we can infer from our competitive ELISA results, native immunolabelling of RML prions through immunogold labelling and immunofluorescence staining that our discontinuous

epitope PrP^{Sc}-specific YEG Sc-G1 will selectively immunoprecipitated both, the full-length PrP^{Sc} and PrP 27-30 in its native conditions.

With all these properties and specificity described for the conformational YEG Sc-G1 monoclonal antibody, we engineered small antibody derivatives conjugated with tissue-specific antibody delivery as potential tools for passive immunotherapy for prion disease. Two different designs were created: (1) we prepared a single chain variable fragment specific to PrP^{Sc}, where a cell-penetrating peptide (CPP) was used as a linker between the two variable domains of the scFv (Skrlić et al., 2013); (2) a bispecific nanobody/VHH, where one specificity is used to target misfolded isoform of the prion protein, PrP^{Sc} (target antigen) and the second specificity is used to target the specific cellular compartment, which is transferrin receptor which will allow our therapeutic antibody to cross the BBB through receptor-mediated transcytosis (RMT) (Pardridge, 2015; Pardridge & Boado, 2012). However, the effectiveness of these therapeutic YEG Sc-G1 antibodies has not been evaluated.

In conclusion, this chapter details the generation, production, extensive characterization and application of a panel of PrP^{Sc}-specific recombinant antibody fragments that were developed using hybridoma DNA technology. The benefits of employing Fabs over full-length antibodies include their ability to penetrate deeply into amorphous aggregates like PrP^{Sc} and the ability to produce them in *E.coli* for a fraction of the cost of hybridoma antibody synthesis (Simmons et al., 2002). Here we have shown the utility of the PrP^{Sc}-specific YEG Sc-G1 monoclonal antibodies in structural analyses via immunogold labelling (structural fold analyses of prion, described in chapter 4), direct detection of prion through cell surface staining, and now we intend to evaluate the use of our engineered therapeutic tools for passive immunotherapy for prion disease in the genetic prion mouse model (Nazor et al., 2005; Sigurdsson et al., 2003).

Chapter 4: Analyzing the Fold of Synthetic
A117V – Gerstmann Sträussler-Scheinker
Peptide using a PrP^{Sc}-specific Antibody

4.1 INTRODUCTION

The central event in the pathogenesis of prion diseases is the misfolding of the cellular prion protein, causing the accumulation of amyloid aggregates which could lead to the formation of amyloid fibrils. Gerstmann-Sträussler-Scheinker disease (GSS), Fatal familial insomnia (FFI), and prion amyloidosis with variable phenotypes are hereditary neurodegenerative diseases.

These genetic prion diseases are caused by missense or insertional mutations in the prion protein gene (*PRNP*) which predisposes mutant PrP^C to spontaneously convert to PrP^{Sc} (Gambetti et al., 2011).

In most prion diseases such as sporadic human disease of Creutzfeldt-Jakob disease (CJD), the digestion of PrP^{Sc} with proteinase K (PK) results in N-terminally truncated PK-resistant PrP aggregates (PrP²⁷⁻³⁰) (Figure. 1-2.D). Depending on the cleavage site, Gly 82 (type 1) and Ser 97 (type 2), digestion yields variably glycosylated C-terminal PrP fragments, whose un-glycosylated PrP^{res} bands show molecular weights of 21 and 19 kDa bands (Parchi et al., 1998).

In contrast, a remarkably different gel electrophoretic profile is observed in the GSS subtype associated with alanine to valine mutation at the *PRNP* position 117 (GSS-A117V) whereby PK-treated GSS-A117V sample only shows an N- and C-terminally truncated, un-glycosylated PrP^{res} band of 7 kDa (Figure 4-1.A). Faint bands of PrP^{res} fragments at higher molecular weight bands at 14 kDa and 21 kDa likely represent its covalently linked multimers (Cracco et al., 2019; Pirisinu et al., 2013). The 7 kDa PrP^{res} fragment of GSS-A117V spanning residues 90-150 is devoid of N and C-terminus and was not recognized by a C-terminus SAF60 monoclonal antibody (Feraudet et al., 2005) that recognizes residues 157-161 at the C-terminus of the human prion protein (Figure 4-1.A).

GSS is characterized clinically by ataxia, pyramidal signs and dementia, and neuropathologically by the presence of extracellular deposits made of small, non-fibrillar, autocatalytic aggregates composed of non-glycosylated and non-glycophosphatidylinositol (GPI) anchored PrP fragments (Figure 4-1.B) (Cracco et al., 2019; Vanni et al., 2020). The non-fibrillar and β -oligomeric structures observed in the brain of GSS-A117V patients were verified with 5 nm gold labelling around the oligomers using a binary method to identify bound anti-PrP Fab 69 antibody (Chapter 2) (Figure 4-1.C).

The self-propagating properties of prions are derived from their structures and structural interactions. Structural studies of PrP^{Sc} have been limited and extremely difficult, owing to difficulties in purification and a high degree of structural disorder. As described in chapters 2 and 3 of this thesis, there is an on-going debate on the structures of PrP^{Sc}. X-ray fiber diffraction of PrP^{Sc} and PrP27-30 amyloid fibrils as well as cryo-electron microscopy of GPI-anchorless PrP27-30 fibrils propose a four-rung beta solenoidal (4R β S) architecture as the key feature of the infectious prion protein (Vazquez-Fernandez et al., 2016; Wille, Bian, et al., 2009). Studies of 2D crystals composed of PrP27-30 and “mini-prion”, PrP^{Sc}106 by electron crystallography was constrained to contain a β -solenoid structure at its core based on the 2D projection maps (Govaerts et al., 2004; Supattapone et al., 1999; Wille et al., 2002). The β -solenoidal structure also complies with a number of structural constraints that have been acquired over time using various biophysical and biochemical techniques. Circular dichroism (CD) and Fourier-transform infrared (FTIR) spectroscopy have both shown that PrP^{Sc} and its N-terminally truncated variant, PrP27-30, had significant β -sheet content (B. Caughey, Raymond, & Bessen, 1998; B. W. Caughey et al., 1991; H. Wille & J. R. Requena, 2018). The recent brain-derived cryo-EM studies proposes a PIRIBS arrangement for the structure of infectious prions.

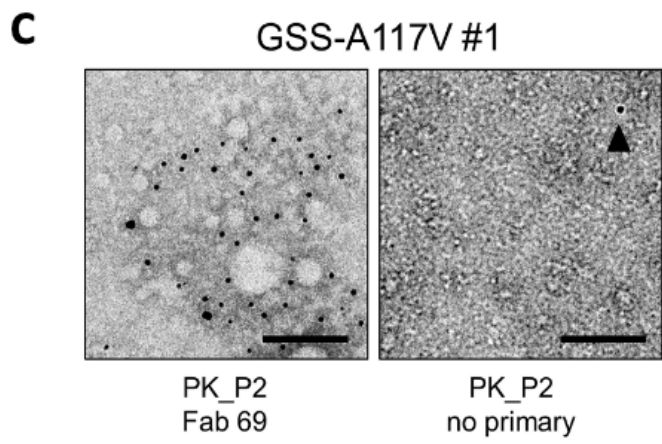
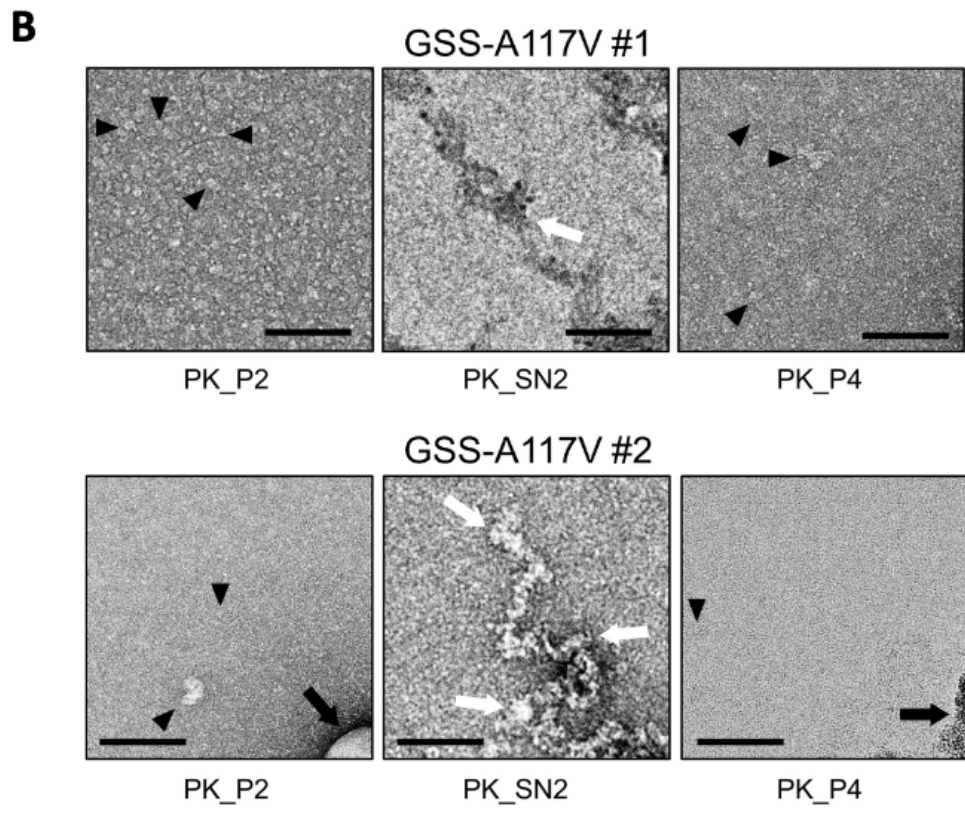
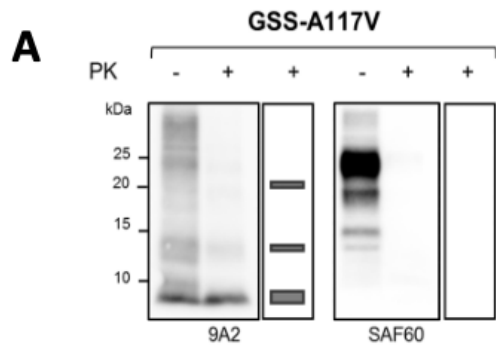


Figure 4-1: Biochemical and structural characterization of human GSS-A117V brain sample.

(A) PK-treated and untreated brain homogenate inocula of human GSS-A117V in bank voles. The first lane shows the total PrP and the second lane shows PrP^{res} in the brain homogenates of the GSS-A117V sample which were analyzed using monoclonal antibodies targeting epitopes at the central region (9A2) and C-terminus region (SAF60) of the human prion protein. The PK-treated GSS-A117V inoculum was characterized by 7kDa PrP^{res} devoid of the C-terminus of the PrP which was recognized by mAb 9A2 but not by the C-terminal antibody, SAF60. This confirms that the 7kDa band is composed of unglycosylated PrP fragment which spans from residue 90-150 of the prion proteins. Multimers of the 7kDa PrP^{res} fragment are observed at higher molecular weights bands at ~14kDa and ~21kDa which are recognized by mAb 9A2 targeting the central region within residues 99-101 of human PrP. **(B)** Representative electron micrographs of purified human brain-derived GSS-A117V samples. The P2 and P4 fractions from the GSS-A117V isolates contained a layer of small amorphous particles that covered the carbon film surface (filled arrowheads on select particles). No amyloid fibrils or larger protein aggregates were observed, and occasional lipid structures and amorphous structures were visualized (black arrows). The SN2 precipitate was composed of amorphous aggregates only (white arrows), which is typical for alcohol precipitates. Grids stained with 2% uranyl acetate. Scale bar = 100 nm. **(C)** The P2 fraction of the human GSS-A117V sample was used for immunogold labelling with our recombinant anti-PrP Fab 69, which recognizes an epitope between residues 87-98 of the human prion protein. The small amorphous aggregates in the GSS-A117V sample were decorated with 5nm gold particles, while a sample that was treated identically except for the omission of the primary Fab showed only one gold particle (filled arrowhead). Because of the size and nature of the GSS-A117V particles, the attached gold labels cannot be assigned to specific particles. These figures were taken from (Vanni et al, 2020)

Cryo-EM study from the brain of two GSS patients associated with a mutation of phenylalanine to serine at position 198 of the *PRNP* revealed amyloid fibrils of PIRIBS conformation consisting of two, three and four protofilament structures (Hallinan et al., 2022). However, these

findings are contrary to the X-ray fiber diffraction proposing a 4R β S structure (Wille, Bian, et al., 2009)

Monoclonal antibodies against PrP have proven to be valuable tools in the investigation of prion disease pathogenesis (Senatore et al., 2020). However, under native conditions, many of the mAbs that are currently available react only with PrP^C, as is the case with 3F4 (Kascsak et al., 1987; Safar et al., 1998), or react equally well with both PrP^C and PrP^{Sc}, for example, our Fabs from the anti-PrP Fab library (Chapter 2). Although several antibodies reported to be specific for PrP^{Sc} have been described (Table 3-1), the use of these antibodies under native conformational conditions has so far been limited (Curin Serbec et al., 2004; Korth et al., 1997; Polymenidou et al., 2008). Monoclonal antibodies such as YEG Sc – G1, are capable of distinguishing different amyloid folds specific to the infectious conformer (PrP^{Sc}) and are useful not only for the diagnosis of prion diseases but also provide an understanding of the various tertiary and quaternary structures involved in disease pathogenesis (detailed explanation in chapter 3).

The underlying cause of the prion pathogenesis is the misfolding and adoption of an abnormal isoform of the prion protein. Recent evidence by Vanni and colleagues showed a direct association between oligomeric GSS – A117V PrP^{res} of ~7 kDa (Figure 4-1.B) and infectivity in bank voles, and a study performed on recombinant PrP^{Sc}, confirmed and strengthened this association, demonstrating that the infectivity is encoded only with structure pertaining mostly of β -fold PrP (Vanni et al., 2020; F. Wang, Wang, Abskharon, & Ma, 2018).

Here we reasoned the high susceptibility of bank voles to GSS prions and designed a 61 residues synthetic GSS – A117V peptide and refolded *in vitro* under eight different biochemical conditions at pH 5.0 and 8.0 for the adoption of β -oligomers and stable amyloid fibrils from

linear peptide and evaluate which β -sheet fold is involved in GSS prion infectivity. In this study, we found that that chemically synthesized 61 residue GSS peptide carrying the A117V mutation was refolded into an isoform rich in β -sheets structure composed of small β -oligomeric aggregates and straight protofilament amyloid fibrils. The results were validated using our PrP^{Sc} – specific monoclonal antibody (YEG Sc-G1 mAb) which discriminated the β -oligomers and amyloid fibrils through our GSS time-dependent folding immunoassay as well as immunogold labelling and electron microscopy. mAb YEG Sc-G1, in addition to being a useful diagnostic research tool, its utility in this work further validates the synthetic GSS-A117V peptide model by showing that the aggregated β -oligomers of GSS-A117V likely adopts a 2R β S fold and shares its structural similarities with the proposed 4R β S structure of PrP²⁷⁻³⁰.

4.2 EXPERIMENTAL PROCEDURES

4.2.1 Synthetic GSS-A117V peptide design

Synthetic peptide spanning truncated GSS subtype (89-149) with a mutation at position 117 of *PRNP* resulting in a substitution for an alanine for a valine (bolded) was synthesized by LifeTein[®] LLC, New Jersey, USA (>99% purity lyophilized powder and peptide mass confirmed by Mass Spectrometry analysis). The length of this short polypeptide was 61 amino acids composed of residues

⁸⁹WGQGGGTHSQWNKPSKPKTNMKHMAGAAVAGAVV**GGLGGY**MLGSAMSRPIIHFGS
DYEDRY₁₄₉ of the human prion protein with a molecular weight of ~6.4 kDa (Cracco et al., 2019). The synthetic peptide has an isoelectric point of 9.2 with a net positive charge of +3.3.

4.2.2 Preparation of GSS-A117V peptide

This peptide was treated like an infectious sample and all the experiments were carried out in a biocontainment level-2 facility. Lyophilized GSS-A117V peptide stored at -80°C was first equilibrated at room temperature for 15 min before dissolving in their respective reconstitution buffers. We decided to use two different pH conditions, 5.0 and 8.0. 10mg of the lyophilized synthetic peptide was dissolved in 10mM sodium acetate buffer, pH 5.0 at a concentration of 10mg/ml (H. Zhang et al., 1995) and additional 10mg of the synthetic peptide was dissolved in phosphate-buffered saline (PBS), pH 8.0 at a concentration of 10mg/ml (Kaneko et al., 2000).

4.2.3 PrP^{Sc} – specific antibody

In this chapter, we used Fab and full-length YEG Sc – G1 monoclonal antibodies, novel tools from our toolbox of recombinant antibody fragments (detailed explanation in chapter 3). The Fab antibody was engineered from the full-length YEG Sc-G1 antibody. Previously shown in chapter 3 the selectivity and specificity of this PrP^{Sc} – specific antibody which has a discontinuous epitope recognizing the native PrP^{Sc} only. The pivotal residues are His 111 and Asp 147 oriented in a pair-wise conformation the β -arc region of the 4R β S model is crucial for the antigen-antibody interaction. In this chapter, we employed monoclonal antibodies recombinant Fab G1 and Parent G1 to validate our results for synthetic GSS-A117V time-dependent folding immunoassay.

4.2.4 Designing GSS fold assay using different biochemical conditions

To form a β -rich conformation, the peptide was resuspended in the indicated biochemical conditions (A-H) in either 10mM sodium acetate at pH 5.0 or 1xPBS at pH 8.0, containing 0mM to 400mM NaCl, with or without 3M urea (Table 4.1 and 4.2). The final peptide concentration was 0.1mg/ml for all the conditions and stored at 4°C for GSS-fold dependent immunoassay.

Table 4-1: Synthetic GSS-A117V peptide reconstituted in sodium – acetate buffer, pH 5.0

Condition	Description	Concentration
A	0mM NaCl + Sodium acetate, pH 5.0	0.1 mg/ml
B	100mM NaCl + Sodium acetate, pH 5.0	0.1 mg/ml
C	200mM NaCl + Sodium acetate, pH 5.0	0.1 mg/ml
D	400mM NaCl + Sodium acetate, pH 5.0	0.1 mg/ml
E	0mM NaCl + Sodium acetate + 3M urea, pH 5.0	0.1 mg/ml
F	150mM NaCl + Sodium acetate + 3M urea, pH 5.0	0.1 mg/ml
G	200mM NaCl + Sodium acetate + 3M urea, pH 5.0	0.1 mg/ml
H	400mM NaCl + Sodium acetate + 3M urea, pH 5.0	0.1 mg/ml

Table 4-2: Synthetic GSS-A117V peptide reconstituted in sodium–phosphate buffer, pH8.0

Condition	Description	Concentration
A	0mM NaCl + PBS, pH 8.0	0.1 mg/ml
B	100mM NaCl + PBS, pH 8.0	0.1 mg/ml
C	200mM NaCl + PBS, pH 8.0	0.1 mg/ml
D	400mM NaCl + PBS, pH 8.0	0.1 mg/ml
E	0mM NaCl + PBS + 3M urea, pH 8.0	0.1 mg/ml
F	100mM NaCl + PBS + 3M urea, pH 8.0	0.1 mg/ml
G	200mM NaCl + PBS + 3M urea, pH 8.0	0.1 mg/ml
H	400mM NaCl + PBS + 3M urea, pH 8.0	0.1 mg/ml

4.2.5 Synthetic GSS-A117V time-dependent folding immunoassay

We used a 96 MicroWell optical-bottom plate with a non-binding surface from Thermo Scientific™ for the GSS fold assay. For each of the GSS-A117V conditions made at pH 5.0 and 8.0, we used independent plates. 100µl of each condition were loaded into each well (A-H).

Enough non-binding ELISA plates were made to run the experiments in triplicate for each time point. The ELISA plates were placed on the Labnet Rocking Platform shaker at 4°C for the next 4 weeks. Each week samples were transferred to SpectraPlates™ binding ELISA plate and an indirect ELISA was carried out as described in section 4.2.6.

4.2.6 Modelling and molecular docking of antigen-antibody complex

As previously described in chapter 3, these molecular dynamic simulation experiments were performed by Dr. Ludymyla Dorosh. The two-rung A117V model was derived from 4RβS conformer (Spagnolli et al., 2019) by C-terminal truncation at residue 150 of the huPrP^{sc} 90-231 and single point mutation A117V, which has been applied in Accelrys VS Discovery studio visualizer. In all simulation runs, the C-terminal and N- terminal extremities of the main chains were kept charged (–COO⁻ and –NH₃⁺), whereas all other titratable amino acids were assigned their canonical state at pH 8.0 or pH 5.0 with the PropKa server software (Sondergaard et al., 2011).

Representative conformations from the production MD trajectories were used as templates for protein-antibody docking using Cluspro serve with Fab G1 antibody were chosen. The top ten docking models (with the highest docking energy) were chosen for the following structural analysis: hydrogen bonds (using Chimera scripts), and inspection of antibody orientation for different modes. Snapshots from trajectories and graphical representations of models were done with Chimera or Discovery Studio. To confirm the stability of docked complexes and test the formation of HBs in solution, production simulations of the constructs were conducted at 310 K temperature and at a pressure of 1 atm with isotropic pressure coupling (NPT ensemble) for

150ns for each system, 1 fs time step. To mimic the major condition of the experiment 0.137 M of NaCl was added to the water solution. Hydrogen bonds evolution along 150 ns MD trajectory was calculated in Chimera using MD/Ensemble analysis tool

2Rung.pH8-A, and 2Rung.pH5-A2, were solvated in a periodic rectangular water box and Cl⁻ or Na⁺ ions were added to electro-neutralized the systems. In systems 2Rung.pH8-H and 2Rung.pH5-H2 additionally, 400mM of NaCl and 3M Urea were solvated in the water box to mimic the conditions of the experiment. Minimizations with gradual release of restraints and equilibration procedures are described previously (Mercer et al., 2018).

4.2.7 Indirect and competitive Enzyme-Linked Immunosorbent

Assays (ELISAs)

Indirect ELISA was performed as described previously in chapter 2.2.6. Samples were coated on ELISA SpectraPlates™ with 10µg of protein (BH and GSS peptide) diluted in their respective buffers and allowed to coat on the binding-surface of the plate, at 4°C overnight. The remainder of the indirect ELISA procedure, the same protocol was followed except for recombinant humanized Fab YEG-Sc-G1 antibody was used instead of other Fab antibodies as described in chapter 2.

Competition ELISA was performed by adding mAb YEG Sc-G1 (Parent G1) with infectious GSS-A117V samples (brain homogenate and purified fractions) in non-binding microplates and allowing it to form an antigen-antibody complex for 1 h at RT. The complex was then transferred to the original binding plate which was coated with non-infectious (PrP^C) brain homogenate and

incubated for 1 h. After washing with TBST, goat anti-mouse HRP secondary antibody was added at a dilution of 1:5000 in 5% non-fat dry milk with TBST and incubated for 45 mins at RT. The plate was then washed 5 times. 100uL of 3,3',5,5'-Tetramethylbenzidine (TMB) substrate was added in the dark until the color was developed, and the reaction was stopped by addition of 2 M sulphuric acid. Absorbance at 450 nm was recorded.

4.2.8 Negative stain electron microscopy

Negative staining was carried out on carbon-coated 400-mesh copper grids (Electron Microscopy Sciences) that were glow discharged prior to the staining (Wille, Baldwin, Cohen, DeArmond, & Prusiner, 1996). 5- μ l of GSS-A117V peptides were adsorbed onto freshly glow-discharged 400 mesh carbon-coated copper grids (Electron Microscopy Sciences) for 2 min and washed in 3 drops of (50 μ l) 0.1M and 0.01M ammonium acetate solutions each. Then, the grids were stained using a freshly filtered 2% solution of uranyl acetate and air-dried after removing the excess stain with filter paper. The stained samples were examined with a Tecnai G20 transmission electron microscope (FEI Company) operating at an acceleration voltage of 200 kV. Electron micrographs were recorded with an Eagle 4k x 4k CCD camera (FEI Company) (Vanni et al., 2020; Wille, Baldwin, et al., 1996).

4.2.9 Immunogold labelling

Immunogold labeling of purified human brain-derived and the synthetic week 4 GSS-A117V samples were performed using anti-PrP Fab 69 (Senatore et al., 2020) and PrP^{Sc}-specific monoclonal Fab YEG Sc-G1 antibodies detecting linear and discontinuous epitopes, respectively. As described in chapter 2, section 2.2.1, Fab 69 was selected from a phage display library for its ability to bind murine PrP. Fab 69's ability to recognize an epitope within residues ₈₇GGWGQGGGTHNQ₉₈ of murine prion protein was essential as this epitope is retained in the 7 kDa PrP^{res} fragments (Kamali-Jamil et al., 2021; Vanni et al., 2020). The recombinant Fab YEG Sc-G1 monoclonal antibody was produced in-house and has been shown to recognize a discontinuous epitope in native PrP^{Sc} only (detailed description in chapter 3).

Based on a previously published immunogold labeling protocol (Kamali-Jamil et al., 2021; Vanni et al., 2020; Wille et al., 2007), 5 µl of purified RML samples were adsorbed onto glow discharged formvar/carbon-coated nickel grids (TedPella, Inc.) for ~5 minutes, and washed using three drops (50 µl) of 0.1M and 0.01M ammonium acetate buffer pH 7.4. Samples used for labeling with Fab 69 antibodies, were treated with 50 µl of 3M urea for 10 minutes, to increase the epitope accessibility. Labelling of GSS samples with Fab YEG Sc-G1 was performed under the native state. Following the washing steps, the grids were stained with 2 drops of freshly filtered 2% sodium phosphotungstic acid (PTA), pH 7.2, then blocked for 90 minutes with 0.3% bovine serum albumin (BSA) in Tris-buffered saline (TBS: 50 mM Tris-HCl, 150 mM NaCl, pH 7.4). Finally, the grids were rinsed with TBS solution and water, and placed onto two drops of 2% PTA for final staining, air-dried, and stored for EM analysis. The control experiments were

conducted similarly except for the omission of the primary antibodies. The samples were analyzed with a Tecnai G20 transmission electron microscope (FEI Company) operating at an acceleration voltage of 200 kV. Electron micrographs were recorded with an Eagle 4k x 4k CCD camera (FEI Company).

4.2.10 PK-Digestion

For Proteinase – K (PK) digestion, pure synthetic GSS-A117V peptide resuspended in its respective buffer condition was used. 5ug of the pure peptide was incubated with PK (New England Biolabs) for 45 mins at 37°C with gentle shaking. The reaction was then stopped by the addition of 10mM Phenylmethylsulfonyl Fluoride (PMSF, Sigma).

4.2.11 Methanol precipitation

Methanol precipitation was performed as previously described (Cracco et al., 2017). The synthetic GSS-A117V sample was mixed with 1:9 volumes of pre-chilled methanol, vortexed and incubated at -30°C overnight. The samples were then centrifuged at 18,200 x g for 45 min at 4°C. The pellets were resuspended in lysis buffer (LB), 100 pH 8.0 (100 mM NaCl, 0.5% Nonidet P-40, 0.5% sodium deoxycholate, 10 mM EDTA, 100 mM Tris-HCl, pH 8.0).

4.2.12 Western blotting

Samples were diluted with gel loading buffer (BioRad) containing SDS and 5% 2-mercaptoethanol and boiled at 100°C for 10 min before electrophoresis. The proteins were separated by SDS-PAGE gel electrophoresis using 12% Bis-Tris NuPAGE gels (Invitrogen) and MES running buffer (Invitrogen), run for 20 min at 70 volts followed by 1 h 10 min at 150 volts and blotted electrically onto a polyvinylidene difluoride (PVDF) membrane (Millipore) at 110 volts for 1 h 20 min. The blotted membranes were blocked with 5% (w/v) non-fat dry milk in Tris-buffered saline solution containing 0.1% Tween 20 (v/v) (TBST) for 1 h. After blocking, the membrane was incubated with primary Ab 3F4, recognizing human PrP residues 106-110 (Kascsak et al., 1987) at a 1:5000 dilution overnight at 4°C. Next, the membranes were washed three times for 5 minutes each in TBST, followed by incubating the blot with anti-mouse IgG conjugated to HRP (BioRad) at 1:10000 dilutions. Membranes were washed three times with TBST. Total and PrP^{res} GSS-A117V protein signals were developed by adding ~2ml ECL chemiluminescent substrate (Pierce™ ECL Plus) and signals were detected by chemiluminescent visualization using ImageQuant (GE Life Science).

4.2.13 ThT fluorescence assay

ThT fluorescence assay for synthetic GSS-A117V peptide was performed using the published protocol used for α -synuclein protein (Wordehoff & Hoyer, 2018). I used a 96-well black

MicroWell optical-bottom plate with a non-binding surface from Thermo Scientific™ for the ThT assay. 100 µl of each sample was distributed per well: 2.5µM of aggregated week 4 and linear monomeric week 0 GSS^{A117V} sample in their indicated biochemical condition and buffer at pH 5.0 and pH 8.0 was used along with 10 µM ThT and 0.05% sodium azide (final concentrations). The fluorescence signal for aggregated and linear GSS peptide was measured every 15 minutes for 60 h using FLUOstar Omega by BMG Labtech (Aylesbury, UK) with excitation at 440 nm and emission at 480 nm and assay temperature was set at 37°C. A negative control (blank well) was setup which was conducted similarly except for the omission of the GSS-A117V peptide. The average of three replicates was plotted after subtracting with the average background fluorescence from the negative control.

4.2.14 Circular Dichroism spectroscopy (CD)

The changes in the secondary structure of synthetic GSS-A117V in eight different biochemical conditions at pH 5 and 8 with or without 3M urea were determined using a Chirascan CD spectrophotometer (Applied photophysics) as described earlier (Paul et al., 2022). The CD spectra of the aggregated week 4 and unstructured week 0 GSS-A117V sample were recorded over a wavelength range of 200 – 280 nm at 25°C, by using 0.1 cm path length quartz cell. The reported spectra were an average of twelve different acquisitions. Baseline correction was performed by subtracting the buffer spectra.

4.2.15 Bioassays

Bioassay experiments will be performed by our collaborators at the Nonno Lab in Rome/Italy as previously described (Vanni et al., 2020). Bioassays will be performed in cohorts of bank voles expressing isoleucine at PrP codon 109 (Bv109I) background. Inoculated voles will be examined twice a week until the appearance of neurological signs, after which they will be examined daily.

4.3 RESULTS

4.3.1 Synthetic GSS-A117V peptide design

Based on evidence by Vanni and colleagues (Vanni et al., 2020), it was discovered that the GSS-A117V infectivity was not directly linked to the larger fibrillar rods that are typically seen in classical prions (C. Terry et al., 2016; Vazquez-Fernandez et al., 2016), but rather to smaller oligomeric assemblies (Figure 4-1.B-C). We decided to further characterize and evaluate the change in fold of the 7 kDa GSS-A117V synthetic peptide under conformational-dependent biochemical changes to associate its infectivity when inoculated in bank voles. Thus, we designed the synthetic peptide corresponding to human PrP spanning residues 89-149 mimicking GSS-A117V features carrying the mutation (Figure 4-2.A).

4.3.2 Specificity of PrP^{Sc}-specific antibody to brain-derived infected prion isolates

We performed Indirect ELISA to validate the specificity of our PrP^{Sc} – specific monoclonal antibody using recombinant Fab and full-length YEG-Sc-G1 antibody (Parent G1) with crude brain homogenates obtained from human GSS-A117V and scrapie-adapted mouse prion isolates. Both antibodies showed higher specificity for the infectious prion isolates. The control experiment was run in parallel with the omission of the primary antibody (Figure 4-2.F).

Competitive ELISA results obtained with the monoclonal antibody YEG Sc-G1 testing crude brain homogenates from GSS-A117V case, fractions collected from the purification of patient-derived GSS A117 mutation on codon 129VV and 129MV background (Vanni et al., 2020) and non-neurologic control brain homogenates produced a clear difference in ELISA signal plotted as a change in OD 450nm as compared to the non-neurologic control samples (Figure 4-2.G)

In detail, YEG Sc-G1 monoclonal antibody also recognized prions from human isolates (data not shown) based on Gerstmann-Sträussler-Scheinker syndrome (GSS-A117V mutation), familial Creutzfeldt-Jakob disease (fCJD E200K mutation), fatal familial insomnia (FFI D178N mutation on codon 129M background), sporadic Creutzfeldt-Jakob disease (sCJD), and variant Creutzfeldt-Jakob disease (vCJD, which is bovine spongiform encephalopathy transmitted to humans).

4.3.3 Computational studies confirm the binding of human GSS-A117V to YEG Sc-G1 monoclonal antibody

Computational modeling of PrP provided an alternative approach by identifying those regions that are likely to adopt secondary structures (Huang et al., 1994). Molecular dynamic simulation performed by Dorosh and colleagues showed the linear peptide of human PrP encompassing residues 90 -150 with a single point mutation at position 117 from alanine to valine mimicking GSS-A117V subtype developed stable secondary structures consisting of 4 beta strands forming stable 2 rung – beta solenoid structure when simulated in their respective buffer conditions and oligomeric confirmation stabilized in the presence of 3M urea (Figure 4-2.B-C). Furthermore,

Dorosh showed protein-antibody interaction through molecular docking using Cluspro server with Fab G1 antibody docked to huPrP 90-150 (GSS-A117V) showing strong covalent interaction between residues H111 and D147 in its monomeric and oligomeric huPrP 90-150 (Figure 4-2.D-E). (Detailed explanation on the epitope characterization of YEG Sc-G1 antibody is discussed in chapter 3)

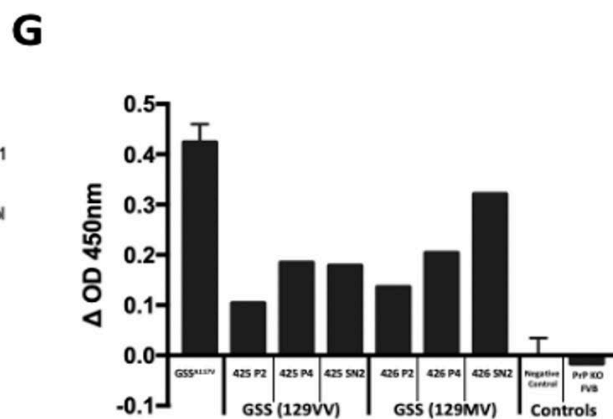
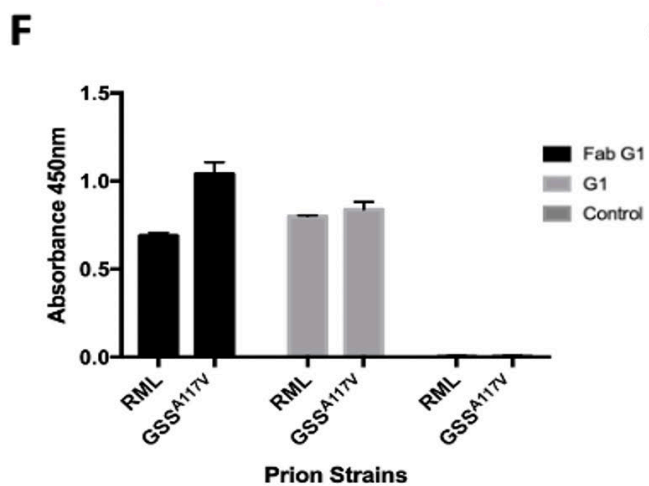
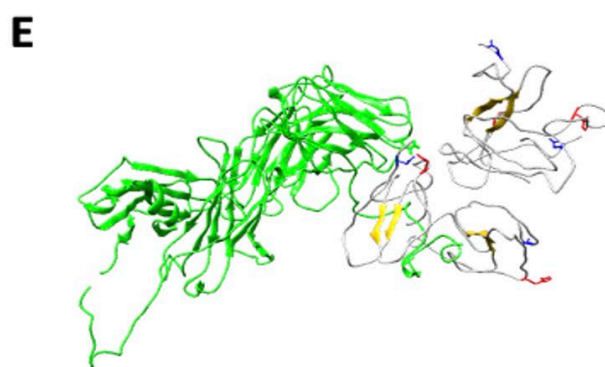
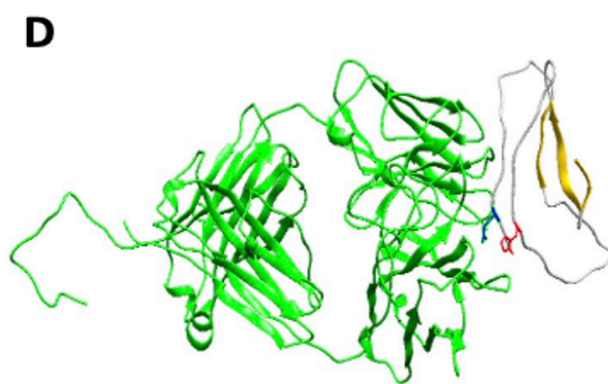
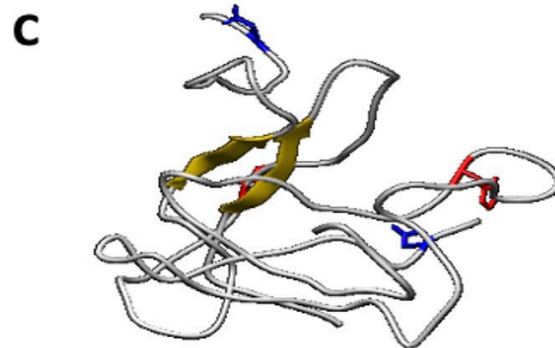
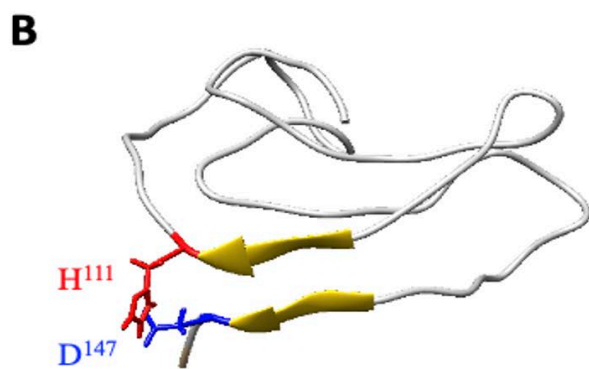


Figure 4-2: Synthetic GSS-A117V peptide and its interaction with mAb YEG Sc-G1 antibody.

(A) The primary structure of the synthetic GSS-A117V peptide spans from residues 89-149 of the human prion protein with a mutation at residue 117, from valine to alanine. This peptide length represents the atypical PrP^{res} GSS-A117V subtype composed of non-glycosylated, C- and N-terminally truncated PrP fragment giving us a ~6.6kDa band. The synthetic linear peptide is unstructured with 61 amino acids in the polypeptide chain with an isoelectric point of ~9.2 and a net charge of +3.3. Residues highlighted in red, and blue represents the epitope of mAb YEG Sc-G1 in a linear peptide. **(B)** Monomer of 2-rung beta solenoid model (2R β S) and, **(C)** multimers of 2-rung beta solenoid model, both extracted from mouse 89-230 4R β S model (Spagnolli et al., 2019). The mutation was applied at residue 117, from alanine to valine as well as converting mouse to human sequence and residues 150 – 230 of the C-terminus prion protein were cut off to create a 7kDa GSS-A117V fragment. The model was then simulated for 40ns to stabilize it. Human GSS-A117V (2R β S) model preserved the symmetry and β -sheet content. **(D)** A monomer of human-2R β S model and **(E)** Multimers of the 2R β S model representing GSS-A117V PrP^{Sc} were docked with Fab YEG Sc-G1 antibody. Docking was done using ClusPro protein-protein docking software. Hydrophilic patch of the Fab G1 antibody with residues N105 and Y55 formed a complex with residues H111 and D147 of the 2R β S GSS-A117V model. **(F)** Indirect ELISA was performed to screen the activity of the untreated brain homogenates of RML and human GSS-A117V prion isolates using PrP^{Sc} – specific antibody (Fab G1). Measurements at OD₄₅₀ for all infectious prion isolates were higher compared to the control samples which were only incubated with the secondary anti-human Fab antibody. **(G)** Competition ELISA was performed to study the selectivity of PrP^{Sc}-monoclonal antibody (YEG Sc – G1, full length) against various GSS-A117 brain purification fractions collected from the previous study (Vanni et al., 2020). We see its specificity and selectivity for only infectious human prion isolated and almost negative measurements at OD_{450nm} observed for uninfected and KO PrP samples. Molecular dynamic docking was performed by Dr. Lyudmyla Dorosh.

4.3.4 Time-dependent folding immunoassay of GSS-A117V peptide

We took advantage of our unique tool namely, the PrP^{Sc}-specific monoclonal antibody, YEG Sc – G1 to perform structural analyses on the synthetic GSS-A117V mutation peptide. Previously described the characteristics of our antibody interacting with native PrP^{Sc} only, whereby H111 and D147 of the human prion protein play a pivotal role in the formation of an antigen-antibody complex (Chapter 3). The orientation of these residues are surface exposed and sitting vertically on-top of each other on the β -arc region of the mouse PrP^{Sc} 4-rung beta solenoid model (Spagnolli et al., 2019). Here we have shown the structural commonalities and conformational changes of the GSS-A117V PrP fragment (89-149) in different biochemical conditions at pH 5.0 and 8.0 using our antibody. Based on our indirect ELISAs performed at weekly time points using recombinant Fab and full-length YEG Sc-G1 monoclonal antibody (Figure 4-3), there was no significant change in structure by week 1 of the linear peptide compared to the signal observed from the crude brain homogenates of GSS-A117V as positive control and non-neurologic negative control (Figure 4-3.A, E). An increase in signal intensity at OD 450nm was observed from the synthetic peptide starting at week 2 and mostly saturated at week 3, suggesting an adoption of a presumed two-rung beta solenoid fold (Figure 4-3 B, C, F, G). Our data indicates stronger antigen-antibody recognition with peptides dissolved in PBS at pH 8.0 with salt concentration ranging from 0mM – 400mM in the presence of 3M urea, suggesting a higher propensity of 2R β S fold and more stable β -oligomers (Baskakov, Legname, Gryczynski, & Prusiner, 2004; Wan et al., 2015) before the fold drifts away to form progressively more intermolecular β -structures suggestive of parallel in-register intermolecular beta structure (PIRIBS) whereby our signal strength would drop (Figure 4-3.D, H) (H. Zhang et al., 1995).

Comparatively, peptides dissolved in sodium acetate at a pH 5.0 with increasing salt concentration showed to have less intensity in signal compared to pH 8.0. Some biochemical conditions at pH 5.0 showed to have low antigen-antibody interaction indicative of more random coil structure and lack of definite secondary structure as the pH is further away from the isoelectric point of the peptide, 9.2 (Guckeisen, Hosseinpour, & Peukert, 2021). However, a more progressive formation of intermolecular β -sheet structure at low pH and spontaneous fibril growth influenced by the concentration-dependent change of NaCl adopting a PIRIBS structure which would abolish the interaction with our mAb YEG Sc – G1 (Goto, Adachi, Muta, & So, 2018; Hallinan et al., 2022; H. Zhang et al., 1995). A similar finding was reported for peptide 106-126 (Selvaggini et al., 1993) and the β -sheet structure of peptide 90-145 at pH 5 was found to form rich in intermolecular interactions in a period of a few days (Gasset, Baldwin, Fletterick, & Prusiner, 1993; H. Zhang et al., 1995). The antigen-antibody interaction is very dependent on the orientation of the epitope of our YEG Sc-G1 monoclonal antibody on different folds adopted in the protein misfolding events, the human 4R β S model (Spagnolli et al., 2019) and brain-derived hamster 263K (Kraus et al., 2021) and GSS-F198S (Hallinan et al., 2022) PIRIBS structure. In order for our antibody to recognize 2R β S or 4R β S PrP^{Sc} fold, the orientation of the epitope residues H111 and D147 have to be in a vertical position at a β -arc region of the presumed solenoid structure for the binding of Fab G1 and Parent G1 (Figure 4-5.A). Comparatively, a decrease in antigen-antibody interaction can be noticed when adopted a fibrillar amyloid structure as the epitope, residues H111 and D147 are orientated on opposite ends on the monomeric hamster PrP^{Sc} which would abolish antibody binding (Figure 4-5.B).

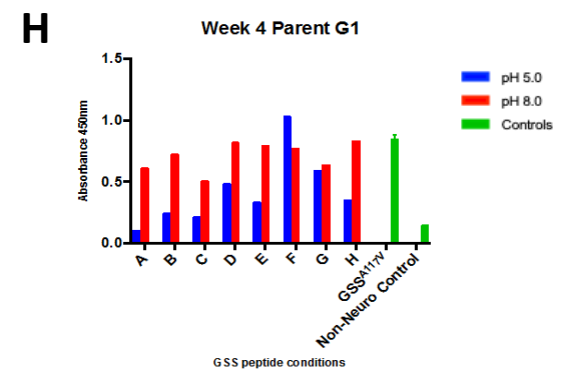
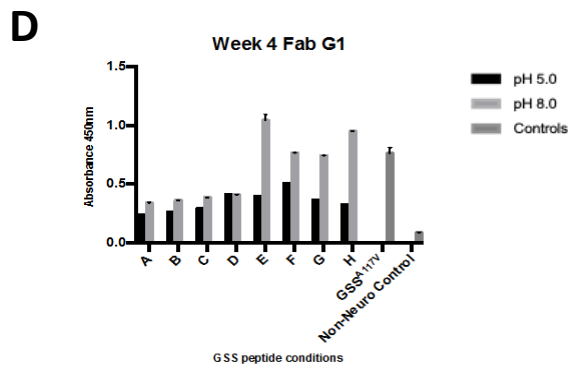
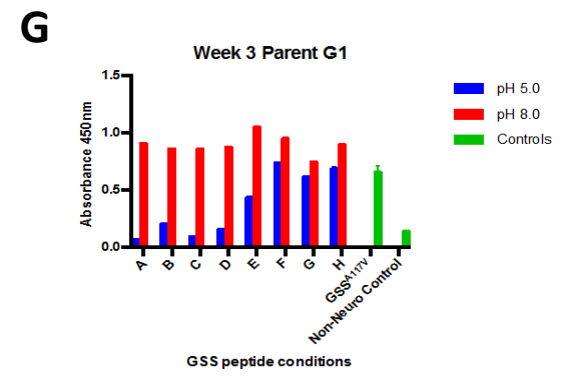
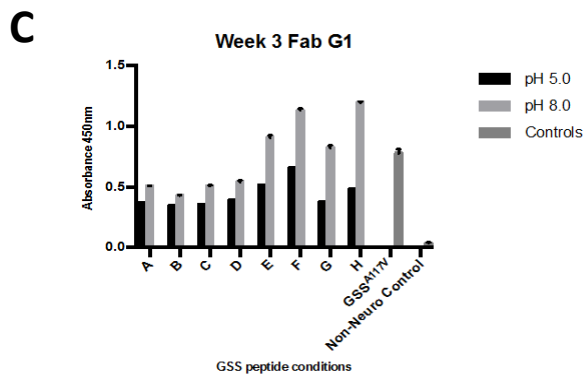
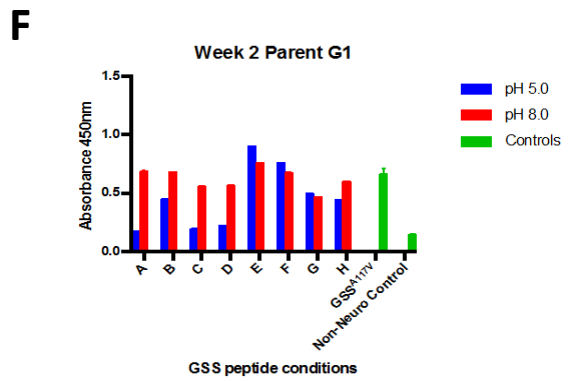
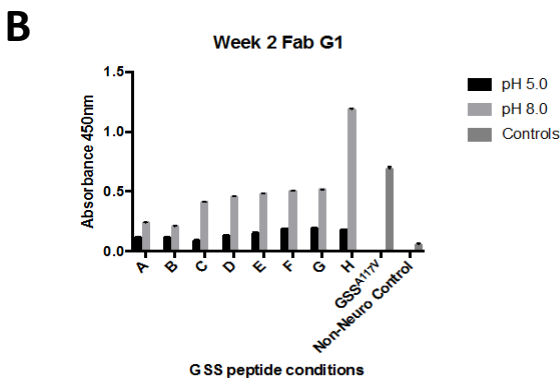
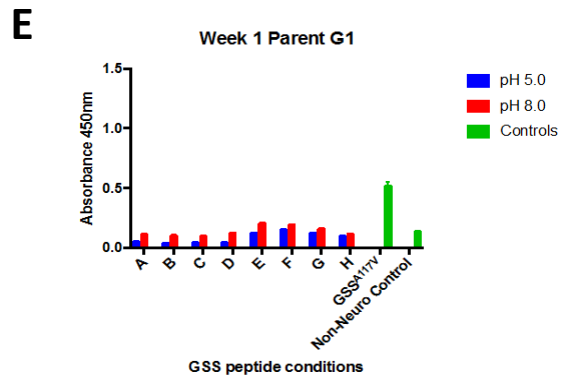
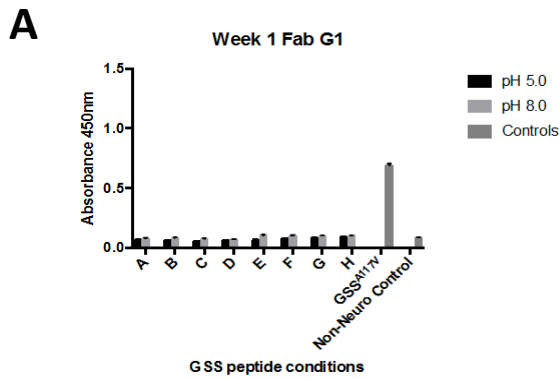
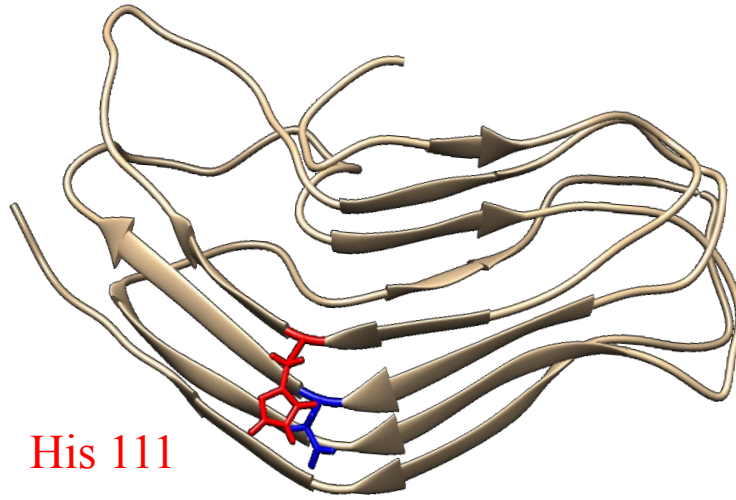


Figure 4-3: Time-dependent folding immunoassay of synthetic GSS^{A117V} peptide in different biochemical conditions using mAb YEG Sc-G1.

Indirect ELISA measurements at OD₄₅₀ nm represent antigen-antibody complex formation between the PrP^{Sc}-specific monoclonal antibody and the GSSA117V fold adopted in eight different biochemical conditions with a positive control which is untreated human GSS-A117V brain homogenate and a negative control which is human non-neurological brain homogenate. GSS-A117V fold adoption was performed for 4 week and ELISA readings were taken weekly. **(A-H)** Represents linear GSSA117V peptide adopting a presumed 2-rung beta solenoid architecture in specific biochemical conditions as the time of aggregation increases (weeks), shown by an increase in OD₄₅₀ nm measurements. We employed the use of **(A-D)** Fab G1 and **(E-H)** full-length G1 (Parent G1) antibodies to quantify the fold change based on the specificity and selectivity of these conformational-dependent PrP^{Sc} - specific antibodies. The PrP^{Sc}-specific antibody has a discontinuous, structured epitope that recognizes the H111 and D147 residue pair when found in a vertical position at the β -arc region of the first two rungs of the 4R β S model.

A

Human 4R β S Model



His 111

Asp 147

B

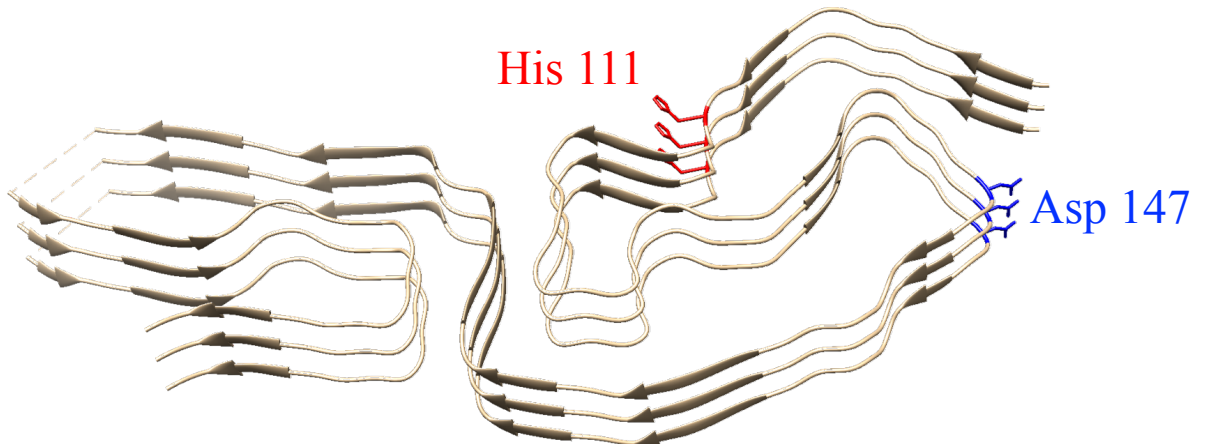
F198S GSS PIRIBS Structure



His 111

C

PIRIBS 263K Structure



His 111

Asp 147

Figure 4-5: Epitope orientation of the mAb YEG Sc-G1 in mouse 4-Rung-Beta Solenoid (4R β S) model and brain-derived GSS-F198S and hamster 263K, Parallel in-Register Intermolecular Beta Sheet Structure (PIRIBS).

(A) The orientation of YEG Sc-G1 monoclonal antibody, epitope (full-length and Fab) sits on the beta-arc region of rungs 1 and 2 of the human 4R β S model. In order to the antibody to form the complex with its antigen, the epitope must be orientated such that the surface exposed residues H111 and D147 are in vertical position and sitting on top of each other of each monomeric PrP^{Sc}. In contrast with the cryo-EM structure of (B) GSS-F198S and (C) hamster 263K prions revealed a PIRIBS structure. The orientation of the YEG-Sc-G1 epitope is found to be on the β -arc region between strand 2 and 3 and strand 4 and 5, H111 and D147 respectively. These residues are surface exposed and facing 180° to each other on each PrP^{Sc} monomer along the fibril axis.

4.3.5 Aggregated synthetic GSS-A117V are morphologically heterogenous at different biochemical conditions

I performed negative stain electron microscopy on synthetic GSS-A117V week 4 peptide reconstituted in all eight different biochemical conditions at pH 5.0 (Figure 4-6) and pH 8.0 (Figure 4-7) which revealed the presence of clumps of amyloid fibrils, structurally indistinct particles and large amorphous aggregates. Electron microscopy analysis of aggregated week 4 GSS-A117V samples at pH 5.0 with the increase in salt conditions (0mM – 400mM) and in the absence of 3M urea, showed no amyloid fibril formation but large indistinct amorphous aggregates (Figure 4-6.A-C). A large population of amyloid fibrils and large amorphous clumps were observed at 400mM NaCl at pH 5.0 (Figure 4-6.D). These observations are in agreement with earlier studies on the salt concentration-dependent fibril formation at pH < physiological (Wan et al., 2015; H. Zhang et al., 1995). In the presence of 3M urea and increasing in salt concentration showed abundant β -oligomeric structure with large amorphous aggregates, a layer of small amorphous particles that covered the carbon film surface, two-dimensional (2D) crystal-like structures (Wille et al., 2002) and short twisted two protofilament fibrils (Figure 4-6.E-H). These observations are consistent with previous studies performed using similar biochemical conditions and measured using various biophysical techniques such as but not limited to electron microscopy, kinetic studies, and X-ray fiber diffraction showing at low salt concentrations there is an abundance of oligomeric structure that are thermodynamically stable (Baskakov et al., 2000; Baskakov et al., 2004) and suggesting β -solenoidal and stacked-sheet structure (Goto et al., 2018; Wan et al., 2015). Fibril morphology of GSS-A117V peptide at week 4 refolded in

PBS at pH 8.0 with an increase in salt concentration and absence of 3M urea showed to consist more of filamentous fibrils stacked together with a mixture of small aggregates covering the carbon film of the grid (Figure 4-7.A-D). In the presence of 3M urea at pH 8.0 displayed more β -oligomers, represented as large amorphous aggregates and short stacked β -sheet fibrils (Figure 4-7.E-H), which are consistent with the morphologies observed at pH 5.0 in the presence of 3M urea. These ultrastructure observations at the biochemical conditions are consistent with previous studies on short PrP peptides revealing long filamentous fibrils formation (Kaneko et al., 2000; Tagliavini et al., 2001) at around 100mM salt concentration and consisting of amorphous aggregates suggesting a structure of a multi-rung solenoid structure and possible PIRIBS conformation of the amyloid fibrils (Vanni et al., 2020; Wan et al., 2015; Wille, Bian, et al., 2009). Additionally, studies with in-vitro generated GSS-P102L mutation PrP through PMCA revealed short rod-like structures with few clumps of amorphous aggregates caused by the sonication during PMCA (Elezgarai et al., 2017).

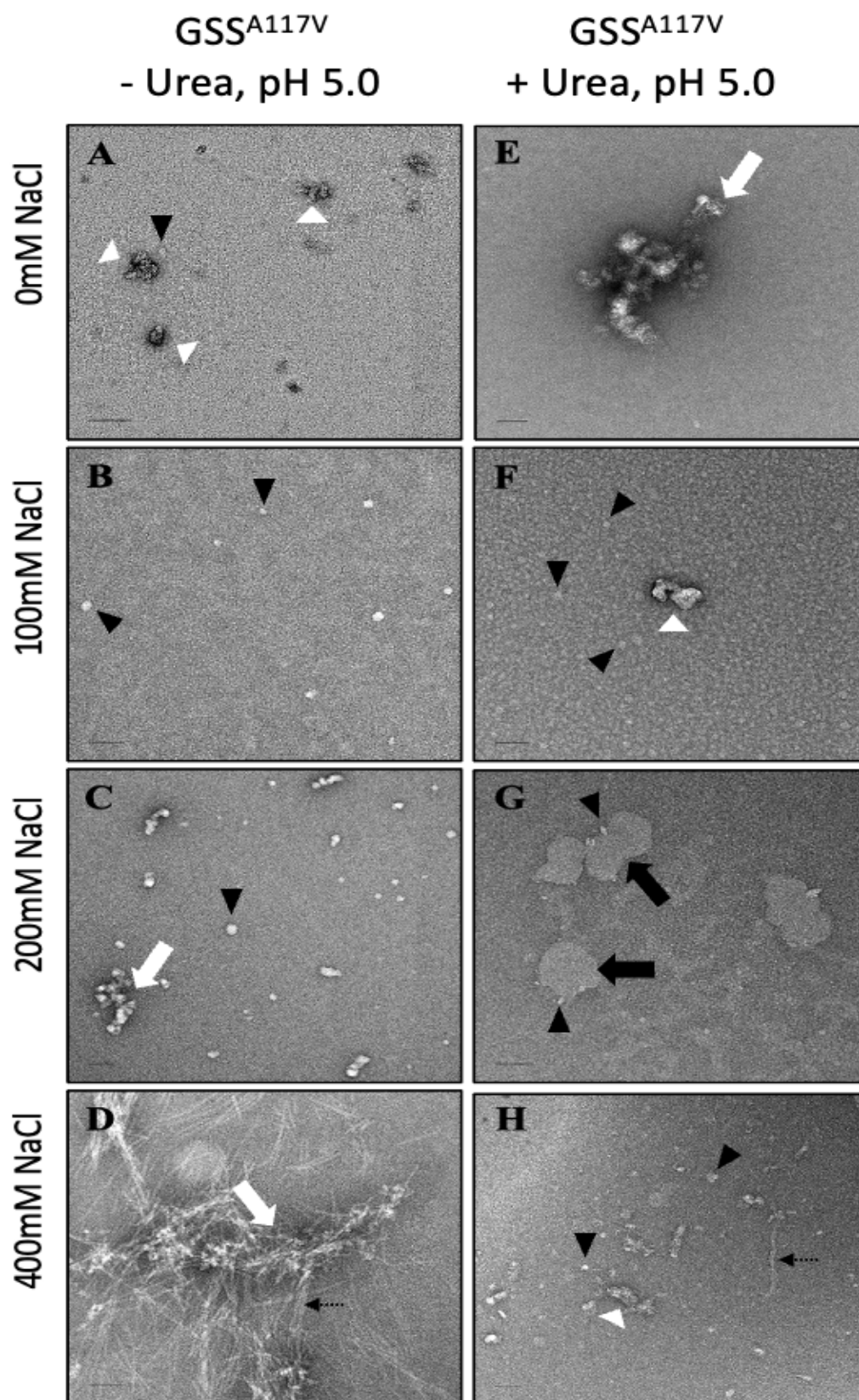


Figure 4-6: Negative stain electron micrographs from week 4 synthetic GSS^{A117V} peptide at pH 5.0.

Representative electron micrographs of week 4 aggregated synthetic GSSA117V peptide prepared in 10mM sodium acetate buffer, pH 5.0 showed to have distinct morphologies including small, non-fibrillar, and fibrillar aggregates (**A-H**) in different eight different biochemical conditions. (**A-C**) No amyloid fibrils but large amorphous aggregates (white arrowhead), small amorphous particles (black arrowheads) large aggregated clumps (white arrows) were observed. (**D**) Contained substantial quantities of amyloid fibrils (black dashed arrows), which tend to aggregate into larger clumps (white arrows). (**E-H**) Samples consisting of 3M urea and varying salt concentrations showed to have mostly, (**E**) large amorphous aggregates, (**F**) a layer of small amorphous particles that covered the carbon film surface, (**G**) 2D crystals like structure (black arrows) along with small amorphous particles, (**H**) small and large large aggregates and short fibril assembly. Samples were stained with 2% uranyl acetate. Scale bars = 100 nm.

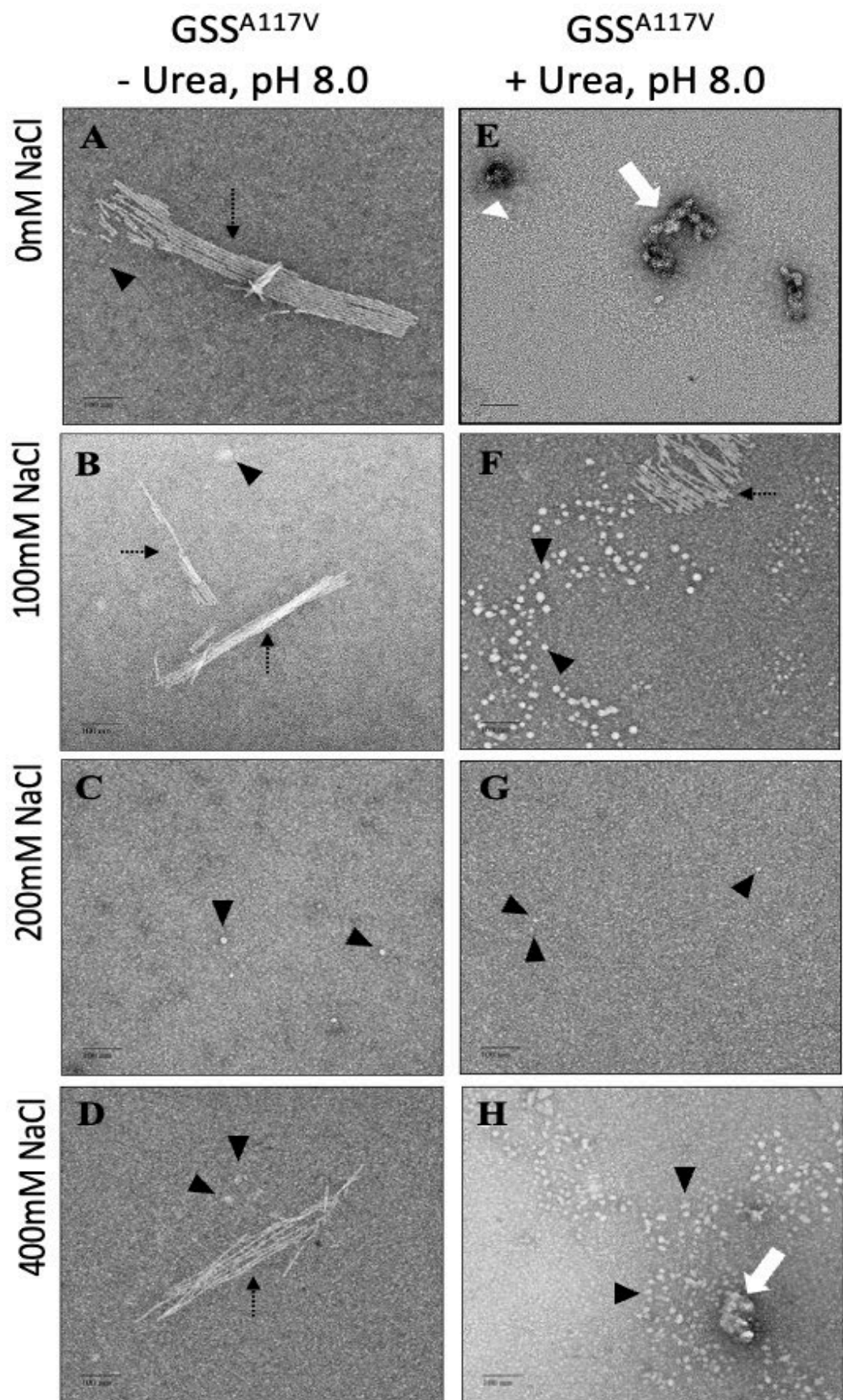


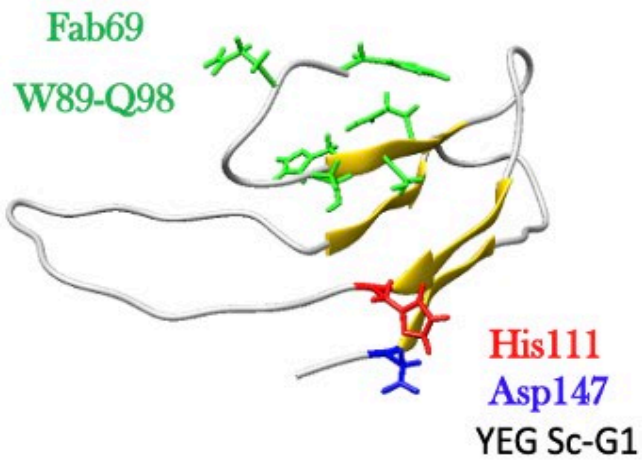
Figure 4-7: Negative stain electron micrographs from week 4 synthetic GSSA117V peptide at pH 8.0.

Representative electron micrographs of week 4 aggregated synthetic GSS-A117V peptide prepared in sodium-phosphate buffer, pH 8.0 showed to have distinct morphologies including small, non-fibrillar, and fibrillar aggregates (**A-H**) in different eight different biochemical conditions. (**A, B, and D**) samples were observed to be heterogenous consisting of substantial amount of large aggregated filamentous amyloid fibrils (black dashed arrows) indicating an adoption of PIRIBS like conformation along with small amorphous particles (black arrowhead). (**E-H**) samples consisting of 3M urea and varying salt concentrations showed to mostly contain, (**E**) large amorphous aggregates (white arrowhead) which tend to aggregate into larger clumps (white arrows), (**F**) composed of short amyloid fibrils and small amorphous particles, (**H**) large amounts of small amorphous aggregates forming larger aggregates. (**C-G**) showed to have common feature of a layer of small amorphous particles that covered the entire carbon film surface. Samples were stained with 2% uranyl acetate. Scale bars = 100 nm.

4.3.6 Immunogold labelling using recombinant anti-PrP Fab 69 and PrP^{Sc} – Fab G1

To ascertain the nature of the structurally indistinct particles and the long filamentous fibrils observed in the GSS-A117V week 4 sample, I performed immunogold labelling experiments with our recombinantly produced Fab fragments; Fab 69 (detailed description in chapter 2) that recognizes an epitope at the truncated N-terminus within residues 87 and 98 of the 7 kDa fragment at the charge cluster 2 region (Figure 4-8) and Fab YEG Sc – G1 (Fab G1) that has a discontinuous epitope recognizing residues H111 and D147 in a solenoid structure (Figure 4-9).

In this chapter, I have used PK – digested week 4 GSS-A117V peptide which was refolded in condition C (200mM NaCl + PBS at pH 8.0) to label it with Fab 69 and Fab G1. Using a binary system to detect bound Fab 69 we were able to decorate the small amorphous ~7 kDa aggregates with 5nm gold particles (Figure 4-8.A-C), while a control sample for which the primary Fab was omitted and showed no gold labelling (Figure 4-8.D). Similarly, the 7 kDa amorphous aggregates were recognized by the conformational antibody, Fab G1 that recognizes native PrP^{Sc} only (Figure 4-9.A-B). As previously described, the long filamentous fibrils observed suggesting a stacked-sheet PIRIBS-like structure appear to be indeed a PIRIBS structure as they were not decorated by our Fab G1 due to the loss of epitope in this particular fold (Figure 4-9.D). The amyloid fibrils and aggregates in the control (no primary Fab G1) remained undecorated (Figure 4-9.D).



PK digested

GSS^{A117V} Condition C pH 8.0 labelled with Fab 69

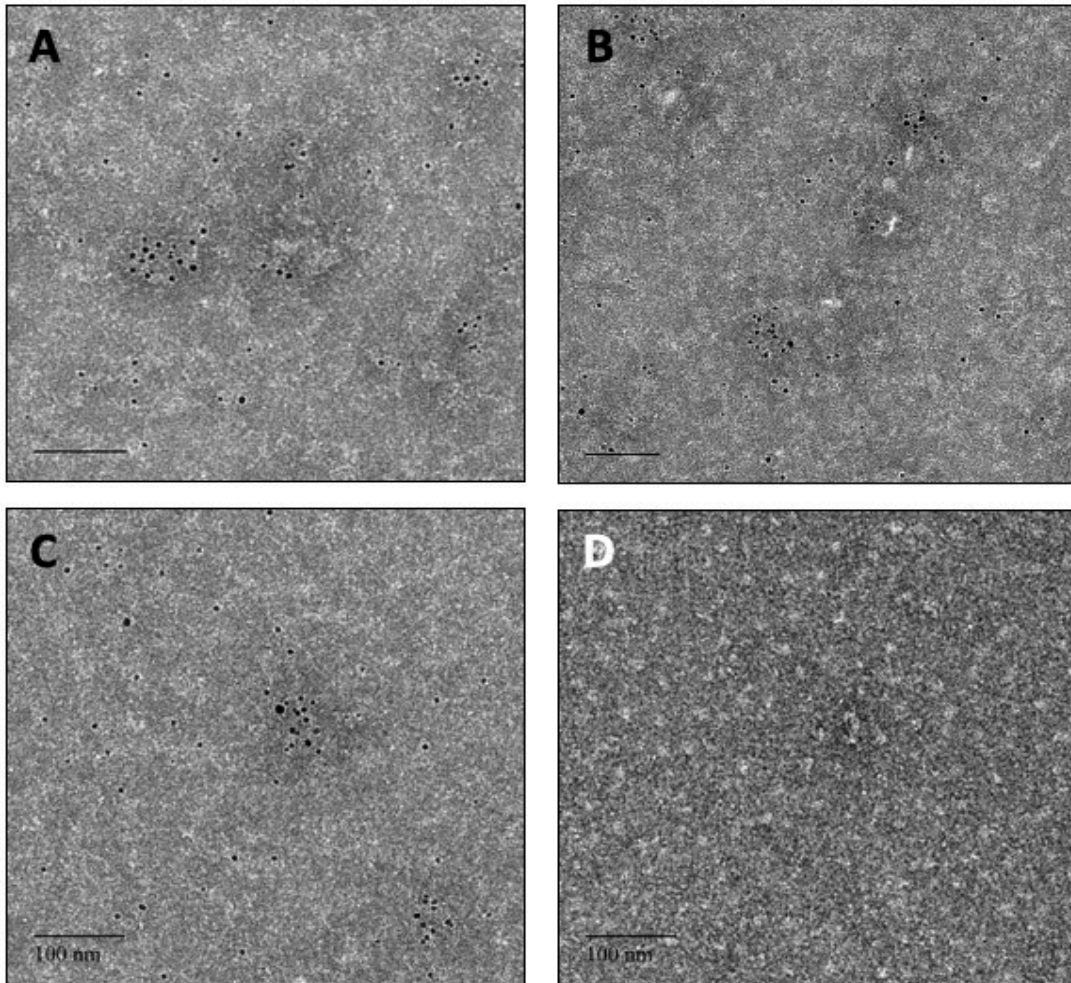
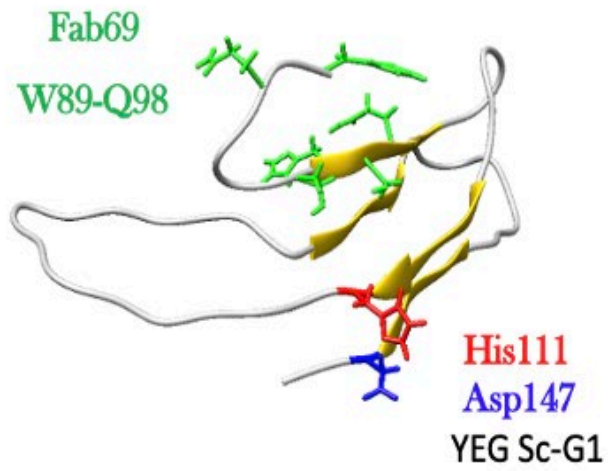


Figure 4-8: Immunogold labelling of week 4 synthetic GSS-A117V sample using Fab 69.

The week 4 aggregated synthetic GSS-A117V reconstituted in sodium phosphate buffer with 200mM NaCl at pH 8.0 was used for immunogold labelling experiments with an anti-PrP Fab 69 which recognizes an epitope between residues 87 and 98 at the CC2 region of the human prion protein. **(A-C)** The small amorphous particles were decorated with many 5nm gold particles, while **(D)** a sample that was treated identically except for the omission of the primary Fab 69 showed no specific gold labelling. Scale bar = 100nm.



PK digested

GSS^{A117V} Condition C pH 8.0 labelled with Fab G1 (Fab YEG Sc-G1)

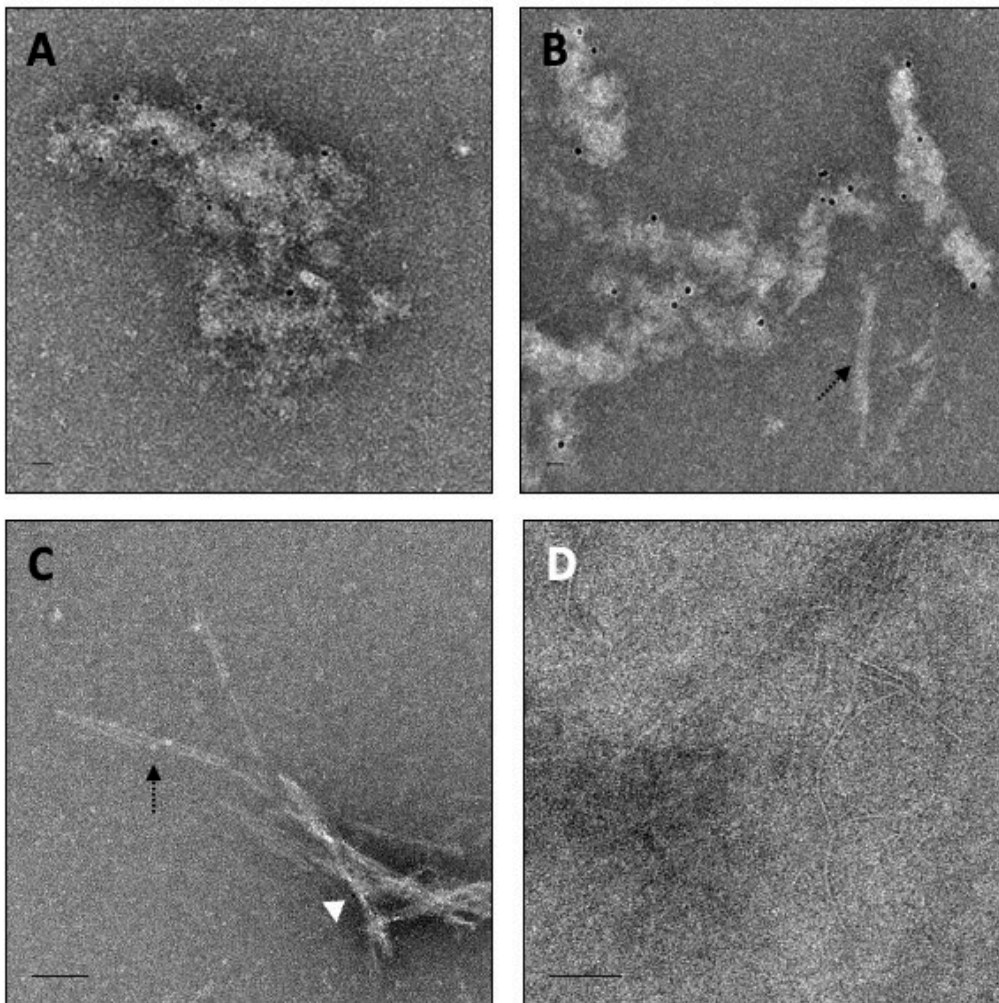


Figure 4-9: Immunogold labelling of week 4 synthetic GSS^{A117V} sample using Fab G1.

The week 4 aggregated synthetic GSS-A117V reconstituted in sodium phosphate buffer with 200mM NaCl at pH 8.0 was used for immunogold labelling experiments with an anti-PrP^{Sc} Fab G1 which recognizes a discontinuous epitope on native PrP^{Sc} only. (A-B) The small amorphous particles and large aggregated clumps were decorated with many 5nm gold particles, while (C) amyloid fibrils suggesting a PIRIBS like fold (black dashed arrows) were not labelled with Fab G1 but small amorphous particle (white arrowhead) was detected by Fab G1 coupled with 5nm gold particle (D) a sample that was treated identically except for the omission of the primary Fab G1 showed no specific gold labelling. Scale bar = 100nm.

4.3.7 GSS-A117V peptide promotes the formation of protease-resistant PrP at week 4

The outcome of recent experiments from brain-derived GSS-A117V sample strongly suggested that the 7 kDa PrP^{res} aggregates that remained after PK digestion which is known to cleave both the N- and C-termini, are indeed responsible for the infectivity and exhibit strain features of GSS-A117V (Vanni et al., 2020). Knowing that short synthetic PrP peptides can interact and induce conformational changes, we asked if a 61-residue synthetic peptide corresponding to GSS-A117 mutation spanning residues 89-149 could become protease resistant after incubation in eight different biochemical conditions. After the β -sheet formation of the GSS-A117V peptide at week 4 in different biochemical conditions (A-H) at pH 5.0 and pH 8.0, we found it to be partially protease-resistant to PK digestion (Figure 4-10. C-D), whereas the random coil linear peptide at week 0 was completely degraded upon PK digestion (Figure 4-10. A-B). Faint multimers of PrP^{res} fragments of ~14 kDa and ~21 kDa share the same antibody reactivity as the ~7 kDa band when immunoblotted with mAb 3F4 and likely represent its covalently linked multimers as reported in previous studies (Cracco et al., 2019; Vanni et al., 2020).

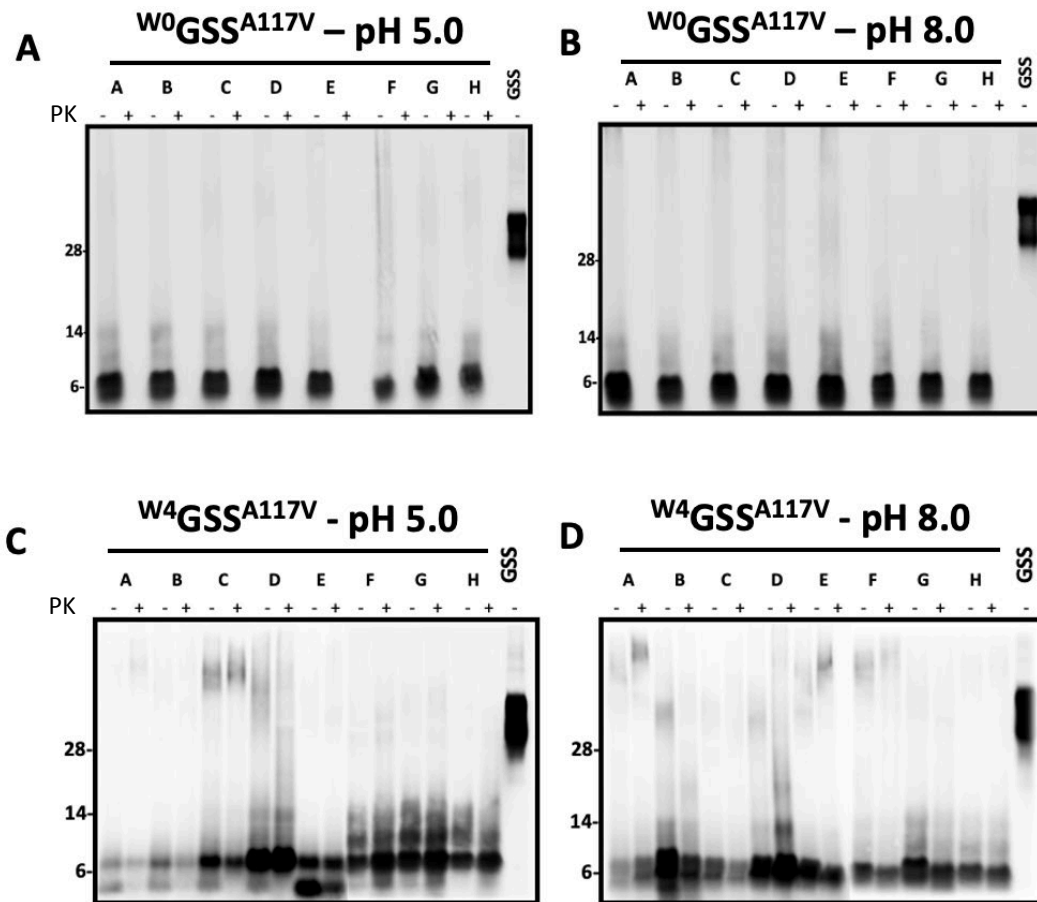


Figure 4-10: Comparison of ~6.6 kDa PrP^{res} band from synthetic GSS-A117V peptide at week 4 aggregated sample versus linear peptide at week 0.

Total PrP and PrP^{res} of synthetic GSSA117V peptide at week 0 and week 4 and (A, C) pH 5.0 and (B, D) 8.0 were analyzed by western blot using monoclonal antibody 3F4 directed to the central region of human PrP. Untreated human GSS-A117V brain homogenate was used as a positive control (shown on the last lane of each blot). The PK-treated GSS-A117V fragment was characterized by ~7 kDa band PrP^{res} devoid of N- and C-terminus of the protein. Multimers of 7 kDa PrP^{res} at higher molecular weight bands of ~14 and ~21 kDa bands were also recognized by the 3F4 antibody. Week 0 GSS-A117V (A-B) peptide showed to have no resistance after PK digestion as it was not recognized by the 3F4 antibody suggesting a linear peptide which did not adopt the suggestive 2R β S fold compared to week 4 GSS-A117V (C-D) peptide showed to have varying PK resistance in eight different biochemical conditions.

4.3.8 Aggregated GSS-A117V binds ThT amyloid dye

To test whether the linear unstructured synthetic GSS-A117V peptide adopted a β -structure consisting of 2R β S or amyloid fibrils we tested its binding to Thioflavin T (ThT). The linear peptide represented random coil structure at week 0 when refold in its indicated biochemical conditions did not bind ThT while the GSS-A117V crude brain homogenate at 2.5 μ M showed a saturated ThT fluorescence reading higher than week 0 samples (Figure 4-11.A-B).

Comparatively, aggregated week 4 GSS-A117V samples in specific biochemical conditions showed a lag phase increment in ThT binding suggestive of a more intense beta sheet structure to that of an amyloid fibril formation and drifting away from the β -oligomeric (2R β S) fold as observed in condition H at pH 5.0 and condition F at pH 8.0 (Figure 4-11. C-D). The length of lag phase varied substantially with a salt concentration in the presence of 3M urea when the GSS-A117V peptide is reconstituted in PBS, pH 8.0. Combining our data from electron micrographs and GSS time-dependent folding immunoassay suggests that the length of the lag phase is also dependent on the heterogeneity of ultrastructure. Condition F at pH 8.0 consists of a large amounts of β -oligomers and stacked beta-sheet amyloid fibrils, indicating that there is a drift in beta structure occurring to form stable amyloid fibrils. Comparatively, conditions with large amounts of beta oligomers at week 4 have a higher ThT fluorescence at 0 h and remain as stable oligomers throughout the time course (0-60 h).

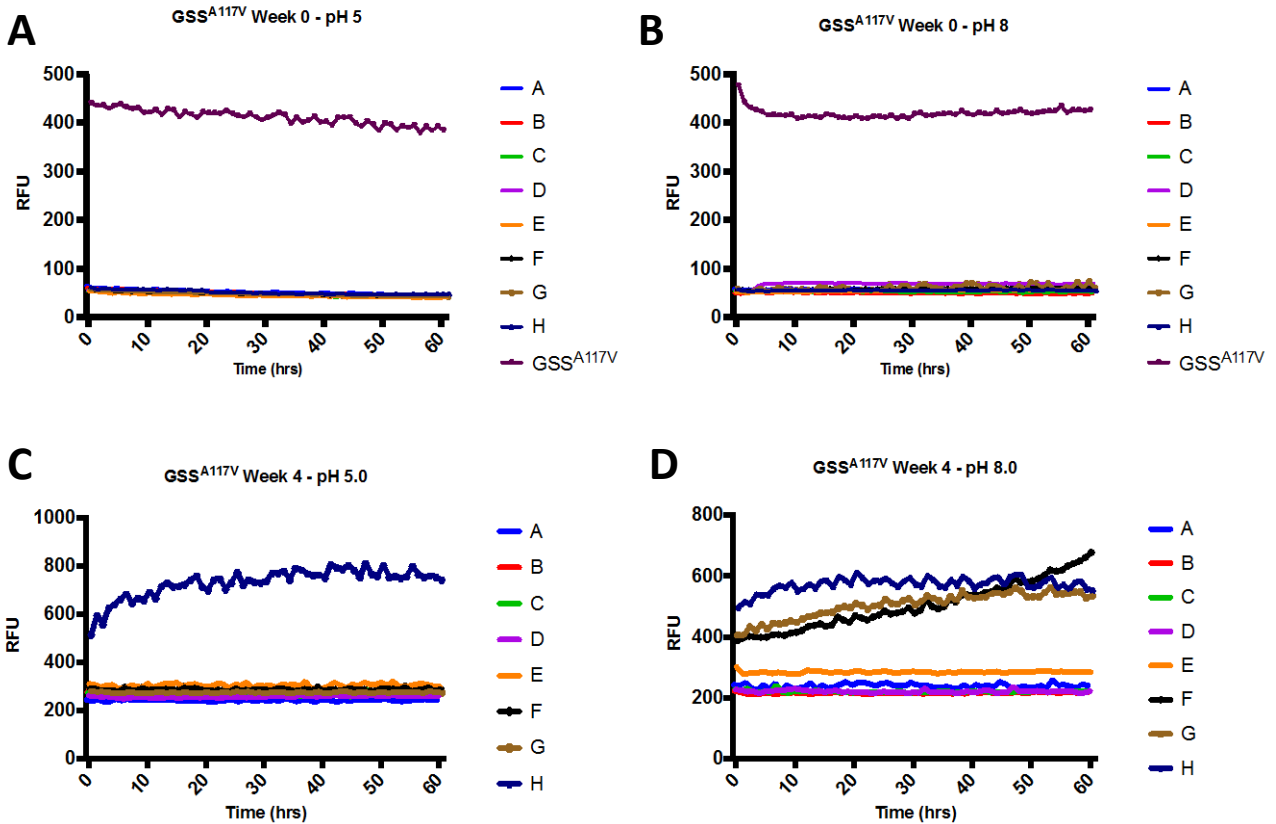


Figure 4-11: ThT fluorescence of the linear and aggregated synthetic GSS-A117V peptide in various biochemical conditions.

ThT fluorescence at the aggregated state and linear state of synthetic GSS-A117V peptide was measured at varying salt concentrations and in the absence and presence of 3M urea for conditions A-H over the course of 60 hours. **(A-B)** ThT fluorescence of linear GSS-A117V peptide at week 0 showed to have almost baseline reading compared to the positive control, human brain GSS-A117V sample. **(C-D)** Showed varied ThT fluorescence readings were observed based on the aggregated structures at their specific biochemical conditions for the week 4 GSS-A117V sample. The final concentration for all peptide conditions was $2.5\mu\text{M}$ and ThT was $10\mu\text{M}$. ThT fluorescence readings are average of triplicate measurements subtracted from the sample with no peptide.

4.3.9 Circular Dichroism spectroscopy

To better understand the structural architecture which transforms the linear peptide into beta-oligomers and eventually forming stacked beta-sheet amyloid fibrils, we performed CD spectroscopy of GSS-A117V peptide reconstituted at a final concentration of 0.1 mg/ml in either 10 mM sodium acetate pH 5 (Figure 4-12), or sodium phosphate pH 8.0 (Figure 4-13). Peptide at week 0 (blue bands) exhibited largely random coil structures with characteristic negative CD band at ~190 nm. After 4 weeks of incubation in different biochemical conditions with an increase in salt concentration (0 mM – 400 mM NaCl) and in the absence of 3M urea, samples showed characteristic β -sheet conformation (red bands) with a minima around 220 nm (Figure 4-12.A-D) and minima around 218 nm (Figure 4-13. A-D) suggesting the presence of β -sheet rich structures (Goto et al., 2018; H. Zhang et al., 1995). Although the nature of the secondary β -structure remains the same but the beta-sheet content increases with salt concentration as revealed by the deconvolution of CD spectra. The effect of 3M urea with an increase in salt concentration of week 4 samples was clearly observed. Week 4 GSS-A117V peptides containing 3M urea displayed spectra suggestive of proteins in a denatured but constrained state lacking long-range order (Figure 4-12.E-H and Figure 4-13.E-H). Urea is commonly used to denature and induce conformational changes in protein secondary and tertiary structure (Frank, Clore, & Gronenborn, 1995). However, the CD spectrum in the presence of urea exhibits most negative ellipticity at the lower wavelength side (195-205 nm) which is consistent with the protein unfolding to a random coil structure (Greenfield, 2006; Kelly, Jess, & Price, 2005).

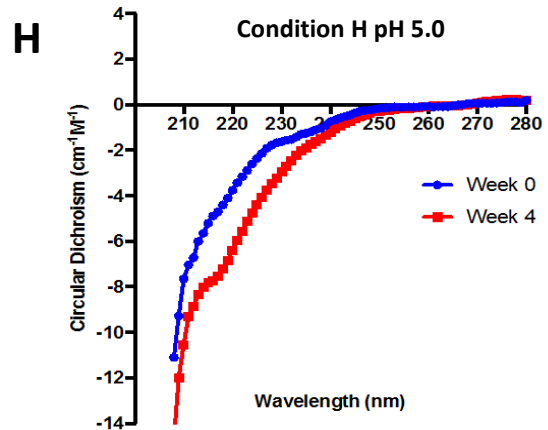
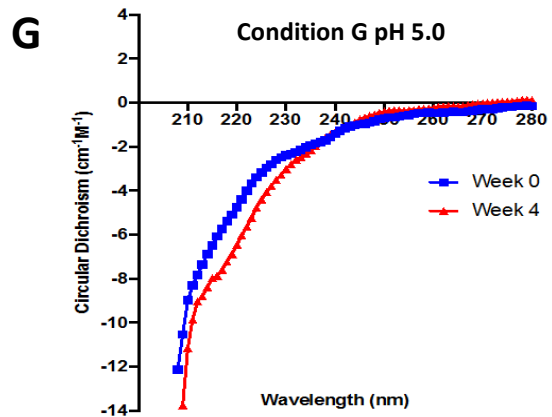
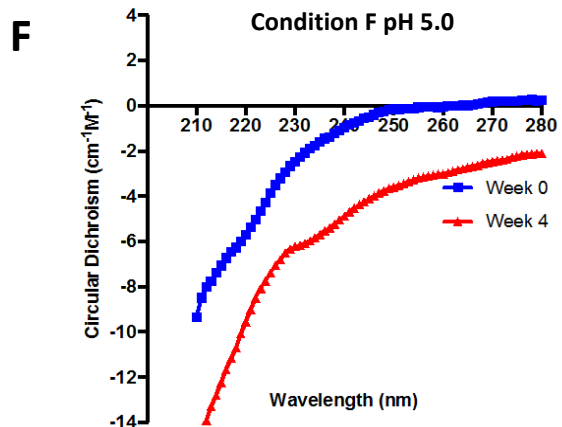
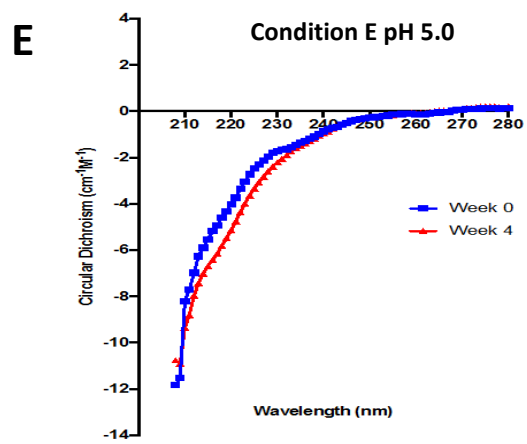
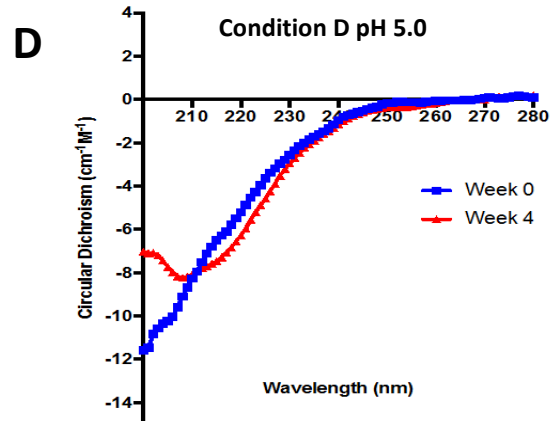
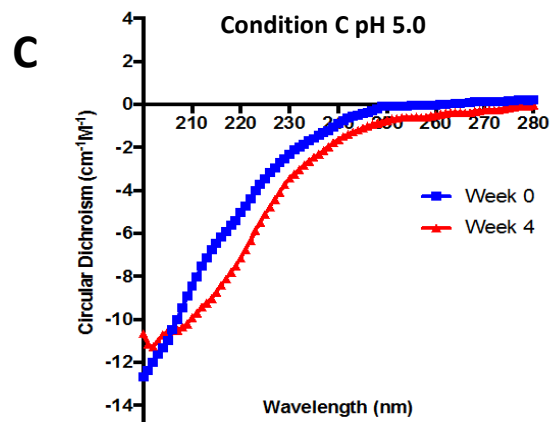
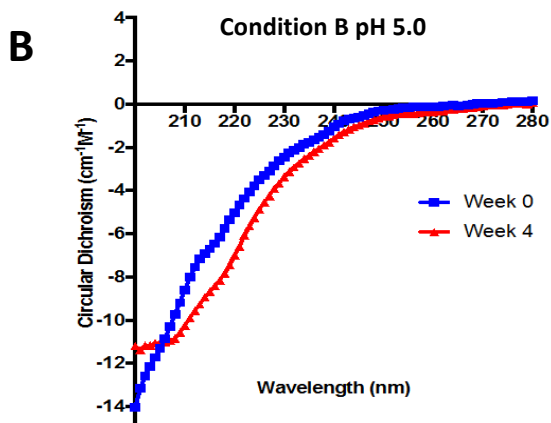
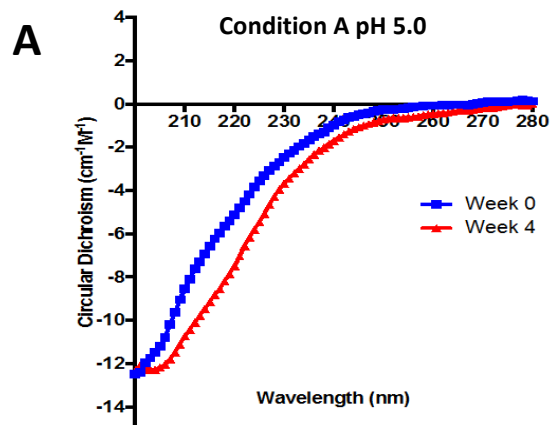


Figure 4-12: Circular Dichroism spectra of week 0 linear and week 4 aggregated synthetic GSS-A117V at pH 5.0.

CD spectra showing change in structural fold of synthetic GSS-A117V peptide between week 0 (blue curves) and week 4 (red curves) at the indicated biochemical conditions **(A)** 0mM NaCl **(B)** 100mM NaCl **(C)** 200mM NaCl **(D)** 400mM NaCl **(E)** 0mM NaCl + 3M urea **(F)** 100mM NaCl + 3M urea **(G)** 200mM NaCl + 3M urea **(H)** 400mM + 3M urea. All these conditions had the synthetic peptide reconstituted in sodium acetate buffer at pH 5.0.

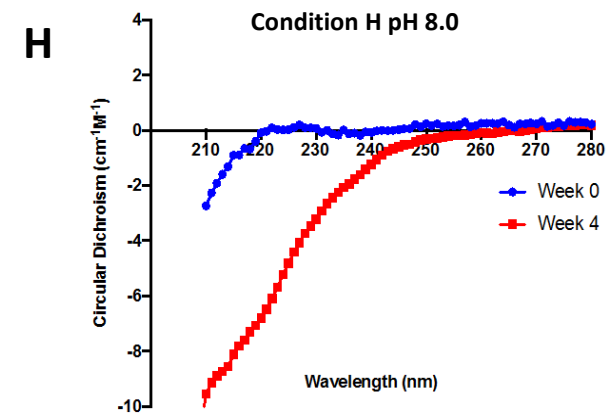
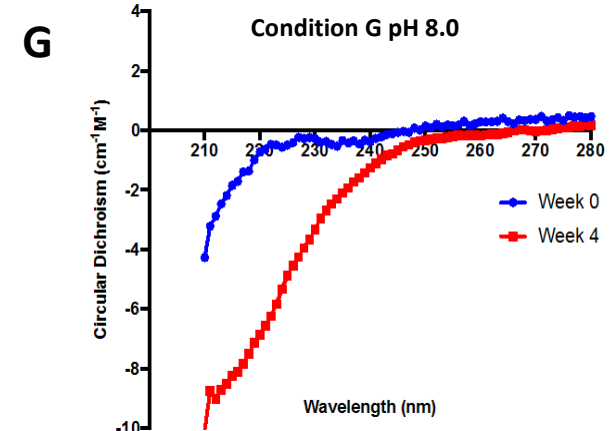
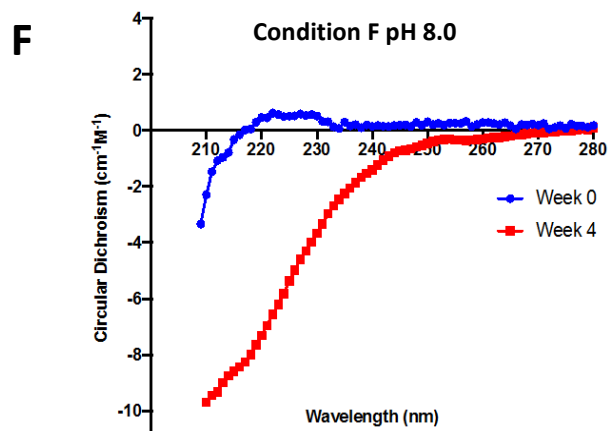
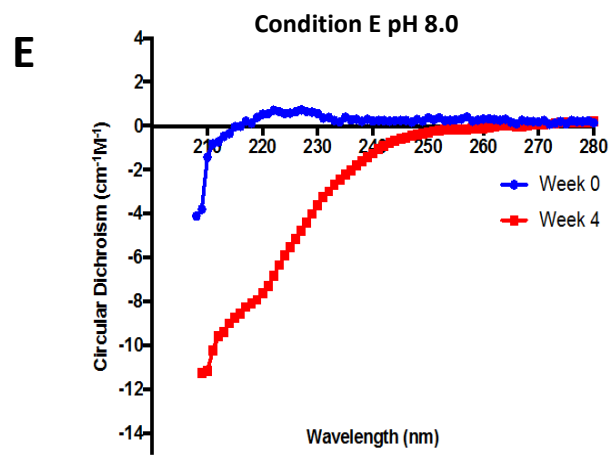
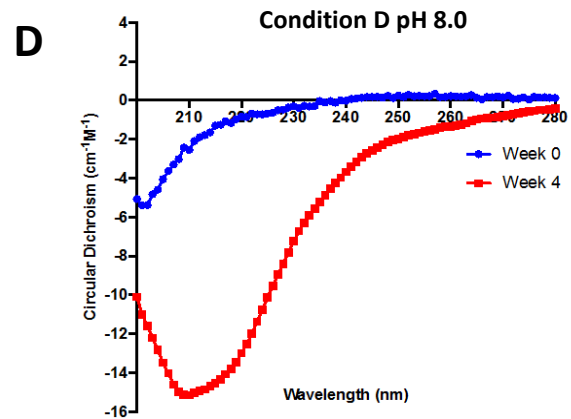
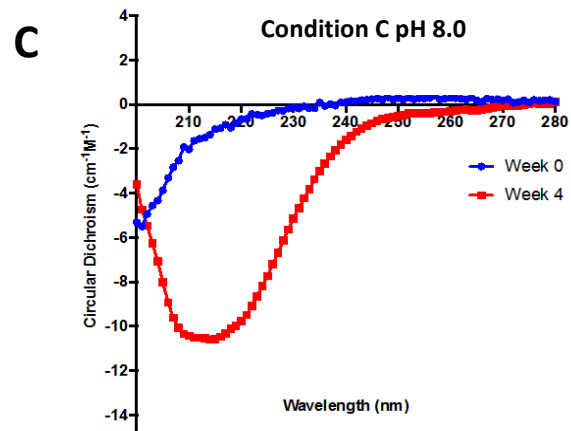
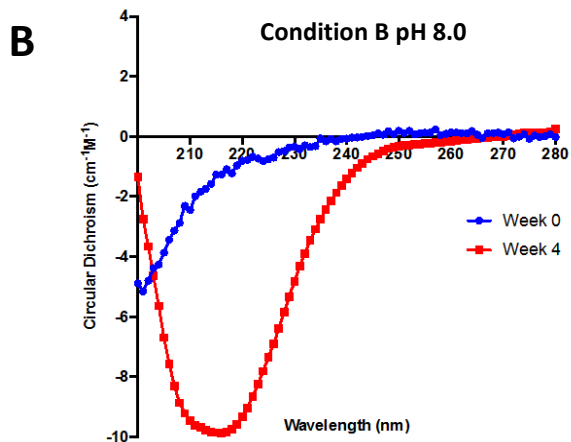
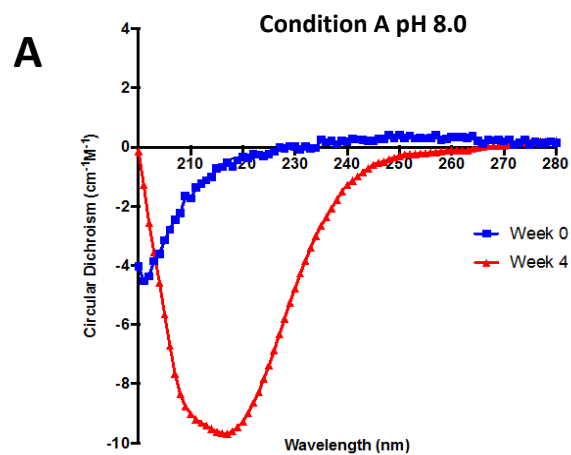


Figure 4-13: Circular Dichroism spectra of week 0 linear and week 4 aggregated synthetic GSS-A117V at pH 8.0.

CD spectra showing change in structural fold of synthetic GSS-A117V peptide between week 0 (blue curves) consisting of linear and unstructured peptide following aggregation to week 4 (red curves) suggesting β -sheet content at the indicated biochemical conditions **(A)** 0mM NaCl **(B)** 100mM NaCl **(C)** 200mM NaCl **(D)** 400mM NaCl **(E)** 0mM NaCl + 3M urea **(F)** 100mM NaCl + 3M urea **(G)** 200mM NaCl + 3M urea **(H)** 400mM + 3M urea. All these conditions had the synthetic peptide reconstituted in sodium phosphate buffer at pH 8.0.

4.3.10 Bioassays

Our bioassay experiments in voles are on-going and being performed by our collaborators at the Nonno lab in Rome, Italy at the Istituto Superiore di Sanita as previously described (Vanni et al., 2020). Since condition H of GSS-A117V sample at pH 5.0 and pH 8.0 contain 3M urea, toxicity assay was performed and showed no apparent toxicity to diluted 3M urea samples in voles.

To investigate if the synthetic GSS-A117V peptide can induce conformational-dependent infectivity, we selected two biochemical conditions (condition A and H) from pH 5.0 and pH 8.0 for our bioassay study in voles. The criteria used to select which inocula to employ was based on the OD 450 measurements at week 4 (Figure 4-3.A-H), ultrastructure observed by negative stain (Figure 4-6 and 4-7), PK resistance (Figure 4-10.A-D), and molecular dynamic simulation (Figure 4-14. A-H). Control inocula were GSS-A117V peptide reconstituted at week 0 of the same condition A and H at pH 5.0 and 8.0.

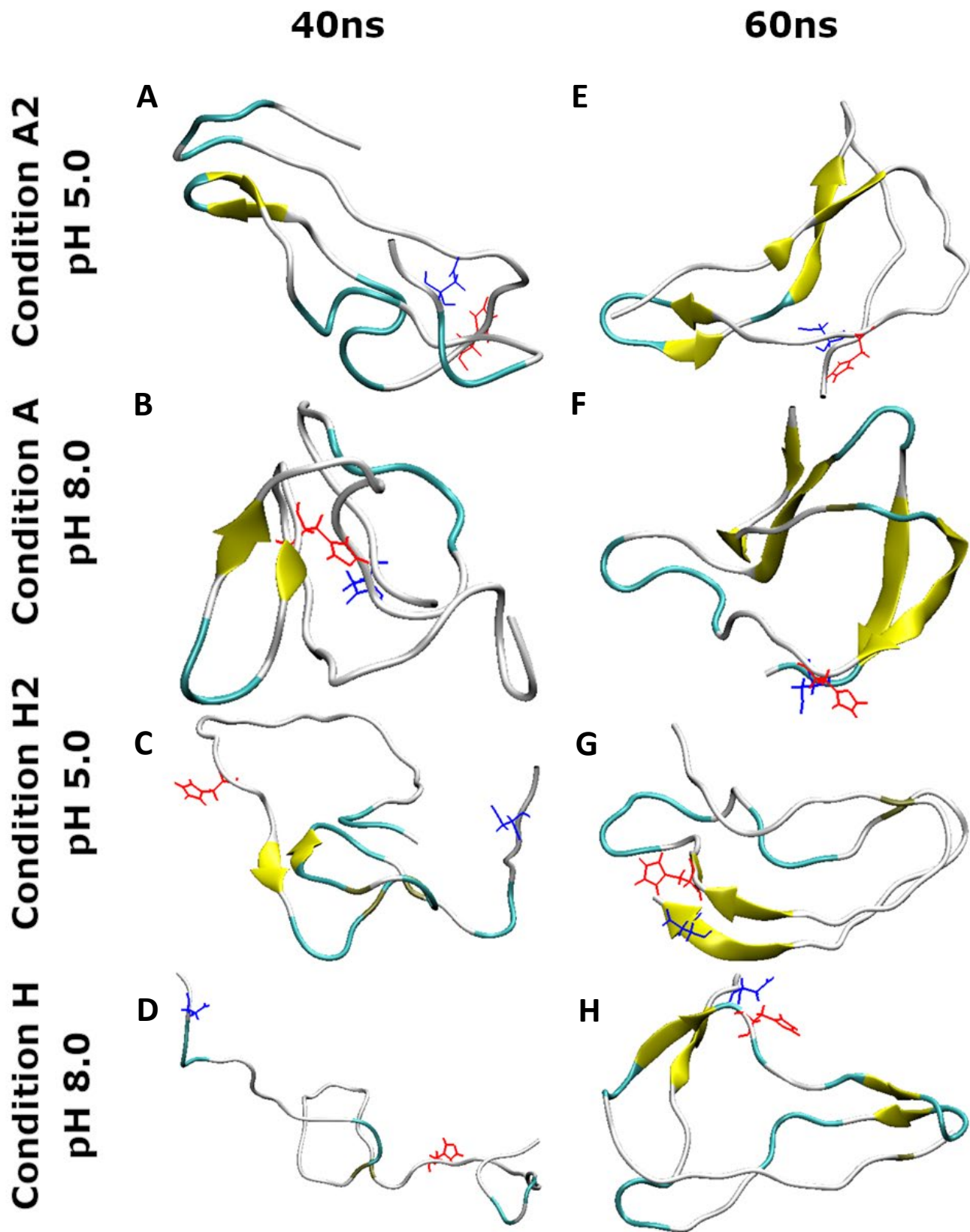


Figure 4-14: Molecular dynamics simulations of human PrP 90-150 stabilized for 40 ns and 60 ns.

Stabilized representative conformation of 2-rung beta solenoid (2R β S) systems encompassing residue 90 – 150 of human GSS-A117V prion protein simulated in selected solvent conditions A (0mM NaCl) and H (400mM NaCl + 3M urea) at pH 5.0 and 8.0. These conditions were of particular interest as they were selected for our bioassays in bank voles. β -strands are shown with yellow ribbons, turns and random coils with grey. At 40 ns MD run, (**A, C**) Random coiled structures of GSS-A117V at pH 5.0 (**A**) simulated in condition A and (**C**) simulated in condition H started to form slow β -rungs. (**B, E**) Random coiled structures of GSS-A117V at pH 8.0 (**B**) simulated in condition A and (**E**) simulated in condition H in the presence of 3M urea remained unstructured at 40 ns. (**E-H**) By 60 ns stable β -strands were preserved with H111 and D147 coming near to orient and forming a pair-wise epitope. These molecular dynamic simulation results validate our earlier ELISA readings on the time-dependent folding of synthetic GSS-A117V peptide. Molecular dynamic simulations were performed by Dr. Lyudmyla Dorosh.

4.4 DISCUSSION

Experimental evidence on biochemical, structural and infectivity investigation on a brain-derived GSS-A117V mutation case have recently reported that amyloid plaque deposits in the brain of GSS patients (Tagliavini et al., 2001) are primarily composed of oligomeric PrP^{Sc} (Vanni et al., 2020) with a low molecular weight PrP fragments derived from the central region of the human PrP and ragged N- and C- termini (Cracco et al., 2019; Pirisinu et al., 2016). It was reported that the 7 kDa, PK resistant core encompassing residues ~90-150 PrP fragment have shown extremely high infectivity titre when inoculated in bank voles (Vanni et al., 2020). Our investigations offer an alternate approach to the study of prions by employing a synthetic GSS-A117V mutation peptide and conformation-dependent PrP^{Sc}-antibody to shed light into the conformational transition in the formation of β -oligomers and amyloid fibrils from a linear unstructured GSS peptide. We show conformational-dependent biochemical alterations and possibly evaluate if these adopted folds induce infectivity when inoculated in bank voles.

In this study, I show how synthetic GSS-A117V linear peptide composed of residues 89-149 adopts a putative two-rung beta solenoid structure in the form of large amorphous aggregates, leading to the formation of energetically stable stacked beta-sheets amyloid fibrils as shown by negative stain electron microscopy. In comparison to week 0 linear peptide by CD spectra, we observed no adoption of beta strands but rather the linear GSS-A117V peptide remained unstructured. The fold changes were analyzed using our PrP^{Sc} – specific antibody, YEG Sc – G1 through an indirect – ELISA assay. Previous studies on minimal sequence PrP peptides have shown PrP to interact and induce multiple conformational changes, such as irregular coiled and

β -sheet rich conformations in different biochemical conditions and acquire pathogenesis or transmission (Nguyen, Baldwin, Cohen, & Prusiner, 1995; H. Zhang et al., 1995). These peptides have shown to be protease-resistant (Prusiner et al., 1983), β -sheet rich in structures (Gasset et al., 1993) and some have corresponded to human-disease causing variants, producing neurodegeneration in Tg-mice (Hegde et al., 1998).

Our findings were in strong agreement with previous structural studies on short PrP peptides corresponding to the amyloidogenic regions, suggesting that the presence of salt (0 – 400mM) is important in promoting intermolecular β -structures in the GSS-A117V peptide (Goto et al., 2018; H. Zhang et al., 1995). The salt-dependent formation of fibrils showed clear optimum, revealing a competition of fibril formation and large amorphous aggregates by 4 weeks. A similar study on Syrian hamster peptide corresponding to residue 90-145 displays a random coil structure when refolded in water and adopts a beta-sheet conformation by 2-3 weeks in the presence of 150 mM NaCl (Kaneko et al., 1995).

In addition, the formation of oligomers is favored at pH below 5.5, whereas optimal pH for the conversion into amyloid fibrils is between 5.0 and 7.2 (Baskakov & Bocharova, 2005).

Interestingly, both abnormal isoforms, the oligomers and the amyloid form, coexist at pH 5.0-8.0 (Figures. 4-6 and 4-7). These pH values are close to the slightly acidic environment of lysosomes and endosome, where the conformational transition into pathological PrP^{Sc} is believed to occur (Arnold et al., 1995; McKinley et al., 1991). Our present findings indicate that changes in environmental conditions may have important implications in determining the structural fold adopted during the misfolding pathways of PrP *in vivo* and the formation of distinct abnormal isoforms.

While these structural properties of synthetic GSS-A117V peptide resemble those of PrP^{Sc}, our peptide also displayed similar biochemical features to partially proteinase K resistant PrP after adopting a β -sheet fold at around week 4, while the linear and random coil fold at week 0 was completely degraded (Figure 4-10). After the proteinase K digestion, the GSS-A117V peptide of residues 89-149 retained its ~6.6 kDa PrP^{res} fragment and its resistance differed according to the biochemical conditions (Conditions A-H). This is analogous to the proteinase K digestion of purified brain-derived GSS-A117V ~7 kDa PrP resistant β -core within residues 89-149 (Figure 4-1.A) (Vanni et al., 2020). The residues encompassing the protease-resistant β -core of GSS-A117V are known to be the most amyloidogenic and have been shown to be infectious in-vivo. Whether this fragment can be converted into an infectious form in-vitro remains to be established (experiments in progress). The protease-resistant β -core adopted by the synthetic GSS-A117V peptide was verified with an anti-PrP Fab 69 antibody which has a binding specificity within residues 87-98 of the human prion protein, demonstrating that the PK-resistant core of ~ 6.6 kDa is indeed comprised of residues 89-149.

The 3D structure of the infectious PrP^{Sc} conformer is a key issue in the prion field, but there are significant challenges to overcome due to the highly aggregated, glycosylated, and GPI-anchored traditional PrP^{Sc} conformers and the difficulty in creating highly infectious synthetic prions. This emphasizes the use of synthetic PrP peptides for biophysical and biochemical studies whose sequence specificity has shown amyloidogenic characteristics. A four-rung β -solenoid structure was identified as the essential component of the infectious conformer by X-ray fiber diffraction of PrP^{Sc} and PrP^{res} fibrils as well as cryo-electron microscopy studies of GPI-anchorless PrP^{res} fibrils (Vazquez-Fernandez et al., 2016; Wille, Bian, et al., 2009). These results suggested that the four-rung β -solenoid structure plays a more extensive function in the autocatalytic

propagation process that underlies prions (Kamali-Jamil et al., 2021; H. Wille & J. Requena, 2018). However, the residues ~89-149 known for the infectivity of GSS-A117V are too small to account for a four-rung β -solenoid structure in the 7 kDa PrP aggregates, which could entail a two-rung beta-solenoid configuration, a structure in alignment with our data from the molecular dynamic simulation. Comparatively, X-ray fiber diffraction studies on synthetic peptide PrP (89-143) corresponding to GSS-P102L mutation support both a two-rung beta solenoidal architecture and a stacked-sheet structure depending on the biochemical conditions of the amyloid formation (Wan et al., 2015). Lastly, solid-state NMR studies on infectious PrP23-144 fibrils showed that its β -core region composed of residues 112-139 was characterized by a parallel in-register beta-sheet structure which is in alignment with the structural studies performed on synthetic PrP23-144, a protein matching the sequence of C-terminally truncated PrP harboured in GSS^{Y145Stop} (Choi et al., 2016). To validate this reasoning with the amyloid morphologies adopted by the synthetic GSS-A117V peptide, we immunolabelled PK-resistant amorphous aggregates and fibrillar GSS-A117V peptide with YEG Sc – G1 antibody, which has displayed a conformational epitope with His 111 and Asp 147 as the pivotal residues in antigen-antibody recognition decorated the amorphous aggregates corresponding to the 2R β S model (Spagnolli et al., 2019) but did not label the fibrillar amyloid structure as it the orientation of His 111 and Asp 147 epitope is buried in brain-derived GSS-F198S PIRIBS structure (Hallinan et al., 2022) or not located in a vertical pair conformation in hamster 263K PIRIBS structure (Kraus et al., 2021).

Despite the fact that purified amyloid proteins typically come in the form of massive aggregates with a fibrillar quaternary structure, there have been reports of nonfibrillar, covalently cross-linked oligomers for a number of amyloid proteins linked to neurodegeneration, including A β ,

tau, and α -synuclein (Cracco et al., 2019; Haass & Selkoe, 2007; Kaye & Lasagna-Reeves, 2013). These oligomers are likely the most toxic species in Alzheimer's, Parkinson's, and other neurodegenerative illnesses, according to mounting evidence over the past two decades (Forloni, Artuso, La Vitola, & Balducci, 2016; Shafiei, Guerrero-Munoz, & Castillo-Carranza, 2017).

There is an ongoing debate over the structural relationship between the small-sized infectious particles in brain homogenate with that of the larger purified fibrils in the presence of detergent. Ilaria and colleagues showed purified GSS-A117V prion particles are non-fibrillar in nature and have highly infectious titres when inoculated into voles which is in agreement with the bioassay performed by Kamali-Jamil and colleagues on purified L-type BSE prions assembled into rod-like assemblies with a common hierarchical assembly consisting of twisted pairs of long protofilament fibrils with a repeating sub-structure (Kamali-Jamil et al., 2021). These observations imply that a fibrillar quaternary structure is not an absolute requirement for prion infectivity, as had been seen with the complete lack of fibrillar assemblies in RML-infected FVB mice (Godsave et al., 2008; Levine et al., 2015). The ability to unequivocally correlate infectivity with a known 3D structure is the necessary basis for understanding the molecular underpinnings of prion infectivity.

Our findings show that synthetic GSS-A117V mutation peptide can adopt an isoform rich in β -sheet structure, composed of small β -oligomeric aggregates and straight protofilament amyloid fibrils by modifying the surrounding chemical environment in-vitro. The folds were evaluated using our unique antibody that recognizes a conformational epitope which fits the PrP^{Sc} oligomeric fold, suggestive of a two-rung beta solenoid structure for 6.6 kDa PrP^{res} through a GSS – fold dependent immunoassay. These results emphasize that the prion misfolding pathway consists of many different β -folds which are then propagated to form energetically stable

amyloid fibril structures consisting of a stacked beta-sheet confirmation. This aligns with the data shown by the X-ray fibril diffraction of consisting 4R β S structure (Kamali-Jamil et al., 2021; Vazquez-Fernandez et al., 2016; Wille, Bian, et al., 2009) and recent cryo-EM structure revealing PIRIBS structure of the infectious prions (Artikis et al., 2022; Hallinan et al., 2022; Kraus et al., 2021). This study also provides a new avenue to study which β -fold plays a critical role in prion infectivity from our bioassays.

Chapter 5: Conclusion and Future Directions

5.1 The role of antibodies in understanding the prion protein

Antibodies are now employed in a variety of applications including research, diagnosis, and therapy (Vidarsson et al., 2014). They are commonly utilized in Western blot, immunogold labelling, immunocytochemistry, or flow cytometry assays. Recombinant antibodies are used to diagnose various pathogens or toxins. In the past decade, various antibodies have been utilized in treatment modalities for a variety of disorders including Prion diseases, Alzheimer's disease and Parkinson's disease (Ma & Ma, 2020).

Human prion diseases are invariably fatal and poorly understood at the molecular level with no treatment options currently available (Prusiner, 1998a). It is well established that the conversion of cellular prion protein (PrP^C) into a toxic, self-replicating form (scrapie, PrP^{Sc}) results in an aggregate formation (Aguzzi & Calella, 2009). However, it is unclear how these aggregates cause toxicity. After decades of intensive research, much is known about the self-templated prion conversion process, a phenomenon that is now understood to be active in other more common neurodegenerative disorders such as Alzheimer's disease, and Parkinson's disease (Mercer & Harris, 2022). Immuno-based approaches are emerging as important therapeutic strategies against these pathologies (Brazier, Mot, White, & Collins, 2013). Generating antibodies against such proteins may be beneficial by opsonizing pathological aggregates and mediating their degradation by phagocytic cells (Schenk et al., 1995). There is ample evidence that both active and passive antibody transfer can actively clear pathological aggregates in preclinical animal models and, to some extent, in affected humans (Mead et al., 2022).

For the longest time, PrP^C has been a therapeutic target for eradicating further misfolding to infectious isomer PrP^{Sc} and accumulation of PrP^{Sc}. Most of the antibodies available in the prion field have been shown to have specificity and affinity towards PrP^C and PrP^{Sc}. Many prion researchers have made efforts to generate PrP^{Sc}-specific antibodies however, in part due to a lack of high-resolution structures of the infectious fibrils until recently, there has been no true PrP^{Sc}-specific antibody. Those claimed PrP^{Sc}-specific antibodies have linear epitopes and have been shown to recognize PrP^{Sc} under denaturing conditions or have shown to recognize the infected as well as uninfected recombinant aggregates (Biasini et al., 2008).

Throughout this thesis, I have outlined the production, engineering and utility of a myriad of recombinant antibody fragments as tools for understanding prion diseases. I have discussed two major groups found in my antibody toolbox, anti-PrP Fabs that recognize linear epitopes found on both PrP^C and PrP^{Sc} generated by phage display technology (Senatore et al., 2020). The other set of antibodies are PrP^{Sc}-specific antibody fragments generated from hybridoma clones that recognize the infectious prion protein only (Rathod et al., manuscript in preparation). I have shown the utility of these various antibody fragments based on their select epitopes and specificity for structural analyses, and direct detection of infectious prions.

5.2 Recombinant anti-PrP antibody fragments

Usually, full-length antibodies such as IgG and IgM (Figure. 1-7.A-B) are ideal as research tools, however, the performance of certain assays is enhanced by using antibody fragments such as Fabs (Vidarsson et al., 2014) (Figure. 1-7.C). The monovalent antigen-binding fragment (Fab) is

composed of a variable heavy chain (VH) and variable light chain (VL) regions and regions of a constant heavy chain (CH) and constant light chain (CL), which makes them smaller in size (~50kDa) than the conventional IgG antibody (~150kDa). Due to their physical characteristic of being smaller in size, active antibody fragments, are able to overcome the difficulty of permeating cell membranes and complex structures, which is limited for a full-length antibody (Holliger & Hudson, 2005).

Our Collaborator, Dr. Adriano Aguzzi showed that antibodies against the so-called globular domain of Prion Protein (PrP) can cause PrP-dependent neurotoxicity (Sonati et al., 2013); however, antibodies against the flexible tail of PrP do not do this such as POM2 (Figure. 1-8), and hence should be favored for therapy (Bardelli et al., 2018). These findings led them to pan a synthetic human antibody phage display library to explore the presence of PrP-binding antibody fragments (Fabs) (Frenzel et al., 2016). Senatore and colleagues from the Aguzzi lab were able to identify >6000 PrP-binding antibodies in a synthetic human Fab phage library, and generate 36 highly specific, highly affine humanized small antibody derivatives that target the whole surface of the prion protein, using the new technologies that combine conventional phage display methodology with next-generation sequencing (NGS) (Senatore et al., 2020). Chapter 2 of this thesis shows the pipeline of producing recombinant anti-PrP antibody fragments and the same protocol was used to express and purify all the recombinant antibody fragments discussed in this dissertation. I demonstrated how these antibody fragment clones can be successfully expressed and purified as a soluble protein in one week under optimum conditions with a good yield in milligram quantities that is cost-effective (Chapters 2 and 3). These anti-PrP antibody fragments were bacterially expressed as Fabs, which are frequently more stable and less susceptible to dimerization than scFv (Arndt et al., 2001). I was able to produce 11 soluble anti-PrP Fabs that

target four major PrP epitopes: the CC1 area (23-50), the OR region (51-90), the CC2 region (91-120), and the GD region (121-230). (Figure 2-1.B). I analyzed the relationship between the anti-PrP Fabs' epitope and its functional activity using various biochemical and biophysical assays. In Chapter 2, I have focused on three linear epitope anti-PrP Fabs; Fab 3, Fab 69 and Fab 29 due to the attractiveness of their epitope targeting the very N-terminus, truncated N-terminus and very C-terminus of the prion protein.

The focus was to use antibody fragments as an alternate approach for structural analyses of infectious prion amyloid aggregates and fibrils through immunogold labelling using the electron microscope. I have shown the utility of these select epitope anti-PrP Fabs to further characterize the morphology of isolated RML, L-type BSE, and CWD fibrils as well as human GSS^{A117V} oligomers (described in chapter 4) via immunogold labelling and electron microscopy (Kamali-Jamil et al., 2021; Vanni et al., 2020). This provided us with information on the orientation of the epitopes in these fibrils and verified that the observed morphologies observed by EM were indeed generated by the polymerization of PrP 27-30, or PrP^{res} monomers in the case of GSS-A117V prion which consists of 7 kDa PK-resistant core (residues 89-149) (Vanni et al., 2020).

5.3 Engineered PrP^{Sc}-specific antibody fragments

As molecular genetics and DNA technology advance, less immunogenic engineered recombinant antibody molecules and their fragments can be produced as the next step in antibody-based treatments for prion diseases (Kim et al., 2005; Morrison et al., 1984). Genetic engineering

techniques have enabled the production of chimeric mouse/human and entirely humanized antibodies (Colcher et al., 1998). Chapter 3 of this dissertation describes the generation of humanized recombinant antibody fragments (Figure. 1-7) in which the complementary determining regions (CDRs) of rodent origin are grafted onto the human antibody framework, effectively maintaining its antigen-binding capacity (Heppner et al., 2001; P. T. Jones et al., 1986; Riechmann et al., 1988). I was able to take advantage of the existing recombinant antibody fragment production method as optimized for anti-PrP Fabs for the expression and purification of the newly engineered antibodies.

Numerous groups as described in Table 3-1 have made efforts in generating PrP^{Sc}-specific antibodies to distinguish PrP^{Sc} from PrP^C. However, a significant number of promising antibodies have shown not to have a discontinuous epitope, that can differentiate the pathogenic (PrP^{Sc}) and the non-pathogenic isoforms in their native form (Biasini et al., 2008). For the first time, I report the generation of recombinant PrP^{Sc}-specific antibody fragments from murine-derived full-length IgG and IgM antibodies. As discussed in Chapter 3, these PrP^{Sc}-specific monoclonal antibodies are an immune response from the “Rationally designed, model-based PrP^{Sc} vaccine” project from the Wille lab (Fang et al., manuscript in preparation). The conformational dependent PrP^{Sc}-specific antibody, namely YEG Sc-G1 has specificity towards the native PrP^{Sc} only when tested against a range of animal and human prion isolates (Figure. 3-1.A-B).

My engineered PrP^{Sc}-specific fluobody, which is a scFv antibody conjugated to an enhanced green fluorescent protein, can function as a tool for molecular detection of aggregates of native PrP^{Sc} only through imaging and diagnostics (Figure. 3.22.C and 3.26.A-C). The fluobody has shown promising preliminary data by specific cell surface labelling of native PrP^{Sc} in RML-

infected CAD5 cells (Figure 3-27.J). This GFP-linked scFv offers a powerful strategy for imaging protein aggregates of various prion strains in living cells or lightly fixed tissues without the need for secondary detection systems.

The epitopes of the mAbs YEG Sc-G1 and YEG Sc-M63 were characterized via a structural epitope mapping and showed that the key residues, H110, D146 and N103, D143 play a pivotal role in the antigen-antibody recognition of these respective antibodies. The epitopes are surface exposed and found in a vertical pair-wise orientation on a 4R β S model of PrP^{Sc} (Figure. 3-33.A)

5.4 Orientation of H110 and D146 in a 4R β S and PIRIBS conformation

Recent cryo-EM structures of brain-derived hamster 263K (Kraus et al., 2021), anchorless RML (Hoyt et al., 2022), RML (S. W. Manka, W. Zhang, et al., 2022), ME7 (Szymon W. Manka et al., 2022) and human GSS F198S (Hallinan et al., 2022) revealed a PIRIBS based structure as a common amyloid fibril conformation observed in these prion strains. These structures contradict the X-ray fiber diffraction (Wille, Bian, et al., 2009), the recent low-resolution structure of L-type BSE prions that proposed a 4R β S architecture (Kamali-Jamil et al., 2021), and the atomic MD model of anchorless RML prion that revealed a 4R β S model (Spagnolli et al., 2019).

Comparing the orientation of the H110 and D146 epitope of the YEG Sc-G1 antibody in a 4R β S model and the PIRIBS structure, we see a profound difference (Figure. 3-33.A-B).

Our immunogold labelling study on the isolated RML prion fibrils utilizing Fab YEG Sc-G1 showed successful labelling of the P2 fraction decorating mostly the PrP 27-30 aggregates and did not show any specific labelling to the isolated amyloid fibrils from the pellet-wash fraction (Figure. 3-15). Similarly, Fab YEG Sc-M63, another conformational PrP^{Sc}-specific antibody recognizing surface exposed residues N103 and D143 that are oriented in a vertical pair-wise form showed to decorate the 2D crystals in their native structure (Figure. 3-16.A-C). In contrast, our Fab YEG Sc – M63 did not show any labelling to the amyloid fibrils (Figure 3-16.E-G) indicating a different structure is observed in the amyloid fibrils compared to the 2D crystal structure of PrP27-30. It has been previously reported that the purified fractions of prions showed a dense amount of the prion rods but also contained 2D crystals that appear to be alternative quaternary structures of native PrP27-30 and expected to be fully infectious (Wille et al., 2007; Wille, Shanmugam, et al., 2009).

The loss of antigen-antibody interaction between the conformational PrP^{Sc}-specific antibody and the infectious amyloid fibrils adopting a PIRIBS conformation is due to the loss of epitope configuration. The orientation of the YEG Sc-G1 is found to be on the β -arc region between strands 2 and 3 and strands 5 and 6, H110 and D146 respectively. These residues are surface exposed and facing 180° to each other on a monomeric RML PrP^{Sc} structure. Whereas the orientation of the YEG Sc-M63 epitope on the RML PIRIBS structure is on the β -strands 2 and 5, N103 and D143 respectively. N103 is surface exposed while the residue D143 is facing inwards toward the hydrophobic core (Figure 3-33.B). These results indicate that there is heterogeneity in the prion sample which is presumably consisting of a 4R β S fold and a PIRIBS structure.

5.5 Is 2R β S or 4R β S a precursor to PIRIBS fibril formation?

There is an ongoing debate in the prion field on the structure of the infectious agent, PrP^{Sc} and possible intermediate conformers and the lingering question of what is the true toxic agent driving prion diseases. Combining all the structural evidence over the decade and the data shown in this dissertation using the PrP^{Sc}-specific antibody indicates that it is impossible to rule out that all the infectious amyloid aggregates adopt a PIRIBS structure.

Based on several structural studies, the fundamental structure of PrP^{Sc} is thought to comprise a 4R β S architecture (H. Wille & J. Requena, 2018). Initially, electron crystallography research on two-dimensional crystals of a truncated prion protein (PrP 27-30) and a mini-prion (PrP^{Sc}106) revealed that PrP^{Sc} molecules consist of a β -solenoid core (Govaerts et al., 2004; Wille et al., 2002). An X-ray fiber diffraction experiment on brain-derived PrP27-30 prions revealed a 19.2Å signal, which is indicative of the height of each 4R β S PrP^{Sc} monomer (Wille, Bian, et al., 2009). The Molecular dynamics simulation study performed based on the proposed models of PrP^{Sc} presented a plausible 4R β S model for the prion molecules (Spagnolli et al., 2019). Recently, a low-resolution negative-stain electron microscope structure of an L-type BSE prion was reported consisting of two different morphologies from the same brain preparation, two- and one- protofilament amyloid fibrils (Kamali-Jamil et al., 2021). The proposed model of L-type BSE prion was in agreement with the previously reported 4R β S model (Kamali-Jamil et al., 2021; Vazquez-Fernandez et al., 2016).

When the height of each 4R β S PrP^{Sc} monomer is compared to current high-resolution cryo-EM structures using a PIRIBS structure (B. Caughey et al., 2022; S. W. Manka, A. Wenborn, et al.,

2022), it is not compatible with the predicted 19.2Å seen in X-ray fiber diffraction and cryo-EM research (Vazquez-Fernandez et al., 2016; Wille, Bian, et al., 2009).

With the reported evidence on the structures of PrP^{Sc}, we asked can the PrP^{Sc}-specific antibody, YEG Sc-G1 be employed to determine the structural heterogeneity in the sample and provide insights into the various folds adopted during the protein misfolding event until the stable amyloid fibril structure is adopted based on the orientation the epitope, H110 and D146. Chapter 4 of this thesis, presents data on the in-vitro refolding of the 7kDa synthetic human A117V-GSS peptide using the conformational PrP^{Sc}-specific antibody. Various biochemical and biophysical methods were employed to see the structural changes of the linear synthetic peptide adopting rich-beta sheet structure in eight different biochemical conditions (Figure. 4-3). Negative electron micrographs revealed heterogeneous morphologies between sample conditions. Some conditions consisted mostly of β -oligomers or long PIRIBS-based structure amyloid fibrils while some conditions consisted of both morphologies in the same sample (Figures. 4-6 and 4-7). Our findings indicate that changes in environmental conditions may have important implications in determining the structural fold adopted during the misfolding pathways of PrP *in vivo* and the formation of distinct abnormal isoforms. Some of these morphologies observed from the synthetic GSS-A117V peptide at week 4 are in agreement with the recently reported morphologies of purified human brain-derived GSS-A117V sample, consisting of β -oligomeric structure and small structurally indistinct particles which proved to have a higher infectivity titre in bank voles, an infectious-dose of 10^9 ID₅₀ (Vanni et al., 2020).

Immunogold labelling using the PrP^{Sc}-specific antibody revealed specific gold labelling to β -oligomeric structure showing the bound YEG Sc-G1 antibody and abolished its interaction when the linear GSS-A117V peptide adopted fibrillar rod architecture (Figure. 4-9). This suggests,

based on the orientation of the H111 and D147 residues, there may be a structural drift from a suggestive 2R β S structure to a PIRIBS-based structure (Figure. 4-5).

Taking into account the results from the recent cryo-EM study of the brain-derived GSS-F198S prion (Hallinan et al., 2022) and some prior research findings (Vanni et al., 2020; Wille, Bian, et al., 2009), including the data from this dissertation, it appears possible that these alternate structures exist in the brain. The observed variety in PrP protein architecture may potentially indicate that many PrP^{Sc} structures co-exist in the brain of one host. The two-rung beta solenoid architecture is also seen in the fungal prions (Wasmer et al., 2008).

5.6 Future directions

My thesis research revolves around the utility of recombinant antibody fragments generated through phage display technology and hybridoma clones recognizing PrP and PrP^{Sc} conformers respectively. These antibodies offer a wide range of use in prion research to understand the molecular mechanism involved in prion diseases. In my dissertation, I have focused on the generation, design and production of recombinant antibody fragments as tools for structural analyses and direct prion detection of infectious prions.

The emphasis on reported conformational dependent PrP^{Sc}-specific antibody fragments that recognize the infectious isoform only under natural conditions has opened up possibilities for usage as a potential treatment tool for prion diseases and a better understanding of prion replication. The approach of using our various PrP^{Sc}-specific antibody fragments along with the

findings presented in this thesis provides a feasible framework for future downstream experiments to isolate the oligomers and amyloid fibril from infectious brain homogenate of different prion strains using immunoprecipitation assay and performing a two-way comparison by performing bioassay study on the precipitated infectious material to understand which β -conformation, the oligomers or the fibrils are the toxic species in causing prion diseases. Overall, the approach of developing a plethora of PrP^{Sc}-specific antibody fragments is not limited to prion diseases but may be used for other vaccine-derived antibodies targeting pathologic proteins that cause neurodegenerative diseases, such as misfolded A β , tau, and α -synuclein. These antibodies have the potential to be employed for protein imaging, one-step detection, or as passive immunotherapy techniques (ongoing projects in the Wille lab).

REFERENCES:

- Adamson, C. S., Yao, Y., Vasiljevic, S., Sy, M. S., Ren, J., & Jones, I. M. (2007). Novel single chain antibodies to the prion protein identified by phage display. *Virology*, 358(1), 166-177. doi:10.1016/j.virol.2006.08.023
- Aguzzi, A., Baumann, F., & Bremer, J. (2008). The prion's elusive reason for being. *Annu Rev Neurosci*, 31, 439-477. doi:10.1146/annurev.neuro.31.060407.125620
- Aguzzi, A., & Calella, A. M. (2009). Prions: protein aggregation and infectious diseases. *Physiol Rev*, 89(4), 1105-1152. doi:10.1152/physrev.00006.2009
- Aguzzi, A., Heikenwalder, M., & Polymenidou, M. (2007). Insights into prion strains and neurotoxicity. *Nat Rev Mol Cell Biol*, 8(7), 552-561. doi:10.1038/nrm2204
- Aguzzi, A., & O'Connor, T. (2010). Protein aggregation diseases: pathogenicity and therapeutic perspectives. *Nat Rev Drug Discov*, 9(3), 237-248. doi:10.1038/nrd3050
- Aguzzi, A., & Zhu, C. (2012). Five questions on prion diseases. *PLoS Pathog*, 8(5), e1002651. doi:10.1371/journal.ppat.1002651
- Ahmad, Z. A., Yeap, S. K., Ali, A. M., Ho, W. Y., Alitheen, N. B., & Hamid, M. (2012). scFv antibody: principles and clinical application. *Clin Dev Immunol*, 2012, 980250. doi:10.1155/2012/980250
- Alles, J., Karaiskos, N., Praktijnjo, S. D., Grosswendt, S., Wahle, P., Ruffault, P. L., . . . Rajewsky, N. (2017). Cell fixation and preservation for droplet-based single-cell transcriptomics. *BMC Biol*, 15(1), 44. doi:10.1186/s12915-017-0383-5
- Altmeppen, H. C., Prox, J., Krasemann, S., Puig, B., Kruszewski, K., Dohler, F., . . . Glatzel, M. (2015). The sheddase ADAM10 is a potent modulator of prion disease. *Elife*, 4. doi:10.7554/eLife.04260
- Andreoletti, O., Berthon, P., Marc, D., Sarradin, P., Grosclaude, J., van Keulen, L., . . . Lantier, F. (2000). Early accumulation of PrP(Sc) in gut-associated lymphoid and nervous tissues of susceptible sheep from a Romanov flock with natural scrapie. *J Gen Virol*, 81(Pt 12), 3115-3126. doi:10.1099/0022-1317-81-12-3115
- Arndt, K. M., Muller, K. M., & Pluckthun, A. (2001). Helix-stabilized Fv (hsFv) antibody fragments: substituting the constant domains of a Fab fragment for a heterodimeric coiled-coil domain. *J Mol Biol*, 312(1), 221-228. doi:10.1006/jmbi.2001.4915
- Arnold, J. E., Tipler, C., Laszlo, L., Hope, J., Landon, M., & Mayer, R. J. (1995). The abnormal isoform of the prion protein accumulates in late-endosome-like organelles in scrapie-infected mouse brain. *J Pathol*, 176(4), 403-411. doi:10.1002/path.1711760412
- Artikis, E., Kraus, A., & Caughey, B. (2022). Structural biology of ex vivo mammalian prions. *J Biol Chem*, 102181. doi:10.1016/j.jbc.2022.102181
- Babelhadj, B., Di Bari, M. A., Pirisinu, L., Chiappini, B., Gaouar, S. B. S., Riccardi, G., . . . Vaccari, G. (2018). Prion Disease in Dromedary Camels, Algeria. *Emerg Infect Dis*, 24(6), 1029-1036. doi:10.3201/eid2406.172007
- Baeten, L. A., Powers, B. E., Jewell, J. E., Spraker, T. R., & Miller, M. W. (2007). A natural case of chronic wasting disease in a free-ranging moose (*Alces alces shirasi*). *J Wildl Dis*, 43(2), 309-314. doi:10.7589/0090-3558-43.2.309

- Baral, P. K., Swayampakula, M., Aguzzi, A., & James, M. N. (2015). X-ray structural and molecular dynamical studies of the globular domains of cow, deer, elk and Syrian hamster prion proteins. *J Struct Biol*, *192*(1), 37-47. doi:10.1016/j.jsb.2015.08.014
- Baral, P. K., Swayampakula, M., Aguzzi, A., & James, M. N. G. (2018). Structural characterization of POM6 Fab and mouse prion protein complex identifies key regions for prions conformational conversion. *FEBS J*, *285*(9), 1701-1714. doi:10.1111/febs.14438
- Baral, P. K., Wieland, B., Swayampakula, M., Polymenidou, M., Rahman, M. H., Kav, N. N., . . . James, M. N. (2012). Structural studies on the folded domain of the human prion protein bound to the Fab fragment of the antibody POM1. *Acta Crystallogr D Biol Crystallogr*, *68*(Pt 11), 1501-1512. doi:10.1107/S0907444912037328
- Baral, T. N., MacKenzie, R., & Arbabi Ghahroudi, M. (2013). Single-domain antibodies and their utility. *Curr Protoc Immunol*, *103*, Unit 2 17. doi:10.1002/0471142735.im0217s103
- Bardelli, M., Frontzek, K., Simonelli, L., Hornemann, S., Pedotti, M., Mazzola, F., . . . Varani, L. (2018). A bispecific immunotweezer prevents soluble PrP oligomers and abolishes prion toxicity. *PLoS Pathog*, *14*(10), e1007335. doi:10.1371/journal.ppat.1007335
- Barnard, G., Hopkins, L., Moorhie, S., Seilly, D., Tonks, P., Dabaghian, R., . . . McConnell, I. (2007). Direct detection of disease associated prions in brain and lymphoid tissue using antibodies recognizing the extreme N terminus of PrPC. *Prion*, *1*(2), 121-127. doi:10.4161/pri.1.2.4439
- Barria, M. A., Mukherjee, A., Gonzalez-Romero, D., Morales, R., & Soto, C. (2009). De novo generation of infectious prions in vitro produces a new disease phenotype. *PLoS Pathog*, *5*(5), e1000421. doi:10.1371/journal.ppat.1000421
- Bartz, J. C., Marsh, R. F., McKenzie, D. I., & Aiken, J. M. (1998). The host range of chronic wasting disease is altered on passage in ferrets. *Virology*, *251*(2), 297-301. doi:10.1006/viro.1998.9427
- Baskakov, I. V., Aagaard, C., Mehlhorn, I., Wille, H., Groth, D., Baldwin, M. A., . . . Cohen, F. E. (2000). Self-assembly of recombinant prion protein of 106 residues. *Biochemistry*, *39*(10), 2792-2804. doi:10.1021/bi9923353
- Baskakov, I. V., & Bocharova, O. V. (2005). In vitro conversion of mammalian prion protein into amyloid fibrils displays unusual features. *Biochemistry*, *44*(7), 2339-2348. doi:10.1021/bi048322t
- Baskakov, I. V., Legname, G., Gryczynski, Z., & Prusiner, S. B. (2004). The peculiar nature of unfolding of the human prion protein. *Protein Sci*, *13*(3), 586-595. doi:10.1110/ps.03457204
- Berek, C., Griffiths, G. M., & Milstein, C. (1985). Molecular events during maturation of the immune response to oxazolone. *Nature*, *316*(6027), 412-418. doi:10.1038/316412a0
- Beringue, V., Mallinson, G., Kaiser, M., Tayebi, M., Sattar, Z., Jackson, G., . . . Hawke, S. (2003). Regional heterogeneity of cellular prion protein isoforms in the mouse brain. *Brain*, *126*(Pt 9), 2065-2073. doi:10.1093/brain/awg205
- Berman, H. M., Westbrook, J., Feng, Z., Gilliland, G., Bhat, T. N., Weissig, H., . . . Bourne, P. E. (2000). The Protein Data Bank. *Nucleic Acids Res*, *28*(1), 235-242. doi:10.1093/nar/28.1.235
- Bett, C., Kurt, T. D., Lucero, M., Trejo, M., Rozemuller, A. J., Kong, Q., . . . Sigurdson, C. J. (2013). Defining the conformational features of anchorless, poorly neuroinvasive prions. *PLoS Pathog*, *9*(4), e1003280. doi:10.1371/journal.ppat.1003280

- Biasini, E., Seegulam, M. E., Patti, B. N., Solforosi, L., Medrano, A. Z., Christensen, H. M., . . . Harris, D. A. (2008). Non-infectious aggregates of the prion protein react with several PrPSc-directed antibodies. *J Neurochem*, *105*(6), 2190-2204. doi:10.1111/j.1471-4159.2008.05306.x
- Bolton, D. C., McKinley, M. P., & Prusiner, S. B. (1982). Identification of a protein that purifies with the scrapie prion. *Science*, *218*(4579), 1309-1311. doi:10.1126/science.6815801
- Bonda, D. J., Manjila, S., Mehndiratta, P., Khan, F., Miller, B. R., Onwuzulike, K., . . . Cali, I. (2016). Human prion diseases: surgical lessons learned from iatrogenic prion transmission. *Neurosurg Focus*, *41*(1), E10. doi:10.3171/2016.5.FOCUS15126
- Boulianne, G. L., Hozumi, N., & Shulman, M. J. (1984). Production of functional chimaeric mouse/human antibody. *Nature*, *312*(5995), 643-646. doi:10.1038/312643a0
- Brazier, M. W., Mot, A. I., White, A. R., & Collins, S. J. (2013). Immunotherapeutic approaches in prion disease: progress, challenges and potential directions. *Ther Deliv*, *4*(5), 615-628. doi:10.4155/tde.13.30
- Brown, K., & Mastrianni, J. A. (2010). The prion diseases. *J Geriatr Psychiatry Neurol*, *23*(4), 277-298. doi:10.1177/0891988710383576
- Brown, P., McShane, L. M., Zanusso, G., & Detwile, L. (2006). On the question of sporadic or atypical bovine spongiform encephalopathy and Creutzfeldt-Jakob disease. *Emerg Infect Dis*, *12*(12), 1816-1821. doi:10.3201/eid1212.060965
- Bruce, M. E., Will, R. G., Ironside, J. W., McConnell, I., Drummond, D., Suttie, A., . . . Bostock, C. J. (1997). Transmissions to mice indicate that 'new variant' CJD is caused by the BSE agent. *Nature*, *389*(6650), 498-501. doi:10.1038/39057
- Castilla, J., Saa, P., Hetz, C., & Soto, C. (2005). In vitro generation of infectious scrapie prions. *Cell*, *121*(2), 195-206. doi:10.1016/j.cell.2005.02.011
- Caughey, B., Orru, C. D., Groveman, B. R., Hughson, A. G., Manca, M., Raymond, L. D., . . . Kraus, A. (2017). Amplified Detection of Prions and Other Amyloids by RT-QuIC in Diagnostics and the Evaluation of Therapeutics and Disinfectants. *Prog Mol Biol Transl Sci*, *150*, 375-388. doi:10.1016/bs.pmbts.2017.06.003
- Caughey, B., Raymond, G. J., & Bessen, R. A. (1998). Strain-dependent differences in beta-sheet conformations of abnormal prion protein. *J Biol Chem*, *273*(48), 32230-32235. doi:10.1074/jbc.273.48.32230
- Caughey, B., Standke, H. G., Artakis, E., Hoyt, F., & Kraus, A. (2022). Pathogenic prion structures at high resolution. *PLoS Pathog*, *18*(6), e1010594. doi:10.1371/journal.ppat.1010594
- Caughey, B. W., Dong, A., Bhat, K. S., Ernst, D., Hayes, S. F., & Caughey, W. S. (1991). Secondary structure analysis of the scrapie-associated protein PrP 27-30 in water by infrared spectroscopy. *Biochemistry*, *30*(31), 7672-7680. doi:10.1021/bi00245a003
- Chao, G., Lau, W. L., Hackel, B. J., Sazinsky, S. L., Lippow, S. M., & Wittrup, K. D. (2006). Isolating and engineering human antibodies using yeast surface display. *Nat Protoc*, *1*(2), 755-768. doi:10.1038/nprot.2006.94
- Chatron, P., & Pontet, F. (1992). [Structure an functions of IgG subclasses]. *Ann Biol Clin (Paris)*, *50*(8), 565-575. Retrieved from <https://www.ncbi.nlm.nih.gov/pubmed/1294012>
- Chen, C., & Dong, X. P. (2016). Epidemiological characteristics of human prion diseases. *Infect Dis Poverty*, *5*(1), 47. doi:10.1186/s40249-016-0143-8

- Choi, J. K., Cali, I., Surewicz, K., Kong, Q., Gambetti, P., & Surewicz, W. K. (2016). Amyloid fibrils from the N-terminal prion protein fragment are infectious. *Proc Natl Acad Sci U S A*, *113*(48), 13851-13856. doi:10.1073/pnas.1610716113
- Clackson, T., Hoogenboom, H. R., Griffiths, A. D., & Winter, G. (1991). Making antibody fragments using phage display libraries. *Nature*, *352*(6336), 624-628. doi:10.1038/352624a0
- Cobb, N. J., Sonnichsen, F. D., McHaourab, H., & Surewicz, W. K. (2007). Molecular architecture of human prion protein amyloid: a parallel, in-register beta-structure. *Proc Natl Acad Sci U S A*, *104*(48), 18946-18951. doi:10.1073/pnas.0706522104
- Colcher, D., Pavlinkova, G., Beresford, G., Booth, B. J., Choudhury, A., & Batra, S. K. (1998). Pharmacokinetics and biodistribution of genetically-engineered antibodies. *Q J Nucl Med*, *42*(4), 225-241. Retrieved from <https://www.ncbi.nlm.nih.gov/pubmed/9973838>
- Collinge, J. (2001). Prion diseases of humans and animals: their causes and molecular basis. *Annu Rev Neurosci*, *24*, 519-550. doi:10.1146/annurev.neuro.24.1.519
- Collinge, J., Palmer, M. S., & Dryden, A. J. (1991). Genetic predisposition to iatrogenic Creutzfeldt-Jakob disease. *Lancet*, *337*(8755), 1441-1442. doi:10.1016/0140-6736(91)93128-v
- Collinge, J., Sidle, K. C., Meads, J., Ironside, J., & Hill, A. F. (1996). Molecular analysis of prion strain variation and the aetiology of 'new variant' CJD. *Nature*, *383*(6602), 685-690. doi:10.1038/383685a0
- Collinge, J., Whitfield, J., McKintosh, E., Beck, J., Mead, S., Thomas, D. J., & Alpers, M. P. (2006). Kuru in the 21st century--an acquired human prion disease with very long incubation periods. *Lancet*, *367*(9528), 2068-2074. doi:10.1016/S0140-6736(06)68930-7
- Collins, P. Y., Insel, T. R., Chockalingam, A., Daar, A., & Maddox, Y. T. (2013). Grand challenges in global mental health: integration in research, policy, and practice. *PLoS Med*, *10*(4), e1001434. doi:10.1371/journal.pmed.1001434
- Coloma, M. J., Larrick, J. W., Ayala, M., & Gavilondo-Cowley, J. V. (1991). Primer design for the cloning of immunoglobulin heavy-chain leader-variable regions from mouse hybridoma cells using the PCR. *Biotechniques*, *11*(2), 152-154, 156. Retrieved from <https://www.ncbi.nlm.nih.gov/pubmed/1931008>
- Costassa, E. V., Iulini, B., Mazza, M., Acutis, P., Maurella, C., Meloni, D., . . . Casalone, C. (2016). Pathogenesis and Transmission of Classical and Atypical BSE in Cattle. *Food Saf (Tokyo)*, *4*(4), 130-134. doi:10.14252/foodsafetyfscj.2016018
- Cracco, L., Notari, S., Cali, I., Sy, M. S., Chen, S. G., Cohen, M. L., . . . Gambetti, P. (2017). Novel strain properties distinguishing sporadic prion diseases sharing prion protein genotype and prion type. *Sci Rep*, *7*, 38280. doi:10.1038/srep38280
- Cracco, L., Xiao, X., Nemani, S. K., Lavrich, J., Cali, I., Ghetti, B., . . . Gambetti, P. (2019). Gerstmann-Straussler-Scheinker disease revisited: accumulation of covalently-linked multimers of internal prion protein fragments. *Acta Neuropathol Commun*, *7*(1), 85. doi:10.1186/s40478-019-0734-2
- Creutzfeldt, H. G. (1989). On a particular focal disease of the central nervous system (preliminary communication), 1920. *Alzheimer Dis Assoc Disord*, *3*(1-2), 3-25. Retrieved from <https://www.ncbi.nlm.nih.gov/pubmed/2663042>
- Curin Serbec, V., Bresjanac, M., Popovic, M., Pretnar Hartman, K., Galvani, V., Ruprecht, R., . . . Jerala, R. (2004). Monoclonal antibody against a peptide of human prion protein

- discriminates between Creutzfeldt-Jacob's disease-affected and normal brain tissue. *J Biol Chem*, 279(5), 3694-3698. doi:10.1074/jbc.M310868200
- Dall'Acqua, W. F., Cook, K. E., Damschroder, M. M., Woods, R. M., & Wu, H. (2006). Modulation of the effector functions of a human IgG1 through engineering of its hinge region. *J Immunol*, 177(2), 1129-1138. doi:10.4049/jimmunol.177.2.1129
- Davies, D. R., Padlan, E. A., & Segal, D. M. (1975). Three-dimensional structure of immunoglobulins. *Annu Rev Biochem*, 44, 639-667. doi:10.1146/annurev.bi.44.070175.003231
- Deleault, N. R., Harris, B. T., Rees, J. R., & Supattapone, S. (2007). Formation of native prions from minimal components in vitro. *Proc Natl Acad Sci U S A*, 104(23), 9741-9746. doi:10.1073/pnas.0702662104
- DeMarco, M. L., & Daggett, V. (2004). From conversion to aggregation: protofibril formation of the prion protein. *Proc Natl Acad Sci U S A*, 101(8), 2293-2298. doi:10.1073/pnas.0307178101
- Desmyter, A., Spinelli, S., Roussel, A., & Cambillau, C. (2015). Camelid nanobodies: killing two birds with one stone. *Curr Opin Struct Biol*, 32, 1-8. doi:10.1016/j.sbi.2015.01.001
- Desta, I. T., Porter, K. A., Xia, B., Kozakov, D., & Vajda, S. (2020). Performance and Its Limits in Rigid Body Protein-Protein Docking. *Structure*, 28(9), 1071-1081 e1073. doi:10.1016/j.str.2020.06.006
- Detwiler, L. A. (1992). Scrapie. *Rev Sci Tech*, 11(2), 491-537. doi:10.20506/rst.11.2.607
- Diebold, C. A., Beurskens, F. J., de Jong, R. N., Koning, R. I., Strumane, K., Lindorfer, M. A., . . . Parren, P. W. (2014). Complement is activated by IgG hexamers assembled at the cell surface. *Science*, 343(6176), 1260-1263. doi:10.1126/science.1248943
- Duffy, P., Wolf, J., Collins, G., DeVoe, A. G., Streeten, B., & Cowen, D. (1974). Letter: Possible person-to-person transmission of Creutzfeldt-Jakob disease. *N Engl J Med*, 290(12), 692-693. Retrieved from <https://www.ncbi.nlm.nih.gov/pubmed/4591849>
- Edelman, G. M., Benacerraf, B., Ovary, Z., & Poulik, M. D. (1961). Structural differences among antibodies of different specificities. *Proc Natl Acad Sci U S A*, 47, 1751-1758. doi:10.1073/pnas.47.11.1751
- Edelman, G. M., & Poulik, M. D. (1961). Studies on structural units of the gamma-globulins. *J Exp Med*, 113, 861-884. doi:10.1084/jem.113.5.861
- El Debs, B., Utharala, R., Balyasnikova, I. V., Griffiths, A. D., & Merten, C. A. (2012). Functional single-cell hybridoma screening using droplet-based microfluidics. *Proc Natl Acad Sci U S A*, 109(29), 11570-11575. doi:10.1073/pnas.1204514109
- Elezgarai, S. R., Fernandez-Borges, N., Erana, H., Sevillano, A. M., Charco, J. M., Harrathi, C., . . . Castilla, J. (2017). Generation of a new infectious recombinant prion: a model to understand Gerstmann-Straussler-Scheinker syndrome. *Sci Rep*, 7(1), 9584. doi:10.1038/s41598-017-09489-3
- Eshaghi, M., Sun, G., Gruter, A., Lim, C. L., Chee, Y. C., Jung, G., . . . Chen, S. L. (2015). Rational Structure-Based Design of Bright GFP-Based Complexes with Tunable Dimerization. *Angew Chem Int Ed Engl*, 54(47), 13952-13956. doi:10.1002/anie.201506686
- Feraudet, C., Morel, N., Simon, S., Volland, H., Frobert, Y., Creminon, C., . . . Grassi, J. (2005). Screening of 145 anti-PrP monoclonal antibodies for their capacity to inhibit PrPSc replication in infected cells. *J Biol Chem*, 280(12), 11247-11258. doi:10.1074/jbc.M407006200

- Fitzpatrick, A. W. P., Falcon, B., He, S., Murzin, A. G., Murshudov, G., Garringer, H. J., . . . Scheres, S. H. W. (2017). Cryo-EM structures of tau filaments from Alzheimer's disease. *Nature*, *547*(7662), 185-190. doi:10.1038/nature23002
- Flego, M., Ascione, A., Zamboni, S., Dupuis, M. L., Imperiale, V., & Cianfriglia, M. (2007). Generation of human scFvs antibodies recognizing a prion protein epitope expressed on the surface of human lymphoblastoid cells. *BMC Biotechnol*, *7*, 38. doi:10.1186/1472-6750-7-38
- Flores-Fernandez, J. M., Rathod, V., & Wille, H. (2018). Comparing the Folds of Prions and Other Pathogenic Amyloids. *Pathogens*, *7*(2). doi:10.3390/pathogens7020050
- Forloni, G., Artuso, V., La Vitola, P., & Balducci, C. (2016). Oligomeropathies and pathogenesis of Alzheimer and Parkinson's diseases. *Mov Disord*, *31*(6), 771-781. doi:10.1002/mds.26624
- Fox, K. A., Jewell, J. E., Williams, E. S., & Miller, M. W. (2006). Patterns of PrPCWD accumulation during the course of chronic wasting disease infection in orally inoculated mule deer (*Odocoileus hemionus*). *J Gen Virol*, *87*(Pt 11), 3451-3461. doi:10.1099/vir.0.81999-0
- Frank, M. K., Clore, G. M., & Gronenborn, A. M. (1995). Structural and dynamic characterization of the urea denatured state of the immunoglobulin binding domain of streptococcal protein G by multidimensional heteronuclear NMR spectroscopy. *Protein Sci*, *4*(12), 2605-2615. doi:10.1002/pro.5560041218
- Frenzel, A., Schirrmann, T., & Hust, M. (2016). Phage display-derived human antibodies in clinical development and therapy. *MAbs*, *8*(7), 1177-1194. doi:10.1080/19420862.2016.1212149
- Gajdusek, D. C., Gibbs, C. J., & Alpers, M. (1966). Experimental transmission of a Kuru-like syndrome to chimpanzees. *Nature*, *209*(5025), 794-796. doi:10.1038/209794a0
- Galatioto, S., Ruggeri, D., & Gullotta, F. (1995). [Gerstmann-Straussler-Scheinker syndrome in a Sicilian patient. Neuropathological aspects]. *Pathologica*, *87*(6), 659-665. Retrieved from <https://www.ncbi.nlm.nih.gov/pubmed/8927427>
- Gambetti, P., Cali, I., Notari, S., Kong, Q., Zou, W. Q., & Surewicz, W. K. (2011). Molecular biology and pathology of prion strains in sporadic human prion diseases. *Acta Neuropathol*, *121*(1), 79-90. doi:10.1007/s00401-010-0761-3
- Gambetti, P., Parchi, P., Petersen, R. B., Chen, S. G., & Lugaresi, E. (1995). Fatal familial insomnia and familial Creutzfeldt-Jakob disease: clinical, pathological and molecular features. *Brain Pathol*, *5*(1), 43-51. doi:10.1111/j.1750-3639.1995.tb00576.x
- Gasset, M., Baldwin, M. A., Fletterick, R. J., & Prusiner, S. B. (1993). Perturbation of the secondary structure of the scrapie prion protein under conditions that alter infectivity. *Proc Natl Acad Sci U S A*, *90*(1), 1-5. doi:10.1073/pnas.90.1.1
- Ghetti, B., Dlouhy, S. R., Giaccone, G., Bugiani, O., Frangione, B., Farlow, M. R., & Tagliavini, F. (1995). Gerstmann-Straussler-Scheinker disease and the Indiana kindred. *Brain Pathol*, *5*(1), 61-75. doi:10.1111/j.1750-3639.1995.tb00578.x
- Gill, A. C., & Castle, A. R. (2018). The cellular and pathologic prion protein. *Handb Clin Neurol*, *153*, 21-44. doi:10.1016/B978-0-444-63945-5.00002-7
- Gilliland, G. L., Luo, J., Vafa, O., & Almagro, J. C. (2012). Leveraging SBDD in protein therapeutic development: antibody engineering. *Methods Mol Biol*, *841*, 321-349. doi:10.1007/978-1-61779-520-6_14

- Giudicelli, V., Duroux, P., Ginestoux, C., Folch, G., Jabado-Michaloud, J., Chaume, D., & Lefranc, M. P. (2006). IMGT/LIGM-DB, the IMGT comprehensive database of immunoglobulin and T cell receptor nucleotide sequences. *Nucleic Acids Res*, 34(Database issue), D781-784. doi:10.1093/nar/gkj088
- Glockshuber, R., Hornemann, S., Riek, R., Wider, G., Billeter, M., & Wuthrich, K. (1997). Three-dimensional NMR structure of a self-folding domain of the prion protein PrP(121-231). *Trends Biochem Sci*, 22(7), 241-242. Retrieved from <https://www.ncbi.nlm.nih.gov/pubmed/9255063>
- Godsave, S. F., Wille, H., Kujala, P., Latawiec, D., DeArmond, S. J., Serban, A., . . . Peters, P. J. (2008). Cryo-immunogold electron microscopy for prions: toward identification of a conversion site. *J Neurosci*, 28(47), 12489-12499. doi:10.1523/JNEUROSCI.4474-08.2008
- Goto, Y., Adachi, M., Muta, H., & So, M. (2018). Salt-induced formations of partially folded intermediates and amyloid fibrils suggests a common underlying mechanism. *Biophys Rev*, 10(2), 493-502. doi:10.1007/s12551-017-0370-7
- Govaerts, C., Wille, H., Prusiner, S. B., & Cohen, F. E. (2004). Evidence for assembly of prions with left-handed beta-helices into trimers. *Proc Natl Acad Sci U S A*, 101(22), 8342-8347. doi:10.1073/pnas.0402254101
- Green, M., & Loewenstein, P. M. (1988). Autonomous functional domains of chemically synthesized human immunodeficiency virus tat trans-activator protein. *Cell*, 55(6), 1179-1188. doi:10.1016/0092-8674(88)90262-0
- Greenfield, N. J. (2006). Using circular dichroism spectra to estimate protein secondary structure. *Nat Protoc*, 1(6), 2876-2890. doi:10.1038/nprot.2006.202
- Groveman, B. R., Dolan, M. A., Taubner, L. M., Kraus, A., Wickner, R. B., & Caughey, B. (2014). Parallel in-register intermolecular beta-sheet architectures for prion-seeded prion protein (PrP) amyloids. *J Biol Chem*, 289(35), 24129-24142. doi:10.1074/jbc.M114.578344
- Guckeisen, T., Hosseinpour, S., & Peukert, W. (2021). Effect of pH and urea on the proteins secondary structure at the water/air interface and in solution. *J Colloid Interface Sci*, 590, 38-49. doi:10.1016/j.jcis.2021.01.015
- Haass, C., & Selkoe, D. J. (2007). Soluble protein oligomers in neurodegeneration: lessons from the Alzheimer's amyloid beta-peptide. *Nat Rev Mol Cell Biol*, 8(2), 101-112. doi:10.1038/nrm2101
- Hafner Bratkovic, I. (2017). Prions, prionoid complexes and amyloids: the bad, the good and something in between. *Swiss Med Wkly*, 147, w14424. doi:10.4414/smw.2017.14424
- Hallinan, G. I., Ozcan, K. A., Hoq, M. R., Cracco, L., Vago, F. S., Bharath, S. R., . . . Vidal, R. (2022). Cryo-EM structures of prion protein filaments from Gerstmann-Straussler-Scheinker disease. *Acta Neuropathol*. doi:10.1007/s00401-022-02461-0
- Hamers-Casterman, C., Atarhouch, T., Muyldermans, S., Robinson, G., Hamers, C., Songa, E. B., . . . Hamers, R. (1993). Naturally occurring antibodies devoid of light chains. *Nature*, 363(6428), 446-448. doi:10.1038/363446a0
- Hannaoui, S., Zemlyankina, I., Chang, S. C., Arifin, M. I., Beringue, V., McKenzie, D., . . . Gilch, S. (2022). Transmission of cervid prions to humanized mice demonstrates the zoonotic potential of CWD. *Acta Neuropathol*, 144(4), 767-784. doi:10.1007/s00401-022-02482-9

- Haraguchi, T., Fisher, S., Olofsson, S., Endo, T., Groth, D., Tarentino, A., . . . et al. (1989). Asparagine-linked glycosylation of the scrapie and cellular prion proteins. *Arch Biochem Biophys*, 274(1), 1-13. doi:10.1016/0003-9861(89)90409-8
- Hegde, R. S., Mastrianni, J. A., Scott, M. R., DeFea, K. A., Tremblay, P., Torchia, M., . . . Lingappa, V. R. (1998). A transmembrane form of the prion protein in neurodegenerative disease. *Science*, 279(5352), 827-834. doi:10.1126/science.279.5352.827
- Heppner, F. L., Musahl, C., Arrighi, I., Klein, M. A., Rulicke, T., Oesch, B., . . . Aguzzi, A. (2001). Prevention of scrapie pathogenesis by transgenic expression of anti-prion protein antibodies. *Science*, 294(5540), 178-182. doi:10.1126/science.1063093
- Hill, A. F., Desbruslais, M., Joiner, S., Sidle, K. C., Gowland, I., Collinge, J., . . . Lantos, P. (1997). The same prion strain causes vCJD and BSE. *Nature*, 389(6650), 448-450, 526. doi:10.1038/38925
- Hill, A. F., Zeidler, M., Ironside, J., & Collinge, J. (1997). Diagnosis of new variant Creutzfeldt-Jakob disease by tonsil biopsy. *Lancet*, 349(9045), 99-100. doi:10.1016/S0140-6736(97)24002-X
- Hiramoto, E., Tsutsumi, A., Suzuki, R., Matsuoka, S., Arai, S., Kikkawa, M., & Miyazaki, T. (2018). The IgM pentamer is an asymmetric pentagon with an open groove that binds the AIM protein. *Sci Adv*, 4(10), eaau1199. doi:10.1126/sciadv.aau1199
- Hoinville, L. J., Tongue, S. C., & Wilesmith, J. W. (2010). Evidence for maternal transmission of scrapie in naturally affected flocks. *Prev Vet Med*, 93(2-3), 121-128. doi:10.1016/j.prevetmed.2009.10.013
- Holliger, P., & Hudson, P. J. (2005). Engineered antibody fragments and the rise of single domains. *Nat Biotechnol*, 23(9), 1126-1136. doi:10.1038/nbt1142
- Horiuchi, M., Karino, A., Furuoka, H., Ishiguro, N., Kimura, K., & Shinagawa, M. (2009). Generation of monoclonal antibody that distinguishes PrP^{Sc} from PrP^C and neutralizes prion infectivity. *Virology*, 394(2), 200-207. doi:10.1016/j.virol.2009.08.025
- Houston, F., & Andreoletti, O. (2019). Animal prion diseases: the risks to human health. *Brain Pathol*, 29(2), 248-262. doi:10.1111/bpa.12696
- Hoyt, F., Standke, H. G., Artikis, E., Schwartz, C. L., Hansen, B., Li, K., . . . Kraus, A. (2022). Cryo-EM structure of anchorless RML prion reveals variations in shared motifs between distinct strains. *Nat Commun*, 13(1), 4005. doi:10.1038/s41467-022-30458-6
- Huang, Z., Gabriel, J. M., Baldwin, M. A., Fletterick, R. J., Prusiner, S. B., & Cohen, F. E. (1994). Proposed three-dimensional structure for the cellular prion protein. *Proc Natl Acad Sci U S A*, 91(15), 7139-7143. doi:10.1073/pnas.91.15.7139
- Huston, J. S., Levinson, D., Mudgett-Hunter, M., Tai, M. S., Novotny, J., Margolies, M. N., . . . et al. (1988). Protein engineering of antibody binding sites: recovery of specific activity in an anti-digoxin single-chain Fv analogue produced in *Escherichia coli*. *Proc Natl Acad Sci U S A*, 85(16), 5879-5883. doi:10.1073/pnas.85.16.5879
- Jankovska, N., Rusina, R., Bruzova, M., Parobkova, E., Olejar, T., & Matej, R. (2021). Human Prion Disorders: Review of the Current Literature and a Twenty-Year Experience of the National Surveillance Center in the Czech Republic. *Diagnostics (Basel)*, 11(10). doi:10.3390/diagnostics11101821
- Jeffrey, M., Martin, S., Gonzalez, L., Ryder, S. J., Bellworthy, S. J., & Jackman, R. (2001). Differential diagnosis of infections with the bovine spongiform encephalopathy (BSE) and scrapie agents in sheep. *J Comp Pathol*, 125(4), 271-284. doi:10.1053/jcpa.2001.0499

- Johnson, G., & Wu, T. T. (1997). A method of estimating the numbers of human and mouse T cell receptors for antigen alpha and beta chain V-genes. *Immunol Cell Biol*, 75(6), 580-583. doi:10.1038/icb.1997.90
- Jones, M., Wight, D., McLoughlin, V., Norrby, K., Ironside, J. W., Connolly, J. G., . . . Head, M. W. (2009). An antibody to the aggregated synthetic prion protein peptide (PrP106-126) selectively recognizes disease-associated prion protein (PrP) from human brain specimens. *Brain Pathol*, 19(2), 293-302. doi:10.1111/j.1750-3639.2008.00181.x
- Jones, P. T., Dear, P. H., Foote, J., Neuberger, M. S., & Winter, G. (1986). Replacing the complementarity-determining regions in a human antibody with those from a mouse. *Nature*, 321(6069), 522-525. doi:10.1038/321522a0
- Jorgensen, W. L., & Tirado-Rives, J. (1988). The OPLS [optimized potentials for liquid simulations] potential functions for proteins, energy minimizations for crystals of cyclic peptides and crambin. *J Am Chem Soc*, 110(6), 1657-1666. doi:10.1021/ja00214a001
- Kajava, A. V., Baxa, U., & Steven, A. C. (2010). Beta arcades: recurring motifs in naturally occurring and disease-related amyloid fibrils. *FASEB J*, 24(5), 1311-1319. doi:10.1096/fj.09-145979
- Kajava, A. V., & Steven, A. C. (2006a). Beta-rolls, beta-helices, and other beta-solenoid proteins. *Adv Protein Chem*, 73, 55-96. doi:10.1016/S0065-3233(06)73003-0
- Kajava, A. V., & Steven, A. C. (2006b). The turn of the screw: variations of the abundant beta-solenoid motif in passenger domains of Type V secretory proteins. *J Struct Biol*, 155(2), 306-315. doi:10.1016/j.jsb.2006.01.015
- Kalman, J., Jardanhazy, T., Cserhati, A., Szekeres, G., Demeter, I., Berek, I., . . . Janka, Z. (1997). [Prion dementias: nosology and diagnostic difficulties in the spectrum of Creutzfeldt-Jakob encephalopathy]. *Orv Hetil*, 138(12), 731-737. Retrieved from <https://www.ncbi.nlm.nih.gov/pubmed/9157343>
- Kamali-Jamil, R., Vazquez-Fernandez, E., Tancowny, B., Rathod, V., Amidian, S., Wang, X., . . . Wille, H. (2021). The ultrastructure of infectious L-type bovine spongiform encephalopathy prions constrains molecular models. *PLoS Pathog*, 17(6), e1009628. doi:10.1371/journal.ppat.1009628
- Kaneko, K., Ball, H. L., Wille, H., Zhang, H., Groth, D., Torchia, M., . . . Cohen, F. E. (2000). A synthetic peptide initiates Gerstmann-Straussler-Scheinker (GSS) disease in transgenic mice. *J Mol Biol*, 295(4), 997-1007. doi:10.1006/jmbi.1999.3386
- Kaneko, K., Peretz, D., Pan, K. M., Blochberger, T. C., Wille, H., Gabizon, R., . . . Prusiner, S. B. (1995). Prion protein (PrP) synthetic peptides induce cellular PrP to acquire properties of the scrapie isoform. *Proc Natl Acad Sci U S A*, 92(24), 11160-11164. doi:10.1073/pnas.92.24.11160
- Kanyo, Z. F., Pan, K. M., Williamson, R. A., Burton, D. R., Prusiner, S. B., Fletterick, R. J., & Cohen, F. E. (1999). Antibody binding defines a structure for an epitope that participates in the PrP^C→PrP^{Sc} conformational change. *J Mol Biol*, 293(4), 855-863. doi:10.1006/jmbi.1999.3193
- Kascsak, R. J., Rubenstein, R., Merz, P. A., Tonna-DeMasi, M., Fersko, R., Carp, R. I., . . . Dinger, H. (1987). Mouse polyclonal and monoclonal antibody to scrapie-associated fibril proteins. *J Virol*, 61(12), 3688-3693. Retrieved from <https://www.ncbi.nlm.nih.gov/pubmed/2446004>
- Kayed, R., & Lasagna-Reeves, C. A. (2013). Molecular mechanisms of amyloid oligomers toxicity. *J Alzheimers Dis*, 33 Suppl 1, S67-78. doi:10.3233/JAD-2012-129001

- Kearney, J. F., Radbruch, A., Liesegang, B., & Rajewsky, K. (1979). A new mouse myeloma cell line that has lost immunoglobulin expression but permits the construction of antibody-secreting hybrid cell lines. *J Immunol*, *123*(4), 1548-1550. Retrieved from <https://www.ncbi.nlm.nih.gov/pubmed/113458>
- Kelley, L. A., Mezulis, S., Yates, C. M., Wass, M. N., & Sternberg, M. J. (2015). The Phyre2 web portal for protein modeling, prediction and analysis. *Nat Protoc*, *10*(6), 845-858. doi:10.1038/nprot.2015.053
- Kelly, S. M., Jess, T. J., & Price, N. C. (2005). How to study proteins by circular dichroism. *Biochim Biophys Acta*, *1751*(2), 119-139. doi:10.1016/j.bbapap.2005.06.005
- Kim, S. J., Park, Y., & Hong, H. J. (2005). Antibody engineering for the development of therapeutic antibodies. *Mol Cells*, *20*(1), 17-29. Retrieved from <https://www.ncbi.nlm.nih.gov/pubmed/16258237>
<https://www.molcells.org/journal/view.html?year=2005&volume=20&number=1&spage=17>
- Kimberlin, R. H., Cole, S., & Walker, C. A. (1987). Temporary and permanent modifications to a single strain of mouse scrapie on transmission to rats and hamsters. *J Gen Virol*, *68* (Pt 7), 1875-1881. doi:10.1099/0022-1317-68-7-1875
- Kipriyanov, S. M., & Le Gall, F. (2004). Generation and production of engineered antibodies. *Mol Biotechnol*, *26*(1), 39-60. doi:10.1385/MB:26:1:39
- Kohler, G., & Milstein, C. (1975). Continuous cultures of fused cells secreting antibody of predefined specificity. *Nature*, *256*(5517), 495-497. doi:10.1038/256495a0
- Korth, C., Stierli, B., Streit, P., Moser, M., Schaller, O., Fischer, R., . . . Oesch, B. (1997). Prion (PrP^{Sc})-specific epitope defined by a monoclonal antibody. *Nature*, *390*(6655), 74-77. doi:10.1038/36337
- Korth, C., Streit, P., & Oesch, B. (1999). Monoclonal antibodies specific for the native, disease-associated isoform of the prion protein. *Methods Enzymol*, *309*, 106-122. doi:10.1016/s0076-6879(99)09010-2
- Kosmac, M., Koren, S., Giachin, G., Stoilova, T., Gennaro, R., Legname, G., & Serbec, V. C. (2011). Epitope mapping of a PrP(Sc)-specific monoclonal antibody: identification of a novel C-terminally truncated prion fragment. *Mol Immunol*, *48*(5), 746-750. doi:10.1016/j.molimm.2010.11.012
- Kotlan, B., & Glassy, M. C. (2009). Antibody phage display: overview of a powerful technology that has quickly translated to the clinic. *Methods Mol Biol*, *562*, 1-15. doi:10.1007/978-1-60327-302-2_1
- Kraus, A., Hoyt, F., Schwartz, C. L., Hansen, B., Artakis, E., Hughson, A. G., . . . Caughey, B. (2021). High-resolution structure and strain comparison of infectious mammalian prions. *Mol Cell*, *81*(21), 4540-4551 e4546. doi:10.1016/j.molcel.2021.08.011
- Kreeger, T. J., Montgomery, D. L., Jewell, J. E., Schultz, W., & Williams, E. S. (2006). Oral transmission of chronic wasting disease in captive Shira's moose. *J Wildl Dis*, *42*(3), 640-645. doi:10.7589/0090-3558-42.3.640
- Lagnel, J., Tsigenopoulos, C. S., & Iliopoulos, I. (2009). NOBLAST and JAMBLAST: New Options for BLAST and a Java Application Manager for BLAST results. *Bioinformatics*, *25*(6), 824-826. doi:10.1093/bioinformatics/btp067
- Leffers, K. W., Wille, H., Stohr, J., Junger, E., Prusiner, S. B., & Riesner, D. (2005). Assembly of natural and recombinant prion protein into fibrils. *Biol Chem*, *386*(6), 569-580. doi:10.1515/BC.2005.067

- Lefranc, M. P. (2014). Antibody Informatics: IMGT, the International ImMunoGeneTics Information System. *Microbiol Spectr*, 2(2). doi:10.1128/microbiolspec.AID-0001-2012
- Legname, G., Baskakov, I. V., Nguyen, H. O., Riesner, D., Cohen, F. E., DeArmond, S. J., & Prusiner, S. B. (2004). Synthetic mammalian prions. *Science*, 305(5684), 673-676. doi:10.1126/science.1100195
- Levine, D. J., Stohr, J., Falese, L. E., Ollesch, J., Wille, H., Prusiner, S. B., & Long, J. R. (2015). Mechanism of scrapie prion precipitation with phosphotungstate anions. *ACS Chem Biol*, 10(5), 1269-1277. doi:10.1021/cb5006239
- Liberski, P. P. (2013). Kuru: a journey back in time from papua new Guinea to the neanderthals' extinction. *Pathogens*, 2(3), 472-505. doi:10.3390/pathogens2030472
- Lindell, B. (1985). [Prion antibodies and structure analysis clarify questions about atypical viruses. Prion structure under the electron microscope]. *Lakartidningen*, 82(6), 406-409. Retrieved from <https://www.ncbi.nlm.nih.gov/pubmed/3920456>
- Linsenmeier, L., Mohammadi, B., Wetzel, S., Puig, B., Jackson, W. S., Hartmann, A., . . . Altmepfen, H. C. (2018). Structural and mechanistic aspects influencing the ADAM10-mediated shedding of the prion protein. *Mol Neurodegener*, 13(1), 18. doi:10.1186/s13024-018-0248-6
- Liu, J., Huang, H. L., & Jiang, S. D. (2002). [Antibody phage display technology: realities approaching to the dream]. *Yi Chuan*, 24(1), 94-99. Retrieved from <https://www.ncbi.nlm.nih.gov/pubmed/15901572>
- Lugaresi, E., Medori, R., Montagna, P., Baruzzi, A., Cortelli, P., Lugaresi, A., . . . Gambetti, P. (1986). Fatal familial insomnia and dysautonomia with selective degeneration of thalamic nuclei. *N Engl J Med*, 315(16), 997-1003. doi:10.1056/NEJM198610163151605
- Ma, Y., & Ma, J. (2020). Immunotherapy against Prion Disease. *Pathogens*, 9(3). doi:10.3390/pathogens9030216
- Manix, M., Kalakoti, P., Henry, M., Thakur, J., Menger, R., Guthikonda, B., & Nanda, A. (2015). Creutzfeldt-Jakob disease: updated diagnostic criteria, treatment algorithm, and the utility of brain biopsy. *Neurosurg Focus*, 39(5), E2. doi:10.3171/2015.8.FOCUS15328
- Manka, S. W., Wenborn, A., Betts, J., Joiner, S., Saibil, H. R., Collinge, J., & Wadsworth, J. D. F. (2022). A structural basis for prion strain diversity. *bioRxiv*, 2022.2005.2017.492259. doi:10.1101/2022.05.17.492259
- Manka, S. W., Wenborn, A., Collinge, J., & Wadsworth, J. D. F. (2022). Prion strains viewed through the lens of cryo-EM. *Cell Tissue Res*. doi:10.1007/s00441-022-03676-z
- Manka, S. W., Zhang, W., Wenborn, A., Betts, J., Joiner, S., Saibil, H. R., . . . Wadsworth, J. D. F. (2022). 2.7 A cryo-EM structure of ex vivo RML prion fibrils. *Nat Commun*, 13(1), 4004. doi:10.1038/s41467-022-30457-7
- Marks, J. D., Hoogenboom, H. R., Bonnert, T. P., McCafferty, J., Griffiths, A. D., & Winter, G. (1991). By-passing immunization. Human antibodies from V-gene libraries displayed on phage. *J Mol Biol*, 222(3), 581-597. doi:10.1016/0022-2836(91)90498-u
- Martin, A. C. (1996). Accessing the Kabat antibody sequence database by computer. *Proteins*, 25(1), 130-133. doi:10.1002/(SICI)1097-0134(199605)25:1<130::AID-PROT11>3.0.CO;2-L
- Mathiason, C. K., Hays, S. A., Powers, J., Hayes-Klug, J., Langenberg, J., Dahmes, S. J., . . . Hoover, E. A. (2009). Infectious prions in pre-clinical deer and transmission of chronic

- wasting disease solely by environmental exposure. *PLoS One*, 4(6), e5916. doi:10.1371/journal.pone.0005916
- Mathiason, C. K., Powers, J. G., Dahmes, S. J., Osborn, D. A., Miller, K. V., Warren, R. J., . . . Hoover, E. A. (2006). Infectious prions in the saliva and blood of deer with chronic wasting disease. *Science*, 314(5796), 133-136. doi:10.1126/science.1132661
- McBride, P. A., Schulz-Schaeffer, W. J., Donaldson, M., Bruce, M., Diringer, H., Kretzschmar, H. A., & Beekes, M. (2001). Early spread of scrapie from the gastrointestinal tract to the central nervous system involves autonomic fibers of the splanchnic and vagus nerves. *J Virol*, 75(19), 9320-9327. doi:10.1128/JVI.75.19.9320-9327.2001
- McCutcheon, S., Langeveld, J. P., Tan, B. C., Gill, A. C., de Wolf, C., Martin, S., . . . Houston, E. F. (2014). Prion protein-specific antibodies that detect multiple TSE agents with high sensitivity. *PLoS One*, 9(3), e91143. doi:10.1371/journal.pone.0091143
- McKinley, M. P., Taraboulos, A., Kenaga, L., Serban, D., Stieber, A., DeArmond, S. J., . . . Gonatas, N. (1991). Ultrastructural localization of scrapie prion proteins in cytoplasmic vesicles of infected cultured cells. *Lab Invest*, 65(6), 622-630. Retrieved from <https://www.ncbi.nlm.nih.gov/pubmed/1684401>
- Mead, S., Khalili-Shirazi, A., Potter, C., Mok, T., Nihat, A., Hyare, H., . . . Collinge, J. (2022). Prion protein monoclonal antibody (PRN100) therapy for Creutzfeldt-Jakob disease: evaluation of a first-in-human treatment programme. *Lancet Neurol*, 21(4), 342-354. doi:10.1016/S1474-4422(22)00082-5
- Mead, S., Stumpf, M. P., Whitfield, J., Beck, J. A., Poulter, M., Campbell, T., . . . Collinge, J. (2003). Balancing selection at the prion protein gene consistent with prehistoric kurulike epidemics. *Science*, 300(5619), 640-643. doi:10.1126/science.1083320
- Medori, R., Tritschler, H. J., LeBlanc, A., Villare, F., Manetto, V., Chen, H. Y., . . . et al. (1992). Fatal familial insomnia, a prion disease with a mutation at codon 178 of the prion protein gene. *N Engl J Med*, 326(7), 444-449. doi:10.1056/NEJM199202133260704
- Mercer, R. C. C., Daude, N., Dorosh, L., Fu, Z. L., Mays, C. E., Gapeshina, H., . . . Westaway, D. (2018). A novel Gerstmann-Straussler-Scheinker disease mutation defines a precursor for amyloidogenic 8 kDa PrP fragments and reveals N-terminal structural changes shared by other GSS alleles. *PLoS Pathog*, 14(1), e1006826. doi:10.1371/journal.ppat.1006826
- Mercer, R. C. C., & Harris, D. A. (2022). Mechanisms of prion-induced toxicity. *Cell Tissue Res*. doi:10.1007/s00441-022-03683-0
- Miller, G. (2009). Neurodegeneration. Could they all be prion diseases? *Science*, 326(5958), 1337-1339. doi:10.1126/science.326.5958.1337
- Miller, M. W., & Wild, M. A. (2004). Epidemiology of chronic wasting disease in captive white-tailed and mule deer. *J Wildl Dis*, 40(2), 320-327. doi:10.7589/0090-3558-40.2.320
- Milstein, C. (2000). With the benefit of hindsight. *Immunol Today*, 21(8), 359-364. doi:10.1016/s0167-5699(00)01660-1
- Mitchell, G. B., Sigurdson, C. J., O'Rourke, K. I., Algire, J., Harrington, N. P., Walther, I., . . . Balachandran, A. (2012). Experimental oral transmission of chronic wasting disease to reindeer (*Rangifer tarandus tarandus*). *PLoS One*, 7(6), e39055. doi:10.1371/journal.pone.0039055
- Mitra, D., Amaratunga, C., Sutherns, R., Pletsch, V., Corneil, W., Crowe, S., & Krewski, D. (2009). The psychosocial and socioeconomic consequences of bovine spongiform encephalopathy (BSE): a community impact study. *J Toxicol Environ Health A*, 72(17-18), 1106-1112. doi:10.1080/15287390903084637

- Mohammadi, B., Song, F., Matamoros-Angles, A., Shafiq, M., Damme, M., Puig, B., . . . Altmeppen, H. C. (2022). Anchorless risk or released benefit? An updated view on the ADAM10-mediated shedding of the prion protein. *Cell Tissue Res*. doi:10.1007/s00441-022-03582-4
- Moon, A. F., Krahn, J. M., Lu, X., Cuneo, M. J., & Pedersen, L. C. (2016). Structural characterization of the virulence factor SdaI nuclease from *Streptococcus pyogenes*. *Nucleic Acids Res*, *44*(8), 3946-3957. doi:10.1093/nar/gkw143
- Morrison, S. L., Johnson, M. J., Herzenberg, L. A., & Oi, V. T. (1984). Chimeric human antibody molecules: mouse antigen-binding domains with human constant region domains. *Proc Natl Acad Sci U S A*, *81*(21), 6851-6855. doi:10.1073/pnas.81.21.6851
- Movaghar Asareh, S., Savei, T., Arjmand, S., Ranaei Siadat, S. O., Fatemi, F., Pourmadadi, M., & Shabani Shayeh, J. (2022). Expression of functional eGFP-fused antigen-binding fragment of ranibizumab in *Pichia pastoris*. *Bioimpacts*, *12*(3), 203-210. doi:10.34172/bi.2021.23219
- Naslavsky, N., Stein, R., Yanai, A., Friedlander, G., & Taraboulos, A. (1997). Characterization of detergent-insoluble complexes containing the cellular prion protein and its scrapie isoform. *J Biol Chem*, *272*(10), 6324-6331. doi:10.1074/jbc.272.10.6324
- Nazor, K. E., Kuhn, F., Seward, T., Green, M., Zwald, D., Purro, M., . . . Telling, G. C. (2005). Immunodetection of disease-associated mutant PrP, which accelerates disease in GSS transgenic mice. *EMBO J*, *24*(13), 2472-2480. doi:10.1038/sj.emboj.7600717
- Nguyen, J., Baldwin, M. A., Cohen, F. E., & Prusiner, S. B. (1995). Prion protein peptides induce alpha-helix to beta-sheet conformational transitions. *Biochemistry*, *34*(13), 4186-4192. doi:10.1021/bi00013a006
- Nonno, R., Di Bari, M. A., Cardone, F., Vaccari, G., Fazzi, P., Dell'Omo, G., . . . Agrimi, U. (2006). Efficient transmission and characterization of Creutzfeldt-Jakob disease strains in bank voles. *PLoS Pathog*, *2*(2), e12. doi:10.1371/journal.ppat.0020012
- Oesch, B., Westaway, D., Walchli, M., McKinley, M. P., Kent, S. B., Aebersold, R., . . . et al. (1985). A cellular gene encodes scrapie PrP 27-30 protein. *Cell*, *40*(4), 735-746. doi:10.1016/0092-8674(85)90333-2
- Oostindie, S. C., Lazar, G. A., Schuurman, J., & Parren, P. (2022). Avidity in antibody effector functions and biotherapeutic drug design. *Nat Rev Drug Discov*. doi:10.1038/s41573-022-00501-8
- Orru, C. D., Favole, A., Corona, C., Mazza, M., Manca, M., Groveman, B. R., . . . Caughey, B. (2015). Detection and discrimination of classical and atypical L-type bovine spongiform encephalopathy by real-time quaking-induced conversion. *J Clin Microbiol*, *53*(4), 1115-1120. doi:10.1128/JCM.02906-14
- Orru, C. D., Groveman, B. R., Hughson, A. G., Zanusso, G., Coulthart, M. B., & Caughey, B. (2015). Rapid and sensitive RT-QuIC detection of human Creutzfeldt-Jakob disease using cerebrospinal fluid. *mBio*, *6*(1). doi:10.1128/mBio.02451-14
- Pan, K. M., Baldwin, M., Nguyen, J., Gasset, M., Serban, A., Groth, D., . . . et al. (1993). Conversion of alpha-helices into beta-sheets features in the formation of the scrapie prion proteins. *Proc Natl Acad Sci U S A*, *90*(23), 10962-10966. doi:10.1073/pnas.90.23.10962
- Parchi, P., Chen, S. G., Brown, P., Zou, W., Capellari, S., Budka, H., . . . Gambetti, P. (1998). Different patterns of truncated prion protein fragments correlate with distinct phenotypes in P102L Gerstmann-Straussler-Scheinker disease. *Proc Natl Acad Sci U S A*, *95*(14), 8322-8327. doi:10.1073/pnas.95.14.8322

- Pardridge, W. M. (2015). Blood-brain barrier drug delivery of IgG fusion proteins with a transferrin receptor monoclonal antibody. *Expert Opin Drug Deliv*, *12*(2), 207-222. doi:10.1517/17425247.2014.952627
- Pardridge, W. M., & Boado, R. J. (2012). Reengineering biopharmaceuticals for targeted delivery across the blood-brain barrier. *Methods Enzymol*, *503*, 269-292. doi:10.1016/B978-0-12-396962-0.00011-2
- Paul, P. S., Cho, J. Y., Wu, Q., Karthivashan, G., Grabovac, E., Wille, H., . . . Kar, S. (2022). Unconjugated PLGA nanoparticles attenuate temperature-dependent beta-amyloid aggregation and protect neurons against toxicity: implications for Alzheimer's disease pathology. *J Nanobiotechnology*, *20*(1), 67. doi:10.1186/s12951-022-01269-0
- Peden, A. H., Head, M. W., Ritchie, D. L., Bell, J. E., & Ironside, J. W. (2004). Preclinical vCJD after blood transfusion in a PRNP codon 129 heterozygous patient. *Lancet*, *364*(9433), 527-529. doi:10.1016/S0140-6736(04)16811-6
- Peretz, D., Williamson, R. A., Matsunaga, Y., Serban, H., Pinilla, C., Bastidas, R. B., . . . Burton, D. R. (1997). A conformational transition at the N terminus of the prion protein features in formation of the scrapie isoform. *J Mol Biol*, *273*(3), 614-622. doi:10.1006/jmbi.1997.1328
- Pettersen, E. F., Goddard, T. D., Huang, C. C., Couch, G. S., Greenblatt, D. M., Meng, E. C., & Ferrin, T. E. (2004). UCSF Chimera--a visualization system for exploratory research and analysis. *J Comput Chem*, *25*(13), 1605-1612. doi:10.1002/jcc.20084
- Pirisinu, L., Di Bari, M. A., D'Agostino, C., Marcon, S., Riccardi, G., Poleggi, A., . . . Nonno, R. (2016). Gerstmann-Straussler-Scheinker disease subtypes efficiently transmit in bank voles as genuine prion diseases. *Sci Rep*, *6*, 20443. doi:10.1038/srep20443
- Pirisinu, L., Nonno, R., Esposito, E., Benestad, S. L., Gambetti, P., Agrimi, U., & Zou, W. Q. (2013). Small ruminant nor98 prions share biochemical features with human gerstmann-straussler-scheinker disease and variably protease-sensitive prionopathy. *PLoS One*, *8*(6), e66405. doi:10.1371/journal.pone.0066405
- Poljak, R. J., Amzel, L. M., Chen, B. L., Phizackerley, R. P., & Saul, F. (1975). Structure and specificity of antibody molecules. *Philos Trans R Soc Lond B Biol Sci*, *272*(915), 43-51. doi:10.1098/rstb.1975.0069
- Polymenidou, M., Heppner, F. L., Pelliccioli, E. C., Urich, E., Miele, G., Braun, N., . . . Aguzzi, A. (2004). Humoral immune response to native eukaryotic prion protein correlates with anti-prion protection. *Proc Natl Acad Sci U S A*, *101* Suppl 2, 14670-14676. doi:10.1073/pnas.0404772101
- Polymenidou, M., Moos, R., Scott, M., Sigurdson, C., Shi, Y. Z., Yajima, B., . . . Aguzzi, A. (2008). The POM monoclonals: a comprehensive set of antibodies to non-overlapping prion protein epitopes. *PLoS One*, *3*(12), e3872. doi:10.1371/journal.pone.0003872
- Porter, D. D., Porter, H. G., & Cox, N. A. (1973). Failure to demonstrate a humoral immune response to scrapie infection in mice. *J Immunol*, *111*(5), 1407-1410. Retrieved from <https://www.ncbi.nlm.nih.gov/pubmed/4200779>
- Prusiner, S. B. (1982). Novel proteinaceous infectious particles cause scrapie. *Science*, *216*(4542), 136-144. doi:10.1126/science.6801762
- Prusiner, S. B. (1998a). The prion diseases. *Brain Pathol*, *8*(3), 499-513. Retrieved from <https://www.ncbi.nlm.nih.gov/pubmed/9669700>
- Prusiner, S. B. (1998b). Prions. *Proc Natl Acad Sci U S A*, *95*(23), 13363-13383. doi:10.1073/pnas.95.23.13363

- Prusiner, S. B., Bolton, D. C., Groth, D. F., Bowman, K. A., Cochran, S. P., & McKinley, M. P. (1982). Further purification and characterization of scrapie prions. *Biochemistry*, *21*(26), 6942-6950. doi:10.1021/bi00269a050
- Prusiner, S. B., Groth, D., Serban, A., Koehler, R., Foster, D., Torchia, M., . . . DeArmond, S. J. (1993). Ablation of the prion protein (PrP) gene in mice prevents scrapie and facilitates production of anti-PrP antibodies. *Proc Natl Acad Sci U S A*, *90*(22), 10608-10612. doi:10.1073/pnas.90.22.10608
- Prusiner, S. B., Groth, D. F., Cochran, S. P., Masiarz, F. R., McKinley, M. P., & Martinez, H. M. (1980). Molecular properties, partial purification, and assay by incubation period measurements of the hamster scrapie agent. *Biochemistry*, *19*(21), 4883-4891. doi:10.1021/bi00562a028
- Prusiner, S. B., McKinley, M. P., Bowman, K. A., Bolton, D. C., Bendheim, P. E., Groth, D. F., & Glenner, G. G. (1983). Scrapie prions aggregate to form amyloid-like birefringent rods. *Cell*, *35*(2 Pt 1), 349-358. doi:10.1016/0092-8674(83)90168-x
- Ravn, U., Gueneau, F., Baerlocher, L., Osteras, M., Desmurs, M., Malinge, P., . . . Fischer, N. (2010). By-passing in vitro screening--next generation sequencing technologies applied to antibody display and in silico candidate selection. *Nucleic Acids Res*, *38*(21), e193. doi:10.1093/nar/gkq789
- Reimann, R. R., Sonati, T., Hornemann, S., Herrmann, U. S., Arand, M., Hawke, S., & Aguzzi, A. (2016). Differential Toxicity of Antibodies to the Prion Protein. *PLoS Pathog*, *12*(1), e1005401. doi:10.1371/journal.ppat.1005401
- Riechmann, L., Clark, M., Waldmann, H., & Winter, G. (1988). Reshaping human antibodies for therapy. *Nature*, *332*(6162), 323-327. doi:10.1038/332323a0
- Riek, R., Hornemann, S., Wider, G., Glockshuber, R., & Wuthrich, K. (1997). NMR characterization of the full-length recombinant murine prion protein, mPrP(23-231). *FEBS Lett*, *413*(2), 282-288. doi:10.1016/s0014-5793(97)00920-4
- Ritchie, D. L., Peden, A. H., & Barria, M. A. (2021). Variant CJD: Reflections a Quarter of a Century on. *Pathogens*, *10*(11). doi:10.3390/pathogens10111413
- Rivera, N. A., Brandt, A. L., Novakofski, J. E., & Mateus-Pinilla, N. E. (2019). Chronic Wasting Disease In Cervids: Prevalence, Impact And Management Strategies. *Vet Med (Auckl)*, *10*, 123-139. doi:10.2147/VMRR.S197404
- Rubenstein, R., Kascsak, R. J., Merz, P. A., Papini, M. C., Carp, R. I., Robakis, N. K., & Wisniewski, H. M. (1986). Detection of scrapie-associated fibril (SAF) proteins using anti-SAF antibody in non-purified tissue preparations. *J Gen Virol*, *67* (Pt 4), 671-681. doi:10.1099/0022-1317-67-4-671
- Saborio, G. P., Permanne, B., & Soto, C. (2001). Sensitive detection of pathological prion protein by cyclic amplification of protein misfolding. *Nature*, *411*(6839), 810-813. doi:10.1038/35081095
- Safar, J., Wille, H., Itri, V., Groth, D., Serban, H., Torchia, M., . . . Prusiner, S. B. (1998). Eight prion strains have PrP(Sc) molecules with different conformations. *Nat Med*, *4*(10), 1157-1165. doi:10.1038/2654
- Sala, C., Morignat, E., Oussaid, N., Gay, E., Abrial, D., Ducrot, C., & Calavas, D. (2012). Individual factors associated with L- and H-type Bovine Spongiform encephalopathy in France. *BMC Vet Res*, *8*, 74. doi:10.1186/1746-6148-8-74

- Sanz-Hernandez, M., Barritt, J. D., Sobek, J., Hornemann, S., Aguzzi, A., & De Simone, A. (2021). Mechanism of misfolding of the human prion protein revealed by a pathological mutation. *Proc Natl Acad Sci U S A*, *118*(12). doi:10.1073/pnas.2019631118
- Schenk, D. B., Rydel, R. E., May, P., Little, S., Panetta, J., Lieberburg, I., & Sinha, S. (1995). Therapeutic approaches related to amyloid-beta peptide and Alzheimer's disease. *J Med Chem*, *38*(21), 4141-4154. doi:10.1021/jm00021a001
- Schumacher, D., Helma, J., Schneider, A. F. L., Leonhardt, H., & Hackenberger, C. P. R. (2018). Nanobodies: Chemical Functionalization Strategies and Intracellular Applications. *Angew Chem Int Ed Engl*, *57*(9), 2314-2333. doi:10.1002/anie.201708459
- Selvaggini, C., De Gioia, L., Cantu, L., Ghibaudi, E., Diomede, L., Passerini, F., . . . Salmona, M. (1993). Molecular characteristics of a protease-resistant, amyloidogenic and neurotoxic peptide homologous to residues 106-126 of the prion protein. *Biochem Biophys Res Commun*, *194*(3), 1380-1386. doi:10.1006/bbrc.1993.1977
- Senatore, A., Frontzek, K., Emmenegger, M., Chincisan, A., Losa, M., Reimann, R., . . . Aguzzi, A. (2020). Protective anti-prion antibodies in human immunoglobulin repertoires. *EMBO Mol Med*, *12*(9), e12739. doi:10.15252/emmm.202012739
- Shafiei, S. S., Guerrero-Munoz, M. J., & Castillo-Carranza, D. L. (2017). Tau Oligomers: Cytotoxicity, Propagation, and Mitochondrial Damage. *Front Aging Neurosci*, *9*, 83. doi:10.3389/fnagi.2017.00083
- Shimizu, Y., Kaku-Ushiki, Y., Iwamaru, Y., Muramoto, T., Kitamoto, T., Yokoyama, T., . . . Tagawa, Y. (2010). A novel anti-prion protein monoclonal antibody and its single-chain fragment variable derivative with ability to inhibit abnormal prion protein accumulation in cultured cells. *Microbiol Immunol*, *54*(2), 112-121. doi:10.1111/j.1348-0421.2009.00190.x
- Sigurdson, C. J., Barillas-Mury, C., Miller, M. W., Oesch, B., van Keulen, L. J. M., Langeveld, J. P. M., & Hoover, E. A. (2002). PrP(CWD) lymphoid cell targets in early and advanced chronic wasting disease of mule deer. *J Gen Virol*, *83*(Pt 10), 2617-2628. doi:10.1099/0022-1317-83-10-2617
- Sigurdson, C. J., Spraker, T. R., Miller, M. W., Oesch, B., & Hoover, E. A. (2001). PrP(CWD) in the myenteric plexus, vagosympathetic trunk and endocrine glands of deer with chronic wasting disease. *J Gen Virol*, *82*(Pt 10), 2327-2334. doi:10.1099/0022-1317-82-10-2327
- Sigurdson, C. J., Williams, E. S., Miller, M. W., Spraker, T. R., O'Rourke, K. I., & Hoover, E. A. (1999). Oral transmission and early lymphoid tropism of chronic wasting disease PrPres in mule deer fawns (*Odocoileus hemionus*). *J Gen Virol*, *80* (Pt 10), 2757-2764. doi:10.1099/0022-1317-80-10-2757
- Sigurdsson, E. M., Sy, M. S., Li, R., Scholtzova, H., Kascsak, R. J., Kascsak, R., . . . Wisniewski, T. (2003). Anti-prion antibodies for prophylaxis following prion exposure in mice. *Neurosci Lett*, *336*(3), 185-187. doi:10.1016/s0304-3940(02)01192-8
- Sikorska, B., Knight, R., Ironside, J. W., & Liberski, P. P. (2012). Creutzfeldt-Jakob disease. *Adv Exp Med Biol*, *724*, 76-90. doi:10.1007/978-1-4614-0653-2_6
- Sim, V. L., & Caughey, B. (2009). Ultrastructures and strain comparison of under-glycosylated scrapie prion fibrils. *Neurobiol Aging*, *30*(12), 2031-2042. doi:10.1016/j.neurobiolaging.2008.02.016
- Simmons, L. C., Reilly, D., Klimowski, L., Raju, T. S., Meng, G., Sims, P., . . . Yansura, D. G. (2002). Expression of full-length immunoglobulins in *Escherichia coli*: rapid and

- efficient production of aglycosylated antibodies. *J Immunol Methods*, 263(1-2), 133-147. doi:10.1016/s0022-1759(02)00036-4
- Skrlj, N., Drevensek, G., Hudoklin, S., Romih, R., Curin Serbec, V., & Dolinar, M. (2013). Recombinant single-chain antibody with the Trojan peptide penetratin positioned in the linker region enables cargo transfer across the blood-brain barrier. *Appl Biochem Biotechnol*, 169(1), 159-169. doi:10.1007/s12010-012-9962-7
- Skrlj, N., Serbec, V. C., & Dolinar, M. (2010). Single-chain Fv antibody fragments retain binding properties of the monoclonal antibody raised against peptide P1 of the human prion protein. *Appl Biochem Biotechnol*, 160(6), 1808-1821. doi:10.1007/s12010-009-8699-4
- Sonati, T., Reimann, R. R., Falsig, J., Baral, P. K., O'Connor, T., Hornemann, S., . . . Aguzzi, A. (2013). The toxicity of antiprion antibodies is mediated by the flexible tail of the prion protein. *Nature*, 501(7465), 102-106. doi:10.1038/nature12402
- Sondergaard, C. R., Olsson, M. H., Rostkowski, M., & Jensen, J. H. (2011). Improved Treatment of Ligands and Coupling Effects in Empirical Calculation and Rationalization of pKa Values. *J Chem Theory Comput*, 7(7), 2284-2295. doi:10.1021/ct200133y
- Soto, C. (2003). Unfolding the role of protein misfolding in neurodegenerative diseases. *Nat Rev Neurosci*, 4(1), 49-60. doi:10.1038/nrn1007
- Spagnoli, G., Rigoli, M., Orioli, S., Sevillano, A. M., Faccioli, P., Wille, H., . . . Requena, J. R. (2019). Full atomistic model of prion structure and conversion. *PLoS Pathog*, 15(7), e1007864. doi:10.1371/journal.ppat.1007864
- Spraker, T. R., Miller, M. W., Williams, E. S., Getzy, D. M., Adrian, W. J., Schoonveld, G. G., . . . Merz, P. A. (1997). Spongiform encephalopathy in free-ranging mule deer (*Odocoileus hemionus*), white-tailed deer (*Odocoileus virginianus*) and Rocky Mountain elk (*Cervus elaphus nelsoni*) in northcentral Colorado. *J Wildl Dis*, 33(1), 1-6. doi:10.7589/0090-3558-33.1.1
- Stahl, N., Baldwin, M. A., Hecker, R., Pan, K. M., Burlingame, A. L., & Prusiner, S. B. (1992). Glycosylinositol phospholipid anchors of the scrapie and cellular prion proteins contain sialic acid. *Biochemistry*, 31(21), 5043-5053. doi:10.1021/bi00136a600
- Stahl, N., Borchelt, D. R., Hsiao, K., & Prusiner, S. B. (1987). Scrapie prion protein contains a phosphatidylinositol glycolipid. *Cell*, 51(2), 229-240. doi:10.1016/0092-8674(87)90150-4
- Stevens, D. J., Walter, E. D., Rodriguez, A., Draper, D., Davies, P., Brown, D. R., & Millhauser, G. L. (2009). Early onset prion disease from octarepeat expansion correlates with copper binding properties. *PLoS Pathog*, 5(4), e1000390. doi:10.1371/journal.ppat.1000390
- Stopschinski, B. E., & Diamond, M. I. (2017). The prion model for progression and diversity of neurodegenerative diseases. *Lancet Neurol*, 16(4), 323-332. doi:10.1016/S1474-4422(17)30037-6
- Supattapone, S., Bosque, P., Muramoto, T., Wille, H., Aagaard, C., Peretz, D., . . . Scott, M. (1999). Prion protein of 106 residues creates an artificial transmission barrier for prion replication in transgenic mice. *Cell*, 96(6), 869-878. doi:10.1016/s0092-8674(00)80596-6
- Suri, C., Fung, B. P., Tischler, A. S., & Chikaraishi, D. M. (1993). Catecholaminergic cell lines from the brain and adrenal glands of tyrosine hydroxylase-SV40 T antigen transgenic mice. *J Neurosci*, 13(3), 1280-1291. Retrieved from <https://www.ncbi.nlm.nih.gov/pubmed/7680068>

- Suter, L., Bruggen, J., & Sorg, C. (1980). Use of an enzyme-linked immunosorbent assay (ELISA) for screening of hybridoma antibodies against cell surface antigens. *J Immunol Methods*, 39(4), 407-411. doi:10.1016/0022-1759(80)90241-0
- Tagliavini, F., Lievens, P. M., Tranchant, C., Warter, J. M., Mohr, M., Giaccone, G., . . . Prelli, F. (2001). A 7-kDa prion protein (PrP) fragment, an integral component of the PrP region required for infectivity, is the major amyloid protein in Gerstmann-Straussler-Scheinker disease A117V. *J Biol Chem*, 276(8), 6009-6015. doi:10.1074/jbc.M007062200
- Taraboulos, A., Jendroska, K., Serban, D., Yang, S. L., DeArmond, S. J., & Prusiner, S. B. (1992). Regional mapping of prion proteins in brain. *Proc Natl Acad Sci U S A*, 89(16), 7620-7624. doi:10.1073/pnas.89.16.7620
- Terry, C., & Wadsworth, J. D. F. (2019). Recent Advances in Understanding Mammalian Prion Structure: A Mini Review. *Front Mol Neurosci*, 12, 169. doi:10.3389/fnmol.2019.00169
- Terry, C., Wenborn, A., Gros, N., Sells, J., Joiner, S., Hosszu, L. L., . . . Wadsworth, J. D. (2016). Ex vivo mammalian prions are formed of paired double helical prion protein fibrils. *Open Biol*, 6(5). doi:10.1098/rsob.160035
- Terry, L. A., Howells, L., Bishop, K., Baker, C. A., Everest, S., Thorne, L., . . . Gough, K. C. (2011). Detection of prions in the faeces of sheep naturally infected with classical scrapie. *Vet Res*, 42, 65. doi:10.1186/1297-9716-42-65
- Thiede, R., Schable, K. F., Bensch, A., Brensing-Kuppers, J., Heim, V., Kirschbaum, T., . . . Zachau, H. G. (1999). The variable genes and gene families of the mouse immunoglobulin kappa locus. *Eur J Immunol*, 29(7), 2072-2081. doi:10.1002/(SICI)1521-4141(199907)29:07<2072::AID-IMMU2072>3.0.CO;2-E
- Tiller, T., Schuster, I., Deppe, D., Siegers, K., Strohner, R., Herrmann, T., . . . Urlinger, S. (2013). A fully synthetic human Fab antibody library based on fixed VH/VL framework pairings with favorable biophysical properties. *MAbs*, 5(3), 445-470. doi:10.4161/mabs.24218
- Tiselius, A., & Kabat, E. A. (1939). An Electrophoretic Study of Immune Sera and Purified Antibody Preparations. *J Exp Med*, 69(1), 119-131. doi:10.1084/jem.69.1.119
- Turk, E., Teplow, D. B., Hood, L. E., & Prusiner, S. B. (1988). Purification and properties of the cellular and scrapie hamster prion proteins. *Eur J Biochem*, 176(1), 21-30. doi:10.1111/j.1432-1033.1988.tb14246.x
- Tycko, R., Savtchenko, R., Ostapchenko, V. G., Makarava, N., & Baskakov, I. V. (2010). The alpha-helical C-terminal domain of full-length recombinant PrP converts to an in-register parallel beta-sheet structure in PrP fibrils: evidence from solid state nuclear magnetic resonance. *Biochemistry*, 49(44), 9488-9497. doi:10.1021/bi1013134
- Uttley, L., Carroll, C., Wong, R., Hilton, D. A., & Stevenson, M. (2020). Creutzfeldt-Jakob disease: a systematic review of global incidence, prevalence, infectivity, and incubation. *Lancet Infect Dis*, 20(1), e2-e10. doi:10.1016/S1473-3099(19)30615-2
- Van Der Spoel, D., Lindahl, E., Hess, B., Groenhof, G., Mark, A. E., & Berendsen, H. J. (2005). GROMACS: fast, flexible, and free. *J Comput Chem*, 26(16), 1701-1718. doi:10.1002/jcc.20291
- Vanni, I., Pirisinu, L., Acevedo-Morantes, C., Kamali-Jamil, R., Rathod, V., Di Bari, M. A., . . . Nonno, R. (2020). Isolation of infectious, non-fibrillar and oligomeric prions from a genetic prion disease. *Brain*, 143(5), 1512-1524. doi:10.1093/brain/awaa078

- Vassallo, N., & Herms, J. (2003). Cellular prion protein function in copper homeostasis and redox signalling at the synapse. *J Neurochem*, *86*(3), 538-544. doi:10.1046/j.1471-4159.2003.01882.x
- Vazquez-Fernandez, E., Alonso, J., Pastrana, M. A., Ramos, A., Stitz, L., Vidal, E., . . . Requena, J. R. (2012). Structural organization of mammalian prions as probed by limited proteolysis. *PLoS One*, *7*(11), e50111. doi:10.1371/journal.pone.0050111
- Vazquez-Fernandez, E., Vos, M. R., Afanasyev, P., Cebey, L., Sevillano, A. M., Vidal, E., . . . Wille, H. (2016). The Structural Architecture of an Infectious Mammalian Prion Using Electron Cryomicroscopy. *PLoS Pathog*, *12*(9), e1005835. doi:10.1371/journal.ppat.1005835
- Vidarsson, G., Dekkers, G., & Rispen, T. (2014). IgG subclasses and allotypes: from structure to effector functions. *Front Immunol*, *5*, 520. doi:10.3389/fimmu.2014.00520
- Wadsworth, J. D., Joiner, S., Linehan, J. M., Asante, E. A., Brandner, S., & Collinge, J. (2008). Review. The origin of the prion agent of kuru: molecular and biological strain typing. *Philos Trans R Soc Lond B Biol Sci*, *363*(1510), 3747-3753. doi:10.1098/rstb.2008.0069
- Walia, R., Ho, C. C., Lee, C., Gilch, S., & Schatzl, H. M. (2019). Gene-edited murine cell lines for propagation of chronic wasting disease prions. *Sci Rep*, *9*(1), 11151. doi:10.1038/s41598-019-47629-z
- Wan, W., Wille, H., Stohr, J., Kendall, A., Bian, W., McDonald, M., . . . Stubbs, G. (2015). Structural studies of truncated forms of the prion protein PrP. *Biophys J*, *108*(6), 1548-1554. doi:10.1016/j.bpj.2015.01.008
- Wang, F., Wang, X., Abskharon, R., & Ma, J. (2018). Prion infectivity is encoded exclusively within the structure of proteinase K-resistant fragments of synthetically generated recombinant PrP(Sc). *Acta Neuropathol Commun*, *6*(1), 30. doi:10.1186/s40478-018-0534-0
- Wang, J., Li, D., Dangott, L. J., & Wu, G. (2006). Proteomics and its role in nutrition research. *J Nutr*, *136*(7), 1759-1762. doi:10.1093/jn/136.7.1759
- Ward, V. K., Schneider, P. G., Kreissig, S. B., Hammock, B. D., & Choudary, P. V. (1993). Cloning, sequencing and expression of the Fab fragment of a monoclonal antibody to the herbicide atrazine. *Protein Eng*, *6*(8), 981-988. doi:10.1093/protein/6.8.981
- Wasmer, C., Lange, A., Van Melckebeke, H., Siemer, A. B., Riek, R., & Meier, B. H. (2008). Amyloid fibrils of the HET-s(218-289) prion form a beta solenoid with a triangular hydrophobic core. *Science*, *319*(5869), 1523-1526. doi:10.1126/science.1151839
- Watts, J. C., Giles, K., Patel, S., Oehler, A., DeArmond, S. J., & Prusiner, S. B. (2014). Evidence that bank vole PrP is a universal acceptor for prions. *PLoS Pathog*, *10*(4), e1003990. doi:10.1371/journal.ppat.1003990
- Wei, X., Roettger, Y., Tan, B., He, Y., Dodel, R., Hampel, H., . . . Du, Y. (2012). Human anti-prion antibodies block prion peptide fibril formation and neurotoxicity. *J Biol Chem*, *287*(16), 12858-12866. doi:10.1074/jbc.M111.255836
- Weissmann, C. (1991). Spongiform encephalopathies. The prion's progress. *Nature*, *349*(6310), 569-571. doi:10.1038/349569a0
- Weissmann, C. (2004). The state of the prion. *Nat Rev Microbiol*, *2*(11), 861-871. doi:10.1038/nrmicro1025
- Wells, G. A., Scott, A. C., Johnson, C. T., Gunning, R. F., Hancock, R. D., Jeffrey, M., . . . Bradley, R. (1987). A novel progressive spongiform encephalopathy in cattle. *Vet Rec*, *121*(18), 419-420. doi:10.1136/vr.121.18.419

- Wesolowski, J., Alzogaray, V., Reyelt, J., Unger, M., Juarez, K., Urrutia, M., . . . Koch-Nolte, F. (2009). Single domain antibodies: promising experimental and therapeutic tools in infection and immunity. *Med Microbiol Immunol*, *198*(3), 157-174. doi:10.1007/s00430-009-0116-7
- Westaway, D., Cooper, C., Turner, S., Da Costa, M., Carlson, G. A., & Prusiner, S. B. (1994). Structure and polymorphism of the mouse prion protein gene. *Proc Natl Acad Sci U S A*, *91*(14), 6418-6422. doi:10.1073/pnas.91.14.6418
- Westergaard, L., Christensen, H. M., & Harris, D. A. (2007). The cellular prion protein (PrP(C)): its physiological function and role in disease. *Biochim Biophys Acta*, *1772*(6), 629-644. doi:10.1016/j.bbadis.2007.02.011
- White, A. R., Enever, P., Tayebi, M., Mushens, R., Linehan, J., Brandner, S., . . . Hawke, S. (2003). Monoclonal antibodies inhibit prion replication and delay the development of prion disease. *Nature*, *422*(6927), 80-83. doi:10.1038/nature01457
- Wilkinson, I. C., Hall, C. J., Veverka, V., Shi, J. Y., Muskett, F. W., Stephens, P. E., . . . Carr, M. D. (2009). High resolution NMR-based model for the structure of a scFv-IL-1beta complex: potential for NMR as a key tool in therapeutic antibody design and development. *J Biol Chem*, *284*(46), 31928-31935. doi:10.1074/jbc.M109.025304
- Will, R. G. (2003). Acquired prion disease: iatrogenic CJD, variant CJD, kuru. *Br Med Bull*, *66*, 255-265. doi:10.1093/bmb/66.1.255
- Will, R. G., Ironside, J. W., Zeidler, M., Cousens, S. N., Estibeiro, K., Alperovitch, A., . . . Smith, P. G. (1996). A new variant of Creutzfeldt-Jakob disease in the UK. *Lancet*, *347*(9006), 921-925. doi:10.1016/s0140-6736(96)91412-9
- Wille, H., Baldwin, M. A., Cohen, F. E., DeArmond, S. J., & Prusiner, S. B. (1996). Prion protein amyloid: separation of scrapie infectivity from PrP polymers. *Ciba Found Symp*, *199*, 181-199; discussion 199-201. Retrieved from <https://www.ncbi.nlm.nih.gov/pubmed/8915611>
- Wille, H., Bian, W., McDonald, M., Kendall, A., Colby, D. W., Bloch, L., . . . Stubbs, G. (2009). Natural and synthetic prion structure from X-ray fiber diffraction. *Proc Natl Acad Sci U S A*, *106*(40), 16990-16995. doi:10.1073/pnas.0909006106
- Wille, H., Govaerts, C., Borovinskiy, A., Latawiec, D., Downing, K. H., Cohen, F. E., & Prusiner, S. B. (2007). Electron crystallography of the scrapie prion protein complexed with heavy metals. *Arch Biochem Biophys*, *467*(2), 239-248. doi:10.1016/j.abb.2007.08.010
- Wille, H., Michelitsch, M. D., Guenebaut, V., Supattapone, S., Serban, A., Cohen, F. E., . . . Prusiner, S. B. (2002). Structural studies of the scrapie prion protein by electron crystallography. *Proc Natl Acad Sci U S A*, *99*(6), 3563-3568. doi:10.1073/pnas.052703499
- Wille, H., & Requena, J. (2018). The Structure of PrP^{Sc} Prions. *Pathogens*, *7*(1), 20. Retrieved from <http://www.mdpi.com/2076-0817/7/1/20>
- Wille, H., & Requena, J. R. (2018). The Structure of PrP(Sc) Prions. *Pathogens*, *7*(1). doi:10.3390/pathogens7010020
- Wille, H., Shanmugam, M., Murugesu, M., Ollesch, J., Stubbs, G., Long, J. R., . . . Prusiner, S. B. (2009). Surface charge of polyoxometalates modulates polymerization of the scrapie prion protein. *Proc Natl Acad Sci U S A*, *106*(10), 3740-3745. doi:10.1073/pnas.0812770106

- Wille, H., Zhang, G. F., Baldwin, M. A., Cohen, F. E., & Prusiner, S. B. (1996). Separation of scrapie prion infectivity from PrP amyloid polymers. *J Mol Biol*, 259(4), 608-621. doi:10.1006/jmbi.1996.0343
- Williams, E. S., & Young, S. (1980). Chronic wasting disease of captive mule deer: a spongiform encephalopathy. *J Wildl Dis*, 16(1), 89-98. Retrieved from <https://www.ncbi.nlm.nih.gov/pubmed/7373730>
- Williamson, R. A., Peretz, D., Pinilla, C., Ball, H., Bastidas, R. B., Rozenshteyn, R., . . . Burton, D. R. (1998). Mapping the prion protein using recombinant antibodies. *J Virol*, 72(11), 9413-9418. doi:10.1128/JVI.72.11.9413-9418.1998
- Williamson, R. A., Peretz, D., Smorodinsky, N., Bastidas, R., Serban, H., Mehlhorn, I., . . . Burton, D. R. (1996). Circumventing tolerance to generate autologous monoclonal antibodies to the prion protein. *Proc Natl Acad Sci U S A*, 93(14), 7279-7282. doi:10.1073/pnas.93.14.7279
- Wordehoff, M. M., & Hoyer, W. (2018). alpha-Synuclein Aggregation Monitored by Thioflavin T Fluorescence Assay. *Bio Protoc*, 8(14). doi:10.21769/BioProtoc.2941
- Wu, T. T., & Kabat, E. A. (1970). An analysis of the sequences of the variable regions of Bence Jones proteins and myeloma light chains and their implications for antibody complementarity. *J Exp Med*, 132(2), 211-250. doi:10.1084/jem.132.2.211
- Wulf, M. A., Senatore, A., & Aguzzi, A. (2017). The biological function of the cellular prion protein: an update. *BMC Biol*, 15(1), 34. doi:10.1186/s12915-017-0375-5
- Yang, Y., Arseni, D., Zhang, W., Huang, M., Lovestam, S., Schweighauser, M., . . . Goedert, M. (2022). Cryo-EM structures of amyloid-beta 42 filaments from human brains. *Science*, 375(6577), 167-172. doi:10.1126/science.abm7285
- Yang, Y., Shi, Y., Schweighauser, M., Zhang, X., Kotecha, A., Murzin, A. G., . . . Goedert, M. (2022). Structures of alpha-synuclein filaments from human brains with Lewy pathology. *Nature*. doi:10.1038/s41586-022-05319-3
- Yokota, T., Milenic, D. E., Whitlow, M., & Schlom, J. (1992). Rapid tumor penetration of a single-chain Fv and comparison with other immunoglobulin forms. *Cancer Res*, 52(12), 3402-3408. Retrieved from <https://www.ncbi.nlm.nih.gov/pubmed/1596900>
- Zhang, H., Kaneko, K., Nguyen, J. T., Livshits, T. L., Baldwin, M. A., Cohen, F. E., . . . Prusiner, S. B. (1995). Conformational transitions in peptides containing two putative alpha-helices of the prion protein. *J Mol Biol*, 250(4), 514-526. doi:10.1006/jmbi.1995.0395
- Zhang, Y. F., & Ho, M. (2017). Humanization of rabbit monoclonal antibodies via grafting combined Kabat/IMGT/Paratome complementarity-determining regions: Rationale and examples. *MAbs*, 9(3), 419-429. doi:10.1080/19420862.2017.1289302